

REDOX-ACTIVE DENDRIMERS AT MOLECULAR PRINTBOARDS

This research has been supported by the Technology Foundation STW, applied science division of NWO and the technology program of the ministry of Economic Affairs (Simon Stevin Nanolithography Award to Prof. dr. ir. David Reinhoudt, project number TST4946).

Publisher: Wöhrmann Print Service, Zutphen, The Netherlands

© C. A. Nijhuis, Enschede, 2006

No part of this work may be reproduced by print, photocopy, or any other means without the permission of the publisher.

Cover design by Matthijs Reinier van Calveen.

Universiteit Twente, Enschede, Nederland

ISBN 90-365-2434-2

REDOX-ACTIVE DENDRIMERS AT MOLECULAR PRINTBOARDS

PROEFSCHRIFT

ter verkrijging van
de graad van doctor aan de Universiteit Twente,
op gezag van de rector magnificus,
prof. dr. W.H.M. Zijm,
volgens besluit van het College voor Promoties
in het openbaar te verdedigen
op vrijdag 3 november om 13.15 uur

door

Christian Albertus Nijhuis

Geboren op 17 januari 1977
te Enschede

Dit proefschrift is goedgekeurd door:

Promotoren: prof. dr. ir. D. N. Reinhoudt
 prof. dr. ir. J. Huskens

Assistent-promotor: dr. B. J. Ravoo

Contents

Chapter 1	General introduction	1
Chapter 2	Electrochemically Controlled Supramolecular Systems	
2.1	Introduction	6
2.2	Motion induced by electrochemistry	6
2.2.1	Conformational change	7
2.2.2	Interlocked molecules based on transition metals	10
2.2.3	Interlocked molecules based on π - π stacking and hydrogen bonds	12
2.3	Self-assembly and disassembly controlled by electrochemistry	16
2.3.1	Host-guest complexes	16
2.3.2	Hydrogen bonding	22
2.3.3	Electrostatic interaction	26
2.3.3.1	Dendrimers	26
2.3.3.2	Modified ferrocenes	29
2.3.3.3	Vesicles	30
2.4	Conclusions	31
2.5	References	31
Chapter 3	Binding Control and Valency of Ferrocenyl Dendrimers at Molecular Printboards	
3.1	Introduction	38
3.2	Results and discussion	39
3.2.1	Synthesis	39
3.2.2	Formation of dendrimer- β CD assemblies	40
3.2.3	Surface plasmon resonance spectroscopy	42
3.2.4	Electrochemistry	45
3.2.5	Simultaneous SPR and CV	49
3.3	Conclusions	54
3.4	Experimental Section	54
3.5	References	59

Chapter 4 Electrochemistry of Dendrimer – β -Cyclodextrin Assemblies in Solution

4.1	Introduction	62
4.2	Results and discussion	62
4.2.1	Cyclic voltammetry and differential pulse voltammetry	62
4.2.2	Scan rate-dependent CV	66
4.2.3	Electrochemical impedance spectroscopy	68
4.3	Conclusions	79
4.4	Experimental Section	80
4.5	References	81

Chapter 5 Biferrocenyl Dendrimers at Molecular Printboards

5.1	Introduction	84
5.2	Results and discussion	85
5.2.1	Synthesis	85
5.2.2	BFc- β CD complexation	86
5.2.3	Dendrimer- β CD assemblies	87
5.2.4	SPR spectroscopy of BFc dendrimers at the molecular printboard	89
5.2.5	Electrochemistry of BFc dendrimers on the molecular printboard	92
5.2.6	Simultaneous SPR and CV	98
5.3	Conclusions	99
5.4	Experimental	100
5.5	References	103

Chapter 6 Redox-Controlled Supramolecular Patterning of Dendrimers at Surfaces

6.1	Introduction	106
6.2	Results and discussion	107
6.2.1	Single molecules on the molecular printboard	107
6.2.2	Supramolecular patterning	108
6.2.3	Imaging by scanning electrochemical microscopy (SECM)	112
6.2.4	Writing with scanning electrochemical microscopy	116
6.3	Conclusions	118
6.4	Experimental	118
6.5	References	120

Chapter 7 Single Electron Tunneling in Dendrimer-Stabilized Gold Nanoparticles

7.1	Introduction	124
7.2	Results and discussion	125
7.2.1	Immobilization of Au nanoparticles	125
7.2.2	STM	126

7.3	Conclusions	130
7.4	Experimental	130
7.5	References	131

Chapter 8 Preparation of Metal – SAM – Metal Junctions by Supramolecular Metal Transfer Printing

8.1	Introduction	134
8.2	Results and discussion	135
	8.2.1 Supramolecular metal transfer printing	135
	8.2.2 Electrostatic metal transfer printing	139
	8.2.3 Electrostatic and supramolecular mTP combined	141
	8.2.4 Negative differential resistance in supramolecular junctions	142
8.3	Conclusions	145
8.4	Experimental	146
8.5	References	148

Summary 151

Samenvatting 155

Dankwoord 159

Curriculum Vitae 161

General Introduction

Miniaturization of electronic devices is necessary to comply with the ever increasing demand of higher data storage densities and increasing processing speeds.¹ Miniaturization of silicon-based technology is limited by the resolution of photolithography and the break-down of the semiconductor material properties at the nanoscale.² However, molecules are building blocks that fall in the regime of about 1 – 10 nm and the number of design possibilities of the molecules which may influence the device output characteristics are virtually endless.³

Using self-assembly and supramolecular chemistry in bottom-up nanofabrication is a promising strategy to obtain large scale devices that are organized at the molecular level.⁴ One of the key issues is the controlled immobilization of molecules at surfaces leading to well-defined and stable nanostructures. For this reason, our group has developed the concept of molecular printboards which are self-assembled monolayers (SAMs) of host molecules to which guest molecules can bind in a supramolecular fashion.⁵ The advantage of supramolecular chemistry, compared to chemi- or physisorption, or covalent chemistry, is that the binding kinetics and thermodynamics can be precisely controlled.⁶ Additionally, supramolecular interactions can also respond to external stimuli to give control over adsorption processes.⁷

For a variety of applications in molecular electronics, switchable molecules or supramolecular assemblies that can be controlled by external stimuli are a prerequisite.⁸ Redox-switchable molecules are of special interest to incorporate into electronic devices.⁹ Moreover, such molecules or supramolecular systems are also of importance in the design of molecular machines, molecular motors, or molecular actuators.¹⁰ Although to date no molecular system exists that can compete with conventional silicon-based technology, a deeper understanding of how molecular scale devices work and differ in properties compared to macroscale devices grows steadily, despite some difficulties in the interpretation of the data.¹¹

Single supramolecular interactions are in general relatively weak, but multivalent interaction increases the stability of supramolecular assemblies dramatically.¹² For this reason, a fundamental understanding of multivalency is required which may, for instance, have a profound influence in the design of new protocols for bottom-up nanofabrication.¹³ In Chapter 2 a literature overview is given about supramolecular systems that can be electrochemically controlled. Of particular interest is the controlled inclusion complex formation of ferrocene

(Fc) and β -cyclodextrin (β CD). Fc forms stable inclusion complexes with β CD, while the oxidized form, the ferrocenium cation (Fc^+), is not able to form inclusion complexes with β CD.

The first part of the thesis (Chapters 3 to 5) deals with the adsorption of multivalent redox active guest dendrimers at SAMs of β CD hosts. Fc-terminated dendrimers form large water soluble supramolecular assemblies by complexation of the end groups to β CD. Chapter 3 deals with the electrochemically controlled adsorption and desorption behavior of these assemblies at and from the host surface. The multivalent binding stoichiometry of these dendrimers with the host surface was assessed for 5 different generations having 4 up to 64 Fc moieties and various tethers. The number of interactions of the dendrimers with the molecular printboard was studied as a function of generation or length of the tethers between the neighboring Fc units.

While Chapter 3 deals only with the electrochemistry of dendrimers adsorbed at the host surface, Chapter 4 gives a detailed electrochemical study of the dendrimers- β CD assemblies at the host surface in equilibrium with the dendrimers- β CD assemblies in solution. Especially electrochemical impedance spectroscopy was used to obtain information about electrontransfer kinetics, mass transport, binding and desorption kinetics, and the binding geometry of the assemblies.

In Chapters 3 and 4 dendrimers having two redox-states are described, but for potential applications in nanoelectronics, it would be desirable to have a supramolecular system with multiple states. Chapter 5 deals with the preparation and the redox-controlled binding to native β CD and β CD SAMs of biferrocene- (BFc-) functionalized dendrimers which have three different oxidation states.

The second part of the thesis (Chapters 6, 7, and 8) concerns the use of the redox-active dendrimer- β CD assemblies in nanofabrication and nanoelectronics. In Chapter 6 the concepts of supramolecular microcontact printing (μ CP) and dip-pen nanolithography (DPN) were used to create patterns of dendrimers at the host surface. Scanning electrochemical microscopy was used to induce local desorption of the dendrimers from the host surface. This method is therefore complementary to DPN and μ CP.

Chapter 7 describes the synthesis of Au nanoparticles inside the dendrimer- β CD assemblies followed by immobilization at the host surface. The Au nanoparticles are shielded from the underlying Au surface and the system is robust due to formation of multivalent host-guest interactions. Images of immobilized dendrimers at the molecular printboard and single electron tunneling characteristics were measured by STM at room temperature.

A key issue in the field of nanoelectronics is to introduce electrodes to single molecules or at SAMs without causing short circuits or destroying the relatively fragile molecules. In Chapter 8 the concept of supramolecular metal transfer printing is introduced to deliver top-electrodes directly onto monolayers of dendrimers at β CD SAMs. Two-terminal devices were prepared consisting of redox-active Fc and BFc dendrimers, and redox-inactive adamantyl

(Ad) terminated dendrimers. The (*I,V*) characteristics of the supramolecular assemblies were measured and clearly showed tunnel characteristics along with negative differential resistance (NDR) waves which were dependent on the type of dendrimers incorporated in the junction.

References

- 1) Ito, T.; Okazaki, S. *Nature* **2000**, *406*, 1027.
- 2) (a) Joachim, C.; Gimzewski, J. K.; Aviram, A. *Nature* **2000**, *408*, 541. (b) Schulz, M. *Nature* **1999**, *399*, 729. (c) Muller, D. A.; Sorsch, T.; Moccio, S.; Baumann, F. H.; Evans-Lutterodt, K.; Timp, G. *Nature* **1999**, *399*, 758.
- 3) (a) Balzani, V. *Small* **2005**, *1*, 278. (b) Flood, A. H.; Stoddart, J. F.; Steuerman, D. W.; Heath, J. R. *Science* **2004**, *306*, 2055.
- 4) (a) Service, R. F. *Science*, **2002**, *295*, 2398. (b) Whitesides, G. M.; Gryzbowski, B. *Science* **2002**, *295*, 2418.
- 5) Auletta, T.; Dordi, B.; Mulder, A.; Sartori, A.; Onclin, S.; Bruinink C. M.; Péter, M.; Nijhuis, C. A.; Beijleveld, H.; Schönherr, H.; Vancso, G. J.; Casnati, A.; Ungaro, R.; Ravoo, B. J.; Huskens, J.; Reinhoudt, D. N. *Angew. Chem. Int. Ed.* **2004**, *43*, 369.
- 6) Schneider, H. J.; Yatsimirsky, A. K. *Principles and Methods in Supramolecular Chemistry*, John Wiley & Sons Ltd: Chichester, **2000**.
- 7) (a) Boulas, O. L.; Gómez-Kaifer, M.; Echegoyen, L. *Angew. Chem. Int. Ed.* **1998**, *37*, 216. (b) Cooke, G. *Angew. Chem. Int. Ed.* **2003**, *42*, 4860. (c) Jing, L.; Yuangang, L.; Yu, F. *Prog. Nat. Sci.* **2005**, *15*, 1057.
- 8) (a) Tseng, H. R.; Wu, D.; Fang, N. X.; Zhang, X.; Stoddart, J. F. *ChemPhysChem* **2004**, *5*, 111. (b) Kahn, O.; Martinez, C. J. *Science* **1998**, *279*, 44. (c) Rueckes, T.; Kim, K.; Joselevich, E.; Tseng, G. Y.; Cheung, C. - L.; Lieber, C. M. *Science* **2000**, *289*, 94. (d) Chen, J.; Reed, M. A.; Rawlett, A. M.; Tour, J. M. *Science* **1999**, *286*, 1550.
- 9) Liu, Z.; Yasserli, A. A.; Lindsey, J. S.; Bocian, D. F. *Science* **2003**, *302*, 1543.
- 10) (a) Schally, C. A.; Beizai, K.; Vögtle, F. *Acc. Chem. Res.* **2001**, *34*, 465. (b) Balzani, V.; Credi, A. *Chem. Rec.* **2001**, *1*, 442. (c) Kay, E. R.; Leigh, D. A. *Top. Curr. Chem.* **2005**, *262*, 133. (d) Feringa, B. L. *Acc. Chem. Res.* **2001**, *34*, 504.
- 11) (a) Akkerman, H. B.; Blom, P. W. M.; De Leeuw, D. M.; De Boer, B. *Nature* **2006**, *441*, 69. (b) Ratner, M. *Nature* **2005**, *435*, 575. (c) Kubatkin, S.; Danilov, A.; Hjort, M.; Cornil, J.; Brédas, J. -L.; Stuhr-Hansen, N.; Hedegård, P.; Bjørnholm, T. *Nature* **2003**, *425*, 698. (d) Service, R. F. *Science*, **2003**, *302*, 556. (e) Troisi, A.; Ratner, M. A. *Small* **2006**, *2*, 172. (f) Stewart, D. R.; Ohlberg, D. A. A.; Beck, P. A.; Chen, Y.; Williams, R. S.; Jeppesen, J. O.; Nielsen, K. A.; Stoddart, J. F. *Nano lett.* **2004**, *4*, 133.
- 12) Mammen, M.; Choi, S. -K.; Whitesides, G. M. *Angew. Chem. Int. Ed.* **1998**, *37*, 2754.
- 13) (a) Badjić, J. D.; Balzani, B. V.; Credi, A.; Silvi, S.; Stoddart, J. F. *Science* **2004**, *303*, 1845. (b) Mulder, A.; Huskens, J.; Reinhoudt, D. N. *Org. Biomol. Chem.* **2004**, *2*, 3409.

Electrochemically Controlled Supramolecular Systems

Large and complex molecular structures can be assembled by supramolecular chemistry and self-organization. For practical purposes it is required that the assembly and disassembly of supramolecular complexes and materials can be directed and controlled by external stimuli in order to prepare, for instance, molecular machines or to build components for molecular electronics. In this respect, redox-responsive molecules or supramolecular complexes are a logical choice since they are directly compatible with existing semiconductor-based microelectronic technology. In this chapter, redox switchable supramolecular assemblies, host-guest complexes and materials are reviewed. The electrochemical action of the redox-active component can be divided into two main categories: i) conformational changes within a molecule and/or the motion of one component with respect to another in interlocked molecules, and ii) the assembly and disassembly of supramolecular complexes. Ferrocenes, viologens, quinones, tetrathiafulvalenes, and transition metals, e.g. Ni and Cu, have two (or three) stable redox-states and their electrochemical conversion is completely reversible. Therefore, these redox centres are frequently used as active components in supramolecular chemistry. The first part of this overview deals with the conformational changes within the molecules, and with electrochemically induced movement of one component with respect to the other in interlocked molecules. The second part describes the electrochemically controlled formation of supramolecular complexes. A wide range of interactions, i.e. hydrophobic interactions, Van der Waals interactions, hydrogen bonds, electrostatic interactions, and π - π stacking can be electrochemically controlled to direct the (relative) motion of molecules and the association or dissociation of complexes.

2.1 Introduction

The miniaturization of electronically active components, such as transistors and diodes, by conventional semiconductor based technology is increasingly difficult below 100 nm.¹ Molecules span the range of roughly 1 nm to 10 nm and are promising candidates to be employed as building blocks to construct devices in the nm regime. Self-assembly and supramolecular chemistry allow the construction of large scale, complicated molecular structures that can be used in electronic circuitry. Moreover, molecules consisting of components that can move relative to each other in response to an external stimulus can be used to construct molecular machines or actuators.^{2,3} Nature provides sophisticated examples of molecular machines composed of multiple subunits that rotate or move along fibers unidirectionally with high efficiency.⁴

To build molecular machinery or devices it is a prerequisite to have control over the self-assembly processes and to include molecules or systems that respond to external stimuli. Molecules or supramolecular complexes that are sensitive to the oxidation state of one or more components are a logical choice to incorporate in electronic circuitry due to the compatibility with silicon-based technology. Here, an overview is given of electrochemically controlled non-covalent supramolecular systems. Altering the redox-state of one the components in an assembly can effect profound structural changes or induce molecular motion. Redox-switchable molecules of which intramolecular conformational changes can be electrochemically controlled, along with rotaxanes and catenanes, which have frequently been the subject in studies for these purposes, are briefly reviewed in section 2.2.^{5,6} Switching between the “on” and “off” states can also be achieved by controlling non-covalent interactions which in addition gives control over assembly processes.^{7,8,9} The electrochemical control over different types of interactions, i.e. hydrophobic interactions, Van der Waals interactions, hydrogen bonding, and electrostatic interactions, will be briefly discussed in section 2.3. Electrochemical control over these interactions can induce, for instance, the bending of self-assembled monolayers (SAMs), vesicle formation, and the orientation of liquid crystals. Cyclodextrin and cucurbituril host molecules are of interest owing to the fact that a variety of small organic molecules can be accommodated in well-defined host-guest complexes.^{10,11,12} The electrochemically controlled binding of the redox-active guests to these hosts is also briefly reviewed. Redox-responsive receptors are potentially useful in sensing applications and constitute another example of how electro-active components in supramolecular chemistry can be used to induce and control molecular recognition.¹³

2.2 Motion induced by electrochemistry

The ability to trigger and control motion in molecular systems by external stimuli is one of the major goals in the field of so-called “molecular machines”.^{14,15,16} Nature uses proteins that

can be considered as molecular machines,⁴ such as F₀F₁ATP synthase.¹⁴ This enzyme is composed of 9 subunits, one of which has a proton tunnel through which protons flow. The proton flux causes a torque between the different subunits resulting in a rotary motion of certain subunits with respect to the other. Other proteins such as myosin and kinesin display linear motion. Motion may proceed via intramolecular conformational change leading to rotation, bending, or flipping of one or more components of a molecule. Artificial molecular machines are still far from perfection but interlocked molecules, i.e. catenanes and rotaxanes, that change shape or conformation in response to, for instance, irradiation, change of pH, or ion exchange, are promising candidates. Here, different types of interlocked molecules based on transition metals and π - π -stacking or hydrogen bonds of which movement of one of the interlocked components with respect to the other one can be electrochemically controlled will be briefly reviewed.

2.2.1 Conformational change

Conformational changes within molecules in response to electrochemical conversion of the redox state have been the subject of a number of investigations to achieve mechanical output on the nanometre scale. Different types of motion, i.e. rotation, bending, flipping, or the orientation of liquid crystals, are possible and – ideally – also need to be controlled. In this context, the group of Tatamoto described a macrocycle based on a two paraphenylenediamine rotors (Figure 2.1).¹⁷ Paraphenylenediamine can undergo a highly reversible two electron oxidation resulting in a paraquinonediimine. This is the basis for the switching when the molecules are incorporated into macrocycles. Two different cyclophanes were prepared by reaction of 4,4'-dimethylenedianiline with duroquinone (DM₄) or anthraquinone (AM₄). According to CV, AM₄ was stable for 100 CV cycles and DM₄ for 10 cycles. In the reductive state, the cyclophanes have a planar conformation with a closed cavity, but oxidation forces the quinones into a face conformation and, thus, induces the opening of the cavity. The “flipping” of the quinones was confirmed in the solid state by X-ray crystallography and in solution by cyclic voltammetry and spectroelectrochemistry.

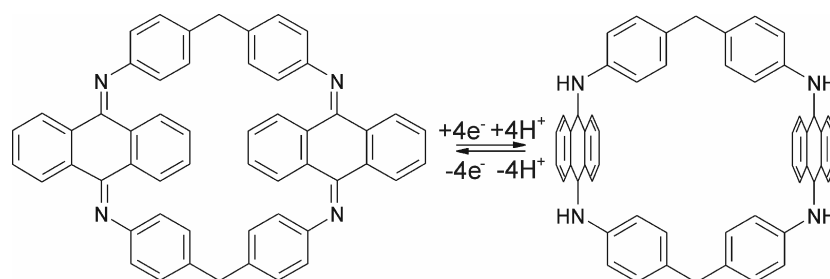


Figure 2.1: Schematic of the redox switchable cyclophane from face to lateral conformation.¹⁷

Oxidation of a quinone covalently linked to a benzene moiety resulted in a conformational change from face-to-face to face-to-edge within the macrocycle (Figure 2.2).¹⁸ In the neutral form, the molecule adopts a face-to-face orientation that is stabilized by π - π interactions of the quinone and benzene moiety. Oxidation of the quinone moiety results in a negatively charged aromatic π -system. The face-to-edge conformer is favored due to electrostatic interactions between the positively charged H-atom of the benzene group and the negatively charged quinone moiety and by the π -H interaction between the π electrons of the quinone and the H-atom of the benzene. The face-to-edge conformer could be stabilized by conversion of the corresponding hydroquinone in the presence of H^+ . The flipping motion could be followed by 1H NMR spectroscopy and CV.

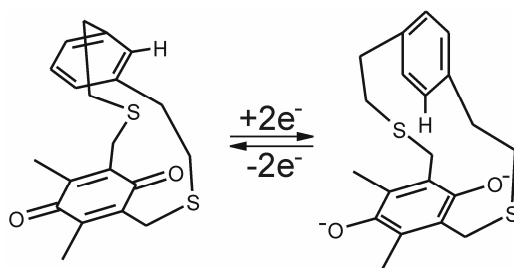


Figure 2.2: Electrochemically induced flipping motion of the benzene ring with respect to the quinone moiety.¹⁸

Hawthorne et al. reported a *commo*-bis-7,8-dicarbollo metallacarborane based on Ni^{3+} and Ni^{4+} of which the two ligands can rotate with respect to each other (Figure 2.3).¹⁹ Metallocenes also show rotation of the ligands with respect of each other with an energy barrier of ca. 2 kcal/mol, but metallocarboranes have barriers of ca. 6 kcal/mol. The ligand possesses two neighboring carbon atoms which normally gives a trans configuration in metallocarborane complexes with Ni^{3+} . On the contrary, Ni^{4+} leads to cis complexes, with both carbon vertices on the same side of the molecule. Electrochemical conversion of Ni^{4+} to Ni^{3+} triggers the rotation of the ligand with respect to each other and a change in conformation from cis to trans. Unidirectional motion could be achieved by introducing a methyl group to both rings in the R^2 and R^4 positions. Therefore, clockwise rotation is preferred upon electrochemical oxidation of the methylated complex, since this prevents overlap of the two methyl groups, as would be the case in counterclockwise rotation.

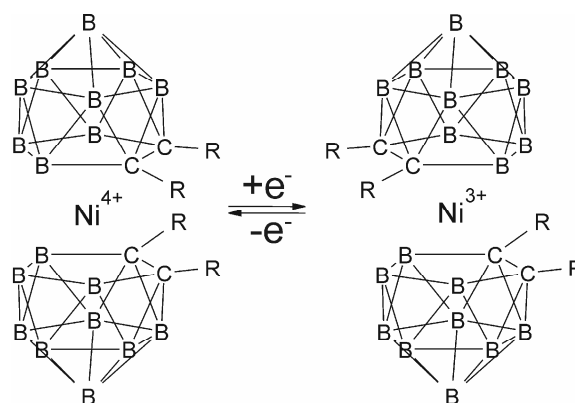


Figure 2.3: Schematic of the electrochemically induced movement of the upper and lower rings with respect to each other, R = H or Me.¹⁹

Electrochemistry can also be used to induce collective motion of molecules in materials. For example, liquid crystals assume orientations that are sensitive to the surface properties which can be electrochemically controlled. Abbott et al. reported SAMs of Fc terminated alkanethiols on Au and alkanethiols at which thermotropic liquid crystals of 4,4'-pentylcyanobiphenyl (5CB) or N-(p-methoxybenzylidene)-p-butylaniline (MBBA) form.²⁰ When CV was applied in the case of 5CB with 35 mM TBAF the reversible oxidation of Fc head groups could be measured together with color changes. When the potential was held at -0.2 V, the 5CB was green, indicating a planar alignment with no azimuthal preference for either electrode, while at 0.28 V yellow regions were observed indicating a perpendicular alignment at the working electrode. The process was reversible and this behavior could not be observed for an alkanethiol reference layer.

Recently, the group of Willner reported redox controlled bending of bipyridinium (= viologen, V) terminated monolayers on Au surfaces.²¹ The monolayers were not densely packed to allow bending of the molecules upon electrochemical conversion of the V head groups. In the V^{2+} form the head groups are electrostatically repelled from the Au electrode and face the exterior of the monolayer at a positive bias. At negative a bias, the head groups are attracted to the Au surface causing the molecules to bend toward the surface. If the bias was sufficiently lowered the head groups were reduced. The bending of the monolayer could be followed by contact angle measurements and electrochemical methods. A monolayer lacking the V head groups showed no bending behavior. A reference monolayer consisting of a short tether between the thiol functionality and V moiety showed only a moderate change in contact angle upon reduction of the V moiety and no significant changes at potentials that cause bending. Recently, a negatively charged carboxylate-terminated monolayer also has been used to bend a monolayer toward the surface upon changing the electrical potential.²²

2.2.2 Interlocked molecules based on transition metals

The group of Sauvage et al. reported Cu-based catenanes and rotaxanes that respond to an electrochemical signal causing one of the interlocked molecules to pirouette around the second one.^{23,24,25,26} The rotaxane consists of an axle that contains a bipy or phenanthroline chelate ligand with two bulky stopper groups and a ring consisting of a bidentate and a tridentate binding site to which copper can bind (Figure 2.4). Cu^+ forms stable 4-coordinate complexes while Cu^{2+} forms 5-coordinate complexes. Electrochemical conversion of Cu^+ to Cu^{2+} results in reorganization from a 4-coordinate to a 5-coordinate complex which can only proceed by pirouetting the ring. The rate of pirouetting depended on the oxidation state of copper. The 5-coordinate copper changed in about 50 ms, but the 4-coordinate copper changed in the order of minutes. The response time could be reduced by lowering the steric hindrance of the axle around the bipy moiety since the rate limiting step is the ligand exchange reaction of the copper (Figure 4 right). The lower limit for the rate constant of the rearrangement for the 5-coordinate- Cu^+ complex to the 4-coordinate- Cu^{2+} was found to be $k > 500 \text{ s}^{-1}$, while the backward reaction proceeded much slower ($k = 5 \text{ s}^{-1}$).²⁷

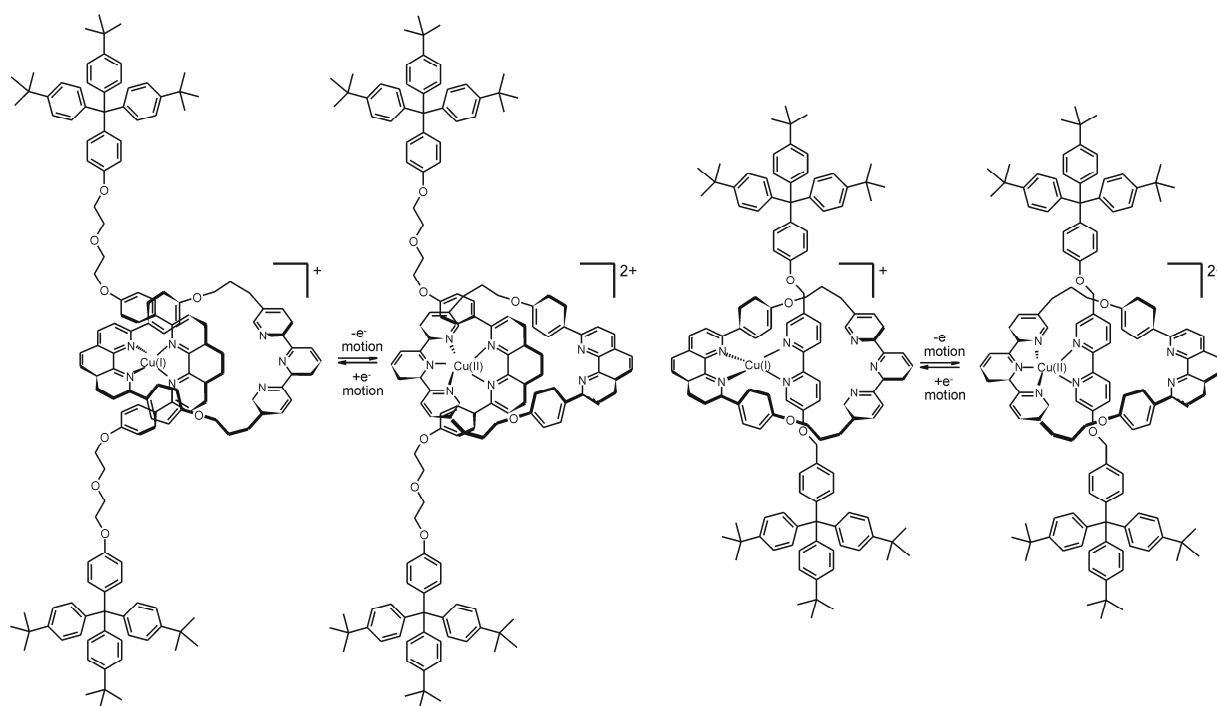


Figure 2.4: Pirouetting rotaxane based on $\text{Cu}^+/\text{Cu}^{2+}$ (left) and one with reduced steric hindrance to decrease the response time (right).²⁷

Woźniak et al. reported electrochemically controlled rotaxanes and catenanes based on transition metal (Ni and Cu) tetraazamacrocyclic complexes and dibenzo[24]crown-8 as building blocks (Figure 2.5).^{28,29,30,31} The major difference with Sauvage's system is that the

metal centres are used as different docking stations for the ring. The macrocycle consisting of two different metal centres adopts a face-to-face geometry. The crown ether aromatic ring interacts with the metal coordinated ring in such a way that a sandwich structure is formed with one of the aromatic rings in between the two metal centres while the second ring coordinates in a parallel fashion outside the ring. The result is a rectangular structure. Electrochemical analysis revealed that the metal centres were not electrochemically communicating unless the linkers are very short.³¹ The most striking feature in the electrochemical data was the observation of the splitting of the oxidation wave for the Ni-centre at lower temperatures. Initially, the crown ether is located at the Ni-centre, but oxidation of the Cu centre initiates the translocation of the crown ether from the Ni-centre to the more positively charged Cu-centre. At lower temperatures or at shorter experimental time scales, the translocation of the ring is slow (5 s^{-1}) and, consequently, a part of the Ni-centres still interact with the crown ether while others are not, resulting in a splitting of the wave.²⁸ A second oxidation of the Ni-centre initiates a second translocation of the crown ether macrocycle back to its original position, i.e. the Ni-centre.

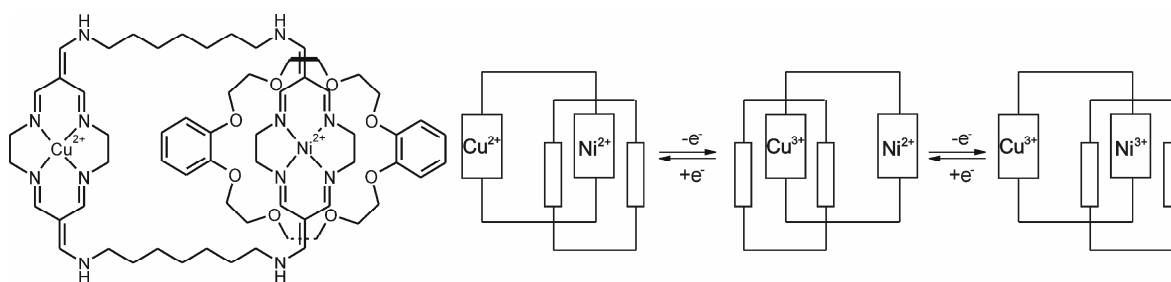


Figure 2.5: Catenane based on a dibenzo[24]crown-8 and a heteronuclear macrocycle with Ni and Cu ions.²⁸

The position of interlocked molecules with respect to each other can be electrochemically controlled. Additionally, the formation of different types of rotaxanes can also be electrochemically induced. The switch between the two oxidation states of ferrocene (Fc) has been used to control the formation of [2]rotaxanes,³² [3]rotaxanes,³³ or pseudo rotaxanes (Figure 2.6).³⁴ A dibenzo[24]crown-8 ring interacts with an axle with a Fc terminus which is bulky enough to prevent dethreading and a *p*-phenylene group capable of having CH- π interactions with the ring.³² Electrochemical oxidation of the Fc moiety triggers the rotaxane formation (Figure 2.6).³⁵ The oxidation potential of the Fc moiety is 80 mV lower due to the stabilization of the Fc^+ by the ring compared to the oxidation potential of the axle in or without the presence of free crown ether. The ring is translocated along the axle due to the attractive positive charge between the ring and the Fc^+ . The oxidation of the Fc moiety of Fc terminated axle in the presence of dibenzo[24]crown-8 also can trigger the formation of a pseudo rotaxane.³⁴ Symmetrically, 1,1'-substituted Fc with two *p*-xylylaminomethyl moieties was able to form both [2] and [3]pseudorotaxanes.³³

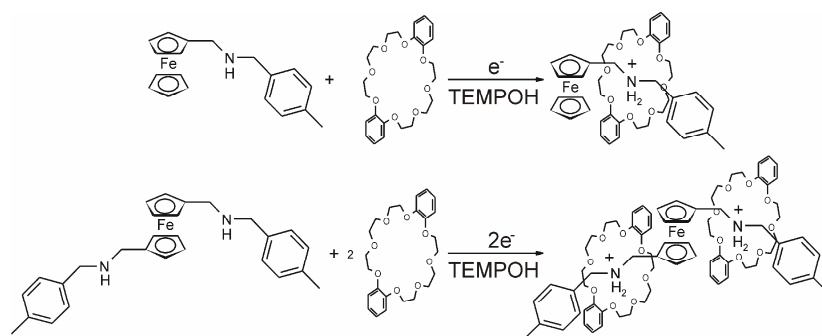


Figure 2.6: The formation of Fc based [2]³⁴ and [3]pseudorotaxane³³ is induced by electrochemical conversion of the Fc moiety in the presence of 1-hydroxy-2,2,6,6-tetramethylpiperidine (TEMPOH), followed by an electron transfer reaction from the nitrogen to the Fc⁺ cation resulting in a cationic radical at the nitrogen (right). Subsequently, transfer of hydrogen from TEMPOH results in a dialkylammonium species followed by rotaxane formation

2.2.3 Interlocked molecules based on π - π -stacking or hydrogen bonding

The immobilization of functional molecular architectures at surfaces can be achieved using two strategies: immobilization of the whole structure at once or step-by-step surface-confined synthesis. The group of Willner reported a monolayer of rotaxanes on Au consisting of the cyclophane, cyclobis(paraquat-*p*-phenylene), that includes a σ -donor diiminobenzene unit stoppered by an adamantyl (Ad) unit (Figure 2.7) by a step-by-step synthesis.^{36,37} The cyclophane is localized on the molecular axle by generating a σ -donor-acceptor complex with the diiminobenzene units of the molecular axle. The cyclophane acts as a molecular shuttle, revealing electrochemically driven mechanical translocations along the molecular axle. The translocation occurs within 70 ms. Reduction of the cyclophane to the respective biradical-dication results in its dissociation from the σ -donor site, and the reduced cyclophane is translocated toward the electrode. Oxidation of the reduced cyclophane reorganizes the σ -donor diiminobenzene sites. The reduced cyclophane moves toward the electrode with a rate constant corresponding to $k_1 = 320 \text{ s}^{-1}$, whereas the translocation of the oxidized cyclophane from the electrode to the σ -donor binding site proceeds with a rate constant of $k_2 = 80 \text{ s}^{-1}$. In situ electrochemical and contact angle measurements reveal that the electrochemically driven translocation of the cyclophane on the molecular axle reversibly controls the wettability of the surface. In the latter system, the translation of the molecular motion into the macroscopic motion of a water droplet was demonstrated. Replacing the Ad stopper by glucose oxidase resulted in a system where the enzyme is “wired” to the Au electrode because the shuttling of the ring assisted in the electron transfer processes.³⁸

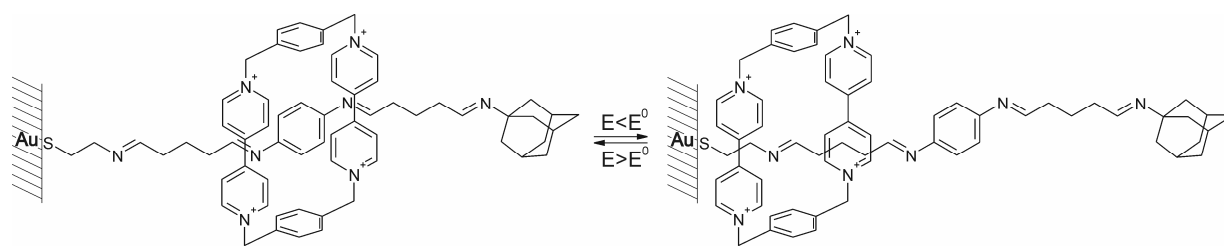


Figure 2.7: A redox switchable rotaxane immobilized at a Au surface with two docking stations and an Ad stopper.^{36,37}

Altieri et al. reported a rotaxane in which the shuttling between two stations only took about 50 μs (Figure 2.8).³⁹ The rotaxane is composed of succinamide and naphthalimide hydrogen bonding stations, separated by seven CH_2 units, and a benzylic amide macrocycle. The formation of hydrogen bonds between the naphthalimide and the ring is sensitive to the redox state of the naphthalimide moiety. The relative binding affinity of the two docking stations is altered by 8 orders of magnitude by reduction of the naphthalimide which triggers the translocation of the ring originally positioned at the succinamide station to the naphthalimide station. CV data demonstrated that a new oxidation wave was observed for the rotaxane compared to the data for the axle without the ring and that the shuttling is reversible at room temperature. Lowering the temperature to 213 K revealed the cathodic wave since the ring is now moving slowly on the electrochemical time scale.

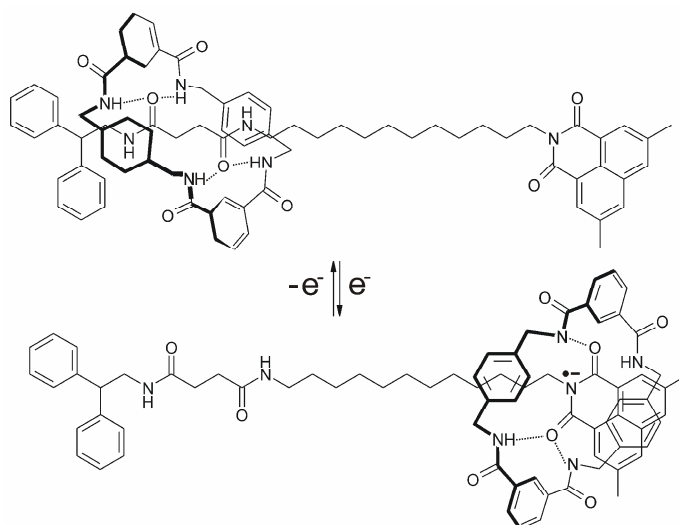


Figure 2.8: An electrochemically switchable, hydrogen bonded rotaxane that has the ring in the neutral state located at the succinamide docking station, while in the reduced form the ring shuttle to the naphthalimide docking station.³⁹

Stoddart et al. reported catenanes and rotaxanes that have two docking stations to which an interlocked macrocycle can bind (Figure 2.9).⁴⁰ The redox state of one of the docking stations determines to which docking station the macrocycle binds. The catenane contains a macrocycle consisting of a tetrathiafulvalene (TTF) and a dioxynaphthalene (DPN) unit that

serve as docking stations linked by ethylene glycol tethers.⁴¹ The second interlocked macrocycle consists of a tetracationic cyclobis(paraquat-*p*-phenylene) (CBPQT⁴⁺) unit. In the “rest” state, the TTF unit is complexed to the CBPQT⁴⁺ ring, but electrochemical conversion of the TTF unit to the monocationic TTF⁺ or dicationic TTF²⁺ form causes electrostatic repulsion between the CBPQT⁴⁺ unit and the positively charged TTF unit. Therefore, the CBPQT⁴⁺ moiety translocates along the ring to the neutral DPN moiety. The movement can be reversed by reduction of the TTF docking station.

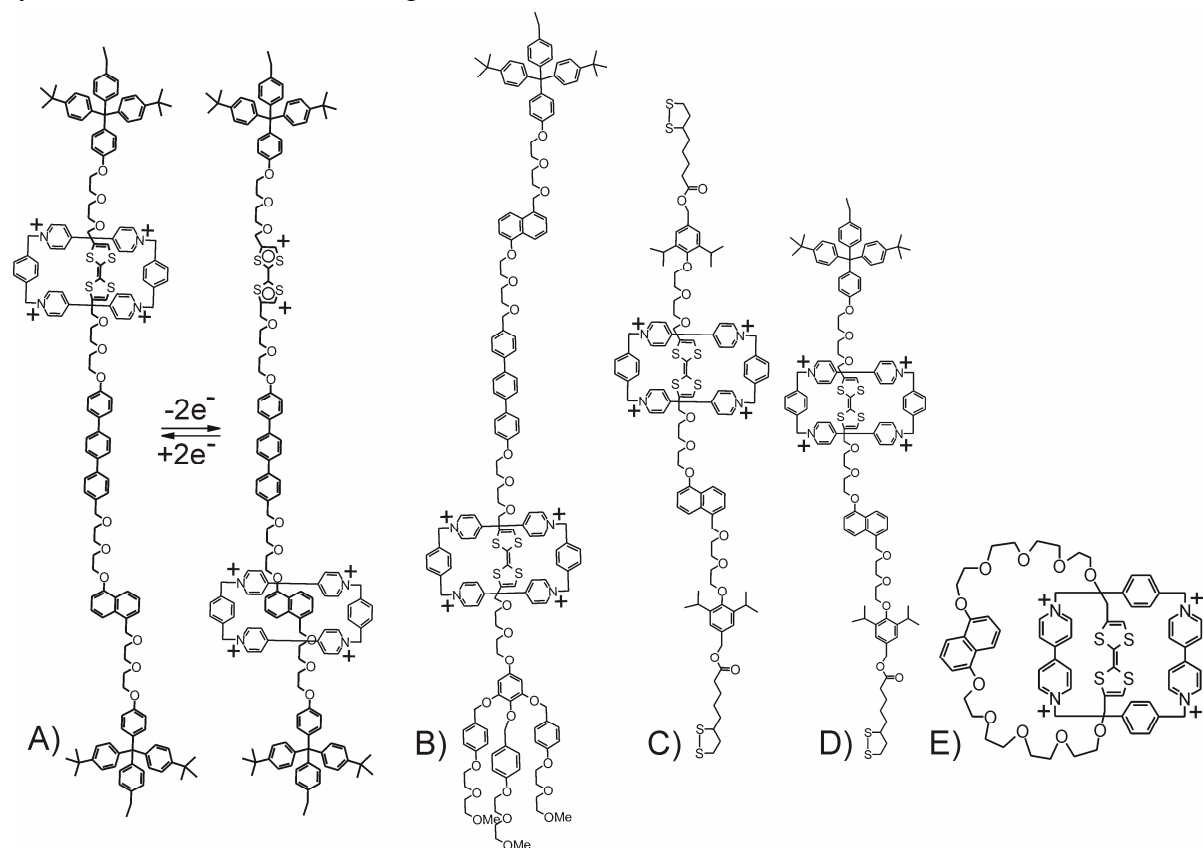


Figure 2.9: The redox triggered movement of the CBPQT⁴⁺ ring is shown for a rotaxane consisting of a rigid terphenyl spacer (A); in the rest state the ring interacts with TTF unit, but electrochemical oxidation of TTF unit forces the ring to move to the DPN docking station due to electrostatic repulsion. The amphiphilic rotaxane used for the preparation of LB-films (B) and disulfide functionalized rotaxanes at both (C) or one (D) stopper used for immobilize at metal surfaces. A typical catenane consisting of a DPN and a TTF docking stations between which the CBPQT⁴⁺ ring can shuttle (E).⁶

Using a similar strategy, Stodart et al. prepared rotaxanes composed of an axle with two bulky stoppers and a TTF and DPN linked by ethylene glycol units with or without an additional rigid terphenylene spacer (Figs. 2.9A-D). The switching behavior of these molecules was studied in great detail in solution by electrochemistry, ¹H NMR spectroscopy, and UV/vis spectroscopy.⁴²

A disulfide tethered rotaxane (Figure 2.9D) was immobilized on Au and the redox-switching behavior was studied by CV at different temperatures.⁴³ According to CV, in about

one out of 10 molecules the CBPQT⁴⁺ ring is located at the DNP centre instead of the TTF unit. A metastable state is observed at high scan rates, in which the ring moved back to a reduced TTF unit too slowly compared to the electrochemical time scale. Therefore, in the first scan the waves corresponding to encapsulated TTF units were observed, while subsequent scans were dominated by the free TTF units. The metastable state has a half life time of 11.7 s at 288 K and of 5 min at 263 K.

Additionally, Langmuir-Blodgett (LB) films of amphiphilic catenanes⁴⁴ (Figure 2.9E) and rotaxanes (Figure 2.9B)^{45,46} could be prepared. The shuttling behavior of a similar rotaxane was also studied in LB-films since in solution the molecules are randomly distributed, while the movement of the ring becomes unidirectional upon surface-confinement. The TTF end is a hydrophobic stopper while the stopper on the DNP end is hydrophilic, or *visa versa*. The shuttling of the CBPQT⁴⁺ after chemical oxidation and reduction could be followed by surface pressure-area isotherm analysis, X-ray reflectometry, and X-ray photoelectron spectroscopy (XPS). Additionally, the shuttling in LB-films at the water-air interface of a different rotaxane lacking the terphenyl moiety could be simulated by molecular dynamics.⁴⁷

The translation of molecular scale motion into the movement of macroscale objects is one of the challenges to achieve true molecular machinery or molecular actuators. Stoddart et al. also described a so-called molecular muscle based on a [3]rotaxane comprised of two pairs of complementary TTF and naphthalene (NP) recognition sites.⁴⁸ Each NP site is enclosed by one CBPQT⁴⁺ unit and the two complementary parts are linked by a rigid spacer. The distance between the two rings can be varied electrochemically from 1.4 nm to 4.2 nm, provided that the molecule adopts a fully stretched conformation. Both cyclophane rings were monofunctionalized with a disulfide tether which allowed immobilization of the rotaxane on one side of Au-coated cantilevers. Oxidation and reduction of the artificial muscle resulted in reversible bending of an atomic force microscope (AFM) cantilever.

The electrochemical release of small guest molecules trapped in a maze of channels inside nanoporous silica particles was recently demonstrated.⁴⁹ A rotaxane (similar to the one shown in Figure 2.9) with a OH-functionality at one of the stoppers was used for immobilization at nanoporous silica particles of an average diameter of 620 nm with highly ordered channels of 1.5-2.0 nm in diameter. The orientation of the rotaxane was such that the TTF unit was located in the upper part of the molecule and the DNP at the lower part of the molecule with respect to the particle. The channels were loaded with Ir(ppy)₃ or rhodamine B and the TTF unit was oxidized in order to close the channel by moving the CBPQT⁴⁺ down to the DNP group. The particles loaded with guest molecules could withstand wash procedures. However, the reduction of the TTF²⁺ unit opened the pores since the ring shuttles back the TTF unit and initiates the release of the guest molecules.

The incorporation of redox-active supramolecular systems in molecular scale junctions is an attractive approach to device miniaturization. Molecular electronic devices were prepared using LB-films of rotaxanes (Figure 2.9B) and catenanes (Figure 2.9D) and the rotaxanes with

the disulfide functionalized stoppers (Figure 2.9C).⁵⁰ Devices were prepared by using LB-films of either the rotaxanes or only the dumbbell shaped axles at the Pt electrodes (Figure 2.9), followed by deposition of Ti top electrodes (Figure 2.10). Both types of devices gave similar (I,V)-characteristics.⁵¹ The switching behavior in these devices was dominated by the properties of the electrode/molecule interface. However, functionalization of both stoppers with disulfides allowed the immobilization of a single molecule between the two Pt electrodes.⁵² The devices prepared with a silicon bottom electrode and a titanium top electrode clearly showed controlled conductivity due to the shuttling.



Figure 2.10: Schematic of the amphiphilic rotaxanes in a tunnel junction where the ring (blue) shuttles between the two docking stations. In the beginning, the ring is located at the TTF unit (green), but oxidation leads to coulomb repulsion forcing the ring to translocate to the DNP unit (red). Reduction of the TTF unit first leads to a metastable state before the ring shuttles back to the TTF unit.^{50a}

2.3 Self-assembly and disassembly controlled by electrochemistry

Controlling non-covalent interactions in supramolecular chemistry and self-assembly is a powerful approach in bottom-up nanofabrication to construct novel materials for potential applications in, for instance, molecular electronics and sensors. The interactions most frequently encountered in supramolecular complexation are hydrophobic interactions, Van der Waals interactions, hydrogen bonds, electrostatic interactions, and π - π stacking. In this section, an overview is given of the electrochemically induced association and dissociation of supramolecular complexes comprised of different types of interactions.

2.3.1 Host-Guest complexes

Cyclodextrins (CDs) and cucurbiturils (CBs) are water soluble host molecules which form stable inclusion complexes with redox-active guest molecules such as Fc, cobaltocene (Cob), and viologen (V). The interplay of the cavity size and the nature of the redox-active guest molecules allows precise control over the host-guest complex formation, stoichiometry, and thermodynamics.

CDs are occurring molecules produced by enzymatic conversion of starch. CDs contain a hydrophobic cavity to which small molecules can bind in aqueous media.⁵³ CDs consist of linked glucose units to yield a chiral macrocycle and the size depends on the number of glucose units. The most common CDs are α -cyclodextrin (α CD), β -cyclodextrin (β CD), and γ -cyclodextrin (γ CD), composed of 6, 7, and 8 glucose units, respectively. Synthetic procedures have been developed to chemically modify β CDs selectively. For instance, the hydroxyl-groups at the upper and lower rim display different reactivities and also monofunctionalized β CDs can be prepared. Figure 2.11 shows the three different CD host molecules along with their characteristic dimensions.

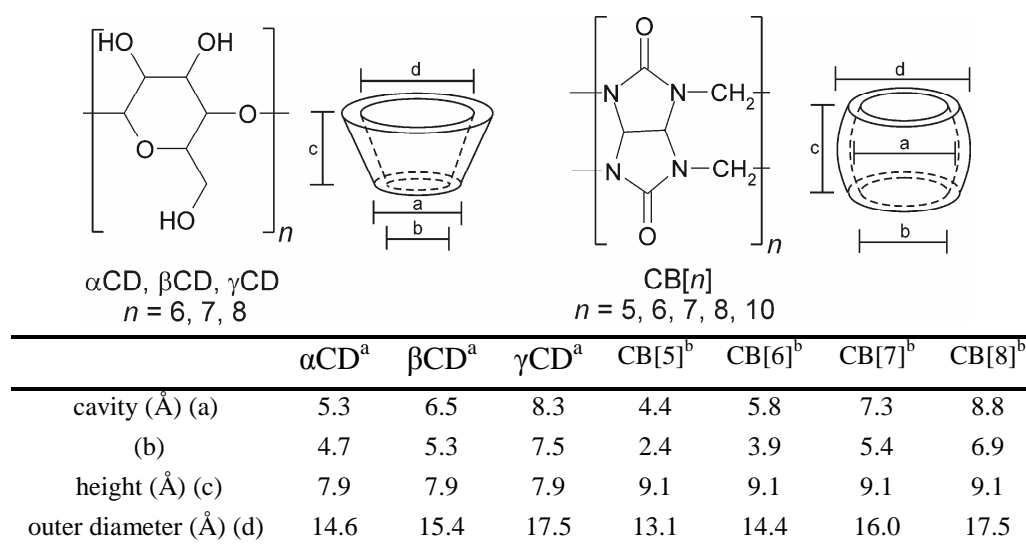


Figure 2.11: Chemical structure of CDs and CBs along with the molecular dimensions; ^a values taken from ref. 62c; ^b values taken from ref. 56.

Cucurbiturils are a class of host molecules that, like CDs, are able to form inclusion complexes with small guest molecules in water. The supramolecular chemistry of cucurbiturils has recently been reviewed.^{54,55,56} Cucurbiturils are synthesized by an acid-catalyzed condensation reaction of glycoluril and formaldehyde. Cucurbiturils are abbreviated as CB[*n*] and *n* indicates the number of glycoluril units (Figure 2.11). The CB[*n*] family span a wide range of cavity sizes ranging from CB[5], CB[6]⁵⁷, CB[7], and CB[8]⁵⁸, and CB[10]^{59,60}. Two CBs which contain one inverted glycoluril unit, i.e. *i*CB[6] and *i*CB[7], have been isolated.⁶¹ The family of CB[*n*] hosts is similar to that of CDs in the sense that the cavity sizes of CB[6], CB[7], and CB[8] are similar to that of α CD, β CD, and γ CD (Figure 2.11). However, the chemical composition and binding properties are different. CBs are achiral and have an equatorial plane of symmetry which is not present in CDs. Thus, CDs have two cavity openings of different sizes with the smaller opening lined by primary OH-groups and the larger opening by twice the number of secondary OH-groups, while CBs have two identical cavity openings lined with carbonyls. In the case of CDs, primarily hydrophobic interactions

are responsible for the formation of stable inclusion complexes with a variety of organic and organometallic compounds. The hydroxyl groups located at the upper and lower rim do not play a profound role in the complexation of guests.⁶² On the contrary, the interactions of CB with guest molecules rely on two types of interactions: i) ion-dipole interactions between the positive charges of the guests and the carbonyl groups at the cavity openings, and ii) hydrophobic interactions. In Figure 2.11 the structure of CB[n] is shown along with a Table summarizing the dimensions of CB[n] with $n = 5$ to 8.

The oxidation state of the guest can strongly affect the stability of CD and CB[n] host-guest complexes. One of the first examples of a redox-controlled host-guest complex is the β CD-Fc inclusion complex.⁶³ A detailed electrochemical study by Matsue et al. of ferrocene carboxylic acid (FcA⁻) in the presence of β CD showed that the peak oxidation potential shifted to higher potentials and the currents decreased upon complexation.⁶⁴ These findings were attributed to a CE mechanism, that is dissociation of the inclusion complex occurs prior to oxidation of FcA⁻. Also, the currents for the inclusion complex are lower than for the free Fc species due to a lower diffusion constant of the complex. The oxidation mechanism is outlined in Figure 2.12. Experimental evidence for the direct oxidation of the Fc- β CD complex could not be found, thus $K_f \gg K'_f$ (Figure 2.12). The oxidized form of FcA⁻ does not bind to β CD. The binding behavior is in sharp contrast to the binding of FcA⁻ to sulfonatocalix[6]arene which causes a negative shift of the peak oxidation potential and to a smaller extent effects the peak currents.⁶⁵ This indicates that the host interacts more strongly with the oxidized form of FcA⁻, which can be explained by the anionic character of both the guest and the host in the reduced form. Kaifer et al. reported later that Fc-ammonium salts also can bind effectively to β CD.⁶⁶

Cobaltocenium (Cob⁺) is, like Fc, a highly stable 18-valence electron complex which can be reduced to the neutral Cob species. Kaifer et al. showed that the reduction of Cob⁺ in the presence of β CD induces the formation of Cob- β CD host-guest complexes and thus Cob⁺ is, in that sense, complementary to Fc.⁶⁷

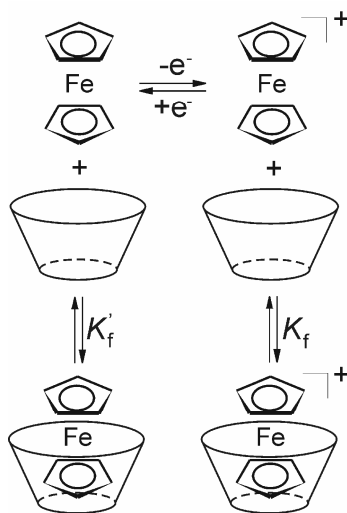


Figure 2.12: Electrochemical oxidation of Fc and its inclusion complex with β CD.⁶⁴

Dendrimers are highly monodisperse polymers bearing all functional end groups at the periphery of the molecule.⁶⁸ This allows to control the stoichiometry of the host-guest complex. Ideally, dendrimers are defect free, highly branched macromolecules with a well-defined three-dimensional structure that can be prepared by a sequence of reactions. The dendrimers have internal cavities to which guest molecules can bind, but also binding to the periphery of the molecules is possible. Functional molecules may be incorporated in the dendritic branches or at the focal point of the dendrimers. Due to these interesting properties, a variety of applications have been found for dendrimers in a variety of fields.⁶⁹ Dendrimers have been prepared with a wide range of end groups of which especially metallo-dendrimers have attracted considerable interest.^{70,71}

Decorating dendritic molecules with redox-active guest functionalities allows control over the formation of large supramolecular assemblies. Poly(propylene imine) (PPI) dendrimers bearing Fc guest functionalities have been prepared,⁷² of which a third generation (G3) is shown in Figure 2.13. PPI Dendrimers decorated with Fc units are virtually insoluble in aqueous media, but complexation of the Fc moieties to β CD resulted in large water soluble supramolecular multisite inclusion complexes of well-defined stoichiometries.⁷³ Addition of a stronger competitive guest, i.e. 2-naphthalenesulfonate, resulted in precipitation of the dendrimers indicating that dendrimers do form multisite inclusion complexes with β CDs. Furthermore, CVs showed one reversible oxidation wave indicating that all end groups are electrochemically similar. The β CD driven dissolution of the apolar dendrimers was effective up to generation 3. Only in the case of the G3-PPI-(Fc)₁₆ two oxidation waves were recorded in the CV spectrum. These waves were attributed to non-complexed and complexed Fc moieties in neutral aqueous media.

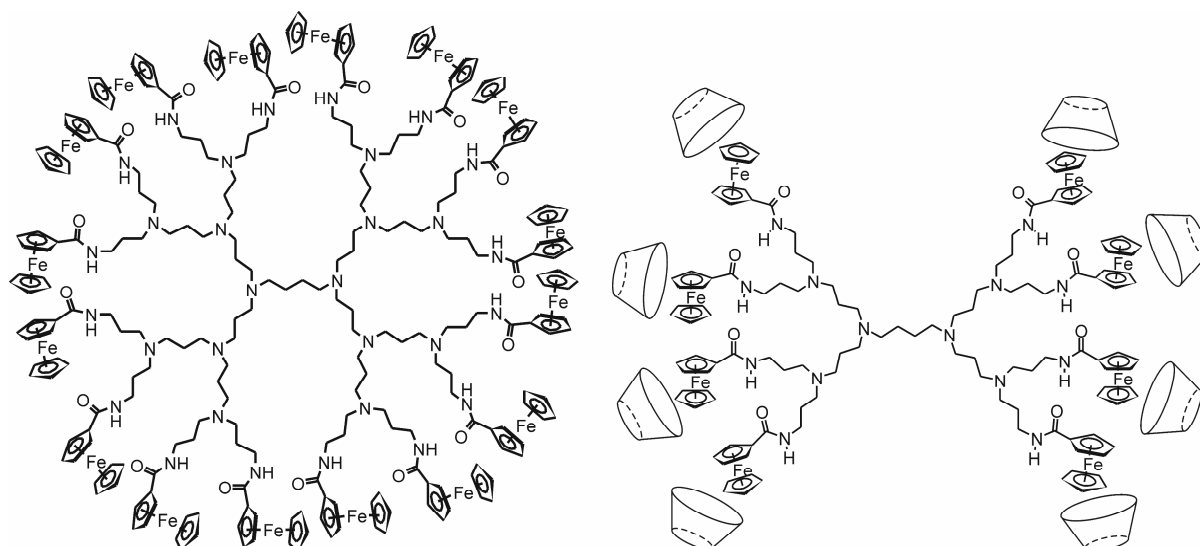


Figure 2.13: A third generation poly(propylene imine) (PPI) dendrimer decorated with Fc moieties (left).⁷² Second generation PPI dendrimer with the Fc end groups complexed to β CD resulting in a water soluble supramolecular assembly (right).⁷³

PPI Dendrimers of G1 to G4 bearing up to 32 cobaltocenium (Cob^+) end groups have been prepared with all end groups in the cationic form. Electrochemical reduction of Cob^+ to Cob triggered the Cob - βCD complex formation resulting in large, water soluble dendrimer- βCD assemblies.⁷⁴ Reduction of the dendrimers without the βCD present in solution resulted in the precipitation of the dendrimers.

Kaifer et al. also reported the preparation of PPI dendrimers containing both Cob^+ and Fc moieties using equimolar amounts of each metallocene, resulting in statistical mixtures of products.^{75,76} A monomeric compound composed of both metallocenes, linked by a small positively charged tether, resulted in a three-state host-guest system of which the binding to βCD can be electrochemically controlled.⁷⁷ The fully oxidized form of the monomeric compound is not able to bind to βCD . However, the fully reduced form binds to two βCD s, and one βCD can bind to the partially reduced compound.

The steric hindrance of large molecules employed in host-guest chemistry has a profound influence on the binding strength of the host-guest complexes. The influence of the increasing steric hindrance by increasing generation on the thermodynamic binding properties was studied.⁷⁸ Newkome-type dendritic wedges containing carboxylic acids at the periphery and a Fc centre in the focal point which can bind to βCD . The binding constant (K_{ass}) of the Fc group with βCD is 950 M^{-1} for G1, but decreases sharply to 250 M^{-1} and 50 M^{-1} for G2 and G3, respectively. These K_{ass} values were obtained by fitting the CV responses and are in accordance with a shift to higher potential as in the case of G1. The K_{ass} value for G1 is comparable to other Fc- βCD inclusion complexes, but it is quite low for G2 and G3. This suggests that for G2, and to a larger extent for G3, the growing dendron partially surrounds the Fc moiety and interferes in the formation of the Fc- βCD inclusion complexes. An opposite trend was observed in a study where the same dendrimers were bound to CB[7].⁷⁹ In the case of G1 an interaction of CB[7] could not be observed at $\text{pH} = 7$ due to the deprotonated form of the carboxylic acid end groups repelling the negatively charged carbonyls at the rim of CB[7]. However, G2 and G3 do bind to CB[7]. Thus, the facts that the number of anodic charges increases by increasing generation, and that complex formation is still favorable, indicate that the charges are located sufficiently far away and do not hinder the complexation. Lowering the pH to 2 resulted in the encapsulation of the Fc moiety by CB[7] in the case of G1.

Cationic guests form stable inclusion complexes with CBs. Kaifer et al. reported that Fc^+ and Cob^+ form highly stable 1:1 inclusion complexes with CB[7], with a K_{ass} larger than 10^6 M^{-1} .⁸⁰ The electrochemical reduction of Fc^+ or Cob^+ only resulted in a modest loss in binding affinity. The ratio of binding constants for Fc/Fc^+ was only 0.4, as could be elucidated by the modest shift of -22 mV in the half-wave oxidation potential. The authors also claimed that the redox mechanism does not proceed via a CE mechanism, as in the case of the Fc- βCD inclusion complex (Figure 2.12), but via direct oxidation of the Fc-CB[7] complex. However, the highest scan rate used was only 2 V/s, while in the case of Fc- βCD scan rates from 50 up

to 200 V/s were used⁶⁴, or low temperatures, to elucidate the redox mechanism. At high scan rates or low temperatures the rate of the chemical reaction becomes rate limiting and hampers the electrochemical reaction. The large association constants for both reduced guests ($K_{\text{ass}} > 4 \times 10^5 \text{ M}^{-1}$ and $K_{\text{ass}} > 3 \times 10^5 \text{ M}^{-1}$ for Fc and Cob respectively) supports the proposed mechanism that dissociation of the inclusion complex is not necessary. It is well-known that strong host-guest complexes, for instance, Ad- β CD ($K_{\text{ass}} \approx 10^5 \text{ M}^{-1}$) complexes, are dynamic and form and dissociate 10^4 times a second.⁸¹

Kim et al. reported a comparative study between the binding behavior of CD and CB hosts to simple cationic and anionic Fc derivatives, and Fc methanol to CB[7].⁸² The authors were able to determine the crystal structure of Fc-CB[7]. The binding constant was found to be $3 \times 10^9 \text{ M}^{-1}$ for Fc methanol and $2\text{-}4 \times 10^{12} \text{ M}^{-1}$ for the cationic Fc derivatives. The negatively charged FcA^- did not show significant binding to CB[7], while the neutral FcAH did. This demonstrated the influence of the presence of the carbonyl oxygens which are partially negatively charged and thus repel the binding of negatively charged guests, but favor the binding of positively charged guests. This is in sharp contrast to β CD, since β CD is able to form inclusion complexes with all Fc derivatives with a K_{ass} in the range of 10^3 to 10^4 .

Changing the redox state of the guest not only alters the binding strength of the host-guest inclusion complexes, but also can control the binding stoichiometry. Methyl viologen dication (MV^{2+}) and monocation (MV^+) form stable inclusion complexes with CB[7] and CB[8] with $K \approx 10^5 \text{ M}^{-1}$ in aqueous media.^{83,84} Above it was described that MV^{2+} does not form stable inclusion complexes with β CD, while the monocationic species MV^+ and the neutral form of MV do ($K_{\text{ass}} \approx 10^4 \text{ M}^{-1}$). This example illustrates one of the main differences in the binding properties of CDs vs. CBs: CDs form stable inclusion complexes with neutral guests, while CBs form inclusion complexes with cationic guests. CB[7] only forms 1:1 complexes with MV^+ , CB[8] can form 1:2 complexes, and MV^{2+} form 1:1 complexes with both hosts. The 1:1 complex of MV^{2+} with CB[8] changes to a 1:2 complex upon reduction of the MV^+ to MV^+ (Figure 2.14).⁸⁴ Kaifer et al. showed dimerization of dendritic wedges, with MV^{2+} in the focal point, upon reduction of to MV^+ in the presence of CB[8].⁸⁵ CB[8] can also form a 1:1:1 complex with 2,6-dihydroxynaphthalene ($\text{Np}(\text{OH})_2$) and MV^{2+} that is stabilized by charge transfer interaction between the electron rich and electron deficient guests inside the hydrophobic cavity.⁸⁶ An equimolar mixture of the 1:1:1 complex in the presence of MV^{2+} could be electrochemically reduced, resulting in the conversion of all MV^{2+} to MV^+ leading to the formation of a 1:2 complex of CB[8] with two MV^+ units.⁸⁷ In contrast, reduction of the MV^{2+} in the presence of dopamine gave a ternary complex of MV^+ , dopamine, and CB[8].⁸⁸ A guest containing both a MV^{2+} and a naphthalen-2-yloxy unit linked to each other by a small tether formed a 1:1 complex with CB[8] with a locked conformation with both units locked inside the cavity. Reduction of the complex in the presence of 1 equivalent of MV^{2+} resulted in the formation of a 1:1:1 complex of CB[8] with one MV^+ from the solution and the guest

with the naphthalen-2-yloxy unit located outside the cavity. Thus, the locked conformation could be electrochemically altered to an unlocked conformation.

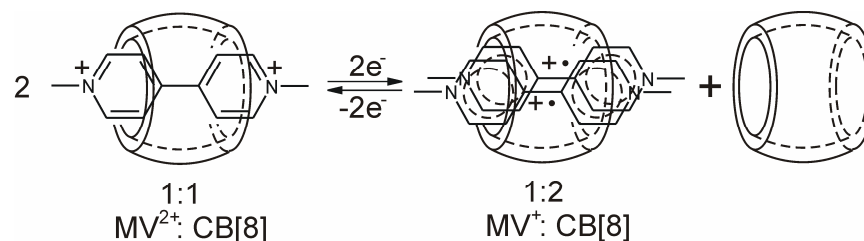


Figure 2.14: The electrochemically controlled complexation of MV^{2+} with $\text{CB}[8]$ forming 1:1 complexes while the reduced MV^+ forms 1:2 complexes.

A different type of redox host molecule is based on the concept of molecular tweezers which are able to bind to guests that are not available for binding to ring shaped hosts.⁸⁹ Vögtle et al. described aromatic molecular tweezers that can bind dendrimers with a viologen core up to G3 (Figure 2.15).⁹⁰ The viologen moiety was functionalized with one or two Fréchet type dendrons resulting in asymmetric or symmetric dendrimers, respectively. The molecular tweezer is composed of a naphthalene and four benzene units which completely quenched the fluorescence of the dendrimers upon binding. The tweezer bound to the dendrimers and dendritic wedges to the viologen moiety in a 1:1 manner. The K_{ass} were $3.4 \times 10^4 \text{ M}^{-1}$ for the G1 wedge and $2.7 \times 10^4 \text{ M}^{-1}$ for the G1 dendrimer and decreased with increasing generation to $1.6 \times 10^4 \text{ M}^{-1}$ and to $0.9 \times 10^4 \text{ M}^{-1}$ for the G2 and G3, respectively. The first reduction wave of the viologen was shifted to more negative potential values while the second wave was unaffected showing that the complexes are stabilized by electron donor-acceptor interactions and dissociate upon reduction.

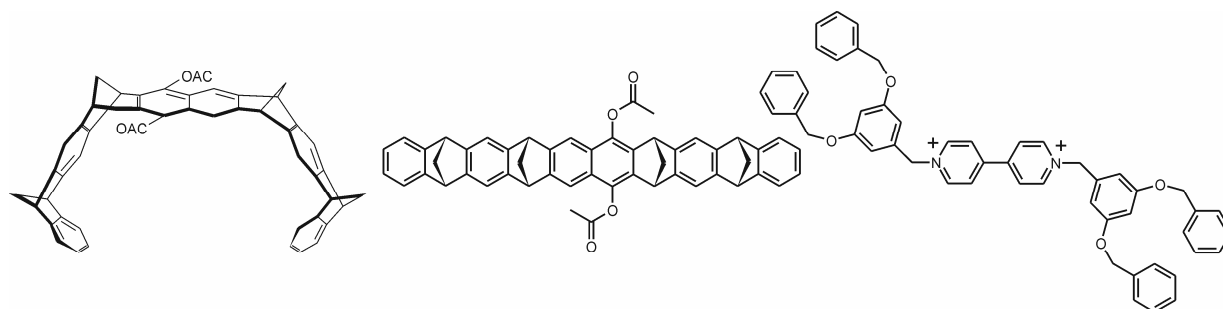


Figure 2.15: A side view of the molecular tweezer (left) and the chemical structure (middle) and a first generation Newkome-type dendrimer with a viologen in the focal point.⁹⁰

2.3.2 Hydrogen bonding

The controlled formation and breaking of hydrogen bonds mediated by electrochemical conversion is another way to control supramolecular assembly. Smith et al. reported the redox-dependent complex formation of diarylurea and nitrobenzene (Figure 2.16)⁹¹ or

dinitrobenzene⁹². The interaction between the urea and nitrobenzene is negligible in the oxidized state, but reduction leads to the formation of a strong complex ($K_{\text{ass}} = 10^5 \text{ M}^{-1}$). Arylureas also form hydrogen bonds with *o*-quinones but electrochemical reduction of the quinones to their radical anions increased the K_{ass} 2000 fold.⁹³

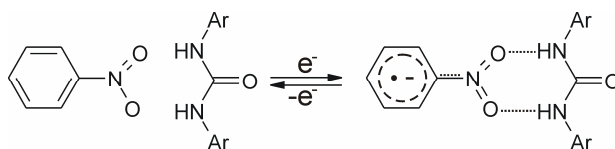


Figure 2.16: Electrochemically controlled hydrogen bond formation of nitrobenzene with diarylureas.⁹¹

Phenyl-urea terminated dendrimers constitute an example of polyfunctional molecules to which phenanthrenequinone can bind leading to large hydrogen bonded supramolecular assemblies (Figure 2.17).⁹⁴ CV data showed a shift of 90 mV of the oxidation wave upon complexation. This shift indicates a stabilization energy of 8.7 kJ/mol of the radical anionic state of the quinone corresponding to a 30-fold increase in binding affinity. CV data showed irreversible behavior at large scan rates (5 V/s) which became reversible at low scan rates (25 mV/s). This observation was attributed to the formation of a large supramolecular species consisting of the quinones and the dendrimer.

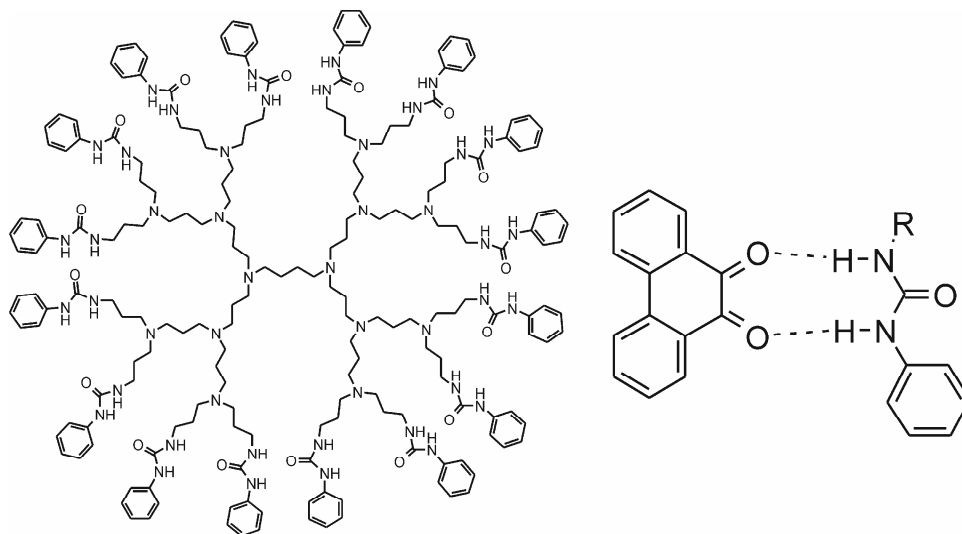


Figure 2.17: Phenyl urea terminated PPI dendrimer capable of interacting with phenanthrenequinone leading to large supramolecular species that can electrochemically be controlled.⁹⁴

Fc moieties can also be used to electrochemically induce host-guest complexation and read-out the properties of the host-guest complex. Tucker and co-workers have shown that Fc receptors comprised of two amidopyridyl groups located at the 1,1'- or 1,3-positions can bind urea and barbiturate derivatives via hydrogen bonding in organic solvents (Figure 2.18).⁹⁵ The receptors bearing two amidopyridyl groups at the same cyclopentadienyl (Cp) ring of the Fc gave larger K_{ass} values since they form a more planar cavity to bind the planar guests.

Electrochemical conversion of Fc to Fc^+ decreased the binding strength by a factor of 10 owing to the electron withdrawing effect of the Fc^+ moiety, thus making the amide moiety a better hydrogen bond donating group. Similar receptors based on bis-amidopyridine Fc and Cob^+ , respectively, were compared to study the influence of the positive charge controlled by the electrochemical redox state of the metal centre on the binding carboxylic acids⁹⁶ or aminoacids,⁹⁷ all forming 1:1 complexes. Both Cp rings functionalized with an amidopyridine of Cob or Fc centres display a similar electrochemically controlled hydrogen bond formation with guest molecules. The difference in the K_{ass} for the oxidized and reduced form is a factor of 20.

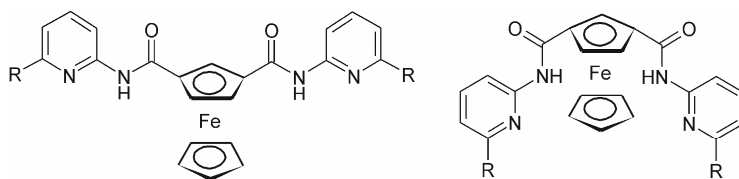


Figure 2.18: Fc receptors with two amidopyridyl groups located at the 1,1'- (left) or 1,3-positions (right).

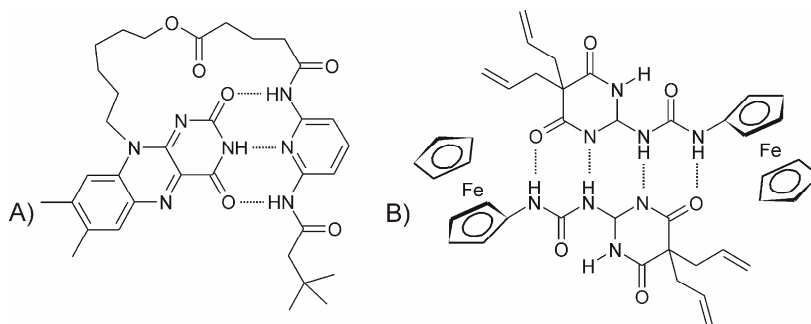


Figure 2.19: Flavin covalently linked to a 2,6-amidopyridine moiety forming intramolecular hydrogen bonds (A);⁹⁸ A Fc derivative that forms a quadruple hydrogen bond motif (B).⁹⁸

Hydrogen bonded systems can also have a profound influence on the mechanism of the redox processes. Rotello and co-workers reported electrochemically controlled hydrogen bonding of isobutylflavin and 2,6-amidopyridines (Figure 2.19A). The binding efficiency increased by a factor of 500 upon reduction of the flavin unit. Flavin is a cofactor that is normally noncovalently bound to several apoenzymes.⁹⁸ Flavin undergoes a reduction process and during reoxidation two waves are observed. The first process is the reversible formation of the flavin anion radical while the second wave arises in the cyclic voltammogram from an ECE process, due to the flavin anion being able to deprotonate flavin in solution resulting in the formation of a protonated flavin radical. This species can undergo a second reduction to give a fully reduced flavin anion which is reoxidized at lower potentials than the unprotonated flavin anion. Upon binding to amidopyridine this second oxidation wave is not observed since the complex formation prevents the ECE mechanism to take place. Recently, a Fc derivative

that can form a quadruple hydrogen-bonded complex consisting of two identical halves (Figure 2.19B) has been reported. The two identical Fc moieties were strongly electrochemically communicating due to the formation of hydrogen bonds.⁹⁹

Hydrogen bonds can also be used to control the adsorption of molecules at surfaces. Phenanthrenequinone binds strongly to ureas¹⁰⁰ and thioureas¹⁰¹ by forming two hydrogen bonds which can be modulated by altering the redox state of the quinone. A self-assembled monolayer (SAM) of a disulfide phenanthrenequinone binds phenyl urea terminated PPI dendrimers by forming multiple interactions. Upon oxidation, the dendrimers bind to the surface 2000-fold stronger ($K_{\text{ass}} = 2.4 \times 10^3 \text{ M}^{-1}$) while for a monovalent model compound a smaller increase of binding strength was observed. Introducing a Fc moiety at the amidopyridine gave additional electrochemical control over the binding to phenanthrenequinone and flavin.¹⁰² Not only the reduction of the phenanthrenequinone or flavin moiety increased the complex stability, but also the oxidation of the Fc centres.

The design and self-assembly of molecular capsules have received considerable attention.¹⁰³ A well-established methodology for capsule formation is the dimerization of two identical calix[4]arenes functionalized with four urea groups on the upper rim.¹⁰⁴ Capsule formation can be electrochemically controlled by introducing Fc groups at the upper rim via a urea linkage.¹⁰⁵ Fc in the neutral form allowed the formation of a dimer in a head-to-head fashion. However, oxidation of the Fc moieties caused dissociation of the dimer (Figure 2.20A). Model compounds in which the Fc moieties were replaced by charged amino groups showed no capsule formation. Thus, the disruption of the Fc-capsules is due to the positive charges generated by oxidation of the Fc centres.

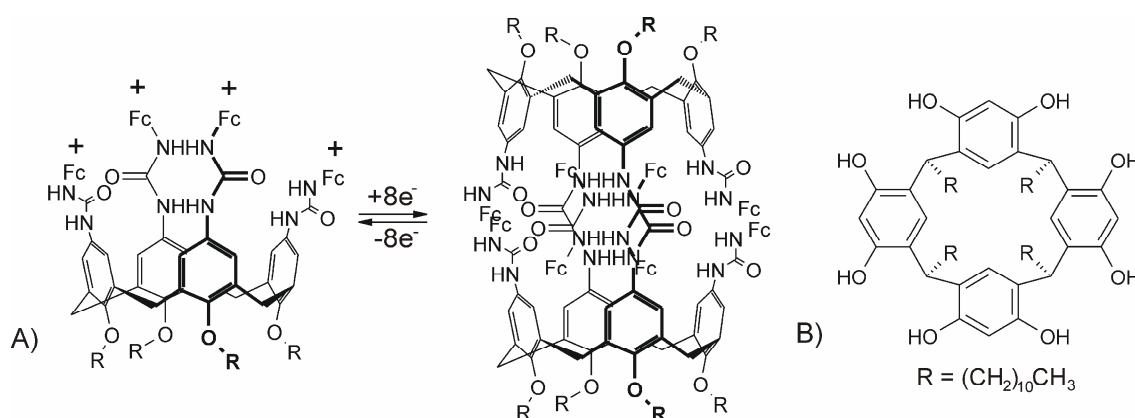


Figure 2.20: Calixarene functionalized with Fc moieties: in the reduced form the urea functionalities form hydrogen bonds with a second calixarene, while in the oxidized form the dimer dissociates due to the repelling cationic charges (A);¹⁰⁵ Resorcinarene that forms a capsule triggered by the presence of Fc^+ (B).¹⁰⁸

The above described example the dissociation of a capsule upon electrochemical oxidation of Fc. In contrast, oxidation of Fc in the presence of resorcinarene (Figure 2.20B) drives capsule formation. Resorcinarene can form capsules consisting of six molecules in an

octahedral geometry held together by hydrogen bonds by the OH groups of the upper rim and residual water molecules.¹⁰⁶ The capsule formation is induced by cationic groups.¹⁰⁷ Kaifer et al. showed that electrochemically generated Fc^+ is a suitable guest for the capsule formation.¹⁰⁸ Six host molecules complex to one Fc^+ . The formation of the complex has a profound influence on the redox behavior of Fc, since the reduction required an overpotential of more than 500 mV and gave rise to a new anodic wave.

2.3.3 Electrostatic interactions

Electrostatic interactions mediated by electrochemical conversion of receptors consisting of one or multiple receptor sites are briefly discussed in this section. Dendrimers have been frequently used to design and test receptors with a large number of independent receptor sites, which has a profound influence in the binding properties of the target molecules. Simple chemical modifications can dramatically alter the binding stoichiometry and binding selectivity, and also the stability. Examples are given of receptors which are relatively simple Fc derivatives with different properties than found for dendritic systems. Additionally, the charge of surfactants can be electrochemically controlled leading to redox-controlled vesicle and lipoplex formation.

2.3.3.1 Dendrimers

Fc-terminated dendrimers (Figure 2.13) have been used in molecular recognition of negatively charged ions.^{109,110} Fc-decorated dendrimers or dendritic wedges are electrochemical exo-receptors for inorganic anions, oxo-anions and biological molecules.¹¹¹ The neutral dendrimers can only form hydrogen bonds with the anionic guests, but the oxidized form of the dendrimers can also have electrostatic interactions to enhance the binding. Usually, the binding of anions is stronger and the selectivity increases by increasing generation. This is the so-called “dendritic effect” which is caused by surface saturation of the higher generation dendrimers, bringing the Fc termini in close proximity with each other, resulting in smaller surface holes. Astruc et al. reported on Fc dendritic wedges immobilized on Au nanoparticles^{112,113,114} and dendrimers^{115,116}. The binding of H_2PO_4^- , HSO_4^- , Cl^- , Br^- and NO_3^- to Fc terminated dendrimers with 3, 9 and 18 Fc end groups was followed by titrations of the anions to the dendrimers followed by CV.¹¹⁵ The largest shift in oxidation potential was found for H_2PO_4^- . After addition of 1 equivalent of H_2PO_4^- the CV remained unchanged indicating 1:1 binding stoichiometry of the H_2PO_4^- to amidoylferrocenyl groups.

Simple modification of the linkages of the Fc units to the dendritic core has a profound influence on the binding stoichiometry to anions. Fc functionalized PPI dendrimers linked via urea moieties have been also used in recognition studies of H_2PO_4^- and compared to HSO_4^- and Cl^- .¹¹⁷ A large shift in oxidation potential of 112 mV was found for H_2PO_4^- , while HSO_4^-

and Cl^- gave shifts of 40 and 16 mV, respectively. In competition experiments with H_2PO_4^- in the presence of equimolar amounts of HSO_4^- or Cl^- , a shift of the oxidation potential of 116 mV nicely demonstrated the selectivity for H_2PO_4^- . Titration of H_2PO_4^- showed that the potential already shifted to a maximum value at 0.5 equivalents of H_2PO_4^- per Fc moiety indicating that each H_2PO_4^- is bound by two end groups of the dendrimers, involving a double hydrogen bond as depicted in Figure 2.21.¹¹⁸

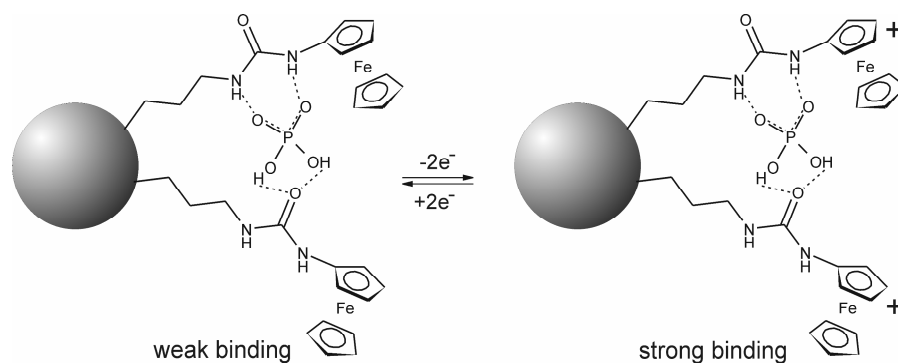


Figure 2.21: Proposed binding mode of H_2PO_4^- forming 2:1 complexes with two Fc-ureas of dendrimer or dendritic wedges, or dendritic wedges immobilized at Au nanoparticles.¹¹⁷

Replacing the Cp of the Fc moieties by pentamethylcyclopentadienyl (Cp^*) leads to Fc^* redox centres with a higher stability and lipophilicity.¹¹⁹ This prevents precipitation on the electrodes after oxidation in CH_2Cl_2 . The scope of anions that can be bound by these dendrimers was limited to phosphates and sulfates, but could be extended to Cl^- and Br^- by introducing $[\text{Fe}(\eta^5\text{-C}_5\text{Me}_5)(\eta^6\text{-N-alkylaniline})]^+$ units.¹²⁰ The recognition, which depends on the synergy between the $\text{X}^- \cdots \text{HN}$ hydrogen bond, the electrostatic interactions, and the shape of the peripheral cavities formed by the dendrimer branches and tripods, could be followed by ^1H NMR spectroscopy.

Besides dendrimers, also dendrons containing Fc moieties attached to Au nanoparticles linked by $\text{Si}(\text{Me})_2$ or amides were used in recognition studies of small anions and ATP^{2-} . Dendrons containing 3 or 9 Fc groups were immobilized onto gold nanoparticles by thiol linkages resulting in particles containing up to about 360 Fc groups (Figure 2.22).¹¹⁴ The recognition was followed by CV and showed a new wave that was attributed to complex formation. HSO_4^- is recognized only by the amido Fc bearing colloids and the interaction is weaker compared to the interaction with H_2PO_4^- due to the lower negative charge density on the oxygen atoms in HSO_4^- with respect to H_2PO_4^- . The dominant interaction is hydrogen bonding between the partially positively charged N-atom in the amido group and the O-atoms of the anions. The Si-atom of the silylferrocene colloids is partially positively charged and this could be the explanation for the difference in selectivity of the two colloids.

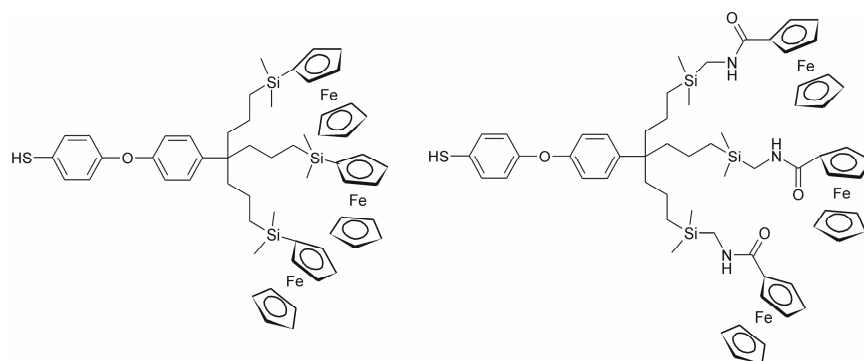


Figure 2.22: First generation dendritic wedges with Fc linked by $\text{Si}(\text{Me})_2$ or amido moieties used to immobilize at Au nanoparticles.¹¹⁴

Recently, Astruc et al. have described PPI dendrimers decorated with transition metal clusters of $[\{\text{CpFe}(\mu_3\text{-CO})\}_4]$ as exo-receptors for ATP^{2-} and H_2PO_4^- .¹²¹ The dendrimers are stable toward oxidation of the tetrairon cluster $\text{Fe}_4^0 \rightarrow \text{Fe}_4^+$ and $\text{Fe}_4^+ \rightarrow \text{Fe}_4^{2+}$ and reduction $\text{Fe}_4^0 \rightarrow \text{Fe}_4^-$. These dendrimers recognized ATP^{2-} better than H_2PO_4^- , while the opposite holds for the metallocene dendrimers described above.

Smith et al. reported a series of dendrimers having the Fc moieties in the focal point which were receptors for Cl^- .^{122,123} Fc was decorated with two Newkome type of branches of G0, G1, and G2 and the binding to chloride was studied by CV and ^1H NMR. The binding to chloride decreased with increasing generation and the dendrimers recognized chloride better than bromide indicating a negative dendritic effect.

So far, only examples have been given of covalently bound dendrimers as receptors for simple anions and ATP. Hydrogen bonded assemblies were reported of amine terminated PPI dendrimers of generation 1 to 5 interacting with dendrons. The dendrons consisted of a *p*-phenyl hydroxyl at the focal point and three terminal double bonds or amidoferrocenyl groups resulting in large assemblies consisting of 192 end groups.¹²⁴ Primary amines and alcohols formed three complementary O – H – N bonds in a 1:1 stoichiometry, which is the basis of the self-assembly between the dendrimers and dendrons. These supramolecular dendrimers bind ATP^{2-} and H_2PO_4^- strongly according to CV titrations. Binding of the anions resulted in the appearance of a new wave at less anodic potentials. As the concentration of anion was increased, the new wave increased at the cost of the original wave. At 0.5 equivalent of anion per end group, the original Fc wave almost completely disappeared and the CV was dominated by the new wave indicating that the anions form 2:1 complexes with the dendritic end groups. A positive dendritic effect in the binding of H_2PO_4^- to the dendrimers was observed as the binding constant increased from $3.4 \times 10^3 \text{ M}^{-1}$ for the dendron to $67 \times 10^3 \text{ M}^{-1}$ for G2 and higher generations. In the case of ATP^{2-} a negative dendritic effect was observed as $K_{\text{ass}} = 2.8 \times 10^3 \text{ M}^{-1}$ for G2 decreased to $1.3 \times 10^3 \text{ M}^{-1}$ for G3 and higher generations.

2.3.3.2 Modified ferrocenes

Amidoferrocene is one of the most widely used receptors to bind to simple anions and to electrochemically read out the sensing properties both at surfaces and in solution.^{125,126,127,128} Beer et al. recently showed that monolayers of 1,1'-bisubstituted disulfide Fc at Au recognized anions consistently better compared to having the receptor in solution (Figure 2.23).¹²⁹ In solution, a cathodic shift for Cl^- , Br^- , and H_2PO_4^- was 40, 20, and 210 mV, while for the surface confined system shifts of 100, 30, and 300 mV were found, respectively. Thus, the surface confined receptors showed a sensing amplification, which is associated with surface preorganization of the host pseudo-macrocycle.

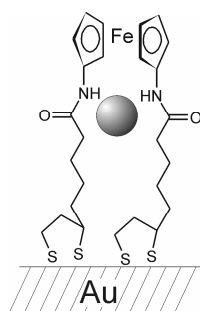


Figure 2.23: Surface enhanced anion binding due to surface induced preorganization of the 1,1'-bisubstituted Fc host.¹²⁹

The surface enhanced recognition became even more apparent in the binding of perrhenate anion (ReO_4^-) in aqueous media. A cathodic shift of 15-20 mV was observed, while in solution no electrochemical sensing was observed. In a $\text{CH}_2\text{CN}/\text{CHCl}_3$ mixture, phosphate was selectively bound by the receptor in competition experiments with perrhenate, while in water perrhenate was selectively sensed.

Moutet et al. reported receptors based on single or multiple Fc moieties that electrochemically bound anions, including F^- . An increase in the number of amidoyl Fc centres increased the binding strength of the oxidized receptors with the anions F^- , H_2PO_4^- , ATP^{2-} , and HSO_4^- and gave better electrochemical responses compared to the monovalent receptors.¹³⁰ The same group also reported a Fc receptor based on a cyclam framework (Figure 2.24).¹³¹ Like the amidoyl Fc receptors, the cyclam-based receptor bound to anions by hydrogen bonds which are reinforced upon electrochemical conversion of Fc to Fc^+ . Alkylation of the amines reduced the binding affinity since hydrogen bond formation is not possible with anions. Complexation of Cu^{2+} gave a receptor that recognized F^- selectively from other halogens.

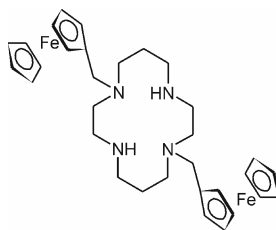


Figure 2.24: Fc receptor based on a cyclam framework.¹³¹

2.3.3.3 Vesicles

Vesicles are potentially useful in drug delivery since water soluble compounds may be entrapped inside the inner aqueous phase, while sparingly water soluble compounds can be captured inside the bimolecular layers. For many applications it is desired that vesicle formation can be controlled so that the release of substances trapped by the vesicle can be triggered by an external stimulus. The group of Abe et al. reported ammonium surfactants with Fc head groups, i.e. bis(11-ferrocenyl(undecyl))-dimethylammonium bromide (BFDMA) which form vesicles of 500 - 2000 nm in diameter (Figure 2.25).¹³² Electrochemical oxidation of the Fc head groups resulted in disintegration of the vesicle into smaller aggregates and micelles of around 50 nm as could be observed by CV and static light scattering. The authors were able to release glucose, trapped in the inner aqueous phase, and benzene, trapped in the bilayer of the vesicles, into the bulk. The same lipid has also been used to complex to DNA and facilitates the transport of DNA across cell membranes.¹³³ It is well-known that cationic lipids form lipoplexes with DNA and can mediate transfection. BFDMA is monocationic, but oxidation of both Fc moieties resulted in a lipid having a charge of 3+. Therefore, the Fc lipid allowed to control transfection since the cationic 3+ form can mediate DNA transport, while the monocationic form cannot. Transfection experiments were conducted using a plasmid encoding enhanced green fluorescent protein (EGFP) and a COS-7 cell line. Lipoplexes were formed with either reduced or oxidized BFDMA and the plasmid followed by incubation with the cells. Cells that were incubated with the lipoplexes formed with the oxidized form of BFDMA showed only expression of the protein comparable to background levels, while lipoplexes formed with the reduced form were transfected and showed significant expression of EGFP.

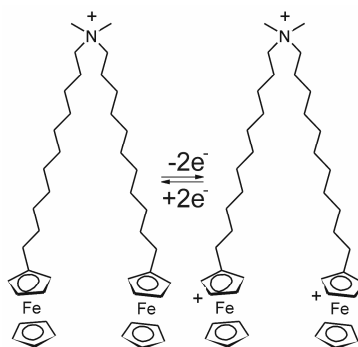


Figure 2.25: Structure of BFDMA.¹³²

2.4 Conclusions

Nature exploits the concepts of self-assembly and supramolecular chemistry at a level of complexity far beyond the chemist's capabilities. For applications in molecular scale fabrication, nanoelectronics, or molecular machines and actuators, a detailed understanding of molecular recognition and self-assembly, as well as the control of recognition and assembly by external stimuli is essential. Nevertheless, at present it is possible to synthesize supramolecular assemblies, even of the size of small proteins, where the assembly and disassembly of components can be exactly controlled by altering the binding affinity of the recognition elements. From a technological point of view, electrochemical control is the most logical choice since it is compatible with modern silicon-based electronic circuitry. A deeper understanding of self-assembly and recognition processes will give rise to redox responsive systems that are promising in sensor applications, data storage, and molecular machinery. In particular, interlocked molecules of which the movement of the different components with respect to each other can be electrochemically controlled are promising.

The incorporation of relatively complex and fragile supramolecular assemblies in molecular scale electronic devices as well as unambiguous proof that the device output characteristics are controlled by the molecules or change of the molecules upon external stimuli is still a major issue. In this thesis, the concept of a supramolecular printboard is employed to position redox-active molecules via multiple host-guest interactions that can be electrochemically controlled.

2.5 References

- 1) (b) Joachim, C.; Gimzewski, J. K.; Aviram, A. *Nature* **2000**, *408*, 541. (b) Schulz, M. *Nature* **1999**, *399*, 729.
(c) Muller, D. A.; Sorsch, T.; Moccio, S.; Baumann, F. H.; Evans-Lutterodt, K.; Timp, G. *Nature* **1999**, *399*, 758.
- 2) Balzani, V.; Credi, A. *Chem. Rec.* **2001**, *1*, 442.
- 3) Schalley, C. A.; Beizai, K.; Vögtle, F. *Acc. Chem. Res.* **2001**, *34*, 465.

- 4) Berg, J. M.; Tymozko, J. L.; Stryer, L.; *Biochemistry*, W. H. Freeman and Company: New York, **2007**.
- 5) Pease, A. R.; Jeppesen, J. P.; Stoddart, J. F.; Luo, Y.; Collier, C. P.; Heath, J. R. *Acc. Chem. Res.* **2001**, *34*, 433.
- 6) Mendes, P. M.; Flood, A. H.; Stoddart, J. F. *Appl. Phys. A.* **2005**, *80*, 1197.
- 7) Boulas, O. L.; Gómez-Kaifer, M.; Echegoyen, L. *Angew. Chem. Int. Ed.* **1998**, *37*, 216.
- 8) Cooke, G. *Angew. Chem. Int. Ed.* **2003**, *42*, 4860.
- 9) Jing, L.; Yuangang, L.; Yu, F. *Prog. Nat. Sci.* **2005**, *15*, 1057.
- 10) Lee, J. W.; Kim, K. *Top. Curr. Chem.* **2003**, *228*, 111.
- 11) Kim, K. *Chem. Soc. Rev.* **2002**, *31*, 96.
- 12) Cardona, C. M.; Mendoza, S.; Kaifer, A. E. *Chem. Soc. Rev.* **2000**, *29*, 37.
- 13) Cooke, G.; Rotello, V. M. *Chem. Soc. Rev.* **2002**, *31*, 275.
- 14) Balzani, V.; Credi, A.; Ferrer B.; Silvi, S.; Venturi, M. *Top. Curr. Chem.* **2005**, *262*, 1.
- 15) Kay, E. R.; Leigh, D. A. *Top. Curr. Chem.* **2005**, *262*, 133.
- 16) Balzani, V.; Credi, A.; Raymo, F. M.; Stoddart, J. F. *Angew. Chem. Int. Ed.* **2000**, *39*, 3348.
- 17) Kanazawa, H.; Higuchi, M.; Yamamoto, K. *J. Am. Chem. Soc.* **2005**, *127*, 16404.
- 18) Kim, H. G.; Lee, C.-W.; Yun, S.; Hong, B. H.; Kim, Y.-O.; Kim, D.; Ihm, H.; Lee, J. W.; Lee, E. C.; Tarakeshwar, P.; Park, S. -M.; Kim, K. *Org. Lett.* **2002**, *4*, 3971.
- 19) Hawthorne, M. F.; Zink, J. I.; Skelton, J. M.; Bayer, M. J.; Liu, C.; Livshits, E.; Baer, R.; Neuhauser, D. *Science* **2004**, *303*, 1849.
- 20) Luk, Y. -Y.; Abbott, N. L. *Science*, **2003**, *301*, 623.
- 21) Wang, X.; Kharitonov, A. B.; Katz, E.; Willner, I. *Chem. Commun.* **2003**, 1542.
- 22) Lahann, J.; Mitragotri, S.; Tran, T. -N.; Kaido, H.; Sundaram, J.; Choi, I. S.; Hoffer, S.; Somorjai, G. A.; Langer, R. *Science* **2003**, *299*, 371.
- 23) Bonnet, S.; Collin, J. -P.; Koizumi, M.; Mobian, P.; Sauvage, J. -P. *Adv. Mater.* **2006**, *18*, 1239.
- 24) Sauvage, J. -P. *Chem. Commun.* **2005**, 1507.
- 25) Collin, J. -P.; Heitz, V.; Sauvage, J. -P. *Top. Curr. Chem.* **2005**, *262*, 29.
- 26) Dietrich-Buchecker, C.; Jimenez-Molero, M. C.; Sartor, V.; J. -P. Sauvage, *Pure Appl. Chem.* **2003**, *75*, 1383.
- 27) Poleschak, I.; Kern, J. M.; Sauvage, J. -P. *Chem. Commun.* **2004**, 474.
- 28) Korybut-Daskiewicz, B.; Więckowska, A.; Bilewicz, R.; Domagał, S.; Woźniak, K.; *Angew. Chem. Int. Ed.* **2004**, *43*, 1668.
- 29) Korybut-Daskiewicz, B.; Więckowska, A.; Bilewicz, R.; Domagał, S.; Woźniak, K.; *J. Am. Chem. Soc.* **2001**, *123*, 9356.
- 30) Bilewicz, R.; Korybut-Daskiewicz, B.; Rogowska, A.; Szydłowska, J.; Więckowska, A.; Domagał, S.; Woźniak, K.; *Electroanalysis* **2005**, *17*, 1463.
- 31) Więckowska, A.; Bilewicz, R.; Domagał, S.; Woźniak, K.; Korybut-Daskiewicz, B.; Tomkiewicz, A.; Mroziński, J. *Inorg. Chem.* **2003**, *42*, 5513.
- 32) Kihara, N.; Hashimoto, M.; Takata, T. *Org. Lett.* **2004**, *6*, 1693.
- 33) Horie, M.; Suzaki, Y.; Osakada, K. *Inorg. Chem.* **2005**, *44*, 5844.
- 34) Horie, M.; Suzaki, Y.; Osakada, K. *J. Am. Chem. Soc.* **2004**, *126*, 3684.
- 35) Osakada, K.; Sakano, T. Horie, M.; Suzaki, Y. *Coord. Chem. Rev.* **2006**, *250*, 1012.
- 36) Katz, E.; Lioubashevsky, O.; Willner, I. *J. Am. Chem. Soc.* **2004**, *126*, 15520.
- 37) Katz, E.; Baron, R.; Willner, I.; Richke, N.; Levine, R. D. *Chem. Phys. Chem.* **2005**, *6*, 2179.
- 38) Katz, E.; Sheeney-Hai-Ichia, L.; Willner, I. *Angew. Chem. Int. Ed.* **2004**, *43*, 3292.

- 39) Altieri, A.; Gatti, F.; Kay, E. R.; Leigh, D. A.; Martel, D.; Paolucci, F.; Slawin, A. M. Z.; Wong, J. K. Y. *J. Am. Chem. Soc.* **2003**, *125*, 8644.
- 40)(a) Tseng, H. -R.; Vignon, S. A.; Celestre, P. C.; Perkins, J.; Jeppesen, J. O.; Fabio, A. D.; Ballardini, R.; Gandolfi, M. T.; Venturi, M.; Balzani, V.; Stoddart, J. F. *Chem. Eur. J.* **2004**, *10*, 155. (b) Jeppesen, J. O.; Vignon, S. A.; Stoddart, J. F. *Chem. Eur. J.* **2003**, *9*, 4611.
- 41)(a) Balzani, V.; Credi, A.; Mattersteig, G.; Matthews, O. A.; Raymo, F. M.; Stoddart, J. F.; Venturi, M.; White, A. J. P.; Williams, D. J. *J. Org. Chem.* **2000**, *65*, 1924. (b) Asakawa, M.; Ashton, P. R.; Balzani, V.; Boyd, S. E.; Credi, A.; Mattersteig, G.; Menzer, S.; Montalti, M.; Raymo, F. M.; Ruffilli, C.; Stoddart, J. F.; Venturi, M.; Williams, D. J. *Eur. J. Org. Chem.* **1999**, 985.
- 42)(a) Tseng, H. -R.; Vignon, S. A.; Stoddart, J. F. *Angew. Chem. Int. Ed.* **2003**, *42*, 1491. (b) Jeppesen, J. O.; Nielsen, K. A.; Perkins, J.; Vignon, S. A.; Fabio, A. D.; Ballardini, R.; Gandolfi, M. T.; Venturi, M.; Balzani, V.; Becher, J.; Stoddart, J. F. *Chem. Eur. J.* **2003**, *9*, 2982.
- 43) Tseng, H. R.; Wu, D.; Fang, N. X.; Zhang, X.; Stoddart, J. F. *ChemPhysChem* **2004**, *5*, 111.
- 44) Collier, C. P.; Mattersteig, G.; Wong, E. W.; Luo, Y.; Beverly, K.; Sampaio, J.; Raymo, F. M.; Stoddart, J. F.; Heath, J. R. *Science* **2000**, *289*, 1172.
- 45) Nørgaard, K.; Laursen, B. W.; Nygaard, S.; Kjaer, K.; Tseng, H. -R.; Flood, A. H.; Stoddart, J. F.; Bjørnholm, T. *Angew. Chem. Int. Ed.* **2005**, *44*, 7035.
- 46) Huang, T. J.; Tseng, H. -R.; Sha, L.; Lu, W.; Brough, B.; Flood, A. H.; Yu, B. -D.; Celestre, P. C.; Chang, J. P.; Stoddart, J. F.; Ho, C. -M. *Nano Lett.* **2004**, *4*, 2065.
- 47) Jang, S. S.; Jang, Y. H.; Kim, Y. -H.; Stoddart, J. F.; Choi, J. W.; Heath, J. R.; Laursen, B. W.; Flood, A. H.; Stoddart, J. F.; Nørgaard, K.; Bjørnholm, T. *J. Am. Chem. Soc.* **2005**, *127*, 14804.
- 48) Liu, Y.; Flood, A. H.; Bonvallet, P. A.; Vignon, S. A.; Northrop, B. H.; Tseng, H. -R.; Jeppesen, J. O.; Huang, T. J.; Brough, B.; Baller, M.; Magonov, S.; Solares, S. D.; Stoddart, J. F.; Ho, C. -M.; Stoddart, J. F. *J. Am. Chem. Soc.* **2005**, *127*, 9745.
- 49) Nguyen, T. D.; Tseng, H. -R.; Celestre, P. C.; Flood, A. H.; Stoddart, J. F.; Zink, J. I. *Proc. Nat. Acad. Sci. USA* **2005**, *102*, 10029.
- 50)(a) Luo, Y.; Collier, C. P.; Jeppesen, J. O.; Nielsen, K. A.; Delonno, E.; Ho, G.; Perkins, J.; Tseng, H. -R.; Yamamoto, T.; Stoddart, J. F.; Heath, J. R. *ChemPhysChem* **2002**, *3*, 519. (b) Chen, Y.; Ohlberg, D. A. A.; Li, X.; Stewart, D. R.; Jeppesen, J. O.; Nielsen, K. A.; Stoddart, J. F.; Olynick, D. L.; Anderson, E. *Appl. Phys. Lett.* **2003**, *82*, 1610. (c) Collier, C. P.; Mattersteig, G.; Wong, E. W.; Luo, Y.; Beverly, K.; Sampaio, J.; Raymo, F. M.; Stoddart, J. F.; Heath, J. R. *Science*, **2000**, *289*, 1172.
- 51) Stewart, D. R.; Ohlberg, D. A. A.; Beck, P. A.; Chen, Y.; Williams, R. S.; Jeppesen, J. O.; Nielsen, K. A.; Stoddart, J. F. *Nano Lett.* **2004**, *4*, 133.
- 52) Yu, H.; Luo, Y.; Beverly, K.; Stoddart, J. F.; Tseng, H. -R.; Heath, J. R. *Angew. Chem. Int. Ed.* **2003**, *42*, 5706.
- 53) Special edition on cyclodextrins: D'Souza, V. T.; Lipkowitz, K. B. *Chem. Rev.* **1998**, *98*, 1741.
- 54) Kim, K.; Selvapalam, N.; Oh, D. H. *J. Incl. Phenom. Macrocycl. Chem.* **2004**, *50*, 31.
- 55) Lagona, J.; Mukhopadhyay, P.; Chakrabarti, S.; Isaacs, L. *Angew. Chem. Int. Ed.* **2005**, *44*, 4884.
- 56) Lee, J. W.; Selvapalam, N.; Kim, H. -J.; Kim, K. *Acc. Chem. Res.* **2003**, *36*, 621.
- 57) Freeman, W. A.; Mock, W. L.; Shih, N. -Y. *J. Am. Chem. Soc.* **1981**, *103*, 7367.
- 58) Kim, J.; Jung, I. -S.; Kim, S. -Y.; Lee, E.; Kang, J. -K.; Sakamoto, S.; Yamaguchi, K.; Kim, K.; *J. Am. Chem. Soc.* **2000**, *122*, 540.
- 59) Day, A.; Blanch, R. J.; Arnold, A. P.; Lorenzo, S.; Lewis, G. R.; Dance, I. *Angew. Chem. Int. Ed.* **2002**, *41*, 1433.
- 60) Liu, S.; Zavalij, P. Y.; Isaacs, L. *J. Am. Chem. Soc.* **2005**, *127*, 16798.

- 61) Isaacs, L.; Park, S. -K.; Liu, S.; Ko, Y. H.; Selvapalam, N.; Kim, Y.; Kim, H.; Zavalij, P. Y.; Kim, G. -H.; Lee, H. -S.; Kim, K. *J. Am. Chem. Soc.* **2005**, *127*, 18000.
- 62)(a) Connors, K. A. *Chem. Rev.* **1997**, *97*, 1325. (b) Rekharsky, M. V.; Inoue, Y. *Chem. Rev.* **1998**, *98*, 1875. (c) Szejtli, J. *Chem. Rev.* **1998**, *98*, 1743.
- 63)(a) Breslow, R.; Czarniecki, M. F.; Emert, J.; Hamaguchi, H. *J. Am. Chem. Soc.* **1980**, *102*, 762. (b) Sigel, B.; Breslow, R. *J. Am. Chem. Soc.* **1975**, *97*, 6869.
- 64) Matsue, T.; Evans, D. H.; Osa, T.; Kobayashi, N. *J. Am. Chem. Soc.* **1985**, *107*, 3411-3417.
- 65) Shinkai, S.; Mori, S.; Koreishi, H.; Tsubaki, T.; Manabe, O. *J. Am. Chem. Soc.* **1986**, *108*, 2409.
- 66) Isnin, R.; Salam, C.; Kaifer, A. E. *J. Org. Chem.* **1991**, *56*, 35.
- 67) Wang, Y.; Mendoza, S.; Kaifer, A. E. *Inorg. Chem.* **1998**, *37*, 317.
- 68)(a) Special issue about dendrimers and dendritic polymers: *Prog. Polym. Sci.* **2005**, *30*. (b) Baars, M. W. P. L.; Meijer, E. W. *Top. Curr. Chem.* **2000**, *210*, 131.
- 69) Vögtle, F.; Gestermann, S.; Hesse, R.; Schwierz, H.; Windisch, B. *Prog. Polym. Sci.* **2000**, *25*, 987.
- 70) Newkome, G. R.; He, F.; Moorefield, C. N. *Chem. Rev.* **1999**, *99*, 1689.
- 71) Cuadrado, I.; Moràn, M.; Casado, C. M.; Alonso, B.; Losada, J. *Coord. Chem. Rev.* **1999**, *193-195*, 395.
- 72)(a) Cuadrado, I.; Morán, M.; Casado, C. M.; Alonso, B.; Lobete, F.; García, B.; Ibisate, M.; Losada, J. *Organometallics* **1996**, *15*, 5278. (b) Takada, K.; Diaz, D.J.; Abruña, H.D.; Cuadrado, I.; Casado, C.; Alonso, B.; Morán, M.; Losada, J. *J. Am. Chem. Soc.* **1997**, *119*, 10763.
- 73) Castro, R.; Cuadrado, I.; Alonso, B.; Casado, C. M.; Morán, M.; Kaifer, A. E. *J. Am. Chem. Soc.* **1997**, *119*, 5760-5761.
- 74)(a) González, B.; Casado, C. M.; Alonso, B.; Cuadrado, I.; Morán, M.; Wang, Y.; Kaifer, A. E. *Chem. Comm.* **1998**, 2569. (b) Takada, K.; Díaz, D. J.; Abruña, H. D.; Cuadrado, I.; González, B.; Casado, C. M.; Alonso, B.; Morán, M.; Losada, J. *Chem. Eur. J.* **2001**, *7*, 1109.
- 75) Casado, C. M.; Conzález, B.; Cuadrado, I.; Alonso, B.; Morán, M.; Losada, J. *Angew. Chem. Int. Ed.* **2000**, *39*, 2135.
- 76) Conzález, B.; Cuadrado, I.; Casado, C. M.; Alonso, B.; Pastor, C. J. *Organometallics* **2000**, *19*, 5518.
- 77) Conzález, B.; Cuadrado, I.; Alonso, B.; Casado, C. M.; Morán, M.; Kaifer, A. *Organometallics* **2002**, *21*, 3544.
- 78) Cardona, C. M.; McCarley, T. D.; Kaifer, A. E. *J. Org. Chem.* **2000**, *65*, 1857.
- 79) Sobransingh, D.; Kaifer, A. E. *Chem. Commun.* **2005**, 5071.
- 80) Ong, W.; Kaifer, A. E. *Organometallics* **2003**, *22*, 4181-4183.
- 81) Zapotoczny, S.; Auletta, T.; De Jong, M.R.; Schnönherr, H.; Huskens, J.; Van Veggel, F.C. J. M.; Reinhoudt, D. N.; Vancso, G. J. *Langmuir*, **2002**, *18*, 6988.
- 82) Jeon, W. S.; Moon, K.; Park, S. H.; H. Chun, Ko, J. Y. H.; Lee, Y.; Lee, E. S.; Samal, S.; Selvapalam, N.; Rekharsky, M. V.; Sindelar, V.; Sobransingh, D.; Inoue, Y.; Kaifer, A. E.; Kim, K. *J. Am. Chem. Soc.* **2005**, *127*, 12984-12989.
- 83) Kim, H. -J.; Jeon, W. S.; Kim, K. *Proc. Natl. Acad. Sci. USA* **2002**, *99*, 507.
- 84) Jeon, W. S.; Kim, H. -J.; Lee, C.; Kim, K. *Chem. Commun.* **2002**, 1828.
- 85) Moon, K.; Grindstaff, J.; Sobransingh, D.; Kaifer, A. E. *Angew. Chem. Int. Ed.* **2004**, *43*, 5496.
- 86) Kim, H. -J.; Heo, J.; Jeon, W. S.; Lee, J.; Kim, S.; Sakamoto, S.; Yumaguchi, K.; Kim, K. *Angew. Chem. Int. Ed.* **2001**, *40*, 1526.
- 87) Jeon, W. S.; Kim, E.; Ko, Y. H.; Hwang, I.; Lee, J. W.; Kim, S. -Y.; Kim, H. -J.; Kim, K. *Angew. Chem. Int. Ed.* **2005**, *44*, 87.
- 88) Sindelar, V.; Cejas, M. A.; Raymo, F. M.; Chen, W.; Parker, S. E.; Kaifer, A. E. *Chem. Eur. J.* **2005**, *11*, 7054.

- 89) Balzani, V.; Bandmann, H.; Ceroni, P.; Giansante, C.; Hahn, U.; Klärner, U.; Müller, W. M.; Verhaelen, C.; Vicinelli, V.; Vögtle, F. *J. Am. Chem. Soc.* **2006**, *128*, 637.
- 90) Balzani, V.; Ceroni, P.; Giansante, C.; Vicinelli, V.; Vögtle, F. Hahn, U. *Angew. Chem. Int. Ed.* **2005**, *44*, 4574.
- 91) Bu, J.; Lilienthal, N. D.; Woods, J. E.; Nohrden, C. E.; Hoang, K. T.; Truong, D.; Smith, D. K. *J. Am. Chem. Soc.* **2005**, *127*, 6423.
- 92) Chan-Leonor, C.; Martin, S. L.; Smith, D. K. *J. Org. Chem.* **2005**, *707*, 10817.
- 93) Ge, Y.; Miller, L.; Quimet, T.; Smith, D. K. *J. Org. Chem.* **2000**, *65*, 8831.
- 94) Cooke, G.; Sindelar, V.; Rotello, V.M. *Chem. Comm.* **2003**, 752.
- 95) (a) Westwood, J.; Coles, S. J.; Collinson, S. R.; Gasser, G.; Green, S. J.; Hursthouse, M. B.; Light, M. E.; Tucker, J. H. R. *Organometallics* **2004**, *23*, 946. (b) Collinson, S. R.; Gelbirch, T.; Hursthouse, M. B.; Tucker, J. H. R. *Chem. Commun.* **2001**, 555.
- 96) Carr, J. D.; Coles, S. J.; Hursthouse, M. B.; Light, M. E.; Tucker, J. H. R.; Westwood, J. *Angew. Chem., Int. Ed.* **2000**, *39*, 3296.
- 97) Miyaji, H.; Gasser, G.; Green, S. J.; Molard, Y.; Strawbridge, S. M.; Tucker, J. H. R. *Chem. Commun.* **2005**, 5355.
- 98) Boyd, A. S. F.; Carroll, J. B.; Cooke, G.; Garety, J. F.; Jordan, B.J.; Mabruk, S.; Rosiar, G.; Rotello, V. M. *Chem. Commun.* **2005**, 2468.
- 99) Sun, H.; Steeb, J.; Kaifer, A. E. *J. Am. Chem. Soc.* **2006**, *128*, 2820.
- 100) Cooke, G.; Couet, J.; Garety, J. F.; Ma, C. -Q.; Mabruk, S.; Rabani, G.; Rotello, V. M.; Sindelar, V.; Woisel, P. *Tetrahedron Lett.* **2006**, *47*, 3763.
- 101) Carroll, J. B.; Gray, M.; Cooke, G.; Rotello, V. M. *Chem. Commun.* **2004**, 442.
- 102) Cooke, G.; de Creniers, H. A.; Duclairoir, F. M. A.; Leonardi, G. R.; Rotello, V. M. *Tetrahedron* **2003**, *59*, 3341.
- 103) (a) Sansone, F.; Baldini, L.; Casnati, A.; Chierici, E.; Faimani, G.; Ugozzoli, F.; Ungaro, R. *J. Am. Chem. Soc.* **2004**, *126*, 6204-6205. (b) Baldini, L.; Ballester, P.; Casnati, A.; Rosa, M.; Hunter, C. A.; Sansone, F.; Ungaro, R. *J. Am. Chem. Soc.* **2003**, *125*, 14181-14189. (c) Kuhnert, N.; Le-Gresley, A. *Chem. Commun.* **2003**, 2426-2427. (d) Hayashida, O.; Shivanyuk, A.; Rebek, J., Jr. *Angew. Chem. Int. Ed.* **2002**, *41*, 3423-3426. (e) Hof, F.; Craig, S. L.; Nuckolls, C.; Rebek, J., Jr. *Angew. Chem. Int. Ed.* **2002**, *41*, 1488-1508. (f) O'Leary, B. M.; Szabo, T.; Svenstrup, N.; Schalley, C. A.; Lützen, A.; Schäfer, M.; Rebek, J., Jr. *J. Am. Chem. Soc.* **2001**, *123*, 11519-11533. (g) Rivera, J. M.; Martín, T.; Rebek, J., Jr. *J. Am. Chem. Soc.* **2001**, *123*, 5213-5220. (h) Hof, F.; Nuckolls, C.; Craig, S. L.; Martín, T.; Rebek, J., Jr. *J. Am. Chem. Soc.* **2000**, *122*, 10991-10996. (i) Rivera, J. M.; Rebek, J., Jr. *J. Am. Chem. Soc.* **2000**, *122*, 7811-7812. (j) Shivanyuk, A.; Paulus, E. F.; Böhmer, V. *Angew. Chem., Int. Ed.* **1999**, *38*, 2906-2909. (k) Conn, M. M.; Rebek, J., Jr. *Chem. Rev.* **1997**, *97*, 1647-1668. (l) Corbellini, F.; van Leeuwen, F. W. B.; Beijleveld, H.; Kooijman, H.; Spek, A. L.; Verboom, W.; Crego-Calama, M.; Reinhoudt, D. N. *New J. Chem.* **2005**, *29*, 243.
- 104) (a) Vysotsky, M. O.; Saadioui, M.; Böhmer, V. *Chem. Commun.* **2003**, 1124-1125. (b) Brewster, R. E.; Shuker, S. B. *J. Am. Chem. Soc.* **2002**, *124*, 7092-7093. (c) Cho, Y. L.; Rudkevich, D. M.; Rebek, J., Jr. *J. Am. Chem. Soc.* **2000**, *122*, 9868-9869. (d) Castellano, R. K.; Craig, S. L.; Nuckolls, C.; Rebek, J., Jr. *J. Am. Chem. Soc.* **2000**, *122*, 7876-7882. (e) Vysotsky, M. O.; Thondorf, I.; Böhmer, V. *Angew. Chem., Int. Ed.* **2000**, *39*, 1264-1266. (f) Rebek, J., Jr. *Chem. Commun.* **2000**, 637-643. (g) Cho, Y. L.; Rudkevich, D. M.; Shivanyuk, A.; Rissanen, K.; Rebek, J., Jr. *Chem. Eur. J.* **2000**, *6*, 3788-3796. (h) Schalley, C. A.; Castellano, R. K.; Brody, M. S.; Rudkevich, D. M.; Siuzdak, G.; Rebek, J., Jr. *J. Am. Chem. Soc.* **1999**, *121*, 4568-4579. (i) Brody, M. S.; Schalley, C. A.; Rudkevich, D. M.; Rebek, J., Jr. *Angew. Chem., Int. Ed.* **1999**, *38*, 1640-1644. (j) Castellano, R. K.; Rebek, J., Jr. *J. Am. Chem. Soc.* **1998**, *120*, 3657-3663. (k) Mogck, O.;

- Pons, M.; Böhmer, V.; Vogt, W. *J. Am. Chem. Soc.* **1997**, *119*, 5706-5712. (l) Castellano, R. K.; Rudkevich, D. M.; Rebek, J., Jr. *J. Am. Chem. Soc.* **1996**, *118*, 10002-10003. (m) Mogck, O.; Böhmer, V.; Vogt, W. *Tetrahedron* **1996**, *52*, 8489-8496. (n) Shimizu, K. D.; Rebek, J., Jr. *Proc. Natl. Acad. Sci. U.S.A.* **1995**, *92*, 12403-12407.
- 105) Moon, K.; Kaifer, A. E. *J. Am. Chem. Soc.* **2004**, *126*, 15016.
- 106) MacGillivray, L. R.; Atwood, J. L. *Nature* **1997**, 389, 469. (b) Gerkensmeier, T.; Iwanek, W.; Agena, C.; Fröhlich, R.; Kotila, S.; Näther, C.; Mattay, J. *Eur. J. Org. Chem.* **1999**, 2257.
- 107) (a) Shivanyuk, A.; Rebek, J. *Proc. Natl. Acad. Sci. U.S.A.* **2001**, *98*, 7662. (b) Shivanyuk, A.; Rebek, J. *Chem. Commun.* **2001**, 2424.
- 108) Philip, I. E.; Kaifer, A. E. *J. Am. Chem. Soc.* **2002**, *124*, 12678.
- 109) Astruc, D.; Blais, J. -C.; Daniel, M. -C.; Martinez, V.; Nlate, S.; Ruiz, J. *Macromol. Symp.* **2003**, *196*, 1.
- 110) (a) Labande A.; Astruc, D. *Chem. Commun.* **2000**, 1007. (b) Daniel, M. -C.; Ruiz, J.; Nlate, S.; Palumbo, J.; Blais, J. -C.; Astruc, D. *Chem. Commun.* **2001**, 2000. (c) Labande, A.; Ruiz, J.; Astruc, D. *J. Am. Chem. Soc.* **2002**, *124*, 1782.
- 111) Astruc, D.; Daniel, M. -C.; Ruiz, J. *Chem. Commun.* **2004**, 2637.
- 112) Valério, C.; Fillaut, J. -L.; Ruiz, J.; Guittard, J.; Blais, J. -C.; Astruc, D. *J. Am. Chem. Soc.*, 1997, **119**, 2588;
- 113) Valério, C.; Alonso, E.; Ruiz, J.; Blais, J. -C.; Astruc, D. *Angew. Chem. Int. Ed.* 1999, **38**, 1747.
- 114) Daniel, M. -C.; Ruiz, J.; Nlate, S.; Blais, J. -C.; Astruc, D. *J. Am. Chem. Soc.* **2003**, *125*, 2617.
- 115) Valério, C.; Fillaut, J. -L.; Ruiz, J.; Guittard, J.; Blais, J. -C.; Astruc, D. *J. Am. Chem. Soc.* **1997**, *119*, 2588.
- 116) Valério, C.; Alonso, E.; Ruiz, J.; Blais, J. -C.; Astruc, D. *Angew. Chem. Int. Ed.* **1999**, *38*, 1747.
- 117) Alonso, B.; Casado, C. M.; Cuadrado, I.; Morán, M.; Kaifer, A. E. *Chem. Commun.* **2002**, 1778.
- 118) Kelly, T. R.; Kim, M. H. *J. Am. Chem. Soc.* **1994**, *116*, 7072.
- 119) Ruiz, J.; Ruiz Medel M. J.; Daniel, M. -C.; Blais, J. C.; Astruc, D. *Chem. Commun.* **2003**, 464.
- 120) Valério, C.; Alonso, E.; Ruiz, J.; Guittard, J.; Blais, J. C.; Astruc, D. *Angew. Chem. Int. Ed.* **1999**, *38*, 1747
- 121) Aranzaes, J. R.; Belin, C.; Astruc, D. *Angew. Chem. Int. Ed.* **2006**, *45*, 132.
- 122) Stone, D. L.; Smith, D. K. *Polyhedron* **2003**, *22*, 763.
- 123) Stone, D. L.; Smith, D. K.; Mcgrail, P. T. *J. Am. Chem. Soc.* **2002**, *124*, 856.
- 124) Daniel, M. -C.; Ba, F.; Aranzaes, J. R.; Astruc, D. *Inorg. Chem.* **2004**, *43*, 8649.
- 125) Beer, P.D.; Gale, P.A.; Chen, G. Z. *Coord. Chem. Rev.* **1999**, *185-186*, 3
- 126) Tucker, J. H. R.; Collinson, S. R. *Chem. Soc. Rev.* **2002**, *31*, 147.
- 127) Beer, P. D.; Gale, P. A. *Angew. Chem. Int. Ed.* **2001**, *40*, 486.
- 128) Beer, P. D. *Acc. Chem. Res.* **1998**, *31*, 71.
- 129) Beer, P. D.; Davis, J. J.; Drillsma-Milgrom, D. A.; Szemes, F. *Chem. Commun.* **2002**, 1716.
- 130) (a) Reynes, O.; Maillard, F.; Moutet, J. -C.; Royal, G.; Saint-Aman, E.; Stanciu, G.; Dutasta, J.-P.; Gossa, I.; Mulatier, J. -C. *J. Organomet. Chem.* **2001**, *637-639*, 356. (b) Reynes, O.; Bucher, C.; Moutet, J. -C.; Royal, G.; Saint-Aman, E. *Chem. Commun.* **2004**, 428.
- 131) Reynes, O.; Bucher, C.; Moutet, J. -C.; Royal, G.; Saint-Aman, E.; Ungureanu, E. -M. J. *Electroanal. Chem.* **2005**, *580*, 291.
- 132) Kakizawa, Y.; Sakai, H.; Yamaguchi, A.; Kondo, Y.; Yoshino, N.; Abe, M. *Langmuir*, **2001**, *17*, 8044.
- 133) Abbott, N. L.; Jewell, C. M.; Hays, M. E.; Kondo, Y.; Lynn, D. M. *J. Am. Chem. Soc.* **2005**, *127*, 11576.

Binding Control and Valency of Ferrocenyl Dendrimers at Molecular Printboards*

In this chapter a detailed study of the multivalent binding of ferrocenyl- (Fc-) terminated dendrimers at molecular printboards is described. Three different types of Fc-functionalized dendrimers of generations 1 to 5 with long, short, and intermediate groups were adsorbed at self-assembled monolayers (SAMs) of heptathioether-functionalized β -cyclodextrin (β CD) on gold. The dendrimers formed kinetically stable supramolecular assemblies at the β CD host surface with up to 8 octavalent supramolecular interactions, but could be efficiently removed from the host surface by electrochemical oxidation of the Fc end groups. Dendrimer desorption and re-adsorption could be repeated a number of times without significant decomposition of the dendrimers or SAMs. The valencies of the dendrimers at the surface were determined using cyclic voltammetry (CV). For the lower dendrimer generations the valencies were quantitatively confirmed by surface plasmon resonance (SPR) titrations of the dendrimers to the β CD SAM. Measuring CV and SPR simultaneously gave crucial mechanistic information on the electrochemically induced desorption of the dendrimers from the host surface. The redox-active dendrimers effectively blocked the host surface for other guest molecules, e.g. adamantyl-functionalized dendrimers, but electrochemically induced release of the blocking layer revealed the host surface to which the adamantyl dendrimers could then bind.

* Parts of this chapter have been published in: (a) Nijhuis, C. A.; Yu, F.; Knoll, W.; Huskens, J.; Reinhoudt, D. N. *Langmuir* **2005**, *21*, 7866. (b) Nijhuis, C. A.; Huskens, J.; Reinhoudt, D. N. *J. Am. Chem. Soc.* **2004**, *126*, 12266. and (c) Auletta, T.; Dordi, B.; Mulder, A.; Sartori, A.; Onclin, S.; Bruinink C. M.; Péter, M.; Nijhuis, C. A.; Beijleveld, H.; Schönherr, H.; Vancso, G. J.; Casnati, A.; Ungaro, R.; Ravoo, B. J.; Huskens, J.; Reinhoudt, D. N. *Angew. Chem. Int. Ed.* **2004**, *43*, 369.

3.1 Introduction

Anchoring (bio)molecules on functionalized surfaces with high accuracy and stability is of high current interest for various applications, e.g. molecular electronics,¹ biochips,² solar cells, and for conducting single molecule experiments. In general, molecules are either covalently attached or physisorbed at surfaces. Disadvantages of chemical, covalent modification of surfaces is that neither self-correction nor intentional desorption are possible. Physisorption allows self-correction, but the thermodynamic and kinetic parameters are difficult to control and neighboring molecule-molecule interactions are usually required for ordering and stabilizing the adsorbed layers. On the other hand, supramolecular interactions allow self-correction, are specific and directional, and are well defined, implying that the binding properties can be manipulated with great precision.³ A disadvantage is that supramolecular interactions are in general weak, but this problem can be overcome by using the concept of multivalency,⁴ which is widely extended throughout nature, e.g. in protein-protein, protein-DNA, and protein-membrane interactions, to enhance the weak monovalent interactions. The concept of multivalency has been used to anchor carbon nanotubes,⁵ dendrimers,⁶ proteins,⁷ and dendritic wedges.⁸ Therefore, a fundamental understanding of multivalency could have a profound influence on, for instance, drug design and bottom-up nanofabrication. The formation of stable assemblies at surfaces, in combination with control over the binding by external stimuli, is essential for applications. However, quantitative information about the specific number of interactions and the resulting binding strength is often hard to obtain, especially for multivalent systems linked to surfaces.

Our group has developed the concept of molecular printboards, which are self-assembled monolayers (SAMs) of molecules consisting of recognition sites to which guest molecules can bind by (multivalent) supramolecular interactions. We have described SAMs of heptathioether-functionalized β -cyclodextrin (β CD) on gold.⁹ This adsorbate forms well-ordered and densely packed monolayers with a hexagonal lattice. Onto these host SAMs a variety of monovalent or multivalent guest molecules were positioned by adsorption from solution.^{6,9} The formation of multiple supramolecular interactions between the guest molecules and the β CD host surface enhanced the surface adsorption dramatically. We coined the term “molecular printboard”, because these SAMs in principle allow binding of molecules with ultimate control over binding thermodynamics and kinetics, and positioning with molecular accuracy.

Dendrimers serve as a particularly suitable class of polyfunctional guest molecules since the number of end groups can be exactly controlled and all end groups are exposed at the periphery of the molecule.¹⁰ Furthermore, the unique properties of dendrimers find applications in many fields such as drug delivery,¹¹ optoelectronics,¹² catalysis,¹³ molecular recognition,¹⁴ and as nanocontainers.¹⁵ Recently, we reported the immobilization of adamantyl- (Ad)⁶ functionalized poly(propylene imine) (PPI) dendrimer guest molecules of

various generations, having 4 – 32 end groups at molecular printboards by forming multiple host-guest interactions. Generation 2, which has 8 Ad functionalities, could be removed from the host surface upon rinsing with competitive aqueous β CD solutions, while generations 3 and 4 formed kinetically stable assemblies due to the formation of multiple host-guest interactions.

It is well-known that Fc forms inclusion complexes with β CD in aqueous media ($K_a \sim 10^3 \text{ M}^{-1}$) and that the complexation is strongly diminished upon electrochemical conversion of the Fc groups to Fc^+ cations.¹⁶ In this chapter, dendrimers decorated with ferrocene moieties of generations 1 to 5 were used in order to investigate the electrochemically controlled binding of the dendrimers to the molecular printboard. The binding stability and the determination of the number of interactions of the dendrimers with the host surface were determined by cyclic voltammetry (CV) and quantitatively confirmed by surface plasmon resonance (SPR) spectroscopy. Furthermore, not only the dependence on the generation, but also the influence of the spacer length between the functionalities and the dendritic core on the number of interactions with the host surface was investigated (Chart 3.1). It is expected that the number of host-guest interactions between the guest dendrimer and the molecular printboard increases for higher generations and also increases with increasing spacer length for a given generation of dendrimers.

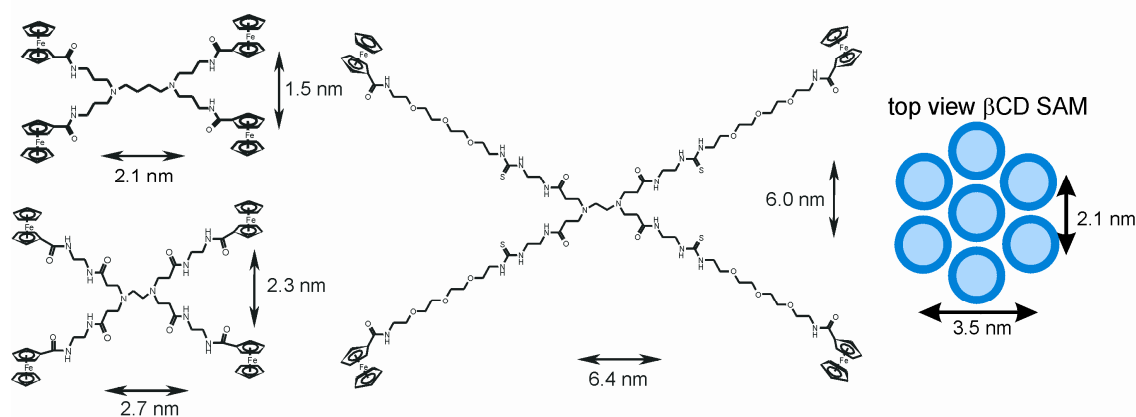


Chart 3.1: Distances of the Fc moieties in the most extended dendrimer conformations derived from CPK models: upper left: G1-PPI-(Fc)₄; lower left: G0-PAMAM-(Fc)₄; center: G0-PAMAM-EG-(Fc)₄; right: top view of the β CD SAM, arrows indicate center-to-center spacing between the β CD cavities.

3.2 Results and discussion

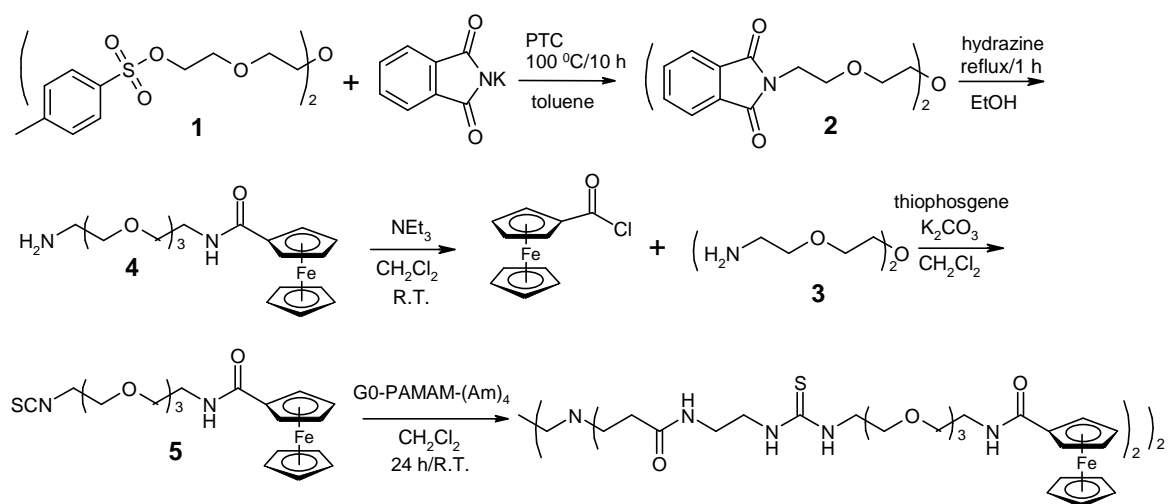
3.2.1 Synthesis

The ferrocenyl-modified poly(propylene imine) (PPI) dendrimers, generations 1 to 5 (see Chart 1), have been prepared by condensation reactions of 1-(chlorocarbonyl)ferrocene with

the terminal amino groups of the parent amino dendrimers according to a literature procedure.¹⁷ Poly(amidoamine) (PAMAM) dendrimers have longer spacer groups compared to PPI dendrimers and three generations G0-PAMAM-(Fc)₄, G1-PAMAM-(Fc)₈, and G2-PAMAM-(Fc)₁₆ have been prepared using a similar procedure as for the PPI dendrimers. The PAMAM dendrimers could be isolated in moderate yields (40% - 75%) as air stable orange powders with similar solubilities as the PPI analogues.

In order to increase the spacer length even more, ethylene glycol units were introduced between the Fc functionalities and the PAMAM dendritic core. G0 and G1 PAMAM dendrimers with four and eight amine functionalities, respectively, were modified with Fc groups containing glycol spacers as is outlined in Scheme 3.1. The tetra(ethylene glycol) ditosylate **1** was converted into the bis(phthalimide) **2** by reaction with potassium phthalimide. Treatment of **2** with hydrazine gave the diamine **3**. The diamine was allowed to react with one equivalent of ferrocene carbonylchloride, and the mono-substituted product **4** could be isolated in 40% yield. The amine functionality of **4** was converted into a more reactive thioisocyanate after reaction with 10 equivalents of thiophosgene for 1 h. Reaction of **5** with the amine-terminated G0-PAMAM-(NH₂)₄ or G1-PAMAM-(NH₂)₈ dendrimers gave the final products G0-PAMAM-EG-(Fc)₄ and G1-PAMAM-EG-(Fc)₈. The first generations of the different types of dendrimers are shown in Chart 1 along with the dimensions estimated from CPK models and a top view of the molecular printboard.

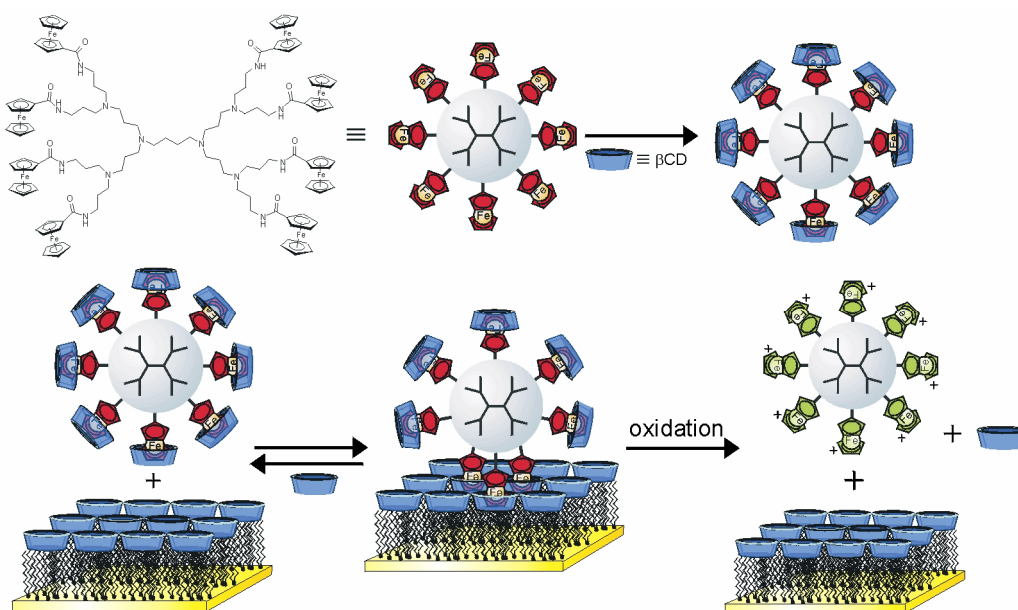
Scheme 3.1: Synthesis of G0-PAMAM-EG-(Fc)₄.



3.2.2 Formation of dendrimer- β CD assemblies

All dendrimers were virtually insoluble in water, but in the presence of native β CD (β CD/Fc = 1.1) and at pH = 2, all dendrimers could be solubilized in water after ultrasonication for 1 – 4 h.¹⁸ Typically, 10 mM solutions (in Fc functionality) of the dendrimers in the presence of 11

mM native β CD were prepared, except for the G5-PPI-(Fc)₆₄ of which typically only 1-2 mM (in Fc functionality) solutions could be prepared. Protonation of the core amines forces the dendrimers to adopt the most extended configuration and, therefore, the native β CD from solution is able to form inclusion complexes with all ferrocenyl endgroups and this results in water-soluble dendrimer- β CD assemblies (Scheme 3.2). CVs of the dendrimer- β CD assemblies showed only one oxidation wave at scan rates (v) varying from 10 to 200 mV/s, indicating that all end groups are accessible for complexation of native β CD from solution (see section 4.2.1). Only G5-PPI-(Fc)₆₄ showed, at low v , two signals in the CV attributed to Fc end groups complexed to β CD and uncomplexed Fc groups, and this explains the observed lower solubility of this particular dendrimer. Kaifer et al. reported PPI- β CD assemblies in neutral aqueous solutions up to generation 3, and G3-PPI-(Fc)₁₆ showed two signals in the CV since not all end groups were interacting with native β CD from solution.¹⁹ The fact that G5-PPI-(Fc)₆₄ is not able to have all end groups interacting with β CD from solution is in good agreement with observations made earlier for adamantyl-functionalized PPI dendrimer- β CD assemblies.¹⁸ From ¹H NMR titration data it was found that only about 40 β CDs complex to the G5-PPI-(Ad)₆₄ dendrimer for steric reasons.¹⁸ Thus, the stoichiometries of the dendrimer – β CD assemblies in solution are Gx-dendrimer-(Fc)_y – β CD_y for all PAMAM dendrimers and the PPI dendrimer up to generation 4, the last having a molecular weight of more than 46 kDa.



Scheme 3.2: G2-PPI-(Fc)₈ and its formation of water soluble assemblies with β CD (top); the adsorption of the dendrimer- β CD assembly at the β CD SAM (bottom) and the electrochemically induced desorption from the molecular printboard.

3.2.3 Surface plasmon resonance spectroscopy

All dendrimers were adsorbed at the β CD host surface from aqueous solutions of the dendrimer- β CD assembly (Scheme 3.2). Because of the intrinsically reversible nature of the host-guest interactions, the dendrimers form densely packed SAMs at the molecular printboards. The dendrimers used in this study are highly flexible molecules, and a full extension of the dendrimers is required to access the maximum number of β CD sites at the surface that is sterically allowed. Additionally, the multivalency principle predicts that molecules will interact (under most conditions) with the maximally allowed number of interactions.²⁰

The stability of the dendrimers at the β CD SAM towards competitive aqueous solutions, e.g. with native β CD present, were studied by SPR for all dendrimers.²¹ In Figure 3.1, two typical examples are shown for G1-PAMAM-(Fc)₈ and G0-PAMAM-EG-(Fc)₄.

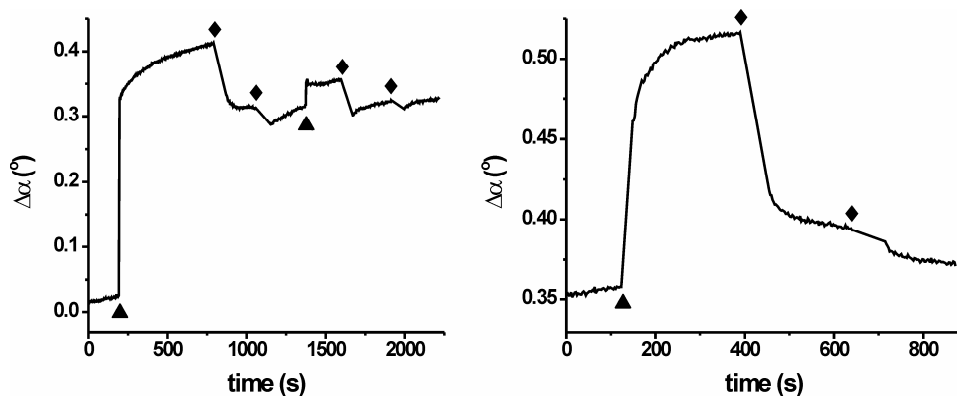


Figure 3.1: SPR sensogram of addition of G1-PAMAM-(Fc)₈ to a β CD SAM (left): ▲ = injection of guest, first injection with concentration of 1.3 μ M guest in 10 mM β CD at pH = 2 and second injection with 0.13 μ M guest; ◆ = wash with an aqueous solution of 10 mM native β CD at pH = 2; on the right addition of G0-PAMAM-EG-(Fc)₄ (25 μ M) to a β CD SAM: ▲ = injection of guest in 10 mM β CD at pH = 2; ◆ = wash with an aqueous solution of 10 mM native β CD at pH = 2.

Addition of G1-PAMAM-(Fc)₈ to a β CD SAM gave a typical adsorption curve as observed by SPR (Figure 3.1, left) and washing with a competitive solvent, e.g. 10 mM solution of native β CD at pH = 2, resulted in a small decrease in SPR signal as only non-specifically bound material was removed. Repeatedly washing left the SPR signal practically unchanged, but injection of a lower concentration of guest resulted in a small increase in signal. The signal dropped to the same value as before the second guest injection upon rinsing with 10 mM solution of native β CD at pH = 2, indicating that after the first injection already a densely packed monolayer of the dendrimers was formed at the β CD SAM and that the increase of the SPR signal after the second injection only stems from non-specifically bound material. This is also reflected by the second injection, which was performed with a lower concentration of guest molecules, resulting in a smaller difference in SPR signal upon washing with 10 mM

β CD at pH = 2, when compared to the first injection, which is attributed to less physisorption in the former case. Similar SPR sensograms were obtained for G3-PPI-(Fc)₁₆, G4-PPI-(Fc)₃₂, G5-PPI-(Fc)₆₄, G2-PAMAM-(Fc)₁₆, and G1-PAMAM-EG-(Fc)₈.

In contrast, upon addition of G0-PAMAM-EG-(Fc)₄ to a β CD SAM, also a typical adsorption curve was observed (Figure 3.1, right), but rinsing with 10 mM solution of native β CD at pH = 2 practically removed all adsorbed guest molecules from the host surface. Similar behavior was also observed for G1-PPI-(Fc)₄, G2-PPI-(Fc)₈, and G0-PAMAM-(Fc)₄. Thus, the larger dendrimers have sufficient Fc- β CD interactions to form kinetically stable assemblies at the β CD surface at room temperature, while the smaller dendrimers can be removed from the surface with competitive solutions indicating that these dendrimers are in equilibrium with native β CD from solution.

In order to determine the number of interactions, p_b , of the dendrimers with the β CD host surface, titrations of aqueous solutions of dendrimer- β CD assemblies of G1-PPI-(Fc)₄, G2-PPI-(Fc)₈, G0-PAMAM-(Fc)₄, and G0-PAMAM-EG-(Fc)₄ to the β CD SAM have been monitored by SPR spectroscopy and fitted to a surface binding model for multivalent host-guest interactions.²⁰ This model assumes that all ferrocene- β CD interactions are equal and independent at the surface as well as in solution, and is based on the high effective concentration (C_{eff}) of host molecules at the surface upon binding of the first guest site of the dendrimer. Furthermore, the model accounts for the free binding sites of the dendrimer and for the competitive β CD in solution. It has been shown before that for small monovalent Fc guests the intrinsic binding constant at the surface ($K_{i,s}$) closely resembles the intrinsic binding constant in solution ($K_{i,l}$)^{22,23} which is $1.2 \times 10^3 \text{ M}^{-1}$ for an individual ferrocene- β CD interaction, as reported by Kaifer.¹⁹ The majority of the molecules will interact with the surface with the maximal number of interactions because $C_{\text{eff}} \gg [\beta\text{CD}]_{\text{tot}}$. Therefore, the binding data can be fitted by optimizing $K_{i,s}$ at various p_b values, but only the results that give plausible $K_{i,s}$ values will correspond to the true p_b values.

The titrations were performed at a constant competitor concentration, e.g. a 10 mM aqueous β CD solution, and the difference in SPR response before and after injection of the dendrimer solutions were plotted versus the concentration of the guest molecule. A typical titration curve for G0-PAMAM-(Fc)₄ is shown in Figure 3.2, and in Table 3.1 fit results are given for G0-PAMAM-(Fc)₄, G0-PAMAM-EG-(Fc)₄, G1-PPI-(Fc)₄, and G2-PPI-(Fc)₈. Figure 3.2 shows also a fit which was obtained assuming three interactions to the surface per molecule, and an intrinsic binding constant at the surface $K_{i,s}$ of $9.2 \times 10^2 \text{ M}^{-1}$ (per Fc- β CD interaction) was found. This compares very well to $K_{i,l}$ while for p_b values of 2 and 4, only implausible $K_{i,s}$ values were obtained (Table 3.1). For instance, fitting the titration data of G0-PAMAM-(Fc)₄ with $p_b = 2$ or $p_b = 4$ gave $K_{i,s}$ values of $4.4 \times 10^3 \text{ M}^{-1}$ and $K_{i,s}$ of $5.4 \times 10^2 \text{ M}^{-1}$, respectively, and both differ significantly from $K_{i,l}$. Therefore, only $p_b = 3$ gave a realistic $K_{i,s}$ value and the main species bound to the surface in the case of G0-PAMAM-(Fc)₄ has three (out of four) Fc- β CD interactions with the surface host sites.

The binding data of G1-PPI-(Fc)₄ gave a best fit with two interactions and G2-PPI-(Fc)₈ with three and gave $K_{i,s}$ values of $5.5 \times 10^2 \text{ M}^{-1}$ and $1.1 \times 10^3 \text{ M}^{-1}$ (per Fc- β CD interaction), respectively. Titration data of G1-PAMAM-EG-(Fc)₄ gave a plausible $K_{i,s}$ of $1.0 \times 10^3 \text{ M}^{-1}$ per β CD-Fc interaction for $p_b = 4$.

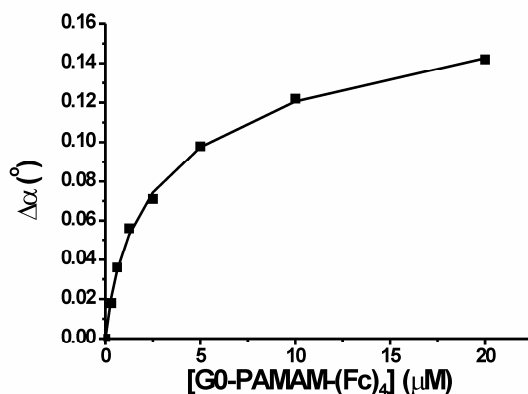


Figure 3.2. SPR titration curve of G0-PAMAM-(Fc)₄ in 10 mM aqueous β CD at pH = 2 at a β CD SAM.

Table 3.1: Optimized $K_{i,s}$ values for SPR titrations of G1-PPI-(Fc)₄, G0-PAMAM-(Fc)₄, G2-PPI-(Fc)₈, and G0-PAMAM-EG-(Fc)₄ to β CD SAMs.

Dendrimer	p_b	$K_{i,s} (\text{M}^{-1})^a$	$\Delta\alpha_{\text{max}} (^\circ)^a$	R
G0-PAMAM-(Fc) ₄	2	4.4×10^3	0.396	0.98
	3	9.2×10^2	0.692	0.98
	4	5.4×10^2	0.949	0.98
G0-PAMAM-EG-(Fc) ₄	2	2.7×10^4	0.494	0.98
	3	3.4×10^3	0.745	0.98
	4	1.0×10^3	1.03	0.98
G1-PPI-(Fc) ₄	1	2.2×10^5	0.209	0.98
	2	5.5×10^2	0.515	0.98
	3	1.0×10^2	0.886	0.98
G2-PPI-(Fc) ₈	2	9.4×10^3	0.410	0.98
	3	1.1×10^3	0.715	0.98
	4	4.4×10^2	1.053	0.98

^a Determined using the multivalency model with $C_{\text{eff,max}} = 0.3 \text{ M}$ and $K_{i,1} = 1.2 \times 10^3 \text{ M}^{-1}$, for varying p_b .

The larger dendrimers have sufficient Fc- β CD interactions to form kinetically stable assemblies at the β CD surface under the present conditions. Given that G0-PAMAM-EG-(Fc)₄ with 4 interactions can effectively be removed from the surface, all kinetically stable dendrimers are likely to have more than four interactions. Dendrimers having less than 4 interactions are still in equilibrium with native β CD in solution. For the G3-PPI-(Fc)₁₆ (which has also 4 interactions) it was not possible to obtain titration curves, probably due to a lower solubility compared to the G0-PAMAM-EG-(Fc)₄. Consequently, under the present

conditions 4 Fc- β CD interactions is an intermediate at which both kinetically stable or equilibrating assemblies may be formed.

3.2.4 Electrochemistry

All dendrimers were adsorbed at the β CD host surface by immersion of β CD host monolayers into aqueous solutions containing the dendrimer- β CD assemblies (Scheme 3.2) followed by rinsing with water and drying under a stream of N_2 . The number of interactions of all dendrimers with the β CD SAM were determined by cyclic voltammetry (CV). A typical desorption initiated and followed by CV is shown in Figure 3.3 for five generations PPI dendrimers and similar CVs were recorded for all dendrimers at different v ranging from 10 to 200 mV/s.

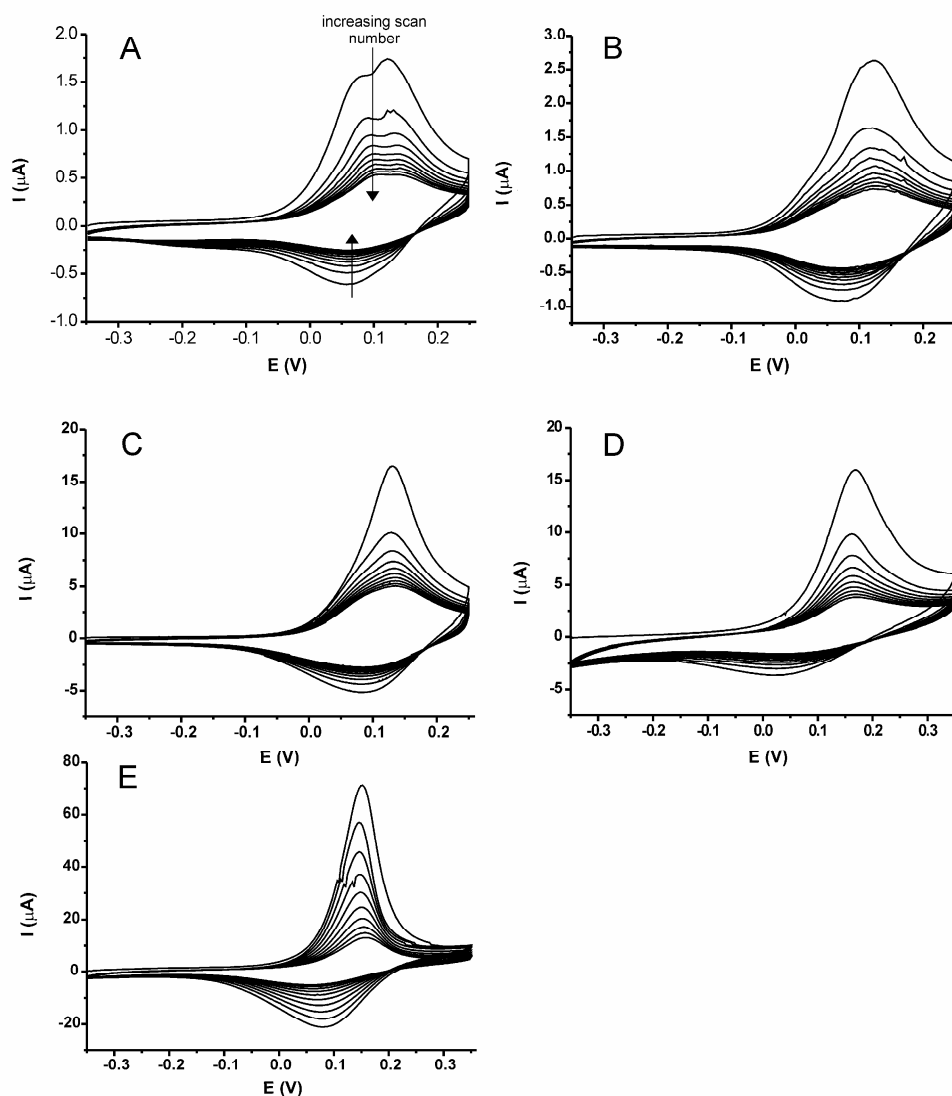


Figure 3.3: Electrochemical desorption of the Fc-functionalized PPI dendrimers from a β CD SAM induced and observed by CV: A) G1, scan rate = 25 mV/s, 0.1 M K_2SO_4 , 10 scans; B) G2, scan rate = 25 mV/s, 0.1 M K_2SO_4 , 10 scans; C) G3, scan rate = 100 mV/s, 0.1 M K_2SO_4 , 10 scans; D) G4, scan rate = 100 mV/s, 0.1 mM NaCl at pH = 2, 10 scans; E) G5, scan rate = 200 mV/s, 0.1 mM NaCl at pH = 2, 10 scans.

As the potential increases, the Fc groups start to oxidize to ferrocenium cations which are not able to form inclusion complexes with β CD leading to desorption of the dendrimers from the β CD SAM and subsequent diffusion into the solution. Upon reduction, only dendrimers remaining close to the surface are reduced and may bind back to the surface, resulting in concomitant decrease in intensity during following scans. Numerous reports state that all redox endgroups are oxidized upon electrochemical oxidation, even for dendrimers consisting of hundreds of endgroups.²⁴ Besides normal electron transfer pathways (e.g. an electron hopping mechanism), another mechanism has been proposed for dendrimers which is based on rotational diffusion of the dendrimers, that is, the dendrimers rotate fast on the electrochemical time scale and for this reason all endgroups are electroactive.²⁵ Here, both types of mechanisms may be accessible simultaneously.

In the case of G1-PPI-(Fc)₄, two signals with equal intensities were recorded at low scan rates (Figure 3.3). This is interpreted by assuming that two of the four Fc end groups are bound to β CD at the surface and the other two unbound (see below). Similar CVs were recorded for the other dendrimers. The signal attributed to bound ferrocene moieties was observed as a shoulder in these cases, because the ratio between bound and unbound end groups decreases for increasing generations (see below).

Integration of the first scan in the (i,E)-curves gives the total charge (Q) from which the surface coverage of the Fc units, G_{Fc} , can be determined using $G_{\text{Fc}} = Q/nFA$, in which n = number of electrons per mole of reaction, F = Faraday constant, and A = surface area of the electrode.²⁶ CVs were recorded at ν ranging from 10 to 200 mV/s to demonstrate the independence of Q on ν as should be for a surface-confined process. The results for the PPI dendrimers are given in Figure 3.4. Also for the PAMAM dendrimers and the PAMAM dendrimers with EG spacer groups it was found that Q remained constant.

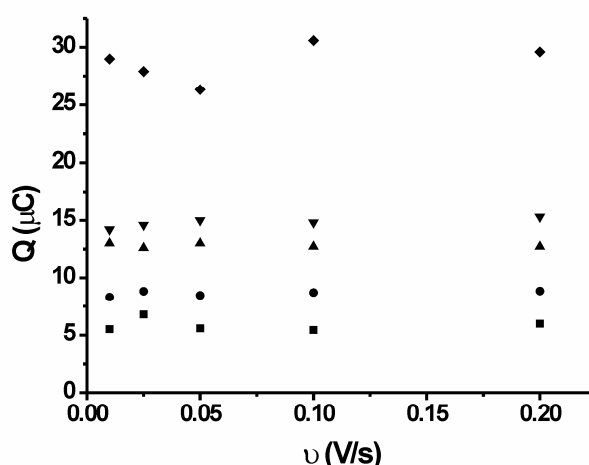


Figure 3.4: Dependence of the total charge Q on the scan rates of the G1-PPI-(Fc)₄ (■), G2-PPI-(Fc)₈ (●) and G3-PPI-(Fc)₁₆ (▲), G4-PPI-(Fc)₃₂ (▼), and G5-PPI-(Fc)₆₄ (◆) Fc-terminated PPI dendrimers recorded at 10, 25, 50, 100 and 200 mV/s.

The surface coverage of the β CD adsorbate molecules, $G_{\beta\text{CD}}$ (8×10^{-11} mol/cm²), was estimated from CPK models, AFM studies,⁹ and from SPR measurements for a calixarene bisadamantyl derivative.²² The relative coverages $G_{\beta\text{CD}}/G_{\text{Fc}}$ provide the number p_b of bound interactions per dendrimer molecule with the host surface, using $p_b = p_{\text{tot}}G_{\beta\text{CD}}/G_{\text{Fc}}$, where p_{tot} is the total number of end groups. The $G_{\beta\text{CD}}/G_{\text{Fc}}$ ratios and the number of interactions p_b are given in Table 3.2. All possible binding modes of a first generation dendrimer with the surface and the theoretical values of the $G_{\beta\text{CD}}/G_{\text{Fc}}$ ratios are depicted in Figure 3.5.

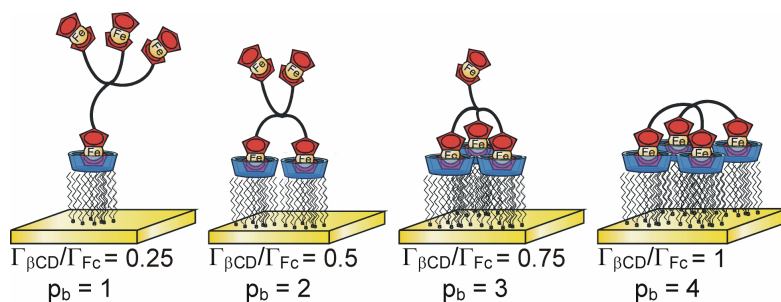


Figure 3.5: Schematic representation of the four possible binding modes of a first generation dendrimer with the numbers, p_b , of bound sites and the predicted $G_{\beta\text{CD}}/G_{\text{Fc}}$ ratios depicted below.

Table 3.2. The number of interactions, p_b , of all dendrimers with the β CD SAM observed by CV and SPR.

Dendrimer	$G_{\beta\text{CD}}/G_{\text{Fc}}^a$	p_b (CV) ^b	p_b (SPR) ^c
G1-PPI-(Fc) ₄	0.56 (0.50)	2	2
G2-PPI-(Fc) ₈	0.38 (0.38)	3	3
G3-PPI-(Fc) ₁₆	0.26 (0.25)	4	-
G4-PPI-(Fc) ₃₂	0.22 (0.22)	7	-
G5-PPI-(Fc) ₆₄	0.11 (0.11)	7 (or 8)	-
G0-PAMAM-(Fc) ₄	0.75 (0.75)	3	3
G1-PAMAM-(Fc) ₈	0.66 (0.67)	5	-
G2-PAMAM-(Fc) ₁₆	0.52 (0.5)	8	-
G0-PAMAM-EG-(Fc) ₄	1.1 (1.0)	4	4
G1-PAMAM-EG-(Fc) ₈	1.0 (1.0)	8	-

^a $G_{\beta\text{CD}} = 8 \times 10^{-11}$ mol/cm² (see text), while G_{Fc} is determined from CV experiments and the theoretical values are given between brackets.

^b $p_b = p_{\text{tot}}G_{\beta\text{CD}}/G_{\text{Fc}}$, (see text and ref. 20).

^c p_b determined from SPR titrations for rapidly equilibrating dendrimers using the surface multivalency model (see text, Table 3.1, and ref. 20).

CPK models provide a coarse indication of the sizes of the dendrimers and of how far the endgroups of one branch or different branches can be maximally spaced in the most extended conformation. The actual sizes and conformations of the dendrimers are strongly dependent on the solvent, pH, and ionic strength.²⁷ Under the present conditions, the dendrimers are forced to adopt a maximally extended conformation for the reason that low pH ensures full

protonation of the core amines and thus the complexation of the maximal amount of β CDs at the surface. Also the dendrimers may change shape upon surface adsorption (Section 4.2.3). Nevertheless, CPK models give a reasonable indication of how the dendrimers may bind the β CD host surface. Chart 1 shows the smallest members of the three different types of dendrimers in the most extended configuration with dimensions estimated from CPK models.

A G_{bCD}/G_{Fc} ratio of 0.56 was found for G1-PPI-(Fc)₄ which implies 2 Fc- β CD interactions with the host surface, while for G0-PAMAM-(Fc)₄ a $G_{\beta CD}/G_{Fc}$ ratio 0.75 was found which indicates 3 interactions. Two Fc moieties at the same branch of a PPI dendrimer are only separated by 1.5 nm and, consequently, cannot interact simultaneously with two b CDs at the molecular printboard, since the center-to-center spacing of two adjacent b CDs at the surface is 2.1 nm which is significantly further apart. On the other hand, two Fc groups of different branches are separated by 2.1 nm and, hence, both can access a β CD site at the surface. Thus, G1-PPI-(Fc)₄ can have only two interactions with the host surface. PAMAM dendrimers consist of longer spacer groups and two adjacent Fc moieties at the same branch are separated by 2.3 nm indicating that both can interact with a b CD at the surface. Two Fc groups of different branches are 2.7 nm separated meaning that a third interaction is feasible, but a fourth is not, since an interaction with the fourth b CD requires a separation of approximately 3.5 nm between two Fc groups (see top view of b CD SAM, Chart 1). Hence, G0-PAMAM-(Fc)₄ can access three β CDs at the molecular printboard, but the spacer groups are not sufficient to have a fourth interaction. G0-PAMAM-EG-(Fc)₄, however, has two Fc groups at the same branch separated by 6.0 nm and of the different branches separated by 6.4 nm indicating that all endgroups can interact with the b CD host surface. For G0-PAMAM-EG-(Fc)₄ a G_{bCD}/G_{Fc} ratio of 1.1 was found indicating that indeed all four endgroups are interacting with the β CD host surface. These findings are in full agreement with the number of interactions found by the SPR titrations, and consistent with the 1:1 peak splitting observed by CV for G1-PPI-(Fc)₄ as described above (Fig. 3.3).

The ratio $\Gamma_{\beta CD}/\Gamma_{Fc}$ for the G1-PAMAM-(Fc)₈ dendrimer was found to be 0.66 and for G2-PAMAM-(Fc)₁₆ 0.52. Thus, G1-PAMAM-(Fc)₈ and G2-PAMAM-(Fc)₁₆ have 5 endgroups (out of 8) and 8 (out of 16) endgroups interacting with β CD host surface, respectively. This is a doubling of the number of interactions compared to the PPI dendrimers, since G2-PPI-(Fc)₈ has only 3 endgroups (out of 8) interacting with surface while G3-PPI-(Fc)₁₆ interacts with 4 out of 16. Apparently, The PAMAM and the PPI dendrimers both have the same number of branches interacting with the surface, but both endgroups of the same branch of a PAMAM dendrimer can interact with the surface causing the increase of the number of interactions. The reason that G1-PAMAM-(Fc)₈ has 5 interactions and not 6 may be due to steric hindrance. The G1-PAMAM-EG-(Fc)₈ has all 4 branches interacting with both endgroups with the surface as a G_{bCD}/G_{Fc} ratio of 1.0 was found. All 8 Fc functionalities apparently are sufficiently spaced and all groups are able to interact with the surface.

For G4-PPI-(Fc)₃₂ and G5-PPI-(Fc)₆₄ the $G_{\beta\text{CD}}/G_{\text{Fc}}$ ratios 0.22, and 0.11, respectively. These values suggest that G4-PPI-(Fc)₃₂ has 7 (out of 32) bound and 25 unbound, and G5-PPI-(Fc)₆₄ has 7 (or 8) (out of 64) bound Fc moieties. For G1-PPI-(Fc)₄ the ratio of 0.56 is significantly higher than the theoretical value of 0.5 for full surface coverage. This indicates that the molecule may slowly desorb from the surface upon rinsing with water. For the other dendrimers, the observed coverages are very close to the theoretical values for full coverage, probably owing to the stronger interactions of the higher generation dendrimers with the surface.

According to CV G1-PAMAM-(Fc)₈ has 5 endgroups interacting with βCD surface and all larger dendrimers have more interactions, meaning that at least 5 interactions are required for the formation of kinetically stable assemblies. This can also be rationalized by the multivalency model which implies that a molecule which has four Fc- βCD interactions with the surface and with 10 mM native βCD in solution present has a K_{surf} in the order of $10^9\sim 10^{10} \text{ M}^{-1}$, and under the same conditions a molecule having 5 interactions has a K_{surf} in the order of $10^{11}\sim 10^{12} \text{ M}^{-1}$. These numbers imply that the desorption rates are too small to be measured with SPR for molecules with 5 or more interactions with the host surface. The higher generation dendrimers, G4-PPI-(Fc)₃₂, G5-PPI-(Fc)₆₄, G2-PAMAM-(Fc)₁₆, and G1-PAMAM-EG-(Fc)₈, which all have more than 5 interactions according to CV, form kinetically stable assemblies at the molecular printboard.

3.2.5 Simultaneous SPR and CV

To gain more insight into the mechanism of the electrochemical desorption process and to demonstrate the full electrochemical binding control of the dendrimers at the host surface, CV was performed and simultaneously the SPR response was measured.²⁸ Combining these two techniques provides information about the efficiency and the desorption rate of the dendrimers upon electrochemical oxidation. Performing CV at a bare βCD SAM left the SPR signal unchanged suggesting that all the observations described below are solely due to changes in the coverage of dendrimers at the surface.

A 0.1 mM (in functionality) solution of G3-PPI-(Fc)₁₆- βCD assembly was added to a βCD SAM in the presence of 10 mM βCD at pH = 2. Immediately after injection the SPR signal increased sharply as the dendrimer adsorbed at the βCD SAM forming a kinetically stable monolayer at the βCD SAM (Figure 3.6). Upon flushing the cell with 10 mM aqueous βCD at pH = 2 a small decrease in signal was observed as non-specifically adsorbed material was removed. Subsequently, CV at a continuous flow of 10 mM βCD at pH = 2 was applied (i.e. with no guest in solution), while recording the SPR signal. While scanning, the dendrimers desorbed from the βCD monolayer, which is reflected in a sharp decrease in the SPR signal to the same value as before guest injection indicating that all dendrimers were removed from the surface upon oxidation. Also, the last CV confirms that all guest molecules were efficiently

removed (not shown). This was repeated another six times demonstrating the reversibility and stability of the system.

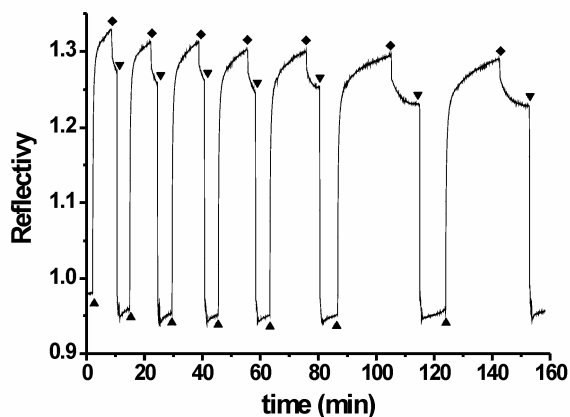


Figure 3.6: SPR response of 7 times an addition of G3-PPI-(Fc)₁₆ followed by rinsing and CV-induced desorption: ▲ = injection of 6.3 μ M aqueous solution of G3-PPI-(Fc)₁₆ with 10 mM β CD at pH = 2; ◆ = rinse with 10 mM aqueous β CD at pH = 2; ▼ = 5 CV scans at 0.1 V/s.

Mechanistic information about the binding of the dendrimers to the surface and of the electrochemically induced desorption was obtained by performing CV and simultaneously measuring the SPR response with the guest present in a stationary solution at the β CD SAM. Under these conditions, the adsorption and desorption processes are limited by diffusion. The same conditions and concentrations were used, as described above, to adsorb G3-PPI-(Fc)₁₆ at the β CD SAM and CV was applied at different v (Figure 3.7).

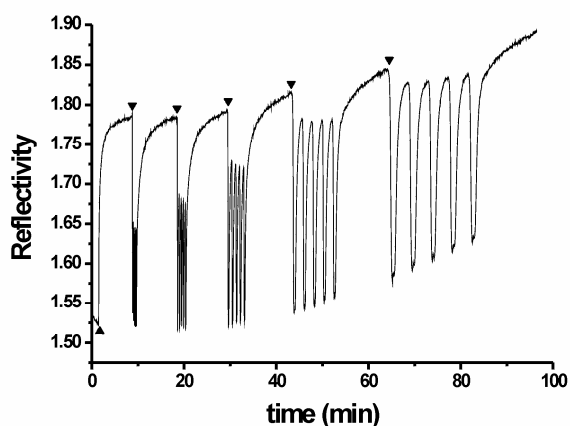


Figure 3.7: SPR response of a β CD SAM with G3-PPI-(Fc)₁₆ in solution while performing CV at different scan rates: ▲ = injection of 6.3 μ M aqueous solution of G3-PPI-(Fc)₁₆ with 10 mM β CD at pH = 2; ▼ = CV 5 scans at 100 V/s, 50 mV/s, 25 mV/s, 10 mV/s, and 5 mV/s from left to right.

Directly before the anodic peak potential (E_{pa}), the dendrimers started to desorb from the monolayer slowly, but just above the E_{pa} virtually all dendrimers were already removed, since all ferrocene groups were oxidized. Further increasing the potential well above E_{pa} left the SPR signal unchanged, as dendrimers binding to the surface from solution will immediately be oxidized, until the potential was lowered below the cathodic peak potential (E_{pc}) during the backward wave. At potentials below E_{pc} adsorbed dendrimers were not oxidized which is reflected in typical adsorption behavior in the SPR response. The dendrimers continued to adsorb at the β CD SAM during the subsequent scan until E_{pa} was reached, and this cycle of adsorption and desorption was repeated as long as CV was performed, and all scans showed the same increase in SPR signal between reduction and oxidation, and a decrease between oxidation and reduction. The amount of dendrimers that can bind to the surface in between two CV cycles is, under these conditions, only dependent on v . At lower values of v , more guest molecules may bind to the β CD SAM during the (longer) time between reduction and oxidation. Most extreme is scanning at 5 mV/s (full right of SPR graph, Figure 3.7) as the time between reduction and oxidation is sufficient to allow the formation of a virtually full monolayer of G3-PPI-(Fc)₁₆ at the β CD SAM between the scans.

Above it was described that below E_{pa} dendrimers bind to the surface, hitherto dendrimers from the bulk solution as well as previously bound reduced dendrimers may both (re)bind to the surface. In order to distinguish between the binding of guest from solution and the amount of rebinding guest molecules, CV was performed without guest in solution while monitoring the SPR response. Again the formation of a SAM of G3-PPI-(Fc)₁₆ at the β CD SAM was followed by SPR under the same conditions as described above and the cell was flushed in order to remove all guest molecules from solution (Figure 3.8, left). During a single CV scan (50 mV/s) all dendrimers were removed just above the E_{pc} as the SPR signals dropped to the original value before guest injection. However, after reduction an increase in SPR signal was observed, which can only be caused by rebinding of reduced dendrimers. Reduced dendrimers may diffuse into solution or may rebind to the β CD SAM and similar behavior was observed during following single scans. Nevertheless, most molecules were removed from the surface during the first scan while after subsequent scans a larger fraction of molecules rebound to the surface. This can be explained by the fact that due to oxidation of all endgroups, a high density of positive charges is created near the surface, as all Fc groups are converted to ferrocenium cations, which may repel each other and, consequently, force the dendrimers into solution. During subsequent scans, however, the degree of bound dendrimers at the surface is lower leading to less repulsion of the oxidized molecules. Performing similar experiments at different v showed exactly the same behavior, but oxidation of higher generations of dendrimers at the surface led to significantly higher charge densities at the surface along with more electrostatic repulsion forcing the dendrimers into solution more efficiently. Similar experiments were performed using G4-PPI-(Fc)₃₂ and G5-PPI-(Fc)₆₄ and the result for G4-PPI-(Fc)₃₂ is shown in Figure 3.8 (right). After the first CV scan, only a relatively small

increase in SPR signal was recorded and after subsequent scans a similar increase in SPR signal was observed. Comparison of the amount of rebinding dendrimers after the first scan in the case of G3-PPI-(Fc)₁₆ (80%) and G4-PPI-(Fc)₃₂ (20%) clearly demonstrates the larger effect of electrostatic repulsion between the oxidized molecules in the latter case.

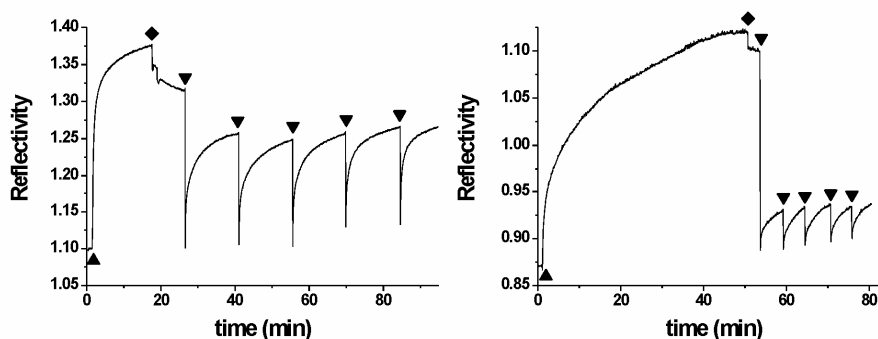
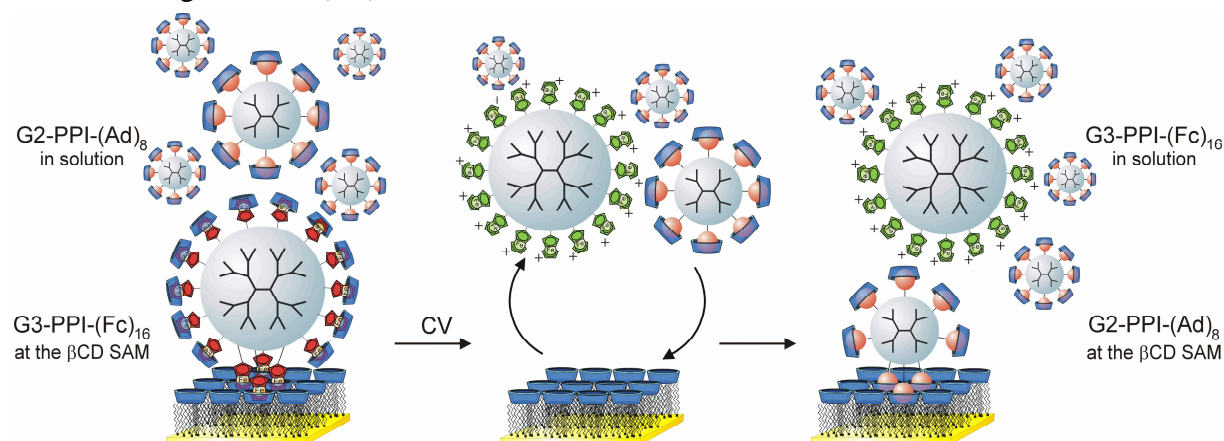


Figure 3.8: SPR response of G3-PPI-(Fc)₁₆ (left) and G4-PPI-(Fc)₃₂ (right) at a β CD SAM while performing 5 single CV: ▲ = injection of 100 μ M (in Fc functionality) aqueous solution of G3-PPI-(Fc)₁₆ or G4-PPI-(Fc)₃₂ with 10 mM β CD at pH = 2; ◆ = wash with 10 mM aqueous β CD at pH = 2; ▼ = single CV scan at 50 mV/s.

G3-PPI-(Fc)₁₆ forms kinetically stable monolayers at the β CD SAM, therefore, other guest molecules are effectively blocked, unless G3-PPI-(Fc)₁₆ is electrochemically removed from the host surface revealing free β CD sites at the surface available for binding of other guest molecules, e.g. G2-PPI-(Ad)₈, as is outlined in Scheme 3.3.



Scheme 3.3. A monolayer of G3-PPI-(Fc)₁₆ at the β CD SAM efficiently blocked the binding of guest molecules from solution, e.g. G2-PPI-(Ad)₈. Only electrochemically induced desorption of G3-PPI-(Fc)₁₆ exposed the free binding sites and G2-PPI-(Ad)₈ can bind to the host surface.

A monolayer of G3-PPI-(Fc)₁₆ was formed at the host surface using the same conditions as described above and the guest from solution was replaced by mixtures of G3-PPI-(Fc)₁₆ and G2-PPI-(Ad)₈ in different ratios. After addition of the mixtures, CV was performed and the results are shown in Figure 3.9 for Fc:Ad ratios of 1:0, 2:1, 1:2 and 0:1 (total concentration of endgroups was 0.1 mM). The advantage of the simultaneous use of SPR and CV is extended

in this case since SPR indicates the total coverage of both types of dendrimers, while the extent of coverage by the electroactive Fc dendrimer is monitored by subsequent CV scans. After the first CV scan all G3-PPI-(Fc)₁₆ were removed, but after reduction both G3-PPI-(Fc)₁₆ and G2-PPI-(Ad)₈ can access the host surface. This is apparent in the SPR sensogram by an increase in signal. Not all material is removed during subsequent CV scans due to the binding of G2-PPI-(Ad)₈ which is not redox active. The most extreme case is that of Fc:Ad ratio of 0:1 (D): all G3-PPI-(Fc)₁₆ was removed during the first scan and the subsequent adsorption of G2-PPI-(Ad)₈ to the surface led to a rapid decrease of redox activity as now only rebinding G3-PPI-(Fc)₁₆ can contribute to a further redox activity. This leads to the conclusion that the binding of G2-PPI-(Ad)₈ can be initiated by electrochemical removal of G3-PPI-(Fc)₁₆. Thus, G3-PPI-(Fc)₁₆ effectively blocks the binding to the βCD SAM, but upon electrochemical removal of the electroactive dendrimer, the βCD SAM may bind guest molecules from solution again. On the other hand, G2-PPI-(Ad)₈ bound to the βCD SAM effectively blocks the electron transfer indicating that ferrocenyl endgroups of the dendrimers only can be oxidized at the βCD SAM if the dendrimers are interacting with the βCD SAM.

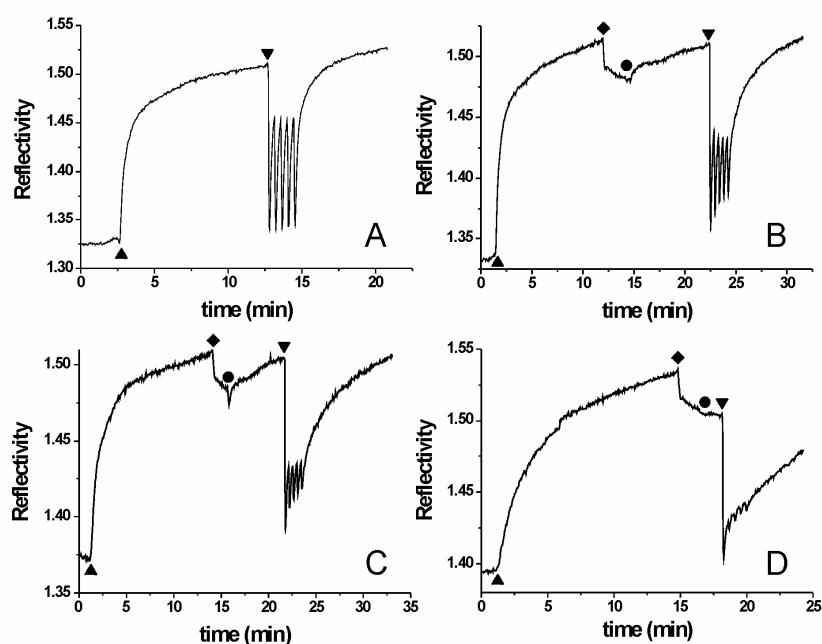


Figure 3.9: SPR response of G3-PPI-(Fc)₁₆ adsorbed at a βCD SAM in a solution with different G3-PPI-(Fc)₁₆:G2-PPI-(Ad)₈ ratios while performing CV ($v = 50$ mV/s); ▲ = injection of 6.3 μM aqueous solution of G3-PPI-(Fc)₁₆ with 10 mM βCD at pH = 2; ◆ = wash with 10 mM aqueous βCD at pH = 2; ▼ = 5 CV scans at 50 mV/s; ● = injection of mixtures of G3-PPI-(Fc)₁₆ and G2-PPI-(Ad)₈ with different Fc:Ad ratios: A) Fc:Ad ratio is 2:0; B) 2:1; C) 1:2 and, D) 0:1 (total endgroup concentration 0.1 mM).

3.3 Conclusions

The observed binding behavior results from multivalency of the dendrimers at the β CD SAMs. Especially the higher generations of dendrimers bind strongly to the host surface and cannot be removed by rinsing with a competitive solvent, e.g. aqueous solutions of 10 mM native β CD, as has been confirmed by SPR. Nevertheless, the electroactive molecules, despite the strong multivalent interactions, could be efficiently removed from the surface in an electrochemical manner, even molecules having 8 Fc- β CD interactions with the host surface.

We have been able to determine the number of interactions of various generations and different types of ferrocenyl-functionalized dendrimers at β CD SAMs. The numbers of interactions increased with increasing dendrimer size and generation, and were quantified by CV and SPR spectroscopy. These findings are in good agreement with the molecular sizes of the dendrimers estimated from CPK models compared to the spacing between the β CD cavities at the surface. Kinetically stable assemblies were obtained if the molecules have at least 5 Fc- β CD interactions, but having 4 interactions or less, the dendrimers could be removed from the host surface by rinsing with competitive aqueous native β CD solutions. Of the lower generation dendrimers not only the number of interactions could be determined, but also thermodynamic data could be obtained.

Measuring CV and SPR simultaneously gave valuable mechanistic information about the electrochemically induced desorption. All dendrimers were removed from the surface instantly at potentials above E_{pa} . At potentials lower than E_{pc} , dendrimers from the bulk solution, as well as reduced dendrimers, bind to the surface. The amount of rebinding is strongly dependent on the generation, since higher generation dendrimers produce a high density of cationic charges close to the surface, that causes electrostatic repulsions between the oxidized dendrimers and, therefore, forces the dendrimers to diffuse into solution rather than reside in close proximity to the surface. In the case of lower generations, the electrostatic repulsion is less pronounced leading to diffusion-controlled rebinding of the dendrimers.

Fc dendrimers that form kinetically stable monolayers at the β CD SAMs were used to block the binding sites of the β CD printboard, but upon electrochemical release of the dendrimers, guest molecules can bind to the clean β CD SAM. This concept is potentially useful in bottom-up nanofabrication as a supramolecular shadow mask to block the binding molecules locally followed by electrochemically induced release of the blocking layer.

3.4 Experimental Section

General Procedures. All moisture sensitive reactions were carried out under argon atmosphere. Reagents were commercial and used without further purification. All dry solvents were prepared according to standard procedures and stored over molecular sieves. ^1H NMR

and ^{13}C NMR spectra were recorded on Bruker AC300 or Bruker AMX400 spectrometers. Spectra are reported in ppm downfield from TMS as internal standard. Matrix-Assisted Laser Desorption Ionization (MALDI) Time-of-Flight (TOF) mass spectra were recorded using a Perkin Elmer/PerSeptive Biosystems Voyager-DE-RP MALDI-TOF mass spectrometer. Analytical TLC was performed using Merck prepared plates (silica gel 60 F-254 on aluminum). Merck silica gel (40-63 μm) was used for flash chromatography. Column chromatography was performed using silica gel (SiO_2 , E. Merck, 0.040-0.063 mm, 230-240 mesh). The ferrocenyl PPI dendrimers¹⁷ and the adamantyl PPI dendrimers²⁹ were prepared according to a literature procedures.

Synthesis

G0-PAMAM-(Fc)₄. The amine-terminated dendrimers were received as a solution in methanol, and prior to use the methanol was removed in vacuo for prolonged period of times. To a solution of amine-terminated G0-PAMAM dendrimer (0.20 g, 0.38 mmol) in DMSO an excess of triethylamine was added and six equivalents of 1-(chlorocarbonyl)ferrocene (0.58 g, 2.3 mmol). The reaction mixture was allowed to stir overnight at room temperature under argon. After removal of the solvent in vacuo the reaction mixture was dissolved in CHCl_3 and washed three times with aqueous saturated NaHCO_3 solution, brine and dried over MgSO_4 . The product was purified by repeated precipitation from CHCl_3 /hexane and isolated as an orange solid, yield (0.39 g, 75 %). ^1H NMR (300 MHz, CDCl_3) δ (ppm): 8.1 (b, 4H, NHCO), 7.5 (b, 4H, NHCO), 7.1 (b, 4H, NH), 6.5 (bt, 1H, NH), 4.7 (8H, t, Fc), 4.3 (8H, t, Fc), 4.2 (20H, Fc), 3.5-3.8 (40H, m, $\text{OCH}_2\text{CH}_2\text{O}$, $\text{OCH}_2\text{CH}_2\text{NHCO}$ and $\text{OCH}_2\text{CH}_2\text{NCS}$), 3.4 (8H, b, dendr), 2.7 (8H, b, dendr), 2.6 (8H, b, dendr), 2.4 (8H, b, dendr). ^{13}C NMR (100 MHz, $\text{MeOD} + \text{DCI}$ (20% DCI in D_2O)) δ (ppm): 172.74 (CO), 172.28 (CO), 75.38, 70.70 (Fc), 69.73 (Fc), 68.31 (Fc), 49.26, 39.42, 38.92, 30.72. MALDI TOF MS Cald. for $\text{C}_{66}\text{H}_{80}\text{N}_{10}\text{Fe}_4\text{O}_8$: $m/z = 1364.4$, Found: $m/z = 1366.1$ [M+H].

G1-PAMAM-(Fc)₈. Same procedure as described for G0-PAMAM-(Fc)₄ but then using 0.20 g (0.14 mmol) of the amine-terminated G1-PAMAM dendrimer and 12 equivalents of 1-(chlorocarbonyl)ferrocene (0.42 g, 1.7 mmol). Yield: (0.28 g, 63%). ^1H NMR (300 MHz, CDCl_3) δ (ppm): 7.7 (b, 8H, NH), 4.7 (16H, s, Fc), 4.3 (16H, s, Fc), 4.2 (40H, Fc), 3.5-3.8 (40H, m, $\text{OCH}_2\text{CH}_2\text{O}$, $\text{OCH}_2\text{CH}_2\text{NHCO}$ and $\text{OCH}_2\text{CH}_2\text{NCS}$), 3.4 (8H, b, dendr), 2.7 (8H, b, dendr), 2.6 (8H, b, dendr), 2.4 (8H, b, dendr). ^{13}C NMR (100 MHz, CDCl_3) δ (ppm): 173, 73 (CO), 172.37 (CO), 171.70 (CO), 75.76, 70.60 (Fc), 68.81 (Fc), 68.41 (Fc), 52.40, 50.48, 49.70, 40.10, 39.56, 37.62, 34.19, 33.13. MALDI TOF MS Cald. for $\text{C}_{150}\text{H}_{192}\text{N}_{26}\text{Fe}_8\text{O}_{20}$: $m/z = 3125.0$, Found: $m/z = 3150.1$ [M+H] and 3165.8 [M+K].

G2-PAMAM-(Fc)₁₆. Same procedure as described for G0-PAMAM-(Fc)₄ but then using 0.50 g (0.15 mmol) of the amine terminated G2-PAMAM dendrimer and 12 equivalents 1-(chlorocarbonyl) ferrocene (0.91 g, 3.6 mmol). Yield: (0.47 g, 47%). ^1H NMR (300 MHz, CDCl_3) δ (ppm): 7.9 (b, 4H, NHCONH), 7.5 (b, 4H, NHCONH), 7.1 (b, 4H, NH), 6.5 (bt, 1H, NH), 4.7 (8H, t, Fc), 4.3 (8H, t, Fc),

4.2 (20H, Fc), 3.5-3.8 (40H, m, OCH₂CH₂O, OCH₂CH₂NHCO and OCH₂CH₂NCS), 3.4 (8H, b, dendr), 2.7 (8H, b, dendr), 2.6 (8H, b, dendr), 2.4 (8H, b, dendr). ¹³C NMR (100 MHz, CDCl₃ + MeOD) δ (ppm): 174.00 (CO), 173.11 (CO), 172.04 (CO), 75.86, 70.85 (Fc), 70.02 (Fc), 68.59 (Fc), 52.59, 50.51, 40.06, 39.55, 37.63, 34.24, 33.18. MALDI TOF MS Cald. for C₃₁₈H₄₀₀N₅₈Fe₁₆O₄₄: *m/z* = 6632, Found: *m/z* = 6655 [M+Na].

1,11-Diphthalimido-3,6,9-trioxoundecane (2). Same procedure as reported by others, but using with tetra(ethylene glycol) di-*p*-tosylate (50 g, 99 mmol) instead of the 1,11-dichloro-3,6,9-trioxoundecane.³⁰ Yield: 31 g (71%). ¹H NMR (300 MHz, CDCl₃) δ (ppm): 7.84 (dd, 4H), 7.10 (dd, 4H), 3.88 (t, 4H, CH₂N, *J* = 5.7 Hz), 3.70 (t, 4 H, CH₂CH₂N, *J* = 5.7 Hz), 3.51-3.59 (m, 8 H). ¹³C NMR (400 MHz, CDCl₃) δ (ppm): 168.46 (CO), 134.10, 132.38, 123.44, 70.78, 70.27, 78.09, 37.47 (CH₂N). MALDI TOF MS Cald. for C₁₉H₂₈N₂FeO₄: *m/z* = 404.1, Found: *m/z* = 405.1 [M+H]. MALDI TOF MS Cald. for C₂₄H₂₄N₂O₇: *m/z* = 452.2, Found: *m/z* = 453.5 [M+H].

1,11-Diamino-3,6,9-trioxoundecane (3). Same procedure as described by others but using **2** (31 g, 0.070 mmol). ¹H NMR (300 MHz, CDCl₃) δ (ppm): 3.51-3.59 (m, 8 H), 3.51 (t, 4H, CH₂CH₂NH₂, *J* = 5.3 Hz), 2.86 (t, 4 H, CH₂NH₂, *J* = 5.3 Hz), 1.41 (b, 2H, NH₂). ¹³C NMR (100 MHz, CDCl₃) δ (ppm): 73.53, 70.47, 70.43, 41.87 (CH₂NH₂). MALDI TOF MS Cald. for C₈H₂₀N₂O₃: *m/z* = 192.3, Found: *m/z* = 193.1 [M+H].

Ferrocenyl ethylene glycol amine (4). To a solution of 1.1 equivalent 1,11-diamino-3,6,9-trioxoundecane **2** (2.4 g, 13 mmol) and excess of triethylamine in CHCl₃ was added dropwise to a solution of one equivalent of 1-(chlorocarbonyl)ferrocene (3.0 g, 12 mmol) in CHCl₃. After addition the reaction mixture was stirred for an additional 15 min at room temperature. The reaction mixture was washed three times with saturated aqueous NaHCO₃ solution, brine and dried over MgSO₄. The product was purified by column chromatography over silica, eluent 5% MeOH/ 95% CH₂Cl₂ to 10% MeOH/ 90% CH₂Cl₂ to 10% MeOH/ 89% CH₂Cl₂/ 1% Et₃N, and isolated as a dark red/orange oil (1.5 g, 39.1%). ¹H NMR (300 MHz, CDCl₃) δ (ppm): 6.55 (bt, 1H, CONH), 4.7 (t, 2H, Fc, *J* = 2.2 Hz), 4.33 (2H, t, Fc, *J* = 2.2 Hz), 4.22 (s, 5H, Fc), 3.7-3.8 (m, 10H, OCH₂CH₂O and OCH₂CH₂NH₂), 3.61 (t, 2H, CH₂CH₂NHCO, *J* = 5.3), 3.56 (t, 2H, OCH₂CH₂NH₂, *J* = 4.7 Hz), 2.9 (2H, t, CH₂NH₂, *J* = 4.9 Hz), 2.17 (br, 2H, NH₂); ¹³C NMR (100 MHz, CDCl₃) δ (ppm): 170.27 (CO), 76.20, 72.26, 70.47, 70.43, 70.34, 70.20, 70.01, 69.78 (Fc), 68.35, 41.40 (CH₂NH), 39.35 (CH₂NH₂). MALDI TOF MS Cald. for C₁₉H₂₈N₂FeO₄: *m/z* = 404.1, Found: *m/z* = 405.1 [M+H].

Ferrocenyl ethylene glycol isothiocyanate (5). To a mixture of **4** (1.0 g, 2.5 mmol) and K₂CO₃ in CHCl₃ was added 10 equivalents of thiophosgene (25 mmol), and the reaction mixture was stirred at room temperature for 1 h. After filtration the volatiles were removed in vacuo and the product was purified by column chromatography, elent 5% MeOH/ 95% CH₂Cl₂, and isolated as a dark red/orange oil (0.94 g, 89.5%). ¹H NMR (300 MHz, CDCl₃) δ (ppm): 6.19 (bt, 1H, CONH), 4.68 (t, 2H, Fc, *J* = 2.0 Hz), 4.3 (t, 2H, Fc, *J* = 2.0 Hz), 4.2 (s, 5H, Fc), 3.7-3.8 (m, 10H, OCH₂CH₂O, OCH₂CH₂NHCO and OCH₂CH₂NCS), 3.60 (t, 2H, CH₂CH₂NHCO, *J* = 6.1 Hz). ¹³C NMR (100 MHz, CDCl₃) δ (ppm): 170.26 (CO), 132.65 (NCS), 76.19, 70.70, 70.56, 70.48, 70.20, 70.04, 69.62 (Fc), 69.23, 68.10, 45.24

(CH₂NH), 39.19 (CH₂NCS). MALDI TOF MS Cald. for C₂₀H₂₆N₂FeO₄S: m/z = 446.4, Found: m/z = 447.1 [M+H].

G0-PAMAM-EG-(Fc)₄. To a solution of the amine-terminated G0-PAMAM in CHCl₃/methanol were added 6 equivalents of **5** and the reaction mixture was stirred overnight. The excess of **5** was removed by column chromatography, eluent 10% MeOH/ 90% CH₂Cl₂ to 10% MeOH/ 89% CH₂Cl₂/ 1% Et₃N and isolated as a dark red/orange oil (0.40 g, 59%). ¹H NMR (300 MHz, CDCl₃) δ (ppm): 7.9 (b, 4H, NHCONH), 7.5 (b, 4H, NHCONH), 7.1 (b, 4H, NH), 6.5 (bt, 1H, NH), 4.7 (8H, t, Fc), 4.3 (8H, t, Fc), 4.2 (20H, Fc), 3.5-3.8 (40H, m, OCH₂CH₂O, OCH₂CH₂NHCO and OCH₂CH₂NCS), 3.4 (8H, b, dendr), 2.7 (8H, b, dendr), 2.6 (8H, b, dendr), 2.4 (8H, b, dendr). ¹³C NMR (100 MHz, CDCl₃) δ (ppm): 181.26 (NHCSNH), 172.74 (CO), 172.28 (CO), 77.49 76.19, 70.72, 70.41, 70.21, 70.36 (Fc), 69.51, 68.10, 49.24 (CH₂NH), 45, 45, 39.59 (CH₂NCS), 39.59, 31.77. MALDI TOF MS Cald. for C₁₀₂H₁₅₂N₁₈Fe₄O₂₀S₄: m/z = 2300.8, Found: m/z = 2302.0 [M+H].

G1-PAMAM-EG-(Fc)₈. Same as described for G0-PAMAM-EG-(Fc)₄ but using (94 mg, 0.066 mmol) of the amine-terminated G1-PAMAM and 12 equivalents of **5** (0.35 g, 0.79 mmol). Yield: (0.11 g, 32%). ¹H NMR (300 MHz, CDCl₃) δ (ppm): 7.9 (b, 4H, NHCONH), 7.5 (b, 4H, NHCONH), 7.1 (b, 4H, NH), 6.5 (bt, 1H, NH), 4.7 (8H, t, Fc), 4.3 (8H, t, Fc), 4.2 (20H, Fc), 3.5-3.8 (40H, m, OCH₂CH₂O, OCH₂CH₂NHCO and OCH₂CH₂NCS), 3.4 (8H, b, dendr), 2.7 (8H, b, dendr), 2.6 (8H, b, dendr), 2.4 (8H, b, dendr). ¹³C NMR (100 MHz, CDCl₃) δ (ppm): 183.29 (NHCSNH), 172.74 (CO), 171.03 (CO), 77.46 76.21, 70.75, 70.43, 70.21, 70.07 (Fc), 69.85, 68.53, 52.79 (CH₂NH), 50.67, 44.53, 39.62 (CH₂NCS), 39.60, 39.85. MALDI TOF MS Cald. for C₂₂₂H₃₃₆N₄₂Fe₈O₄₄S₈: m/z = 4999.8, Found: m/z = 5007 [M+H].

Materials and methods. All glassware used to prepare monolayers was immersed in piranha solution (conc. H₂SO₄ and 33% H₂O₂ in a 3:1 ratio). (Warning: piranha should be handled with caution; it can detonate unexpectedly). Next, the glassware was rinsed with large amounts of Milli-Q water. All adsorbate solutions were prepared prior to use. All solvents used in monolayer preparation were of p.a. grade.

Substrate preparation. Glass-supported gold substrates for SPR and for electrochemistry (2.54 cm diameter; 47.5 nm and 200 nm metal thickness, respectively, with a 2 nm titanium adhesion layer) were obtained from SSENS bv (Hengelo, The Netherlands). Gold substrates were cleaned by brief immersion in piranha³¹ and the resulting oxide layer was removed by leaving the substrates for 10 min in absolute EtOH. The substrates were subsequently immersed in the adsorbate solution (0.1-1 mM) for ca. 16 h at 60°C. Next, the samples were removed from the solutions and rinsed thoroughly with chloroform, ethanol, and Milli-Q water. Adsorption of the dendrimers was carried out by immersing a preformed β CD SAM on Au in an aqueous solution of the corresponding dendrimer- β CD assemblies solutions (0.1 or 1.0 mM in ferrocene functionality in the presence of 11 mM β CD at pH = 2) for at least 1 h. Subsequently the samples were thoroughly rinsed with Milli-Q water (at pH = 2 to ensure full protonation of the amines) and dried in a stream of N₂.

Surface Plasmon Resonance Spectroscopy. SPR measurements were performed in a two-channel vibrating mirror angle scan set-up based on the Kretschmann configuration, described by Kooyman *et al.*³² Light from a 2 mW HeNe laser is directed onto a prism surface by means of a vibrating mirror. The intensity of the light is measured by means of a large-area photodiode. This set-up allows determination of changes in plasmon angle with an accuracy of 0.002°. The gold substrate with the monolayer was optically matched to the prism using an index matching oil. A Teflon cell was placed on the monolayer *via* an O-ring, to avoid leakage, and filled with 800 μL of βCD buffer solution at the same concentration as in the guest solution. After stabilization of the SPR signal, titrations were performed by removing an amount of solution from the cell and by adding the same amount of a 50 μM stock solution (in ferrocene functionality) of G2-PPI-(Fc)₈, G0-PAMAM-(Fc)₄, and G1-PAMAM-EG-(Fc)₄, in the presence of 10 mM βCD at pH = 2. Between additions of the dendrimers the cell was thoroughly washed with 10 mM native βCD solution (700 μL , 3 times) and again 200 s later. Then a solution of 10 mM βCD at pH = 2 in Milli-Q water was added to a final volume of 800 μL to restore the proper buffer concentration. For G1-PPI-(Fc)₄ a stock solution of 0.1 M (in ferrocene functionality) in the presence of 0.11 mM βCD at pH = 2. Between additions of the G1-PPI-(Fc)₄ the cell was thoroughly washed with 10 mM native βCD solution (700 μL , 5 times) and then a solution of 0.11 mM βCD at pH = 2 in Milli-Q water was added to a final volume of 800 μL to restore the proper buffer concentration. The SPR measurements were repeated 3 times.

Electrochemistry. Electrochemical measurements were performed with an AUTOLAB PGSTAT10, in a custom built three-electrode setup equipped with a platinum counter electrode, a mercury sulfate reference electrode ($V_{\text{MSE}} = +0.61 V_{\text{NHE}}$) and a screw cap holding the gold working electrode (area exposed to the solution = 0.44 cm^2). Cyclic voltammograms were recorded in an aqueous solution 0.1 M K_2SO_4 , between $-0.35 V_{\text{MSE}}$ and $0.25 V_{\text{MSE}}$ or $0.35 V_{\text{MSE}}$, at scan rates of 10, 25, 50, 100 and 200 mV/s.

Electrochemistry and SPR combined. The electrochemistry SPR setup is very similar to that described earlier by the group of Knoll.²⁸ The SPR setup in the Kretschmann configuration was obtained from Resonant Probes GmbH. The beam of a NeHe laser (JDS Uniphase, 10 mW, $\lambda = 633$ nm) passes through a chopper that is connected to a lock-in amplifier (EG&G, 7256). The modulated beam then passes through two polarizers (Owis) by which the intensity and the plane of polarization of the laser can be adjusted. Then the beam is reflected off the base of the coupling prism (Scott, LASFN9) and is focused by a lens (50 mm, Owis) into a photodiode detector.

The glass supported Au SPR substrates at the prism were clamped against a Teflon cuvette with O-rings providing a liquid-tight seal. The CVs were performed with an AUTOLAB PGSTAT10 in a three-electrode setup with the Au SPR substrates at the prism as the working electrode, a Ag/AgCl reference electrode and a platinum wire as counter electrode. The CV induced desorption processes on gold were detected by monitoring reflectivity changes as a function of time at a fixed incident angle, θ .

3.6 References

- 1) (a) Joachim, C.; Gimzewski, J. K.; Aviram, A. *Nature* **2000**, *408*, 541. (b) Tour, J. M. *Acc. Chem. Res.* **2000**, *33*, 791.
- 2) (a) Mehta, A. D.; Rief, M.; Spudich, J. A. *Science* **1999**, *283*, 1689. (b) Weiss, S. *Science* **1999**, *283*, 1676.
- 3) Schneider, H. J.; Yatsimirsky, A. K. *Principles and Methods in Supramolecular Chemistry*, John Wiley & Sons Ltd: Chichester, **2000**.
- 4) Mammen, M.; Choi, S.-K.; Whitesides, G. M. *Angew. Chem. Int. Ed.* **1998**, *37*, 2754.
- 5) Banerjee, I. A.; Yu, L.; Matsui, H. *J. Am. Chem. Soc.* **2003**, *125*, 9542.
- 6) Huskens, J.; Deij, M. A.; Reinhoudt, D. N. *Angew. Chem. Int. Ed.* **2002**, *41*, 4467.
- 7) (a) Dietrich, C.; Schmitt, L.; Tampe, R. *Proc. Natl. Acad. Sci. U.S.A.* **1995**, *92*, 9014. (b) Thess, A.; Hutschenreiter, S.; Hofmann, M.; Tampé, R.; Baumeister, W.; Guckenberger, R. *J. Biol. Chem.* **2002**, *277*, 36231.
- 8) Auletta, T.; Dordi, B.; Mulder, A.; Sartori, A.; Onclin, S.; Bruinink, C. M.; Péter, M.; Nijhuis, C. A.; Beijleveld, H.; Schönherr, H.; Vancso, G. J.; Casnati, A.; Ungaro, R.; Ravoo, B. J.; Huskens, J.; Reinhoudt, D. N. *Angew. Chem. Int. Ed.* **2004**, *43*, 369.
- 9) (a) Beulen, M. J. W.; Bügler, J.; Lammerink, B.; Geurts, F. A. J.; Biemond, E. M. E. F.; Leerdam, K. G. C.; Van Veggel, F. C. J. M.; Engbersen, J. F. J.; Reinhoudt, D. N. *Langmuir*, **1998**, *14*, 6424. (b) Beulen, M. J. W.; Bügler, J.; De Jong, M. R.; Lammerink, B.; Huskens, J.; Schönherr, H.; Vancso, G. J.; Boukamp, B. A.; Wieder, H.; Offenhäuser, A.; Knoll, W.; Van Veggel, F. C. J. M.; Reinhoudt, D. N. *Chem. Eur. J.* **2000**, *6*, 1176.
- 10) (a) Tomalia, D. A. *Prog. Polym. Sci.* **2005**, *30*, 294. (b) Chase, P. A.; Klein Gebbink, R. J. M.; Van Koten, G. *J. Organometal. Chem.* **2004**, *689*, 4016. (c) Bosman, A. W.; Janssen, H. M.; Meijer, E. W. *Chem. Rev.* **1999**, *99*, 1665.
- 11) Boas, U.; Heegaard, M. H. *Chem. Soc. Rev.* **2004**, *33*, 43.
- 12) Balzani, V.; Ceroni, P.; Maestri, M.; Vicinelli, C. S. V. *Top. Curr. Chem.* **2003**, *228*, 159.
- 13) Twyman, L. J.; King, A. S. H.; Martin, I. K. *Chem. Soc. Rev.* **2002**, *31*, 69.
- 14) (a) Daniel, M.-C.; Ruiz, J.; Nlate, S.; Blais, J.-C.; Astruc, D. *J. Am. Chem. Soc.* **2003**, *125*, 2617. (b) Ong, W.; Gomez-Kaifer, M.; Kaifer, A. E. *Chem. Commun.* **2004**, 1677.
- 15) (a) Michels, J. J.; Huskens, J.; Reinhoudt, D. N., *J. Chem. Soc., Perkin Trans. 2* **2002**, 102. (b) Crooks, R. M.; Lemon III, B. I.; Sun, Lee L.; Yeung, K.; Zhao, M. *Topics Curr. Chem.* **2001**, *212*, 81.
- 16) Kaifer, A. E. *Acc. Chem. Res.* **1999**, *32*, 62.
- 17) Cuardo, I.; Morán, M.; Casado, C. M.; Alonso, B.; Lobete, F.; García, B.; Ibisate, M.; Losada, J. *Organometallics* **1996**, *15*, 5278.
- 18) Michels, J. J.; Baars, M. W. P. L.; Meijer, E. W.; Huskens, J.; Reinhoudt, D. N. *J. Chem. Soc., Perkin. Trans. 2* **2000**, 1914.
- 19) Castro, R.; Cuadrado, I.; Alonso, B.; Casado, C. M.; Morán, M.; Kaifer, A. E. *J. Am. Chem. Soc.* **1997**, *119*, 5760.
- 20) Huskens, J.; Mulder, A.; Auletta, T.; Nijhuis, C. A.; Ludden, M. J. W.; Reinhoudt, D. N. *J. Am. Chem. Soc.* **2004**, *126*, 6784.
- 21) Knoll, W. *Ann. Rev. Phys. Chem.* **1998**, *49*, 569.
- 22) Mulder, A.; T. Auletta, T.; Sartori, A.; Del Ciotto, S.; Casnati, A.; Ungaro, R.; Huskens, J.; Reinhoudt, D. N. *J. Am. Chem. Soc.* **2004**, *126*, 6627.
- 23) De Jong, M. R.; Huskens, J.; Reinhoudt, D. N. *Chem. Eur. J.* **2001**, *7*, 4164.
- 24) (a) Newkome, G. R.; He, E.; Moorefield, C. N. *Chem. Rev.* **1999**, *99*, 1689. (b) Cuardo, I.; Morán, M.; Casado, C. M.; Alonso, B.; Losada, J. *Coord. Chem. Rev.* **1999**, *193-105*, 395.

- 25)(a) Nlate, S.; Ruiz, J.; Blais, J.-C.; Astruc, D. *Chem. Commun.* **2000**, 417. (b) Green, S. J.; Pietron. J. J.; Stokes, J. J.; Hostetler, M. J.; Vu, H.; Wuelfing, W. P.; Murray, R. W. *Langmuir* **1998**, *14*, 5612
- 26) Bard, A. J.; Faulkner, L. R. *Electrochemical Methods: Fundamentals and Applications* John Wiley & Sons: New York, **2001**.
- 27) Ballouff, M.; Likos, C.N. *Angew. Chem. Int. Ed.* **2004**, *43*, 2998.
- 28)(a) Xia, C.; Advincula, R. C.; Baba, A.; Knoll, W. *Langmuir* **2002**, *18*, 3555. (b) Baba, A.; Park, M.-K.; Advincula, R. C.; Knoll, W. *Langmuir* **2002**, *18*, 4648. (c) Baba, A.; Advincula, R. C.; Knoll, W. *J. Phys. Chem. B* **2002**, *106*, 1581. (d) Aust, E. F.; Ito, S.; Sawondny, M.; Knoll, W. *Trends Polym. Sci.* **1994**, *2*, 313.
- 29) Baars, M. W. P. L.; Karlsson, A. J.; Sorokin, V.; de Waal, B. F. W.; Meijer E. W. *Angew. Chem. Int. Ed.* **2000**, *39*, 4262.
- 30) Ciuffarin, E.; Isola, M.; Leoni, P. *J. Org. Chem.* **1981**, *46*, 3064.
- 31) Dobbs, D. A.; Bergman, R. G.; Theopold, K. H. *Chem. Eng. News* **1990**, *68*, 2.
- 32) Lenferink, A. T. M.; Kooyman, R. P. H.; Greve, J. *Sens. Actuators B* **1991**, *3*, 261.

Electrochemistry of Ferrocenyl Dendrimer – β -Cyclodextrin Assemblies in Solution in Contact with molecular printboards

In the previous chapter an in-depth analysis of the adsorption and the stability of ferrocenyl-(Fc-) functionalized dendrimers at the molecular printboard was given. The present chapter shows the detailed electrochemistry of the dendrimers present in solution and adsorbed at the molecular printboard. Scan rate-dependent cyclic voltammetry revealed that β CD SAM-decorated Au electrodes induce a drastic change of the electrochemical behavior of the Fc dendrimers of generations 1 to 5 compared to bare Au electrodes. At the host surface, the strong binding of the dendrimers dominates the electrochemical behavior. Electrochemical impedance spectroscopy allowed to describe the system in terms of an equivalent circuit revealing detailed information of the electron transfer processes, the diffusion behavior of the dendrimers, and the shape of the dendrimers adsorbed at the host surface as well as in solution.

4.1 Introduction

In the previous chapter the multivalency¹ of redox-active dendrimers at the molecular printboard² were studied in detail. Also, the electrochemically induced desorption of the ferrocenyl- (Fc-) functionalized dendrimers at the host surface was shown unambiguously. This chapter describes a detailed electrochemical study of solutions of the five generations of PPI dendrimers bearing Fc moieties in equilibrium with β -cyclodextrin (β CD) SAM-decorated Au electrodes, by scan rate-dependent cyclic voltammetry (CV) and electrochemical impedance spectroscopy (EIS).

In chapter 2 the electrochemistry of Fc- and cobaltocenium- (Cob⁺-) functionalized dendrimers was introduced as well as their electrochemical behavior in aqueous solution in the presence of β CD.³ Kaifer et al. reported Fc dendrimer- β CD complexes in neutral aqueous solutions up to generation 3.⁴ More detailed studies were reported on monovalent Fc- and Cob⁺- β CD inclusion complexes.⁵ The electrochemical characterizations were all based entirely on DC methods such as CV.

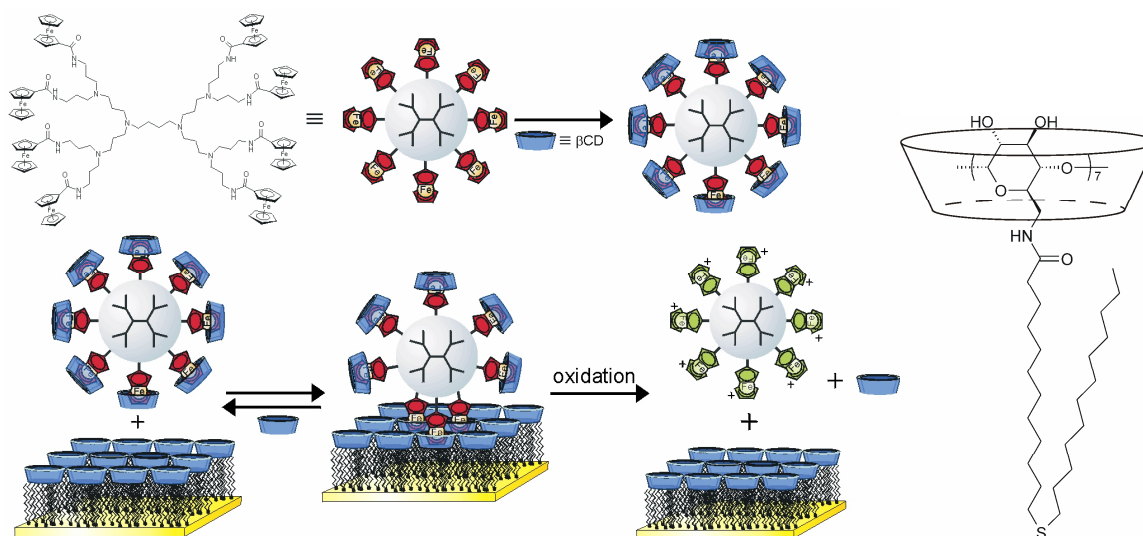
EIS is a powerful technique which has been used in corrosion studies,⁶ processes in fuel cells,⁷ solar cells,⁸ (bio)sensors,⁹ and to study processes of biomolecules.¹⁰ A major advantage of EIS compared to other electrochemical techniques is that it allows the characterization of the system in thermodynamic equilibrium. However, to date there are only a few examples in which EIS was employed in supramolecular studies.¹¹ In this chapter a detailed analysis is given of the electrochemistry of Fc dendrimers in the electrolyte solution in equilibrium with the β CD SAM-decorated Au electrodes by CV and potential-dependent EIS. Dendrimers desorb electrochemically from the molecular printboard can be replaced by dendrimers from solution. Scan rate-dependent CV revealed rebinding phenomena of dendrimers at the molecular printboard and EIS gave more detailed data about the processes in different time domains. The aim was to obtain a description of the system in terms of an equivalent circuit and to reveal detailed information about the desorption processes, electron transfer processes, binding conformations of the dendrimers at the host surface, and diffusion phenomena.

4.2 Results and discussion

4.2.1 Cyclic voltammetry and differential pulse voltammetry

Five generations (G1 to G5) of ferrocenyl- (Fc-) functionalized poly(propylene imine) (PPI) dendrimers were synthesized according to a literature procedure.^{3a} Complexation of the end groups to native β CD resulted in water-soluble dendrimer- β CD assemblies (Scheme 4.1). The complexation of all Fc moieties to β CD up to generation 4 was proven by cyclic voltammetry. G5-PPI-(Fc)₆₄ can only complex up to about 40 β CDs (Table 4.1) (see below). As described in chapter 3, SPR and CV data showed that the dendrimers form densely packed monolayers

at the β CD SAM and the number of interacting end groups (p_b) could be determined for all generations (Table 4.1). At neutral pH, the solubility of the dendrimer- β CD assemblies decreased rapidly with increasing generation.⁴ However, at pH = 2, aqueous solutions could be prepared up to generation 4 of 10 mM in Fc functionality and G5-PPI-(Fc)₆₄ up to 2 mM in Fc functionality.



Scheme 4.1: Schematic of the formation of water soluble dendrimer- β CD assemblies shown for G2 (top) and its adsorption at the β CD host surface and the electrochemically induced desorption (bottom). The molecular structure of the β CD adsorbate is shown on the right.

Table 4.1: Properties of the Fc PPI dendrimers: binding stoichiometry, p_b , at the β CD host surface and to β CD in solution, formal oxidation potentials at bare Au electrodes and at a β CD SAM determined by DPV, and the diameter of the dendrimer estimated from CPK models.

	Number of interactions (p_b) ^a	Stoichiometry in solution ^b	$E^{0'}$ (at bare Au)	$E^{0'}$ (at β CD SAM)	diameter (nm) ^d
G1-PPI-(Fc) ₄	2	4	136	145	1.7
G2-PPI-(Fc) ₈	3	8	135	151	2.8
G3-PPI-(Fc) ₁₆	4	16	145	159	3.9
G4-PPI-(Fc) ₃₂	7	32	190 ^d	163	5.0
G5-PPI-(Fc) ₆₄	7 (or 8)	~40	194 ^c	208 (129) ^f	6.1

^a Section 3.2.4.

^b determined by CV and DPV.

^c derived from CPK models (see chapter 3).

^d a post-wave is visible due to strong adsorption of reactant.

^e a post-wave and a pre-wave are visible due to strong adsorption of reactant and partial complexation of the Fc end groups, respectively.

^f the oxidation potential between brackets refers to $E^{0'}$ of non-complexed Fc end groups.

The interaction of the five generations of dendrimer- β CD assemblies in aqueous solutions with β CD SAMs at Au was characterized by CV and differential pulse voltammetry (DPV) and compared to bare Au electrodes. DPV has the advantage over CV that charging currents can be discriminated against Faradaic currents because charging currents decay more rapidly than Faradaic currents.¹⁴ DPV uses fixed potential pulses of a small amplitude superimposed on a slowly changing bias. The current is measured just before and at the end of the pulse to allow nonfaradaic currents to decay. The two currents are subtracted and plotted versus the potential. The differential pulse voltammograms for G1-PPI-(Fc)₄ and G5-PPI-(Fc)₆₄ at a β CD SAM and a bare Au electrode are shown in Figure 4.1. The formal oxidation potentials $E^{0'}$ of all generations were determined by DPV using $E^{0'} = E_p - \Delta E/2$ ($\Delta E = 10$ mV), and are given in Table 4.1. At bare electrodes, the $E^{0'}$ for G1-PPI-(Fc)₄ and for G2-PPI-(Fc)₈ are similar, but $E^{0'}$ increases for G3-PPI-(Fc)₁₆, G4-PPI-(Fc)₃₂, and G5-PPI-(Fc)₆₄. Differential pulse voltammograms of the dendrimer- β CD assemblies at bare Au electrodes showed one oxidation wave for G1-PPI-(Fc)₄, G2-PPI-(Fc)₈, G3-PPI-(Fc)₁₆, and G4-PPI-(Fc)₃₂, while a prewave is present in the case of G5-PPI-(Fc)₆₄ which is due to the non-complexed Fc moieties. This was also observed in CV experiments and is in agreement with a previous ¹H NMR study of adamantyl- (Ad-) functionalized dendrimer- β CD assemblies.¹²

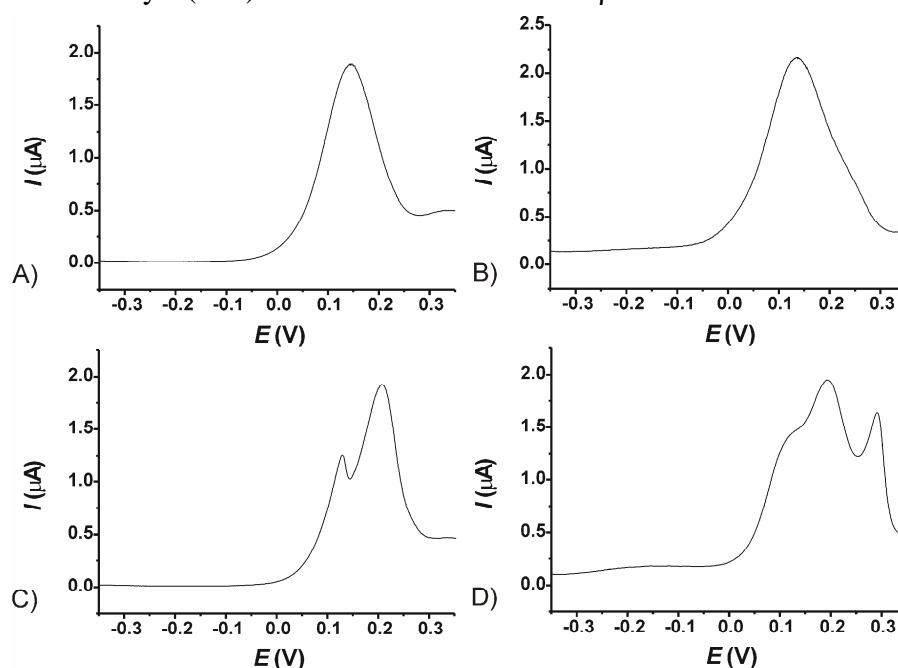


Figure 4.1: Differential pulse voltammograms of aqueous solutions of 1 mM (in Fc functionality) of G1-PPI-(Fc)₄ (A and B) and G5-PPI-(Fc)₆₄-(β CD)₄₀ (10 mM β CD at pH = 2) at a bare Au electrode (B and D) and at a β CD SAM (A and C).

In the case of G4-PPI-(Fc)₃₂ and G5-PPI-(Fc)₆₄ at bare Au electrodes a small post wave was observed in the differential pulse voltammograms due to adsorption of the dendrimers which increased during scanning. This post wave may also be present for the other dendrimers but the interaction may be too weak to be observed. For G5-PPI-(Fc)₆₄, $E^{0'}$ of the post-wave is

308 mV (Figure 4.1), while for G4-PPI-(Fc)₃₂ the post wave could only be observed as a shoulder. The Au electrode remained electroactive (not shown) after replacing the electrolyte solution by a solution without the dendrimers, but the redox-activity decreased during scanning. The adsorption of dendrimers at Pt electrodes from organic solvents was also observed and studied in detail by Kaifer et al.¹³ They also found that the adsorption was time- and concentration-dependent and that the electrode remained redox-active after removal of the dendrimer solution. Thus, the dendrimer- β CD assemblies adsorb at bare Au surfaces but do not form stable layers at the Au surface.

The differential pulse voltammograms of the dendrimer- β CD assemblies at β CD SAMs showed quite different characteristics, e.g. the post-wave due to adsorption was not observed, and all $E^{0'}$ values were shifted to slightly higher potentials by about 15 mV (Table 4.1). All DPV spectra showed a single oxidation wave, except G5-PPI-(Fc)₆₄ (Fig. 4.1), which showed a distinct wave at lower potentials. Since the DPV spectra at the β CD SAMs do not show a post wave, thus, it is not possible to discriminate between bound and unbound Fc units at the host surface. In contrast, as is shown in Section 3.2.4 in CV experiments of monolayers of dendrimers at β CD SAMs, it was possible to discriminate between interacting and non-interacting groups if no β CD nor dendrimers were present in the electrolyte solution. Figure 4.2 shows CV data of G3-PPI-(Fc)₁₆-(β CD)₁₆ assemblies at β CD SAM-covered and at bare Au electrodes both recorded at a scan rate of 0.5 V/s. On the β CD SAMs, the currents were lower than the currents observed with bare Au electrodes. Moreover, the reduction wave is not visible at β CD SAM-covered electrodes.

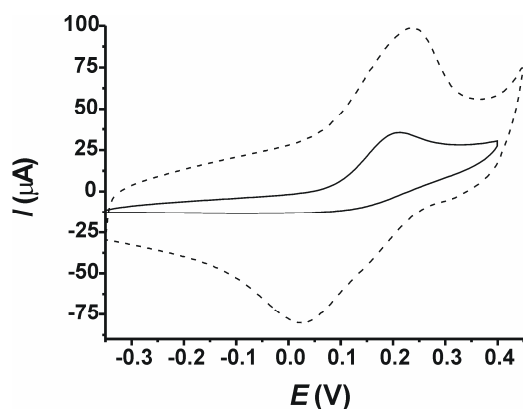


Figure 4.2: Cyclic voltammograms of an aqueous solution of 1 mM (in Fc functionality) of G3-PPI-(Fc)₁₆-(β CD)₁₆ (10 mM β CD at pH = 2) at 0.5 V/s at a bare Au electrode (dashed line) and at a β CD SAM (solid line).

The small differences between the $E^{0'}$ values observed for the dendrimer- β CD assemblies at bare Au electrodes and at β CD-SAM covered electrodes, indicate a strong interaction of the Fc moieties with the β CD SAM. Normally, a SAM, like octadecanethiol (ODT), in combination with weakly interacting redox species in solution causes a large shift of $E^{0'}$, i.e. the SAM is then effectively blocking the redox process.¹⁴ The fact that the currents in β CD

SAM-coated Au electrodes are reduced, caused by the long alkyl chains, unambiguously proves the presence of the β CD SAM. The reduction wave is not visible since the oxidized cationic dendrimers do not interact strongly with the host surface (see below).

4.2.2 Scan rate-dependent cyclic voltammetry

To obtain more insight in the mechanism of the adsorption and desorption processes of the G1 – G5 dendrimers to and from the host surface, CVs were recorded at different scan rates (v) ranging from 0.005 to 2.5 V/s at β CD SAM-decorated electrodes. The results shown in Figure 4.3A-C are for G3-PPI-(Fc)₁₆-(β CD)₁₆ assemblies in solution at a β CD SAM-decorated Au electrode at v of 0.01 V/s, 0.5 V/s and 2.5 V/s. Additionally, data are shown for G5-PPI-(Fc)₆₄ at $v = 2.5$ V/s (Fig 4.3D). At β CD SAM-covered electrodes, an almost completely reversible behavior is observed at low v (Fig. 4.3A). This is more pronounced for G1-PPI-(Fc)₄ and G2-PPI-(Fc)₈ compared to the higher generation dendrimers. At intermediate v the reduction wave is completely absent (Fig. 4.3B). For G1-PPI-(Fc)₄ and G2-PPI-(Fc)₈ the reduction wave is also absent at high v , up to 2.5 V/s. However, at high v a reduction wave was visible in the case of G3-PPI-(Fc)₁₆ (Fig. 4.3C), which is more pronounced for G4-PPI-(Fc)₃₂ and G5-PPI-(Fc)₆₄ (Fig. 4.3D).

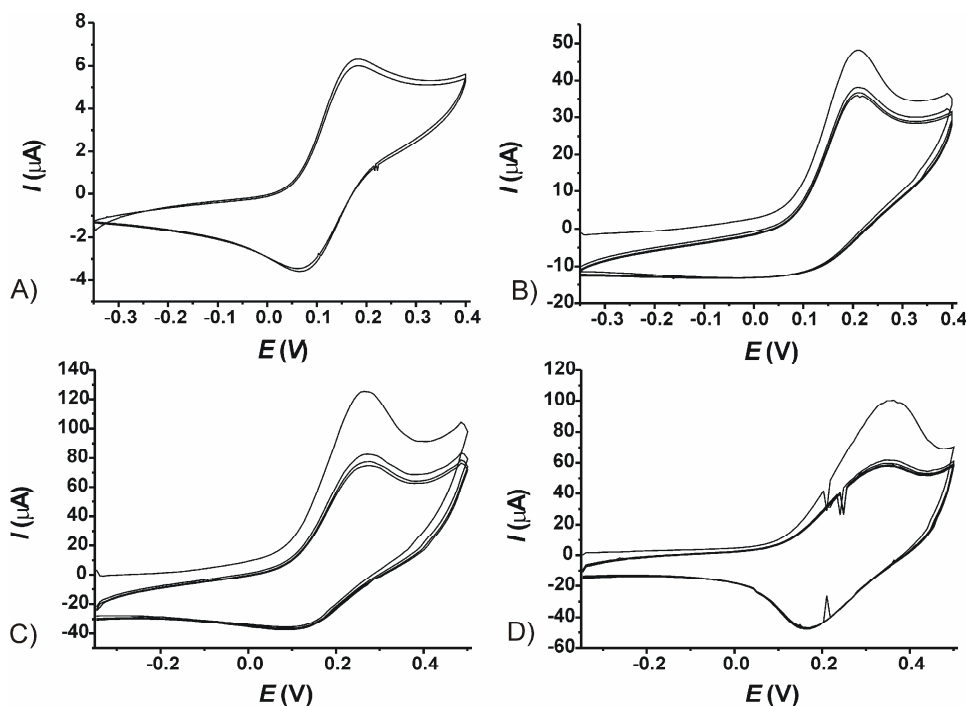


Figure 4.3: Cyclic voltammograms of an aqueous solution of 1 mM (in Fc functionality) of G3-PPI-(Fc)₁₆-(β CD)₁₆ (10 mM β CD at pH = 2) at a β CD SAM at 0.010 V/s (a); at 0.5 V/s (b); at 2.5 V/s (c); and of an aqueous solution of 1 mM (in Fc functionality) of G5-PPI-(Fc)₆₄-(β CD)₄₀ (10 mM β CD at pH = 2) at 2.5 V/s (d).

Upon oxidation of the Fc moieties to Fc^+ , the Fc- β CD interaction is diminished, while during reduction the neutral Fc is regenerated and the Fc- β CD inclusion complexes are restored. This complexation may be hampered at high ν due to the diffusion of β CD and of the dendrimers to and from the surface causing a large shift of E_p values and a broadening of the reduction wave, or its absence. This behavior is predominant in the case of G1-PPI-(Fc)₄ and G2-PPI-(Fc)₈ since at 2.5 V/s the CV spectrum is dominated by the formation of host-guest complexes which is reflected by the absence of the reduction wave. At low ν the CVs are diffusion-controlled and show almost reversible behavior for all dendrimer generations.

CVs of the assemblies at the β CD SAM-covered Au electrodes show a clear reduction wave in the case of generations 3, 4, and 5 at large ν . In the case of generation 5, this effect is more pronounced compared to G3-PPI-(Fc)₁₆ due to the lower diffusion constant of the assemblies (Fig. 4.3D). Moreover, the first scan is higher in intensity than subsequent scans since initially a full monolayer of dendrimers is present at the β CD SAM. At high ν the difference in intensity between the first and subsequent scans is roughly a factor two, while at low ν the difference is negligible. This suggests that during reduction only dendrimers remaining in close proximity to the surface are reduced which may re-bind to the host surface. During subsequent scans, mainly bound and re-bound molecules are repeatedly oxidized and reduced. This also explains the large difference in the anodic peak currents (I_{pa}) between the first and subsequent scans. Thus, at higher scan rates the CV spectra are dominated by the breaking and formation of host-guest complexes. At low ν the cyclic voltammograms are dominated by diffusion processes and, thus, a large difference in I_{pa} is not observed.

The diffusion-controlled behavior at low ν , the host-guest controlled behavior at intermediate ν , and the rebinding which is predominant at large ν , is also reflected in the shifts of E_{pc} and E_{pa} . The values of E_{pc} and E_{pa} as a function of ν which are shown in Figure 4.4A for a solution of a G3-PPI-(Fc)₁₆-(β CD)₁₆ assembly in contact with a β CD SAM-covered Au electrode. At low ν both peak anodic potential (E_{pa}) and the peak cathodic potential (E_{pc}) are square root-dependent on ν , while the E_{pa} is independent of ν at large ν . The large increase of E_{pa} to 165 mV at ν above 0.5 V/s reflects the reduction of rebound dendrimers. In the case of G4-PPI-(Fc)₃₂ and G5-PPI-(Fc)₆₄ the E_{pc} value increased, to 193 mV and 210 mV, respectively, and gradually decreased to values close to 165 mV. The same applies for E_{pa} which also reflected the two processes, as is shown in Figure 4.4A. Additionally, the shift in E_{pa} at low scan rates, e.g. in the range of 0.005 to 0.050 V/s, of 15 mV is much smaller than the shift in E_{pc} of 66 mV. Thus, the anodic electron transfer process are faster than the cathodic reaction. This stems from the fact that the dendrimers in the reduced form, in sharp contrast to the oxidized form, interact strongly with the host surface, hence, improving electron transfer processes.

This behavior is not observed at bare Au electrodes at which an increase in ν only causes an increase in the difference in E_{pa} and E_{pc} in the case of all generations (Figure 4.4B for a solution of G3-PPI-(Fc)₁₆-(β CD)₁₆). This unambiguously proves that the observed ν -

dependent behavior is solely due to the multivalent host-guest interactions of the dendrimers with the host surface.

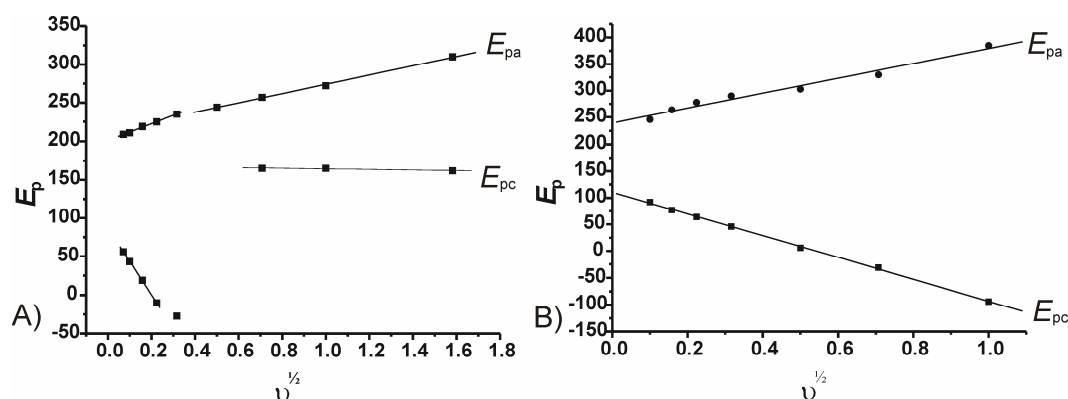


Figure 4.4: The peak oxidation (E_{pc}) and reduction potential (E_{pa}) plotted vs. $v^{-1/2}$ of an aqueous solution of 1 mM (in Fc functionality) of G3-PPI-(Fc)₁₆-(β CD)₁₆ (10 mM β CD at pH = 2) at a β CD SAM (a) (E_{pa} at $v = 0.5$ V/s could not be determined) and at a bare Au electrode (b). The lines are a guide to the eye.

4.2.3 Electrochemical impedance spectroscopy

Electrochemical impedance spectroscopy (EIS) is an AC technique and uses only a very small alternating excitation amplitude (here: 5 mV) of which the frequency is varied.¹⁴ EIS studies an electrochemical system in a wide frequency range which allows to separate different kinetic processes, e.g. charge transfer, adsorption, and diffusion. In general, the spectra can be approximated to a high degree using an equivalent circuit. The circuit elements can then may be correlated to physical or chemical processes. To gain a better insight in all redox-controlled binding processes of the dendrimers at the printboard, potential-dependent EIS measurements were performed with aqueous solutions of five generations of PPI dendrimers at β CD SAMs in the frequency range of 10 kHz to 10 mHz at potentials ranging from -0.15 V to 0.15 V at intervals of 15 mV. All measurements were performed using the same conditions, in aqueous solutions of the dendrimers of 1 mM in Fc functionality and 10 mM β CD at pH = 2. The data were Kramers-Kronig (KK) transformable which indicates that the data are not prone to, for instance, sample aging or slight temperature changes, and, thus of high quality.¹⁵ KK-analysis also proves whether the data are linear, i.e. no higher harmonics are present, and that the system is stable and not changing, i.e. in thermodynamic equilibrium. The χ^2_{KK} values found were in the range of 1 - 10×10^{-6} . For G1 and G2 larger χ^2_{KK} values were found at potentials above 0.12 V. At potentials higher than 0.15 V a dramatic increase in χ^2_{KK} was observed for all generations, probably due to decomposition of the oxidized ferrocenyl moieties and thus the data at potentials higher than 0.15 V were omitted.

Nyquist plots at potentials ranging from -0.15 V to 0.15 V at intervals of 30 mV of an aqueous solution of G4-PPI-(Fc)₃₂-(β CD)₃₂ at a β CD SAM-covered Au electrode are shown in

Figure 4.5. At low potentials the spectra appear to be mainly capacitive in character (Fig. 4.5A). Upon increasing the potentials, the charge transfer resistances and the resistance of the β CD SAM are lowered, reflected in two well-defined semicircles in the high frequency domain and the Warburg element for diffusion at low frequencies (Figs. 4.5A to 5F).

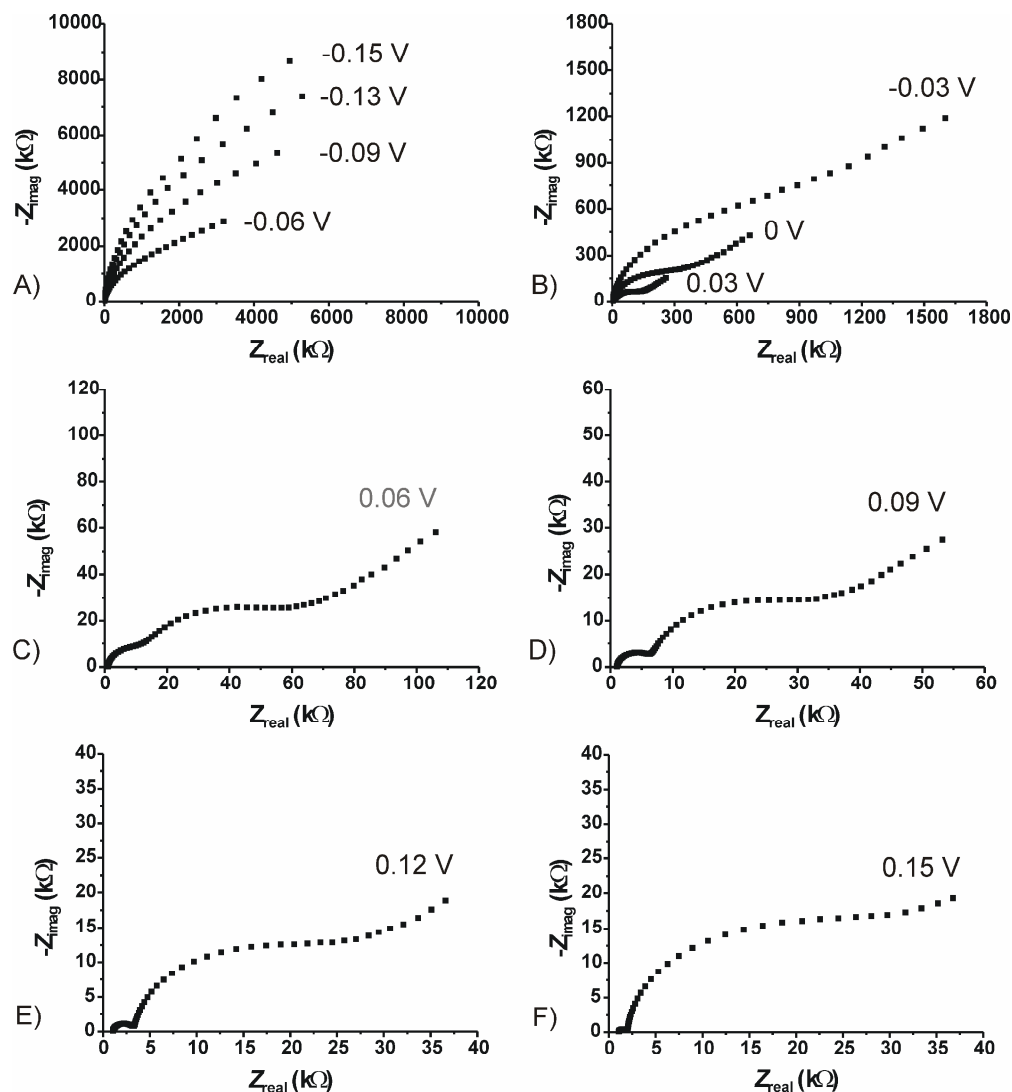


Figure 4.5: Nyquist plots of an aqueous solution of 1 mM (in Fc functionality) of G4-PPI-(Fc)₃₂-(β CD)₃₂ (10 mM CD at pH = 2) at a β CD SAM. The EIS spectra were recorded in the range of -0.15 V to 0.15 V at intervals of 15 mV, data are shown at intervals of 30 mV: EIS spectra recorded at -0.15 V, -0.12 V, -0.09 V, -0.06 V (A); -0.03 V, -0.0 V, 0.03 V (B); 0.06 V (C); 0.09 V (D); 0.12 V (E); and 0.15 V (F).

For all generations the data obtained for the entire frequency range were analyzed using the same equivalent circuit shown in Figure 4.6. This equivalent circuit was obtained by a complex nonlinear least squares fit (CNLS) procedure developed by Boukamp.¹⁶ The χ^2 of the fits were in the range of 1×10^{-6} to 10×10^{-6} which was attributed to noise. To obtain high quality fits, a small contribution ($R_{\text{ref}}C_{\text{ref}}$) which is probably due the reference electrode, was also included in the equivalent circuit. R_s is the solution resistance, $C_{\beta\text{CD SAM},1}$ and $C_{\beta\text{CD SAM},2}$

are two capacitances of the β CD SAM, $R_{\beta\text{CD SAM},1}$ and $R_{\beta\text{CD SAM},2}$ are two resistances of the β CD SAM, C_{dl} is the double-layer capacitance, R_{ct} is the charge transfer resistance, and W is the Warburg element for diffusion. At low potentials it was not possible to resolve the two sets of resistances and capacitances for the β CD SAM and the equivalent circuit simplified to one $C_{\beta\text{CD SAM,tot}}$ in parallel with one $R_{\beta\text{CD SAM,tot}}$.

In general, a Randles-equivalent circuit consisting of a R_s in series with C_{dl} , R_{ct} , and W , models the electrochemical impedance of an interface. However, the Randles-equivalent circuit modeled our data poorly in the entire frequency range. At low potentials, a capacitance in parallel with a resistance attributed to the β CD SAM added to the equivalent circuit in a parallel fashion gave satisfactory fitting results. At higher potentials, an additional contribution of the β CD SAM, i.e. a resistance in series with a capacitance, was required to obtain high quality fits. To fit the high frequency range an extra capacitance C_{ref} in parallel with a resistance R_{ref} was added in series to the equivalent circuit which is probably due to the reference electrode.

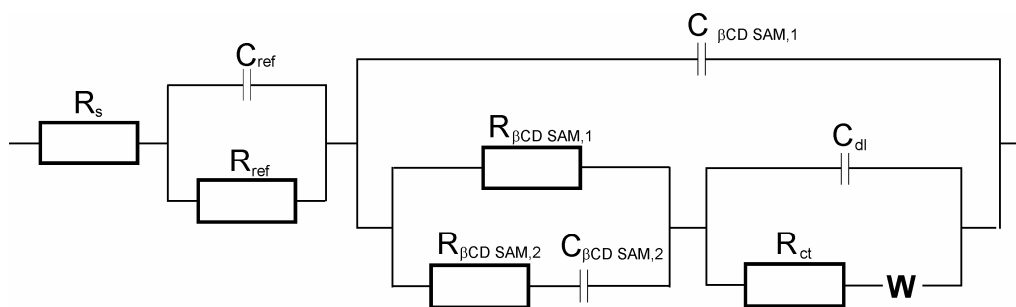


Figure 4.6: The equivalent circuit used to fit the frequency scans, where R_s is the solution resistance, $C_{\beta\text{CD SAM},1}$ and $C_{\beta\text{CD SAM},2}$ are capacities of the β CD SAM, $R_{\beta\text{CD SAM},1}$ and $R_{\beta\text{CD SAM},2}$ are the resistances of the β CD SAM, C_{dl} is the double-layer capacitance, R_{ct} is the charge transfer resistance, and W is the Warburg element for diffusion. A small capacity C_{ref} and resistance R_{ref} most likely due to the reference electrode was also included to obtain high quality fits.

The fitting results for G1-PPI-(Fc)₄-(β CD)₄ assemblies at a β CD SAM-covered Au electrode using the equivalent circuit in Figure 4.6 are shown in Figure 4.7. All circuit elements are strongly dependent on the potential, except R_s which remains constant at 2.4 k Ω cm². The capacitance of the β CD SAM ($C_{\beta\text{CD SAM,tot}}$) remained constant at 2.3×10^{-6} F/cm² up to potentials of around -50 mV after which a gradual increase to 6.4×10^{-6} F/cm² was observed. The value of $C_{\beta\text{CD SAM}}$ of 2.3×10^{-6} F/cm² is similar to the value previously reported of 2.6×10^{-6} F/cm² measured at -0.2 V using an aqueous solution of K₃Fe(CN)₆/K₄Fe(CN)₆ and 0.1 M K₂SO₄.^{2a} The increase in $C_{\beta\text{CD SAM}}$ at higher potentials is probably caused by the decrease in interaction strength of the dendrimers with the molecular printboard. At potentials above 135 mV $C_{\beta\text{CD SAM}}$ decreased, probably due to degradation of the system. Moreover, at potentials above 0.15 V the system shows significant non-KK behavior and, thus, the data are

not reliable. The capacitance of the double layer (C_{dl}) varied one order of magnitude and increased from 4×10^{-6} F/cm² to 4×10^{-5} F/cm² in the potential range of 0 V to 0.15 V, while at lower potentials, i.e. -0.15 V to 0 V the C_{dl} remained constant. This indicates that at low potentials C_{dl} is determined by a monolayer of dendrimers on the β CD SAM, while at higher potentials the dendrimers are desorbed and, consequently, C_{dl} is determined by the β CD SAM only. The Warburg impedance (Q_{diff}), increased 2 orders of magnitude from 4×10^{-5} Ss^{1/2} to 3×10^{-3} Ss^{1/2}. The resistance of the β CD SAM ($R_{\beta CD SAM}$) decreased by more than two orders of magnitude from $6.3 \times 10^5 \Omega$ to $4.4 \times 10^3 \Omega$. The charge transfer resistance (R_{ct}) also decreased from $2.2 \times 10^5 \Omega$ to $3.2 \times 10^3 \Omega$.

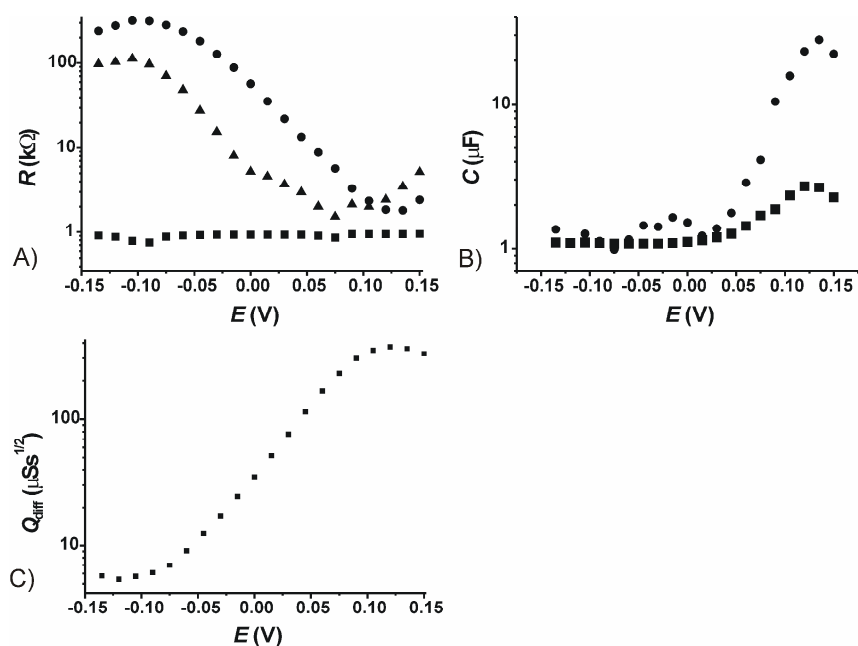


Figure 4.7: The resistances (A), capacitances (B), and Q_{diff} as a function of the potential of an aqueous solution of 1 mM (in Fc functionality) of G1-PPI-(Fc)₄-(β CD)₄ (10 mM β CD at pH = 2) at a β CD SAM; EIS spectra were measured at potentials ranging from -0.15 V to 0.15 at intervals of 15 mV. Left: \bullet = $R_{\beta CD SAM}$, \blacktriangle = R_{ct} , \blacksquare = R_s ; Right: \bullet = C_{dl} , \blacksquare = $C_{\beta CD SAM}$.

To explain the potential dependence of the different elements in more detail and to rule out differences in the quality of the β CD SAM from sample to sample, the influence of the dendrimer generation was investigated by recording EIS spectra of the dendrimers at the same β CD SAM. G1-PPI-(Fc)₄ to G4-PPI-(Fc)₃₂ were measured in a smaller potential range, from -20 mV to 85 mV, to prevent degradation of the oxidized dendrimers. All aqueous solutions of the dendrimers were prepared using the same pH corrected for the protonated core amines of the dendrimers. This is reflected in the R_s which is close to 2.4 k Ω cm² for all dendrimer solutions. The $C_{\beta CD SAM}$ remained virtually constant during the whole experiment indicating that no significant degradation took place and that all changes can be attributed to the increase of the generation number of the dendrimers. The data for G3-PPI-(Fc)₁₆ are shown in Figure

4.8. Similar trends were observed as discussed above for G1-PPI-(Fc)₄ and they were also observed for the other generations.

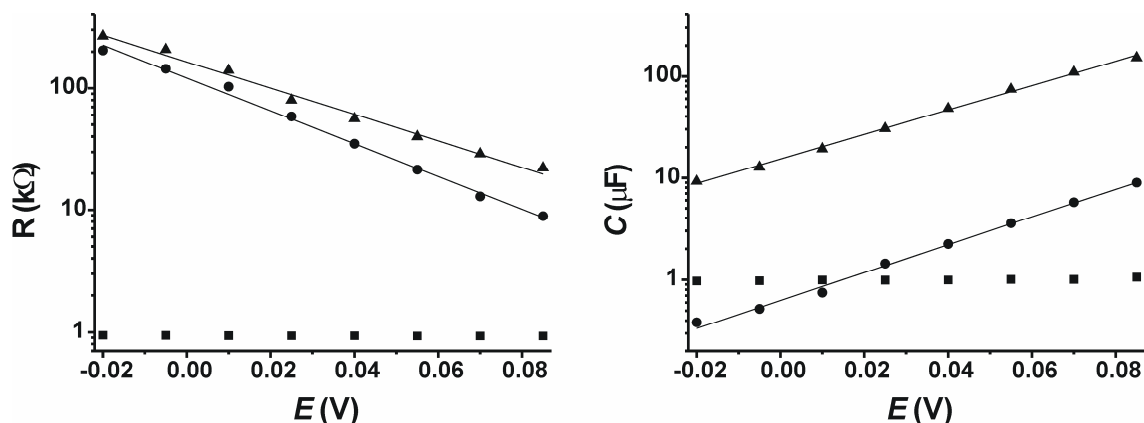


Figure 4.8: The resistances (left) and capacitances (right) as a function of the potential of an aqueous solution of 1 mM (in Fc functionality) of G3-PPI-(Fc)₁₆-(β CD)₁₆ (10 mM β CD at pH = 2) at a β CD SAM; EIS spectra were measured at potentials ranging from -0.15 V to 0.15 at intervals of 15 mV. Left: $\bullet = R_{\beta\text{CD SAM}}$, $\blacktriangle = R_{ct}$, $\blacksquare = R_s$; Right: $\bullet = C_{dl}$, $\blacktriangle = W$, $\blacksquare = C_{\beta\text{CD SAM}}$.

C_{dl} increased with increasing dendrimer generation, except for G1. C_{dl} is determined by the thickness of the monolayer of adsorbed dendrimers. C_{dl} is related to the monolayer thickness d by eq. (1):

$$d = \frac{\epsilon_0 \epsilon_r A}{C_{dl}} \quad (1)$$

In this equation, A is the surface area of the electrode, ϵ_0 is the permittivity in vacuum, and ϵ_r is the relative permittivity. The monolayer thickness of the dendrimer is not only determined by the generation, but also by the number of interactions. Figure 4.9 shows a plot of C_{dl} versus the ratio of number of end groups (p_{tot}) to the number of interactions (p_b) for G1 to G4 (Table 4.1). G1 gave a much higher C_{dl} value because, under the present conditions, G1-PPI-(Fc)₄ can not form a densely packed monolayer at the β CD SAM due to the high β CD concentration in the electrolyte solution. This observation is in agreement with the observed increase of C_{dl} with increasing potential (Fig. 4.7) leading to lower surface coverages of the dendrimers at the molecular printboard.

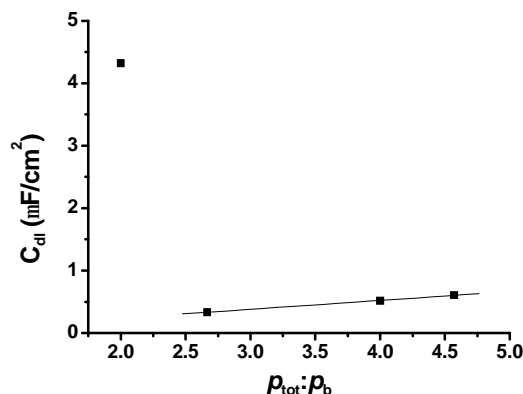


Figure 4.9: A plot of C_{dl} vs. the ratio of the number of end groups (p_{tot}):number of interactions (p_b) measured at -5 mV for generations 1 to 4. The line is a guide to the eye.

C_{dl} is linearly dependent on the ratio $p_{tot}:p_b$. Under the present conditions, e.g. 10 mM β CD at pH = 2, the dendrimers are forced to adopt a fully extended conformation due to the protonation of the core amines and the complexation of all end groups with β CD from solution. However, an increase in d should result in a decrease in C_{dl} , while a linear increase is observed. The C_{dl} is also dependent on the nature of the electrode-electrolyte interface. The electrode-electrolyte interface may be influenced by the presence of protonated core amines and counterions of the dendrimers. The linear behavior of C_{dl} with the ratio $p_{tot}:p_b$ suggests that the dendrimers are attached to the surface as fully extended sphere-like structures which is in agreement with the Stokes-Einstein behavior of the dendrimers in solution (see below) and the observed trend in R_{ct} (see below).

C_{dl} is determined by the adsorbed monolayer of dendrimers. Thus, there are two extreme values for C_{dl} when the surface coverage of the dendrimers ($\Gamma_{dendrimer}$) is maximal at low potentials and when $\Gamma_{dendrimer}$ is minimal at high potentials. The potential-dependent change of C_{dl} could be fitted according to eq. (2):

$$C_{dl} = C_{dl,1}q + C_{dl,2}(1-q) \text{ with } q = \frac{e^{\frac{nF}{RT}(h-h_0)}}{1 + e^{\frac{nF}{RT}(h-h_0)}} \quad (2)$$

In this equation $C_{dl,1}$ and $C_{dl,2}$ denotes the C_{dl} value at high and low potentials, respectively, n , F , R , and T have their usual electrochemical meaning, θ is the fraction of adsorbed dendrimers, η_0 is the equilibrium potential with respect to the reference electrode, and η is the potential difference with respect to the reference electrode. Thus, C_{dl} can be expressed as the fractional summation of the $C_{dl,1}$ and $C_{dl,2}$ values of the contribution which is dependent on the potential. Thus, the ratio $C_{dl,1}/C_{dl,2}$ is a measure for the difference in $\Gamma_{dendrimer}$ at high and low potentials.

The dielectric capacitance of the β CD SAM is represented by $C_{\beta CD \text{ SAM},1}$ which has virtually the same value for all β CD SAM-dendrimer associates. In a number of spectra the electronic

path through the β CD SAM could be resolved into two parallel resistances, of which one was coupled through a second capacitance, $C_{\beta\text{CD SAM},2}$. In other spectra the separation could not be made due to a too small contribution to the overall impedance spectrum. The observed combination of $R_{\beta\text{CD SAM},1}$ and $R_{\beta\text{CD SAM},2}$ with $C_{\beta\text{CD SAM},2}$ can be easily explained through the presence of two different alkyl chains: one directly attached to the β CD, R_1 , and one chain that is not directly chemically bonded to the β CD cavity, but only via the sulfur-atom, R_2 (Scheme 4.1). It may be assumed that AC conductivity is possible through both alkyl chains, where the “freestanding” chain is capacitively coupled to the chemically bound chain and possibly also to the β CD. $R_{\beta\text{CD SAM},2}$ is about 2-5 times larger than $R_{\beta\text{CD SAM},1}$. An example is given for the G4-PPI-(Fc)₃₂-(β CD)₃₂ assembly in solution in contact with a β CD SAM decorated Au-electrode (Fig. 4.10). Both $R_{\beta\text{CD SAM},1}$ and $R_{\beta\text{CD SAM},2}$ decrease with increasing potential. The $C_{\beta\text{CD SAM},2}$ depends on the potential while $C_{\beta\text{CD SAM},1}$ only increases gradually at high potentials. The exact nature of the increase of $C_{\beta\text{CD SAM},2}$ is not fully understood at present.

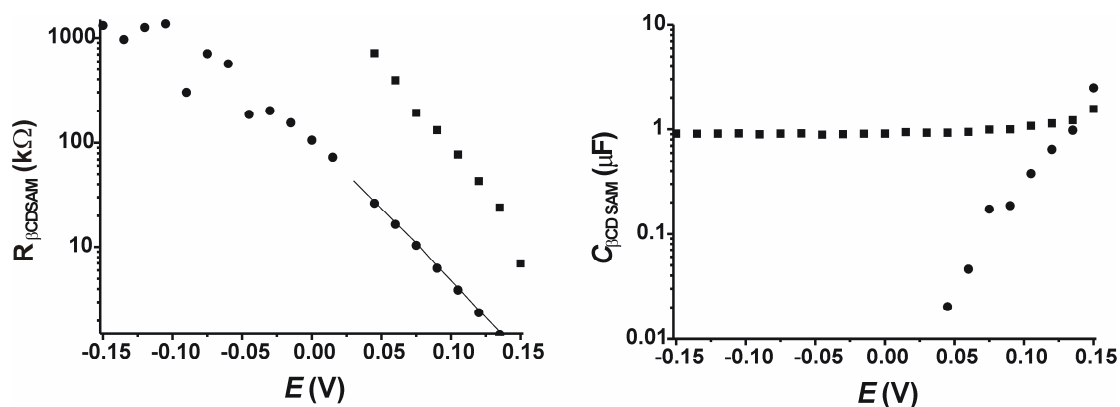


Figure 4.10: Left: $R_{\beta\text{CD SAM},1}$ (●) and $R_{\beta\text{CD SAM},2}$ (■) as a function of the potential. The line indicates $R_{\beta\text{CD SAM,tot}}$ ($1/(1/R_{\beta\text{CD SAM},1} + 1/R_{\beta\text{CD SAM},2})$); Right: The change of $C_{\beta\text{CD SAM},1}$ and $C_{\beta\text{CD SAM},2}$ with the potential. At potentials below 60 mV only $R_{\beta\text{CD SAM,tot}}$ and $C_{\beta\text{CD SAM,tot}}$ could be found.

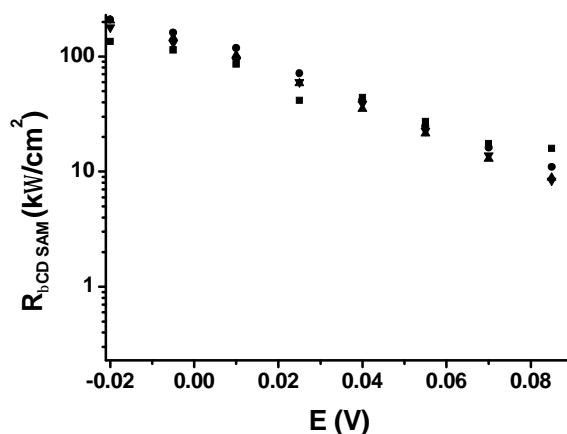


Figure 4.11: $R_{\beta\text{CD SAM,tot}}$ as a function of the potential for G1-PPI-(Fc)₄ (■), G2-PPI-(Fc)₈ (▲), G3-PPI-(Fc)₁₆ (▼), and G4-PPI-(Fc)₃₂ (●).

Although the $R_{\beta\text{CD SAM,tot}}$ values depends on the potential, it remained constant for all generations, as is shown in Figure 4.11. The fact that the $C_{\beta\text{CD SAM}}$ (not shown) and the behavior of $R_{\beta\text{CD SAM}}$ remained the same during the experiment for all generations indicates that the $\beta\text{CD SAM}$ was stable in this potential range and during the course of the experiment.

R_{ct} increased with increasing dendrimer generation (Figure 4.12). R_{ct} of G4-PPI-(Fc)₃₂ was found to be almost the same as that of G3-PPI-(Fc)₁₆. R_{ct} is related to the exchange current (i_0) by eq. (3):

$$R_{ct} = \frac{RT}{nFi_0}. \quad (3)$$

The heterogeneous electron transfer constant (k^0) is related to i_0 by eq. (4):

$$i_0 = nFAk^0 C_o^* e^{-anf(E_{eq}-E^0')} \text{ with } f = RT/F. \quad (4)$$

Despite the fact that the bulk concentration of Fc^+ is not known, these relations hold since the measurements were performed under thermodynamic equilibrium and therefore the ratio of Fc/Fc^+ is defined by the Nernst equation. Therefore, R_{ct} directly provides qualitative information about the heterogeneous reaction rates. Hence, the larger dendrimers show slower heterogeneous reaction rates. The reaction rate is probably reduced by the increase in monolayer thickness of the dendrimers since the diameter of the dendrimers increases with increasing generation (Table 4.1). The fact that the R_{ct} values for G3-PPI-(Fc)₁₆ and G4-PPI-(Fc)₃₂ are similar reflects the small difference in $p_{\text{tot}}:p_{\text{b}}$ ratio which is 4 and 4.5, respectively. This indicates that the monolayer thickness of both dendrimers at the $\beta\text{CD SAM}$ is similar, as was indicated by C_{dl} . But in the case of G4-PPI-(Fc)₃₂ the higher density of the Fc moieties may improve the electron transfer processes.

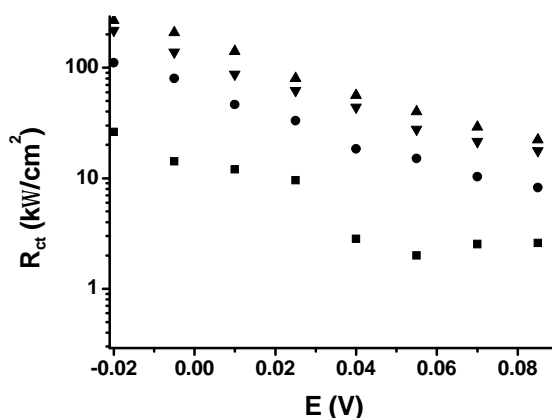


Figure 4.12: Charge transfer resistance (R_{ct}) as a function of the potential of G1-PPI-(Fc)₄ (■), G2-PPI-(Fc)₈ (●), G3-PPI-(Fc)₁₆ (▲), and G4-PPI-(Fc)₃₂ (▼).

Q_{diff} increased dramatically with increasing potential (Fig. 4.7) and is also dependent on the dendrimer generation as is shown in Figure 4.13. Q_{diff} increases with increasing generation because the diffusion constant decreases and thus increasingly impedes mass transport.

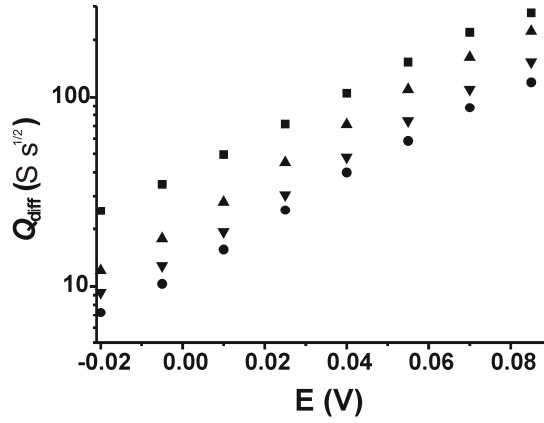


Figure 4.13: σ as a function the potential of G1-PPI-(Fc)₄ (■), G2-PPI-(Fc)₈ (▲), G3-PPI-(Fc)₁₆ (▼), and G4-PPI-(Fc)₃₂ (●).

For simple redox processes at an inert electrode, the diffusion element is given by (in impedance form) eq. (5):

$$Z = s(w)^{-1/2}(1-j) \text{ with } s = \frac{1}{Q_{diff} \sqrt{2}} = \frac{RT}{n^2 F^2 A \sqrt{2}} \left(\frac{1}{C_o^* \sqrt{D_o}} + \frac{1}{C_R^* \sqrt{D_R}} \right) \quad (5)$$

In eq. 5 σ is the Warburg coefficient which is dependent on diffusion coefficients of the oxidized D_o and reduced D_R species, on the bulk concentrations of the oxidized C_o^* and reduced C_R^* species. R , T , n and F have their usual electrochemical meaning. The diffusion coefficients for the oxidized species are not identical since the reduced form forms Fc- β CD inclusion complexes which have a lower diffusion constant than the oxidized form which can not form inclusion complexes. A ratio of D_o/D_R of 0.25 to 0.55 has been reported for different water soluble substituted ferrocenes.¹⁷ In the CNLS-analysis the diffusion coefficient is expressed as its admittance according to eq. (6):

$$Q_{diff} = s^{-1} \quad (6)$$

In Figure 4.7 it is clearly visible that Q_{diff} changes from a nearly constant value at low potentials to a maximum at high potentials, followed by the onset of a steady decrease with increasing potential. The right hand side of the Q_{diff} - η curve can easily be explained by assuming the total concentration of Fc dendrimers, $C_{Fc,tot}^0$, is constant leading to eq. 7 where θ is the fraction of oxidized species:

$$C_{Fc,tot}^0 = C_o^* + C_R^* = [qC_{Fc,tot}^0]_O + [(1-q)C_{Fc,tot}^0]_R \quad (7)$$

This fraction is potential-dependent according to eq. (8) where η_0 is the potential for which $\theta = 0.5$:

$$\frac{q}{q-1} = e^{\frac{nF}{RT}(h-h_0)} = K_q \quad (8)$$

Insertion in eq. (7) and the transformation to the admittance representation yields eq. (9):

$$Q_{\text{diff}} = Q_0 \frac{1}{\left(1 + \frac{1}{K_q}\right) \left(1 + K_q \sqrt{\frac{D_o}{D_R}}\right)}, \text{ with } Q_0 = \frac{n^2 F^2 A \sqrt{2}}{RT} C_{\text{Fc,tot}}^0 \sqrt{D_o} \quad (9)$$

This expression has been fitted to the right hand side of the $Q_{\text{diff}}-\eta$ curve. Subtraction showed a more or less constant Q_{diff} value for the low potential side, possibly indicating that in this region a parallel diffusion process takes place. Incorporating this process in the fit procedure yields the continuous line in Figure 4.14 for a G2-PPI-(Fc)₈-(β CD)₈ assembly in contact with a β CD SAM decorated Au electrode. Considering the limited quality of the data at the extremes of the potential range, as presented by the relatively high values for the data validation, the fit of this model to the obtained diffusion coefficients is quite convincing. EIS measurements performed at bare Au electrodes showed normal Warburg behavior (eq. 5), i.e. the Q_{diff} increased to reach a maximum at η_0 followed by a decrease of Q_{diff} at higher potentials.

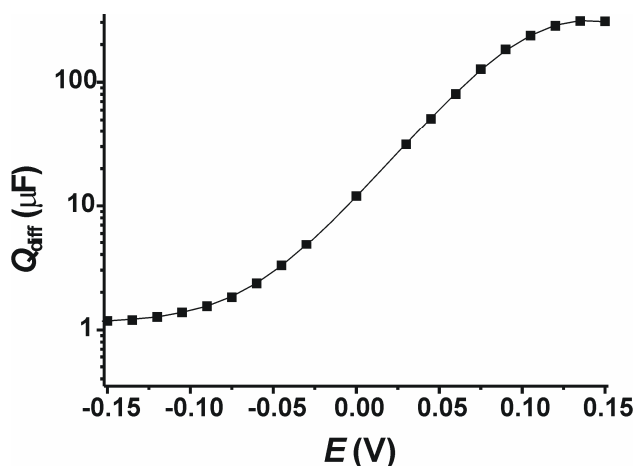


Figure 4.14: Q_{diff} as a function of the potential for G2-PPI-(Fc)₈-(β CD)₈ assembly (1 mM in Fc functionality with 10 mM β CD at pH = 2) measured at a β CD SAM-decorated Au electrode.

According to the Stokes-Einstein relation, the diffusion constant (D) is inversely related to the diameter (r) of the molecule by eq. (11) where k is the Boltzmann constant, T is the temperature, and η is the viscosity:

$$D = \frac{kT}{6\hbar\pi r} \quad (11)$$

Equations 5 and 11 predict a linear relationship between the Q_{diff} and $(1/r)^{-1/2}$ where r stands for the diameter of the dendrimer. Since r is directly related to the generation of the dendrimer, r can be replaced by Gx where x indicates the generation number. Figure 4.15 shows the Q_{diff} corrected for the concentration and the number of electrons n involved per molecule plotted vs. $(1/Gx)^{-1/2}$. The linear dependence indicates that the dendrimers behave in solution like spheres and that the dendrimers adopt a fully extended conformation. Other

studies have shown that it is difficult to obtain reliable diffusion data with electrochemical techniques since non-linear behavior was observed, while Stokes-Einstein behavior could be proven with non-electrochemical techniques.¹⁸ The electrochemical techniques used in those studies only allowed to study a system under non-steady state and non-equilibrium conditions. Here, the data were acquired while the system is in thermodynamic equilibrium and EIS allows to obtain data about mass transport kinetics well separated from electron transfer processes due to the large difference of the time constants of both processes.

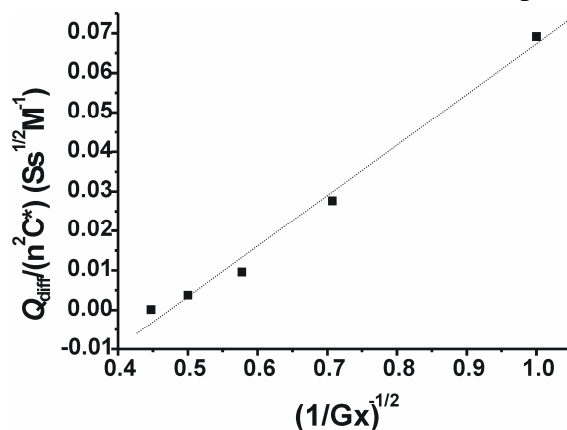


Figure 4.15: The W admittance corrected for the concentration of dendrimers and the number of electrons involved per molecules plotted vs the square root of generation⁻¹.

Rebach and Sluyters have described a kinetic description for strongly adsorbed redox-active species and their response in EIS.¹⁹ Performing CV while measuring the SPR signal showed that at potentials above E_{pc} the surface coverage $\Gamma_{dendrimer}$ is approximately 0, but at potentials well below E_{pc} , $\Gamma_{dendrimer}$ is maximal. At potentials well above E_{pc} the dendrimers from solution may bind to the host surface and undergo oxidation immediately followed by desorption. This results in an equilibrium between adsorption and desorption of the dendrimers where $\Gamma_{dendrimer}$ is close to 0. $\Gamma_{dendrimer}$ only depends on the concentration of the dendrimer and β CD in solution, the electrochemical reaction rates, and the D_O and D_R . At intermediate potentials, $\Gamma_{dendrimer}$ will decrease with increasing potential since the rate of desorption increases with increasing potential. The kinetic scheme is shown in Figure 4.16. The dendrimers in the reduced form in solution (Red_{sol}) can adsorb at the β CD SAM, in the scheme shown as Red_{ads} . In principle, Red_{sol} is in equilibrium with Red_{ads} , but especially for the higher generations, the rate of adsorption (k_{ar}) for the reduced form will be much larger than the rate of desorption (k_{dr}), hence $k_{ar} \gg k_{dr}$. The oxidized form (Ox_{ads}) has low affinity with the β CD SAM and will desorb from the surface into solution (Ox_{sol}) fast (k_{do}) while the rate of adsorption of the oxidized form will be very slow (k_{ao}), thus $k_{do} \gg k_{ao}$.

This model accounts for the potential dependence of the elements in the EIS spectra. For instance, the $C_{\beta CD SAM, tot}$ remains constant, and also the R_s is independent of the potential. Only at high potentials $C_{\beta CD SAM}$ increases. The increase of C_{dl} can be explained if C_{dl} is the

result of a charged double layer determined by the dendrimer monolayer. $\Gamma_{\text{dendrimer}}$ decreases as the potential increases thus causing an increase of Q_{dl} . Also the strong decrease of R_{ct} can be explained since at low potentials a double layer impedes the charge transfer, while at high potentials only the β CD SAM impedes charge transfer.

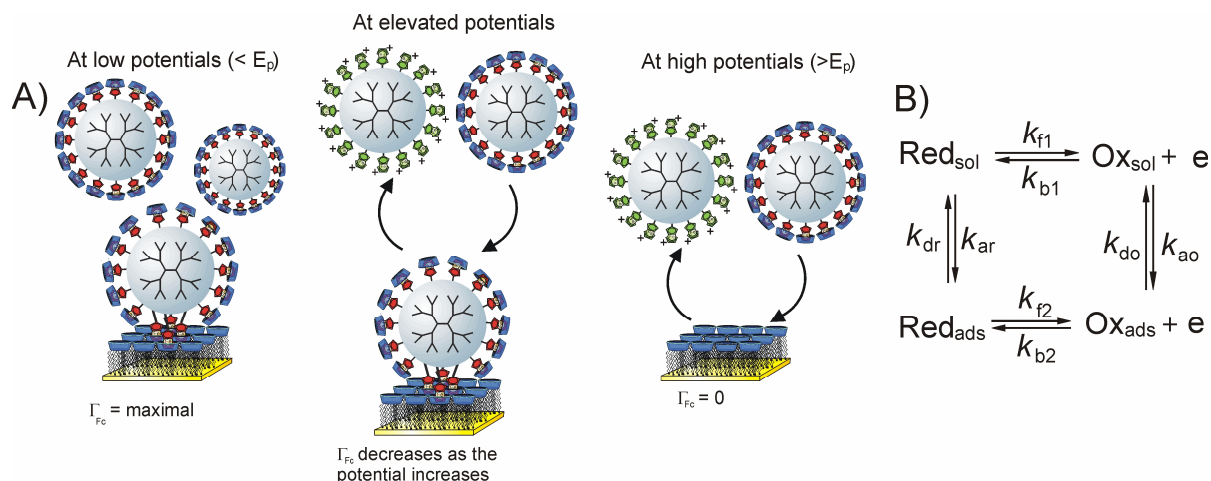


Figure 4.16: Schematic of the potential-dependent surface coverage of the dendrimers (left), and a scheme of adsorption and desorption kinetics (right), Red_{sol} = reduced dendrimers in solution, Red_{ads} = dendrimers adsorbed at the β CD SAM, Ox_{sol} = oxidized dendrimers in solution, Ox_{ads} = oxidized dendrimers at the surface; k_{dr} , k_{ar} , k_{do} and k_{ao} are adsorption (a) and desorption (d) rates of oxidized (o) and reduced (r) dendrimers; k_b and k_f are electrochemical rate constants.

4.3 Conclusions

The adsorption of the Fc dendrimers at the β CD host surfaces can be electrochemically controlled. The stability of the supramolecular system in aqueous media at $\text{pH} = 2$, is remarkable. Potential-dependent EIS measurements were performed over 8 h and showed only some non-KK behavior at potentials close to or above E^0 , probably due to decomposition of the oxidized ferrocenyl moieties. Despite the long experimental times, no multilayer formation of the dendrimers at the host surface could be observed.

Scan rate-dependent CV revealed almost reversible behavior at low scan rates for all generations, but irreversible behavior at high scan rates. In the case of the larger dendrimers, however, the cyclic voltammograms at high scan rates were dominated by rebinding of the dendrimers to the host surface. The fact that the oxidized form of the dendrimers can not bind with the host surface and that the larger dendrimers diffuse slowly away from the host surface accounts for the complex electrochemical behavior. The fact that the oxidized form has a much lower interaction with the host surface explains the absence of the reduction wave. The higher generations diffuse too slowly and thus may be reduced and consequently rebind.

A full description in terms of an equivalent circuit could be obtained by electrochemical impedance spectroscopy (EIS). EIS revealed that the capacitance of the charged double layer

dendrimer monolayer on the β CD SAM depends on the electrolyte-interface and the generation and the number of interactions. This suggests that the dendrimers adopt a fully extended spherical conformation at the host surface. This is in sharp contrast to physisorbed dendrimers at for instances Au or Pd surfaces at which the dendrimers are flattened.

Larger dendrimer generations show an increase of the charge transfer resistance. The larger dendrimers have relatively slow electron transfer kinetics, while the smaller generations show fast kinetics. This can be rationalized by electrons hopping from metal centre to metal centre and that the electrons have to hop longer distances in the case of larger dendrimers.

The desorption of the dendrimers upon oxidation could be studied in great detail by EIS. Especially the double-layer capacitance (C_{dl}) is sensitive to adsorption of the dendrimers. The difference in C_{dl} , which is inversely proportional to the monolayer thickness, at low and high potentials, was over two orders of magnitude, indicating that at potentials around $E^{0'}$ the surface coverage by the dendrimers is very close to 0.

Using EIS it was even possible to discriminate between different electron transfer processes within the β CD SAM. This SAMs contains two different alkyl chains, one directly attached to the β CD cavity and the second one is bound indirectly via the sulfur-atom. Both have a similar resistance but different capacitances. The difference in capacitance stems from a different distance the electrons have to overcome.

Electrochemical impedance spectroscopy provided an unique way to probe a complex supramolecular system by a small AC perturbation, and allowed to discuss the properties in terms of an equivalent circuit. A good understanding of supramolecular systems is a prerequisite for applications in, for instance, molecular electronics.

4.4 Experimental Section

General Procedures. All moisture sensitive reactions were carried out under argon atmosphere. Reagents were commercial and used without further purification. All dry solvents were prepared according to standard procedures and stored over molecular sieves. The ferrocenyl^{3a} and adamantyl PPI dendrimers²⁰ were prepared according to literature procedures.

Materials and methods. All glassware used to prepare monolayers was immersed in piranha solution (conc. H_2SO_4 and 33% H_2O_2 in a 3:1 ratio). (Warning: piranha should be handled with caution; it can detonate unexpectedly).²¹ Next, the glassware was rinsed with large amounts of Milli-Q water. All adsorbate solutions were prepared prior to use. All solvents used in monolayer preparation were of p.a. grade.

Substrate preparation. Glass-supported gold (2.54 cm diameter; 200 nm metal thickness, with a 2 nm titanium adhesion layer) were obtained from SSENS bv (Hengelo, The Netherlands). Gold substrates were cleaned by brief immersion in piranha and the resulting oxide layer was removed by leaving the substrates for 10 min in absolute EtOH. The substrates were subsequently immersed in the

adsorbate solution (0.1-1 mM) for ca. 16 h at 60°C. Next, the samples were removed from the solutions and rinsed thoroughly with chloroform, ethanol, and Milli-Q water.

Electrochemistry. Electrochemical measurements were performed with an AUTOLAB PGSTAT10, in a custom built three-electrode setup equipped with a platinum counter electrode, a mercury sulfate reference electrode ($V_{\text{MSE}} = +0.61 V_{\text{NHE}}$) and a screw cap holding the gold working electrode (area exposed to the solution = 0.44 cm²). All aqueous solutions of the dendrimers solutions were 1 mM in Fc functionality and contained 10 mM β CD at pH = 2. Electrochemical impedance measurements were performed by measuring 80 frequencies in the range of 10 kHz to 10 mHz at different potentials ranging from -0.15 V_{MSE} to 0.15 V_{MSE} in steps of 15 mV with a superimposed sinusoidal potential with an amplitude of 10 mV. After increasing the voltage by 15 mV, the system was allowed to equilibrate for 5 min before measuring the subsequent EIS spectrum.

Differential pulse voltammograms were recorded using a modulation time of 0.5 s, an interval time of 0.2 s, a step potential of 1 mV, and a modulation amplitude of 10 mV.

Cyclic voltammograms were recorded at scan rates of 0.005, 0.010, 0.025, 0.050, 0.10, 0.25, 0.50, 1.0, and 2.5 V/s at β CD SAMs covered electrodes, while for measurement at bare electrodes the scan rate at 0.005 V/s was omitted. At scan rates from 0.1 to 2.5 V/s it was found that the after 5 scans the CV spectra were stable, at lower scan rates stable spectra were already achieved after 3 scans. The E_p values at (nearly) steady state were used.

4.5 References

- 1) (a) Mammen, M.; Choi, S.-K.; Whitesides, G. M. *Angew. Chem. Int. Ed.* **1998**, *37*, 2754. (b) Mulder, A.; Huskens, J.; Reinhoudt, D. N. *Org. Biomol. Chem.* **2004**, *2*, 3409.
- 2) (a) Beulen, M. J. W.; Bügler, J.; Lammerink, B.; Geurts, F. A. J.; Biemond, E. M. E. F.; Leerdam, K. G. C.; Van Veggel, F. C. J. M.; Engbersen, J. F. J.; Reinhoudt, D. N. *Langmuir*, **1998**, *14*, 6424. (b) Beulen, M. J. W.; Bügler, J.; De Jong, M. R.; Lammerink, B.; Huskens, J.; Schönherr, H.; Vancso, G. J.; Boukamp, B. A.; Wieder, H.; Offenhäuser, A.; Knoll, W.; Van Veggel, F. C. J. M.; Reinhoudt, D.N. *Chem. Eur. J.* **2000**, *6*, 1176.
- 3) (a) Cuadrado, I.; Morán, M.; Casado, C. M.; Alonso, B.; Lobete, F.; García, B.; Ibisate, M.; Losada, J. *Organometallics* **1996**, *15*, 5278. (b) Takada, K.; Diaz, D.J.; Abruña, H.D.; Cuadrado, I.; Casado, C.; Alonso, B.; Morán, M.; Losada, J. *J. Am. Chem. Soc.* **1997**, *119*, 10763. (c) González, B.; Casado, C. M.; Alonso, B.; Cuadrado, I.; Morán, M.; Wang, Y.; Kaifer, A. E. *Chem. Comm.* **1998**, 2569. (d) Takada, K.; Díaz, D. J.; Abruña, H. D.; Cuadrado, I.; González, B.; Casado, C. M.; Alonso, B.; Morán, M.; Losada, J. *Chem. Eur. J.* **2001**, *7*, 1109. (e) Casado, C. M.; Conzález, B.; Cuadrado, I.; Alonso, B.; Morán, M.; Losada, J. *Angew. Chem. Int. Ed.* **2000**, *39*, 2135. (f) Conzález, B.; Cuadrado, I.; Casado, C. M.; Alonso, B.; Pastor, C. J. *Organometallics* **2000**, *19*, 5518. (g) Conzález, B.; Cuadrado, I.; Alonso, B.; Casado, C. M.; Morán, M.; Kaifer, A. *Organometallics* **2002**, *21*, 3544.
- 4) Castro, R.; Cuadrado, I.; Alonso, B.; Casado, C.M.; Morán, M.; Kaifer, A.E. *J. Am. Chem. Soc.* **1997**, *119*, 5760.
- 5) a) Breslow, R.; Czarniecki, M. F.; Emert, J.; Hamaguchi, H. *J. Am. Chem. Soc.* **1980**, *102*, 762. (b) Sigel, B.; Breslow, R. *J. Am. Chem. Soc.* **1975**, *97*, 6869. (c) Matsue, T.; Evans, D. H.; Osa, T.; Kobayashi, N. *J. Am. Chem. Soc.* **1985**, *107*, 3411-3417. (d) Wang, Y.; Mendoza, S.; Kaifer, A. E. *Inorg. Chem.* **1998**, *37*, 317.

- 6) Hu, J. M.; Zhang, J. Q.; Cao, C. N. *Prog. Org. Coat.* **2003**, *46*, 273.
- 7) (a) Andreaus, B.; Scherer, G. G. *Solid State Ionics* **2004**, *168*, 311. (b) Wagner, N. *J Appl. Electrochem.* **2002**, *32*, 859. (c) Boukamp, *Solid State Ionics* **2004**, *169*, 65. (d) Gomadam, P. M.; Weidner, J. W.; *Int. J. Energy Res.* **2005**, *29*, 1133.
- 8) Wang, Q.; Moser, J. -E. Grätzel, M. *J. Phys. Chem. B* **2005**, *109*, 14945.
- 9) (a) Guan, J. -G.; Miao, Y. -Q.; Zhang, Q. -J. *J. Biosci. Bioeng.* **2004**, *97*, 219. (b) Janshoff, A.; Steinem, C.; Michalke, A.; Henke, C.; Galla, H. -J. *Sens. Actuators B* **2000**, *70*, 243. (c)
- 10)(a) Naumann, R.; Baumgart, T.; Gräber, T.; Jonczyk, A.; Offenhäuser, A.; Knoll, W. *Biosens. Bioelectr.* **2002**, *17*, 25. (b) Naumann, R.; Schmidt, E. K.; Jonczyk, A.; Fendler, K.; Kadenbach, B.; Liebermann, T.; Offenhäuser, A.; Knoll, W. *Biosens. Bioelectr.* **2002**, *17*, 25.
- 11)(a) Ion, A.; Ion, I.; Moutet, J. -C.; Pailleret, A.; Popescu, A.; Saint-Aman, E.; Ungureanu, E.; Siebert, E.; Ziessel, R. *Sens. Actuators B*, **1999**, *59*, 118. (b) Janshoff, A.; Steinem, C.; Michalke, A.; Henke, C.; Galla, H. -J. *Sens. Actuators B*, **2000**, *70*, 243. (c) Zhang, S.; Echegoyen, L. *J. Am. Chem. Soc.* **2005**, *127*, 2006. (d) Flink, S.; Van Veggel, F. C. J. M.; Reinhoudt, D. N. *J. Phys. Chem. B* **1999**, *103*, 6515. (e) Flink, S.; Boukamp, B. A.; Van den Berg, A.; Van Veggel, F. C. J. M.; Reinhoudt, D. N. *J. Am. Chem. Soc.* **1998**, *120*, 4652. (f) Katz, E.; Lioubashevsky, O.; Willner, I. *J. Am. Chem. Soc.* **2004**, *126*, 15520.
- 12)Michels, J. J.; Baars, M. W. P. L.; Meijer, E. W.; Huskens, J.; Reinhoudt, D. N. *J. Chem. Soc., Perkin. Trans. 2* **2000**, 1914.
- 13)Takada, K.; Diaz, D.J.; Abruña, H.D.; Cuadrado, I.; Casado, C.; Alonso, B.; Morán, M.; Losanda, J. *J. Am. Chem. Soc.* **1997**, *119*, 10763.
- 14)Bard, A. J.; Faulkner, L. R. *Electrochemical Methods: Fundamentals and Applications* John Wiley & Sons: New York, **2001**.
- 15)Boukamp, B. A. *J. Electrochem. Soc.* **1995**, *142*, 1885.
- 16)Boukamp, B. A. *Solid State Ionics* **1986**, *20*, 31.
- 17)(a) Matsue, T.; Evans, D. E.; Osa, T.; Kobayashi, N. *J. Am. Chem. Soc.* **1985**, *107*, 3411. (b) Osella, D.; Carretta, A.; Nervi, C.; Ravera, M.; Gobetto, R. *Organometallics* **2000**, *19*, 2791.
- 18)(a) Sun, H.; Chen, W.; Kaifer, A. E. *Organometallics* **2006**, *25*, 1828 (b) Goldsmith, J. I.; Takada, K.; Abruña, H. D. *J. Phys. Chem. B* **2002**, *106*, 8504.
- 19)Sluyters-Rehbach, M.; Sluyters, J. H. *J. Electroanal. Chem.* **1975**, *65*, 831.
- 20)Baars, M. W. P. L.; Karlsson, A. J.; Sorokin, V.; de Waal, B. F. W.; Meijer E. W. *Angew. Chem. Int. Ed.* **2000**, *39*, 4262.
- 21)Dobbs, D. A.; Bergman, R. G.; Theopold, K. H. *Chem. Eng. News* **1990**, *68*, 2.

Biferrocenyl Dendrimers at Molecular Printboards*

This chapter describes the synthesis and electrochemistry of biferrocenyl dendrimers, and their β -cyclodextrin (β CD) inclusion complexes in solution and at surfaces. Three generations of poly(propylene imine) (PPI) dendrimers, decorated with 4, 8, and 16 biferrocenyl (BFc) units respectively, were synthesized. The dendrimers were solubilized in aqueous media by complexation of the BFc end groups to β CD in a similar fashion as was described in chapter 3 for ferrocenyl- (Fc-) functionalized dendrimers. The dendrimers were adsorbed at the β CD molecular printboard and the binding valency was determined. The complexation of BFc to β CD is sensitive to the oxidation state of the BFc units. Oxidation of one iron centre (oxidation of neutral BFc- $Fe_2(II,II)$ to the cationic mixed-valence biferrocenium- $Fe_2(II,III)^+$) resulted in dissociation of the host-guest complexes. Scan rate-dependent cyclic voltammetry and differential pulse voltammetry of dendrimer- β CD assemblies immobilized at the β CD host surface and in solution revealed that the dendrimers are oxidized in three steps. The surface β CD-bound BFc moieties are first oxidized to the mixed valence state, followed by the oxidization of the non-interacting groups. The third step consists of the oxidization of all mixed-valence BFc moieties to the $Fe_2(III,III)^{2+}$ form.

* This chapter has been published in: Nijhuis, C. A.; Dolatowska, K. A.; Ravoo, B. J.; Huskens, J.; Reinhoudt, D. N. *Chem. Eur. J.* **2006**, in press.

5.1 Introduction

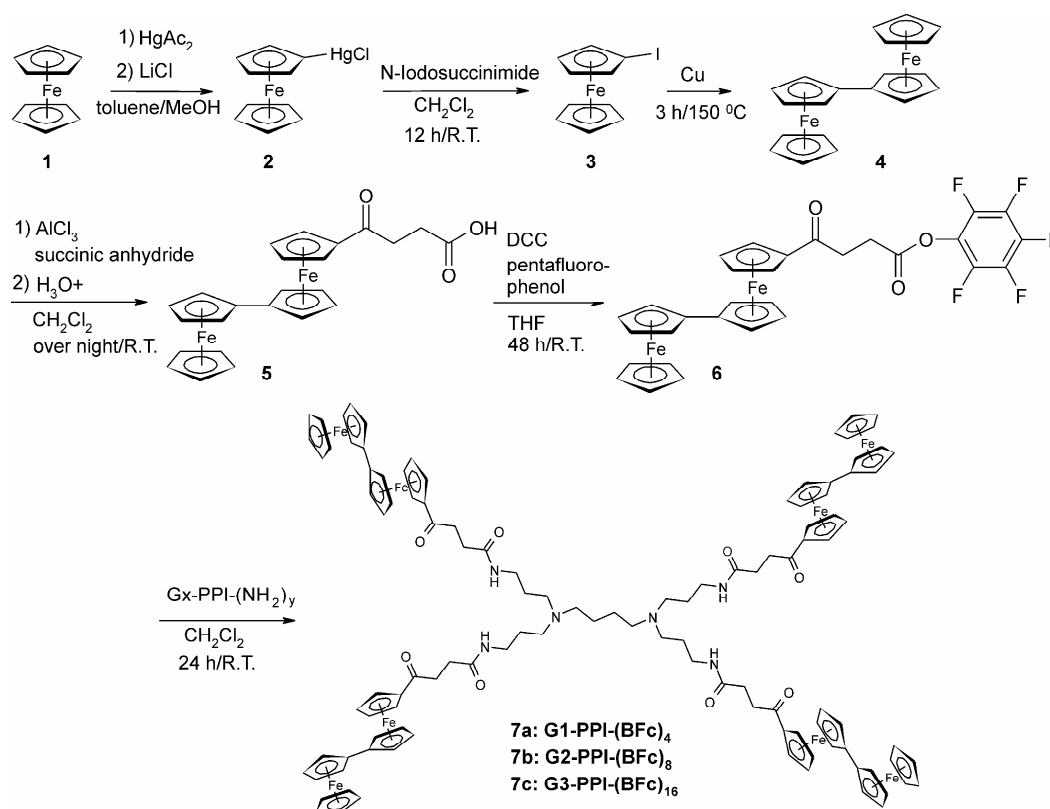
Organometallic polymers and dendrimers based on ferrocene (Fc) or ferrocene conjugates have attracted considerable attention to prepare macromolecular materials which may find applications in a variety of fields owing to their high thermal stability, reversible redox properties and synthetic versatility.¹ Conjugated Fc units are of special interest since mixed valence states are accessible with noticeable electron mobilities and interesting electrical, redox, and magnetic properties.² The degree of electrochemical interaction between the conjugated ferrocenes is normally expressed as the difference in redox potentials of the interacting units. Electronically communicating ferrocenes, for instance, via a bridging Si³ or N-atom,⁴ or alkene or alkyne tethers,⁵ have a difference of oxidation potential (ΔE_p) in range of 10-180 mV depending largely on the length of the tether and the degree of conjugation. Directly linked ferrocene oligomers, like biferrocene (BFc), have strongly electronically interacting metal centres with a ΔE_p in the range of 240-300 mV.^{1,2,5} The BFc groups can selectively be oxidized by I₂ yielding the mixed valence Fe₂(II,III)⁺ complexes.⁶ BFc moieties have been immobilized at gold nanoparticles and gold surfaces⁷ and used in complexation studies of alkali and alkaline earth metal ions.⁸

In view of the interesting properties of BFc and its promising potential especially in molecular electronics, the possibilities to confine BFcs at the β CD molecular printboard was investigated. PPI dendrimers of generation 1-3 terminated with 4, 8, and 16 BFc moieties, respectively, were prepared. The ability of BFc to form inclusion complexes with β CD was studied by isothermal titration microcalorimetry. The adsorption of the water-soluble dendrimer- β CD assemblies at β CD SAMs on gold was studied by surface plasmon resonance (SPR) spectroscopy. The number of host-guest interactions for each dendrimer was investigated by electrochemistry and SPR titrations. The BFc moiety can exist in three oxidation states, in the neutral Fe₂(II,II), the cationic Fe₂(II,III)⁺, and the dicationic Fe₂(III,III)²⁺ states. The redox processes which control the ability of the dendrimers to form inclusion complexes with β CD were studied by cyclic voltammetry (CV) and differential pulse voltammetry (DPV).

5.2 Results and discussion

5.2.1 Synthesis

Three generations of BFc-terminated PPI dendrimers were prepared as outlined in Scheme 5.1. Ferrocene **1** was *in situ* converted to FcHgAc which after reaction with LiCl gave the FcHgCl **2**, which could be easily separated from the disubstituted product. Subsequent reaction with N-iodosuccinimide gave the monofunctionalized iodoferrocene **3**.⁹ Ullmann coupling gave the BFc **4**.¹⁰ Friedel-Craft acylation with succinic anhydride gave the monoacylated product **5** in moderate yields (32%) and, subsequently, the carboxylic acid was converted to the more reactive ester **6**. The final BFc-decorated PPI dendrimers **7a** – **7c** were obtained in 69% to 95% yield by reaction of **6** with the corresponding amino terminated PPI dendrimers, G1-PPI-(NH₂)₄, G2-PPI-(NH₂)₈, or G3-PPI-(NH₂)₁₆. All BFc dendrimers and intermediates were characterized by ¹H NMR, ¹³C NMR, elemental analysis, and MS. All analytical data were consistent with the molecular structures.



Scheme 5.1: Synthesis of BFc-functionalized dendrimers; of the end products **7**, only **7a** is shown for clarity.

5.2.2 BFc- β CD complexation

The BFc carboxylic acid **5** is quite soluble in water at high pH and the complexation to β CD was studied by isothermal titration microcalorimetry (ITC). Figure 5.1 shows the exothermic heat profile vs. the molar ratio $[\beta\text{CD}]/[\mathbf{5}]$ obtained by titration of a solution of β CD to a solution of **5**. The inflection point was very close to a molar ratio of 1:1 and the data were fitted to a model for a 1:1 interaction of the BFc guest with the β CD host. The intrinsic binding constant K_i and the enthalpy ΔH° of complexation are $K_i = 2.5 \times 10^4 \text{ M}^{-1}$ and $\Delta H^\circ = -8.5 \text{ kcal/mol}$, respectively. A rather large unfavorable entropy term was found ($T\Delta S^\circ = -2.7 \text{ kcal/mol}$), indicating that the formation of BFc- β CD complex is enthalpy driven.

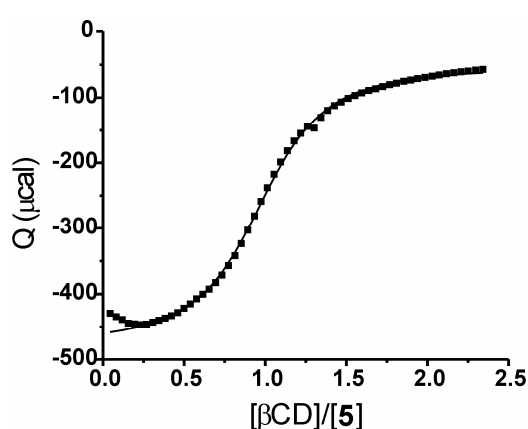


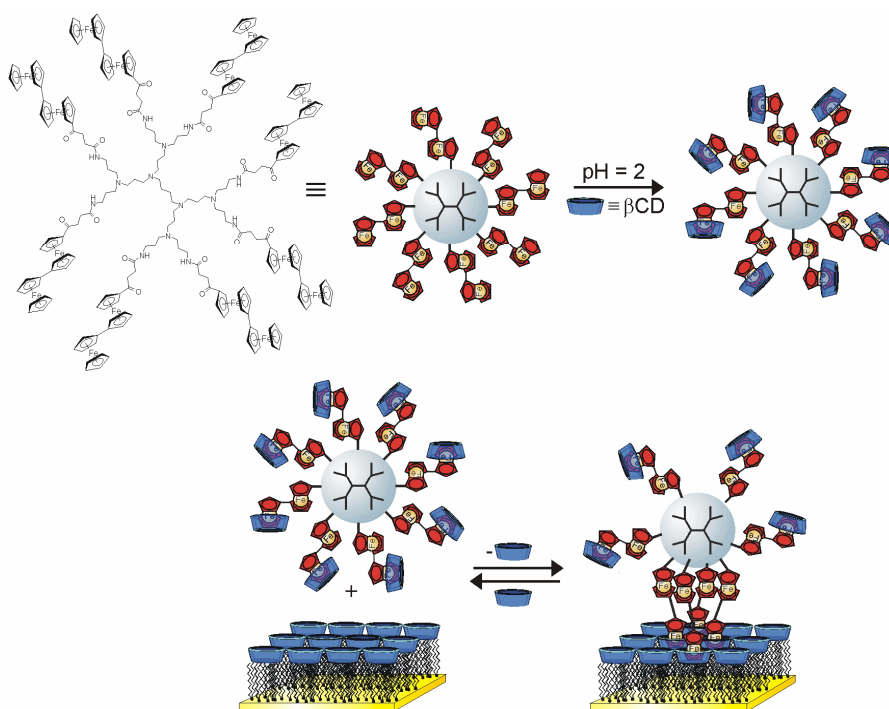
Figure 5.1: Heat evolved per injection plotted vs. the molar ratio $[\beta\text{CD}]/[\mathbf{5}]$ (markers) and fit (solid line) for the calorimetric titrations of 10 mM β CD to 1 mM of **5**, in water at pH = 12 (NaOH) at 295 K.

Typical K values for ferrocene derivatives are one order of magnitude smaller: for ferrocene carboxylate $K_i = 2.1 \times 10^3 \text{ M}^{-1}$, $\Delta H^\circ = -3.6 \text{ kcal/mol}$ and $T\Delta S^\circ = 0.9 \text{ kcal/mol}$, and for ferrocene quaternary ammonium salts, K_i values ranging from 7.1×10^2 to $4.8 \times 10^4 \text{ M}^{-1}$, ΔH° values ranging from -5.1 to -6.8 kcal/mol , and $T\Delta S^\circ$ values ranging from -0.5 to -2.1 have been reported.¹¹ Ferrocenemethanol gave a comparable binding constant of $9.9 \times 10^3 \text{ M}^{-1}$, but with a less favorable $\Delta H^\circ = -6.1 \text{ kcal/mol}$ and a more favorable $T\Delta S^\circ = -0.7 \text{ kcal/mol}$.¹² The large difference in ΔH° of biferrocene compared to ferrocene can be explained by the so-called “expanded hydrophobic surface” which has been proposed to explain trends observed for the inclusion of linear alkyl guests with increasing number of aliphatic carbon atoms (N_c).¹¹ Guest molecules with increasing N_c gave more negative ΔG° and ΔH° values while $\Delta G/N_c$ and $\Delta H/N_c$ remained constant. This can be rationalized from the hypothesis that in the case of longer chain lengths at least one methylene group is forced to stay outside the hydrophobic cavity and, hence, increases the exposed hydrophobic surface. Due to complexation of a guest, that is only partly included, water molecules surrounding the complex must solvate part of the guest. Both the release of water molecules from the cavity and the rearrangement

of water molecules play a crucial role in the unfavorable complexation entropy of BFc compared to ferrocenemethanol. The BFc moiety is much larger than the Fc moiety and, therefore, β CD cannot accommodate a BFc moiety as well as it can accommodate a Fc moiety. This results in a more negative ΔH° by 2.4 kcal/mol compared to Fc which is partly compensated by an unfavorable $T\Delta S^\circ$ resulting in a high K_i compared to Fc guests.

5.2.3 Dendrimer- β CD assemblies

The apolar dendrimers were virtually insoluble in water, but a decrease of the pH to 2 and the addition of β CD (β CD/BFc = 10) resulted in water-soluble dendrimer- β CD assemblies, which is similar to the procedure for the Fc dendrimers described in Chapter 3. All dendrimers could be solubilized in water after prolonged ultrasonication. The dendrimer- β CD assembly **7b**·(β CD)₈ is depicted schematically in Scheme 5.2.¹³



Scheme 5.2: G2-PPI-(BFc)₈ (**7b**) and its formation of water-soluble assemblies with β CD (top) and the adsorption of the dendrimer- β CD assembly at the β CD SAM (“molecular printboards”) (bottom).

The solubilities of the BFc dendrimer- β CD assemblies are relatively low compared to the solubilities of the ferrocenyl (Fc) or adamantyl (Ad) analogs (section 3.2.2). The G1-PPI-(BFc)₄ is relatively soluble and solutions up to 1-2 mM in BFc functionality could be prepared at pH = 2 in the presence of an excess of β CD. The solubility decreased with increasing generation, e.g. solutions of G2-PPI-(BFc)₈ up to about 0.5 mM in BFc could be prepared, while G3-PPI-(BFc)₁₆ was only soluble up to 0.2 mM in BFc. In comparison, solutions of the Fc and Ad dendritic analogs of typically 10 mM in functionality could be prepared for all generations. The lower solubility of the complexes can be explained by the fact that,

compared to Fc and Ad, the biferrrocenyl group is shielded less efficiently by the β CD cavity. Consequently a large hydrophobic surface area is still exposed to the solution which increases at increasing generation altering the solubility significantly.

The BFc dendrimer- β CD assemblies were characterized by CV and DPV. Two oxidation waves were observed, which correspond to the oxidation of both metal centers in a two-step one-electron redox process (Figure 5.2). Upon oxidation of the first metal center at $E_{p,1} = 50$ mV, the BFc moiety changes from a neutral $\text{Fe}_2(\text{II},\text{II})$ complex to a positively charged mixed valence state $\text{Fe}_2(\text{II},\text{III})^+$. The second oxidation at $E_{p,2} = 350$ mV results in a dicationic $\text{Fe}_2(\text{III},\text{III})^{2+}$ complex. The large difference in oxidation potential ΔE_p of 300 mV indicates that the metal centres communicate electrochemically strongly. This is consistent with values reported for other biferrrocenes.^{1,2,5} The comproportionation constant K_{com} can be calculated using ΔE_p , according to $K_{\text{com}} = e^{-\left(\frac{RT}{F}\right)\Delta E_p}$, and was found to be 1.2×10^5 . This value of K_{com} suggests that the BFc dendrimers belong to Class II according to the Robin-Day classification.¹⁴ This classification implies that some charge delocalization takes place in the mixed-valence state, but not completely, and that the charge resides mostly at the most electron rich-metal centre, i.e. the terminal ferrocene.

All end groups undergo oxidation and reduction at the same potentials indicating that all end groups are identical and are interacting with β CD in solution. It is well known that all redox end groups of dendrimers (even for large dendrimers containing hundreds of end groups) behave independently and are oxidized at the same potential.¹⁵ Besides normal electron transfer pathways (for instance, an electron hopping mechanism), another mechanism has been proposed for dendrimers which is based on rotational diffusion of the dendrimers.¹⁶ Therefore, it can be safely assumed that all end groups of the BFc dendrimers in the present study are redox active.

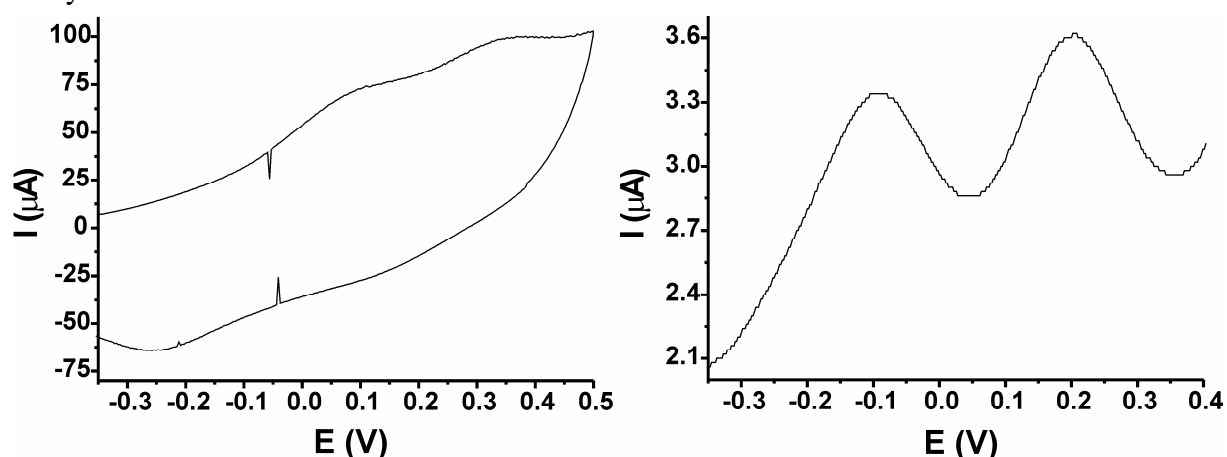


Figure 5.2: Left: CV of G1-PPI-(BFc)₄- β CD assembly at a bare Au-electrode, 1 mM (in functionality) in the presence of 10 mM β CD, pH = 2, 0.1 M NaCl, scan rate = 1 V/s; right: DPV of the same solution, scan rate = 1 mV/s.

5.2.4 SPR spectroscopy of BFc dendrimers at the molecular printboard

The BFc dendrimers were adsorbed at the β CD host surface from aqueous solutions of the dendrimer- β CD assemblies (Scheme 5.2). The dendrimers bind strongly to the printboard owing to the high effective concentration of host sites at the surface and high local concentration of guest groups at the dendrimers. The dendrimers readily form densely packed monolayers at the host surface for a number of reasons: i) the individual host-guest interactions are by nature reversible, ii) the PPI dendrimers are flexible and can extend to access the maximum number of β CD sites at the surface that is sterically allowed, and iii) the multivalency principle prescribes that molecules will interact with the maximum number of interactions p_b (see Chapter 3).

The adsorptions and stabilities of dendrimer- β CD assemblies at the host surface with respect to competitive solutions were examined by SPR.¹⁷ Injection of guest molecules resulted in typical adsorption curves as illustrated in Figure 5.3. Rinsing with a competitive solution of 10 mM aqueous β CD at pH = 2 after adsorption of G1-PPI-(BFc)₄ resulted in desorption of most dendrimers from the surface (Fig. 5.3A), whereas G2-PPI-(BFc)₈ (Fig. 5.3B) and G3-PPI-(BFc)₁₆ (Fig. 5.3C) could not be removed from the host surface even upon rinsing extensively. After rinsing with β CD at pH = 2 only a small decrease in the SPR sensogram could be observed in the case of G2-PPI-(BFc)₈ and a second guest injection resulted in a small increase, but after washing again with 10 mM aqueous β CD at pH = 2 the signal decreased to a similar extent as before the second guest injection. These observations confirm that already after the first injection a densely packed monolayer of dendrimers at the host surface was formed. The small decrease in SPR signal upon rinsing after guest injection indicates removal of non-specifically bound guest molecules. In addition, in the case of G2-PPI-(BFc)₈ a small but steady decrease in SPR signal was observed during rinsing. This decrease implies that the G2-PPI-(BFc)₈ serves as an intermediate case in terms of stability since G1-PPI-(BFc)₄ can be removed completely and G3-PPI-(BFc)₁₆ can not be removed at all from the surface. The two larger dendrimers have sufficient BFc- β CD interactions to form kinetically stable assemblies at the β CD surface at room temperature.

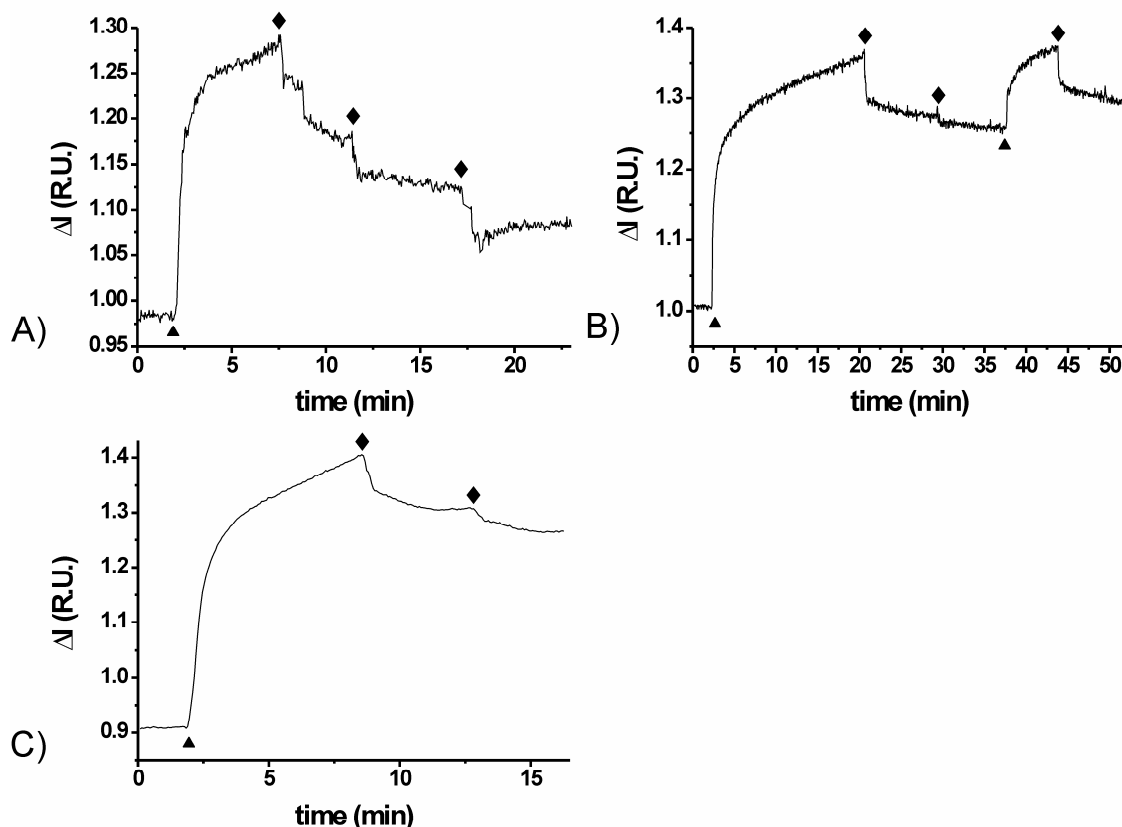


Figure 5.3: SPR sensograms of the adsorption and (attempted) desorption of G1-PPI-(BFC)₄ (**7a**) (A), G2-PPI-(BFC)₈ (**7b**) (B), and G3-PPI-(BFC)₁₆ (**7c**) (C) adsorption at a β CD SAM; ▲ = injection of guest (concentration of **7a** is 50 μ M, **7b** is 13 μ M, and **7c** is 6.3 μ M) in 10 mM β CD; ◆ = wash with an aqueous solution of 10 mM native β CD at pH = 2.

The number of interactions p_b of the dendrimers with the β CD host surface can be determined from SPR titrations of aqueous solutions of dendrimer- β CD assemblies to the host surface. The changes in SPR signal due to the adsorption of guest as a function of guest concentration can be fitted to a surface binding model for multivalent host-guest interactions.¹⁸ This model is based on the assumption that all biferrocene- β CD interactions are independent and equivalent in solution and at the surface. The model interprets multivalent interactions in terms of the high effective concentration (C_{eff}) of available host molecules at the surface upon binding of the first guest group of the dendrimer and accounts for the free binding sites of the dendrimer as well as for the competitive interaction with β CD in solution. Previously, we have shown that for small monovalent guests the intrinsic binding constant at the surface ($K_{i,s}$) closely resembles the intrinsic binding constant in solution ($K_{i,l}$).^{19,20} To prove that this also holds for biferrocene, titrations of **5** (aqueous solution at pH = 12) to the β CD SAM were performed and followed by SPR. Figure 5.4 shows the binding data and the fit to a Langmuir isotherm. From the isotherm, we obtained a binding constant $K_i = 2.2 \times 10^4 \text{ M}^{-1}$, which is very similar to the binding constant in solution obtained by ITC.

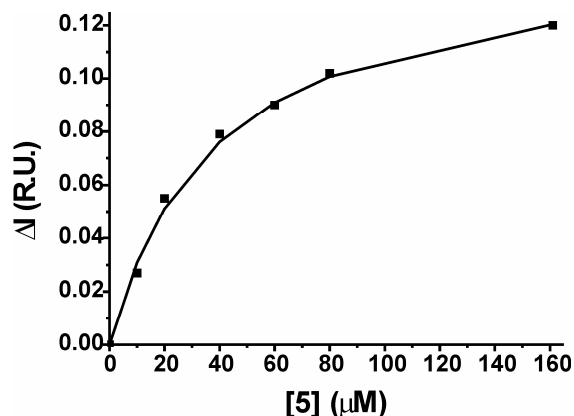


Figure 5.4: SPR titration curve of **5** (aqueous solution at pH = 12) at a β CD SAM (markers) and the fit (solid line) to a Langmuir isotherm.

The BFc dendrimers interact with the surface with the maximum number of interactions because the effective concentration C_{eff} of β CD hosts at the surface (0.3 M) is much larger than the concentration of β CD in solution. The binding curve for the dendrimers can be fitted by optimizing $K_{i,s}$ for various p_b values, but only those fits that give plausible $K_{i,s}$ values, i.e. $K_{i,s} \approx K_{i,l}$, will correspond to the real p_b value (see also section 3.2.4). Titrations were performed with G1-PPI-(BFc)₄ using a constant competitive solution (10 mM β CD at pH = 2), as the other two dendrimers form kinetically stable assemblies. Figure 5.5 shows a typical titration curve and in Table 5.1 the fitting solutions are given for $p_b = 2, 3$, or 4. Figure 5.5 also shows a fit that was found assuming three interactions to the surface per molecule ($p_b = 3$). An intrinsic binding constant at the surface $K_{i,s}$ of $2.1 \times 10^4 \text{ M}^{-1}$ per BFc- β CD interaction was obtained in this case, which compares very well to $K_{i,l} = 2.5 \times 10^4 \text{ M}^{-1}$. On the contrary, for p_b values of 2 and 4, only implausible $K_{i,s}$ values were found (Table 5.1).

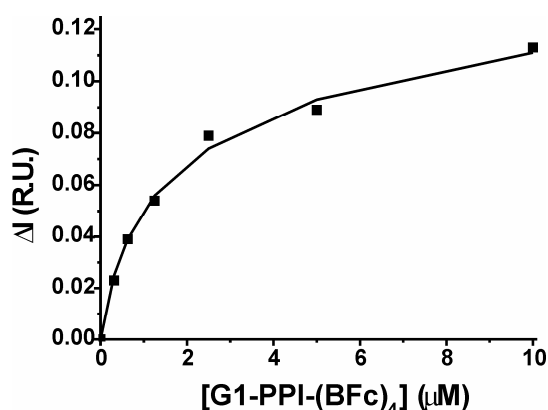


Figure 5.5: SPR titration curve of G1-PPI-(Fc)₄ (**7a**) with 10 mM native β CD at pH = 2 to a β CD SAM with a fit for 3 interactions.

Table 5.1: Optimized $K_{i,s}$ values for SPR titrations of G1-PPI-(BFC)₄ (**7a**) to β CD SAMs.

p_b	$K_{i,s}$ (M ⁻¹) ^a	SPR max ^a	R
2	1.3×10^5	0.33	0.98
3	2.1×10^4	0.56	0.98
4	9.4×10^3	1.0	0.98

^a Determined using the multivalency model with $C_{\text{eff,max}} = 0.3 \text{ M}$ and $K_{i,1} = 2.5 \times 10^4 \text{ M}^{-1}$, for varying p_b .

This observation agrees very well with the stability study of Fc dendrimers of various types and generations (Chapter 3). In comparison with the Fc dendrimers, the BFc dendrimers have a small dendritic core with short tethers between the end group and the dendritic core and a higher $K_{i,s}$, and also give kinetically stable assemblies at $p_b \geq 4$.

5.2.5 Electrochemistry of BFc dendrimers on the molecular printboard

CV and DPV spectra of the BFc dendrimer- β CD assemblies at bare Au electrodes showed two oxidation waves of similar intensity (Figure 5.2). In contrast, CVs of the G1-PPI-(BFC)₄ – β CD in solution at a β CD SAM showed a pronounced first wave while the second oxidation wave was hardly visible (Fig. 5.6A). DPV spectra clearly showed the second oxidation wave of the assemblies at the host surface in the case of G1-PPI-(BFC)₄ – β CD (**6B**). Again the first signal is intense and sharp, while the second signal is very broad and significantly less pronounced. These observations can be explained by the hypothesis that a single oxidation diminishes the BFc- β CD interaction, because of charge delocalization over the BFc moiety. The most electron rich metal centre is the terminal Fc without the electron withdrawing carbonyl linker implying that the part of the BFc moiety complexed to the β CD is (more) positively charged in the mixed valence state. This suggests that oxidation of one iron centre in the BFc leads to desorption of the dendrimers from the host surface and, therefore, a second oxidation is more difficult. This scenario is supported by the shifts of both oxidation potentials compared to the experiments performed at bare Au electrodes (Fig. 5.2). $E_{p,a,1}$ is shifted by 40 mV to higher oxidation potentials due to the presence of the β CD SAM, while $E_{p,a,2}$ is shifted by 120 mV to higher potentials, leading to a large ΔE_p 374 mV, compared to a ΔE_p 301 mV at bare Au electrodes.

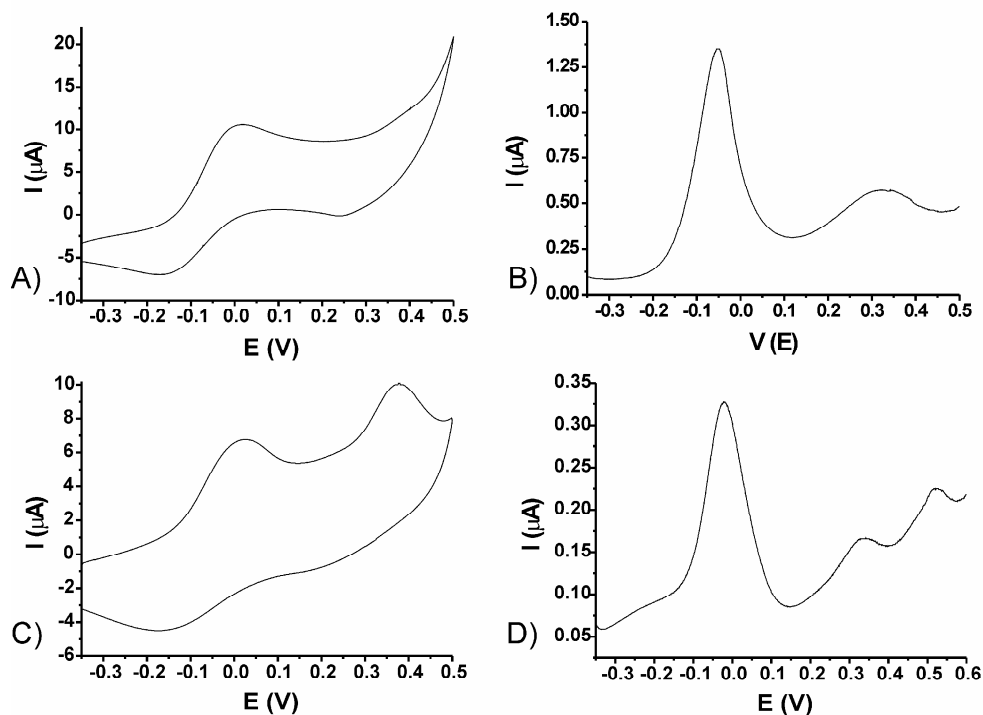
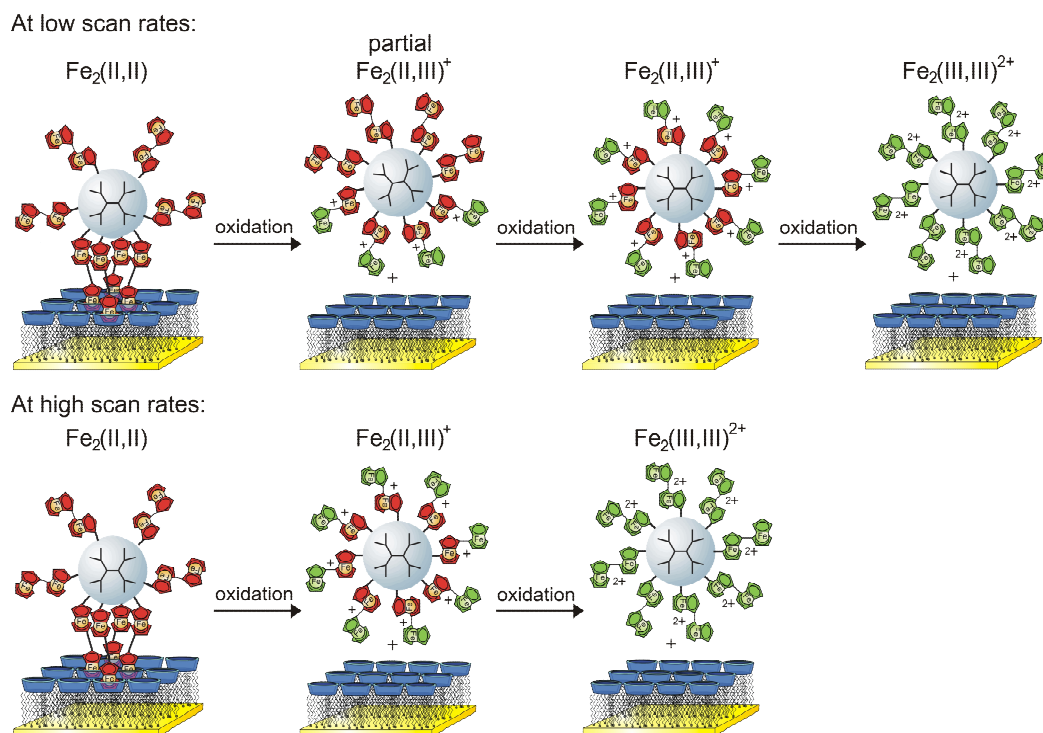


Figure 5.6: CV (A (0.1 V/s) and C (20 mV/s)) and DPV (B and D) of 1 mM (in functionality) aqueous solution of G1-PPI-(BFC)₄ (**7a**) and G3-PPI-(BFC)₁₆ (**7c**) with 10 mM native β CD at pH = 2 at Au electrodes covered with a β CD SAM).

A similar behavior was observed for G2-PPI-(BFC)₈ (not shown) and G3-PPI-(BFC)₁₆. However, for G3-PPI-(BFC)₁₆ a second oxidation wave was clearly visible in the CV spectra under the same conditions (Fig. 5.6C). Additionally, DPV spectra of both G2-PPI-(BFC)₈ (not shown) and G3-PPI-(BFC)₁₆ (Fig. 5.6D) revealed the presence of a third wave at around 490 mV and 501 mV, respectively. This suggests a complicated oxidation mechanism due to the host-guest chemistry of the dendrimers and the molecular printboard involving a three-step oxidation process of the molecules at the host surface. A possible explanation is outlined in Scheme 5.3. During the first step ($E_p = -24$ mV) the interacting BFC moieties are oxidized resulting in partially oxidized dendrimers that interact weakly with the β CD SAM. Subsequently, the non-interacting groups are oxidized ($E_p = 340$ mV) and finally all end groups undergo a second oxidation ($E_p = 520$ mV). More details and evidence in support of this proposed mechanism are discussed below.



Scheme 5.3: Schematic of the proposed oxidation mechanism of biferrrocenyl dendrimers in solution and immobilized at the βCD host surface outlined for $\text{G2-PPI}(\text{BFc})_8$ which has four interactions with the host surface (see below). The proposed oxidation and desorption are scan rate-dependent.

The $\text{G3-PPI}(\text{BFc})_{16}(\beta\text{CD})_{16}$ assemblies have a ΔE_p of 352 mV and $\text{G2-PPI}(\text{BFc})_8$ has a ΔE_p of 360 mV. The increase in ΔE_p at the host surface is caused by the fact that the dendrimers have a strong interaction with host surface. The interaction of the mixed valence state dendrimers (partially or with all moieties in the $\text{Fe}_2(\text{II},\text{III})^+$ state) may not be entirely negligible. The interaction of these species can be estimated from eq. 1 and 2:

$$\Delta\Delta E_{p,1} = E_{p,2} - E_{p,1} = \left(\frac{RT}{F}\right) \ln \left(\frac{K_i}{K_{1,1}}\right) \quad (1)$$

$$\Delta\Delta E_{p,2} = E_{p,3} - E_{p,2} = \left(\frac{RT}{F}\right) \ln \left(\frac{K_{1,1}}{K_{1,2}}\right) \quad (2)$$

In eq. 1 and 2 K_i , $K_{1,1}$ and $K_{1,2}$ are the equilibrium constants of βCD with BFc , with BFc in the $\text{Fe}_2(\text{III},\text{III})$, partial $\text{Fe}_2(\text{II},\text{III})^+$, and $\text{Fe}_2(\text{II},\text{III})^+$ states, respectively.²¹ This equation holds if the system is reversible and the $[\beta\text{CD}] \gg [\text{BFc}]$. These conditions are met if the scan rates are low and $[\text{BFc}] = 0.1 \text{ mM}$ and $[\beta\text{CD}] = 10 \text{ mM}$. The $K_i = 2.5 \times 10^4 \text{ M}^{-1}$ and the difference in ΔE_p leading to $\Delta\Delta E_{p,1}$ and $\Delta\Delta E_{p,2}$ for the second and third oxidation wave gives $K_{1,1}$ and $K_{1,2}$ at bare Au electrodes and the βCD SAM decorated electrodes, respectively. For the partially oxidized dendrimers $\Delta\Delta E_{p,1}$ values of 73 mV, 69 mV, and 52 mV for $\text{G1-PPI}(\text{BFc})_4$, $\text{G2-PPI}(\text{BFc})_8$, and, $\text{G3-PPI}(\text{BFc})_{16}$, respectively, were found resulting in $K_{1,1}$ values of 11 M^{-1} , 20

M^{-1} and $117 M^{-1}$. Thus, the assemblies have a small, but significant interaction with the host surface in the partial mixed valence state. The third oxidation wave has a $\Delta\Delta E_{p,2}$ of more than 200 mV which leads to $K_2 \ll 1 M^{-1}$ indicating that the dendrimers in the $\text{Fe}_2(\text{II,III})^+$ state do not have any significant interaction with the host surface.

To elucidate the complex redox behavior of the dendrimers at the host surface and to determine the number of interactions of all dendrimers, scan rate-dependent CV was performed of monolayers of the dendrimers at the host surface. The dendrimers were adsorbed at the βCD host surface by immersion of preformed βCD host monolayers into aqueous solutions containing the dendrimer- βCD assemblies (Scheme 5.2) followed by rinsing with water and drying under a stream of N_2 . The electrochemically induced desorption of the dendrimers from the molecular printboard is shown in Figure 5.7. In a typical experiment ten successive CV scans were recorded at different substrates with the scan rate v ranging from 5 mV/s to 10 V/s. As the potential increases to 50 mV, the BFc groups are oxidized and mixed valence biferrocenium cations $\text{Fe}_2(\text{II,III})^+$ are formed. The BFc $\text{Fe}_2(\text{II,III})^+$ cations form only very weak inclusion complexes with βCD resulting in desorption of the dendrimers from the βCD SAM and diffusion into the solution.

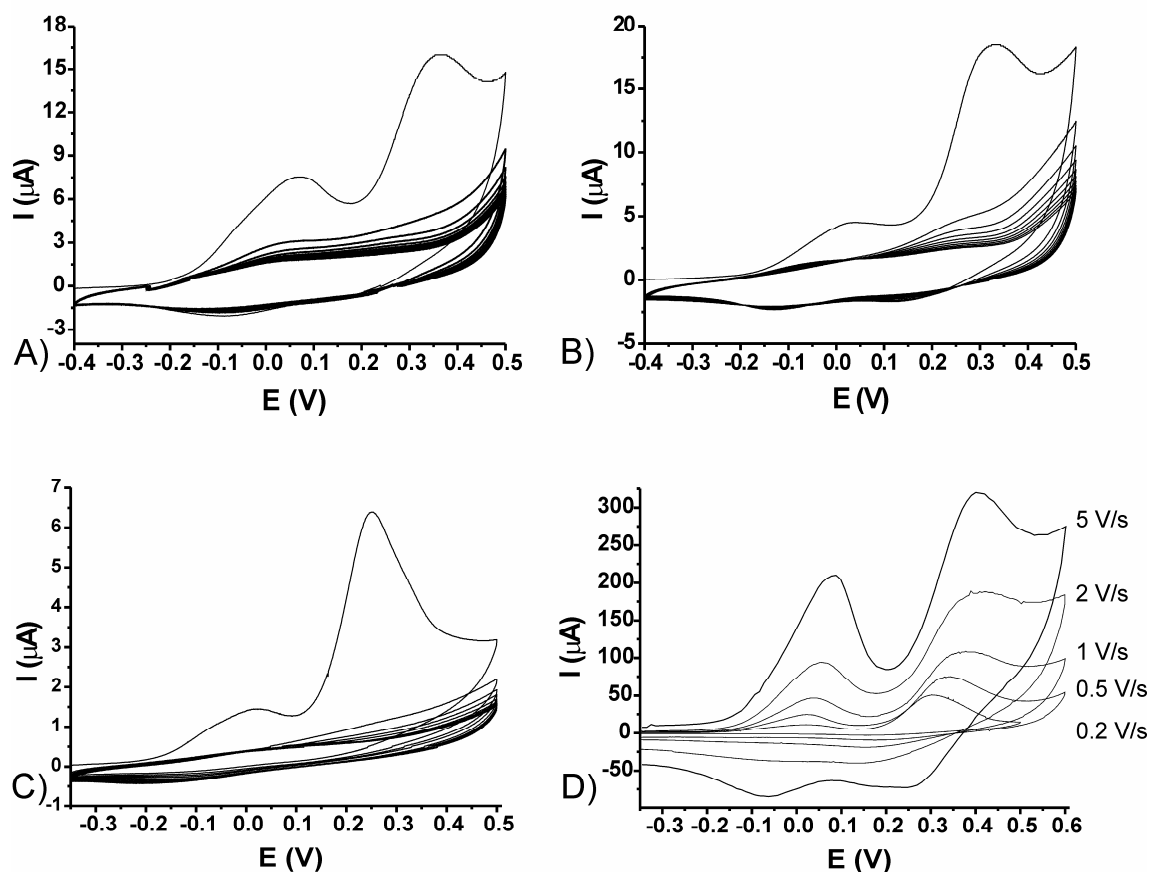


Figure 5.7: Electrochemical desorption of G1-PPI-(BFc)_4 (**7a**) from a βCD SAM induced and observed by CV, scan rate = 200 mV/s, 0.1 M K_2SO_4 , 10 scans (A); the same for G2-PPI-(BFc)_8 (**7b**) at 100 mV/s (B) and G3-PPI-(BFc)_{16} (**7c**) at 25 mV/s (C); only the first scan of similar desorption experiments at scan rates of 0.2, 0.5, 1, 2, and 5 V/s (D) for G3-PPI-(BFc)_{16} .

The electrochemically induced desorption of the BFc dendrimers is completely analogous to that of Fc dendrimers (Chapter 3). Only dendrimers that remain in close proximity to the surface may be reduced and rebound to the surface. During subsequent scans only rebound dendrimers are oxidized resulting in a rapid decrease of peak intensity. In fact, already after the first scan most dendrimers are removed from the surface at low v as is shown in Figure 5.7A-C. By increasing v to 5 V/s, as is shown for G3-PP-(BFc)₁₆ in Figure 5.7D, not all dendrimers have sufficient time to diffuse away from the host substrate and a significant fraction is reduced and readsorbed.

The numbers of interactions p_b were determined from the relative surface coverages of the surface-confined bCD (G_{bCD}) and the BFc units (G_{BFc}) as described in detail in section 3.2.4. The Γ_{BFc} was determined from the CV data by integration of both oxidation waves of the first scan of the (i, E)-curves which gives the total charge (Q_{tot}) and using the relation $\Gamma_{BFc} = Q_{tot}/nFA$.²² Q_{tot} is independent of v ranging from 5 mV/s to 10 V/s indicating surface-confined processes.

For G1-PPI-(BFc)₄ a G_{bCD}/G_{BFc} ratio of 0.77 was found which implies that $p_b = 3$ and thus three BFc- β CD interacting end groups (out of 4) with the host surface. For G2-PPI-(BFc)₈ a G_{bCD}/G_{BFc} ratio was 0.55 which indicates $p_b = 4$ interactions (out of 8), and for G3-PPI-(BFc)₁₆ the ratio was 0.26 suggesting $p_b = 4$ interactions (out of 16). Two BFc moieties at the same branch are separated by 2.2 nm and, consequently, both may interact simultaneously with two bCD s at the molecular printboard, since the center-to-center spacing of two adjacent bCD s at the surface is 2.1 nm. However, two BFc groups of different branches are separated by 2.8 nm, implying that G1-PPI-(BFc)₄ can have only three interactions with the host surface since to complex a fourth bCD at the surface a distance of 3.5 nm has to be covered. The maximal distance of two BFc groups of G2-PPI-(BFc)₈ is 3.9 nm, which is sufficient for having four interactions. Thus, the number of interactions found by electrochemistry corresponds very well with the estimated sizes of the molecules compared to the lattice periodicity of the molecular printboard. The number of interactions for the first generation is in full agreement with the SPR results. The maximal distance between two end groups of G3-PPI-(BFc)₁₆ is 5.3 nm, indicating that 7-8 interactions would have been possible, but the number of interactions of G3-PPI-(BFc)₁₆ is only 4 due to steric hindrance since the dendritic core is relatively small. In comparison, G3-PPI-(Fc)₁₆ lacks the tether and has 4 interactions (section 3.2.4). This indicates that the small tether between the dendritic core and the BFc moiety is not sufficient to overcome the steric hindrance and to increase the number of interactions.

The surface areas of both waves of the first scan are different and the ratio of the charge of the first wave Q_1 and the second wave Q_2 is dependent on the dendrimer generation (Fig. 5.7 A-C) as well as on the scan rate v (Fig. 5.7D). In all cases Q_1 was smaller than Q_2 at low v . The $Q_1:Q_2$ ratio was 0.63 for G1-PPI-(BFc)₄, 0.33 for G2-PPI-(BFc)₈, and 0.14 for G3-PPI-(BFc)₁₆. The same three-step oxidation mechanism that was proposed to explain the CV and

DPV data for the solution experiments can also be used here. During the first oxidation only the iron center of the BFc end groups interacting with the surface are oxidized, while during the second oxidation the remaining metal centres of the entire dendrimer are oxidized as is outlined in Scheme 5.3. This implies that in the case of the G1-PPI-(BFc)₄, which has three interactions, during the first oxidation 3 metal centers are oxidized whereas during the second oxidation the remaining 5 metal centers are oxidized leading to a ratio of $Q_1:Q_2$ of 0.60 (3/5). For G2-PPI-(BFc)₈ with 16 Fe-centers and four interactions the ratio is 0.33 (4/12) and for G3-PPI-(BFc)₁₆ with 32 Fe centers and four interactions the theoretical ratio is 0.14 (4/28). The theoretical $Q_1:Q_2$ ratios compare very well to the found ratios.

Increasing v led to an increase of the $Q_1:Q_2$ ratios until at high v the $Q_1:Q_2$ ratio increased to a maximum of 1 and remained constant for all dendrimers. This is illustrated in Figure 5.7D for G3-PPI-(BFc)₁₆ at v ranging from 0.2 V/s to 5 V/s and in Figure 5.8 for G3-PPI-(BFc)₁₆ at v ranging from 5 mV/s to 10 V/s and the $Q_1:Q_2$ ratios are plotted versus v . Additionally, in Figure 5.8 the linear dependency of $Q_1:Q_2$ ratio on v is shown when the $Q_1:Q_2$ ratio changes (between 50 mV/s and 2 V/s for G3-PPI-(BFc)₁₆). The other dendrimers behaved the same.

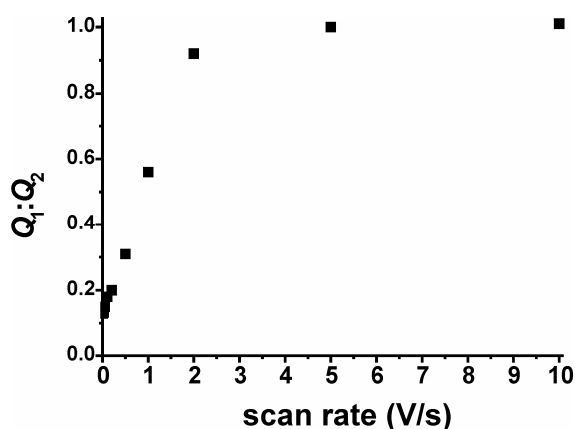


Figure 5.8: Scan rate dependency of the $Q_1:Q_2$ ratio for G3-PPI-(BFc)₁₆ adsorbed at the host surface determined at 0.005, 0.010, 0.025, 0.05, 0.1, 0.2, 0.5, 1, 2, 5 and 10 V/s.

These observations support the oxidation process illustrated in Scheme 5.3. The redox mechanism of the oxidation of the BFc dendrimers adsorbed at the surface is a two-step single-electron redox process for all end groups, but the potential at which the bound end groups undergo the first oxidation is lower than for the non-interacting moieties. The oxidation potential of the non-interacting groups is almost the same as at which the second metal center of the BFc moieties are oxidized (Scheme 5.3, upper part). At very low scan rates, e.g. 1 mV/s or lower, a shoulder is observed at the second oxidation wave. The dissociation of the BFc - bCD inclusion complexes is fast compared to the electrochemical time scale at low v , but becomes comparable at intermediate v . Therefore, the $Q_1:Q_2$ ratio gradually increases by increasing v linearly which is characteristic for a surface-confined process. (For diffusion-dependent processes, a square root relationship is expected). At high v

the dissociation is slow on the electrochemical time scale and all BFc end groups undergo oxidation to the mixed valance state at the same potential to give $Q_1 = Q_2$ (Scheme 5.3, lower part).

This interpretation is consistent with the CV and DPV experiments of the dendrimer- β CD assemblies in solution at the β CD SAM where DPV showed three distinct oxidation waves. The increase of the observed $K_{1,2}$ values with increasing generation can be rationalized by the increase of the number of non-interacting end groups, i.e. 1, 4 and 12 for generations 1, 2 and 3, respectively.

5.2.6 Simultaneous SPR and CV

In order to prove unambiguously that oxidation of one iron centre of the BFc units leads to dissociation of the BFc- β CD host-guest complex and, consequently, to desorption of the dendrimers from the host surface, CV was performed in combination with SPR.²³ Combining these two techniques gives crucial information about the efficiency and the desorption rate of the dendrimers upon electrochemical oxidation, since the electrochemical time scale can be coupled to the SPR time scale. The experiments were performed in stationary solutions, i.e. the dendrimer- β CD assemblies were present in solution and at the β CD SAM, because under those conditions the adsorption and desorption processes are limited by diffusion. A solution of G1-PPI-(BFc)₄ was added to a β CD SAM (1 mM solution in functionality in the presence of 10 mM β CD at pH = 2) and a typical adsorption curve was observed as was described in the SPR section (Fig. 9). Five successive CV scans were applied at scan rates of 50 mV/s and 25 mV/s and at potentials directly before the first cathodic peak potential ($E_{p,c,1}$), the dendrimers desorbed from the monolayer slowly, but just above $E_{p,c,1}$ virtually all dendrimers were already removed. At this potential the BFc units are in the mixed valance state $Fe_2(II,III)^+$ confirming unequivocally that oxidation of one metal center dramatically diminishes the BFc- β CD interaction. The SPR signal did not change upon increasing the potential well above $E_{p,c,1}$ and above the second oxidation potential $E_{p,c,2}$, because any dendrimer binding to the surface from solution would directly be oxidized. When the potential (during the backward scan) reached the first anodic peak potential ($E_{p,a,1}$), the dendrimers started to adsorb again at the β CD SAM which is apparent from the characteristic adsorption curve in the SPR response. At potentials below $E_{p,a,1}$ the adsorbed dendrimers were not oxidized. During subsequent scans the dendrimers continued to adsorb at the host surface until $E_{p,c,1}$. This cycle of adsorption and desorption was repeated, and all CV scans caused the same increase in SPR response between reduction and oxidation, and a decrease between oxidation and reduction. Since stationary conditions were used, the degree of monolayer formation of the dendrimers at β CD SAM is only dependent on the scan rate ν . Lower scan rates increase the time between reduction and oxidation in successive scans, e.g. $E_{p,a,1}$ and $E_{p,c,1}$, thus the adsorption and desorption times of the dendrimers.

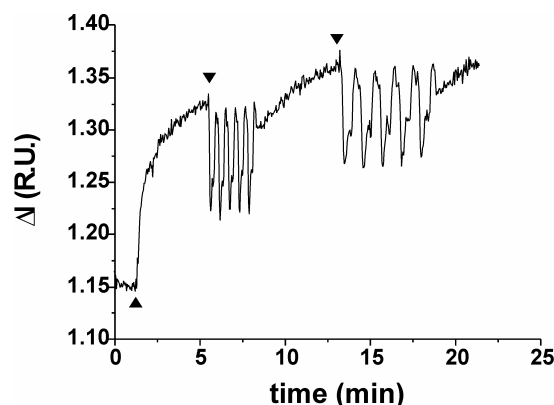


Figure 5.9: SPR response upon performing CV at a 0.25 mM solution of G1-BFc-(Fc)₄ at a β CD SAM with 10 mM native β CD at pH = 2: \blacktriangle = injection 0.25 mM solution of G1-BFc-(Fc)₄ with 10 mM β CD at pH = 2; \blacklozenge = 5 CV scans at 50 mV/s (left) and 25 mV/s (right).

5.3 Conclusions

A new type of dendrimer consisting of electrochemically communicating BFc end groups has been prepared. Biferrocenyl carboxylate **5** readily forms stable inclusion complexes with β CD and the binding constant was found to be $2.5 \times 10^4 \text{ M}^{-1}$ which is an order of magnitude larger than for ferrocene- β CD complexes. The higher complexation constant is caused by a favorable ΔH° . SPR titrations showed that BFc also forms inclusion complexes with β CD SAMs with a binding constant similar as found in solution. Three generations of BFc dendrimers could be dissolved in water in the presence of β CD. The β CD complexes to all BFc end groups and the dendrimer- β CD assemblies adsorb at β CD SAMs on gold. The dendrimers formed stable monolayers at the host surface due to the formation of multivalent host-guest complexes which were quantified by electrochemistry for all dendrimers and by SPR titrations in the case of the G1-PPI-(BFc)₄.

These findings are in full agreement with the study described in Chapter 3 of the binding behavior for Fc-functionalized dendrimers to the molecular printboard. However, the electrochemically controlled binding of BFc dendrimers to β CD and β CD SAMs is more complex and different compared to that for ferrocenyl dendrimers. Oxidation of only one iron centre in the BFc- β CD complex results in dissociation of the host-guest complexes and desorption of the dendrimers from the host surface. In the mixed valence state $\text{Fe}_2(\text{II,III})^+$ the BFc moiety is only hardly able to form inclusion complexes with β CD. This also caused a dramatic change in the redox processes of the dendrimers at the host surface. At bare Au electrodes the BFc moieties were all oxidized first to $\text{Fe}_2(\text{II,III})^+$ and subsequently to $\text{Fe}_2(\text{III,III})^{2+}$. At the host surface three oxidation waves were observed. The first oxidation only resulted in the oxidation of the bound BFc moieties and the second oxidation step the remaining BFc moieties were oxidized leading to $\text{Fe}_2(\text{II,III})^+$ for all BFc groups. During the

third oxidation step all end groups undergo a second oxidation leading to molecules with all moieties in the $\text{Fe}_2(\text{III,III})^{2+}$ state. This mechanism was supported by scan rate-dependent measurements of immobilized dendrimers at the βCD host surface. Thus, the redox chemistry is strongly influenced by the ability of the BFc moiety to form inclusion complexes with βCD .

Electronically communicating materials may lead to the development of new and interesting devices. The combination of self-assembly, multivalency and redox activity, provide the ability to alter and control immobilization of molecules precisely. Precise understanding of the redox processes of molecules on surfaces are a prerequisite for applications in, for instance, molecular electronics.

5.4 Experimental

General Procedures. All moisture sensitive reactions were carried out under argon atmosphere. Reagents were commercial and used without further purification. All dry solvents were prepared according to standard procedures and stored over molecular sieves. ^1H NMR and ^{13}C NMR spectra were recorded on Bruker AC300 or Bruker AMX400 spectrometers. Spectra are reported in ppm downfield from TMS as internal standard. Matrix-Assisted Laser Desorption Ionization (MALDI) Time-of-Flight (TOF) mass spectra were recorded using a Perkin Elmer/PerSeptive Biosystems Voyager-DE-RP MALDI-TOF mass spectrometer. Analytical TLC was performed using Merck prepared plates (silica gel 60 F-254 on aluminum). Merck silica gel (40-63 μm) was used for flash chromatography. Column chromatography was performed using silica gel (SiO_2 , E. Merck, 0.040-0.063 mm, 230-240 mesh). Chloromercuriferrocene,⁹ iodoferrocene⁹ and biferrocene¹⁰ were prepared according to literature procedures.

Synthesis

4-Biferrocenyl-4-one butyric acid (5). A mixture of 0.5 g (1.4 mmol) of biferrocene and 0.16 g (1.5 mmol) of succinic anhydride was dissolved in CH_2Cl_2 and cooled to 0 °C. Aluminiumtrichloride (0.45 g, 3.4 mmol) was added to the solution as a powder and the reaction mixture was stirred at room temperature over night. Subsequently, 50 ml of aqueous 10% hydrochloric acid was added and stirring was continued for 1hr. The organic layer was separated and washed thrice with 50 ml portions of 10% hydrochloric acid after which the organic extract was dried over MgSO_4 . Removal of solvent in vacuo gave a dark brown oil that was purified by column chromatography over silica, eluent 5% MeOH/95% CH_2Cl_2 , and isolated a dark red/brown oil. Yield = 32% (0.24 g). m.p. 151.5-152 °C. ^1H NMR (400 MHz, CDCl_3) δ (ppm): 2.60 (t, 2H, $J = 6.7$ Hz, CH_2COOH), 2.81 (t, 2H, $J = 6.3$ Hz, CH_2CO), 3.9 (s, 5H, Cp), 4.22 (t, 4H, $J = 1.7$ Hz, Cp), 4.25 (t, 4H, $J = 1.7$ Hz, Cp), 4.36 (t, 2H, $J = 1.7$ Hz, Cp), 4.37 (t, 2H, $J = 1.9$ Hz, Cp), 4.41 (t, 2H, $J = 1.7$ Hz, Cp), 4.62 (t, 2H, $J = 1.9$ Hz, Cp). ^{13}C NMR (100 MHz, CDCl_3) δ (ppm): 28.00 (CH_2COOH), 34.30 (CH_2CO), 66.55 (Cp), 67.60 (Cp), 68.45 (Cp), 69.50 (Cp), 70.40 (Cp), 71.40 (Cp), 73.30 (Cp), 79.20 (Cp), 81.50 (Cp), 86.90 (Cp), 170.00 (CO), 200.00 (BFcCO). FAB MS Cald. for $\text{C}_{24}\text{H}_{22}\text{O}_3\text{Fe}_2$: $m/z = 470.14$, found: $m/z = 470.1$ [M + H]. Elem. Analysis: Cald. for $\text{C}_{24}\text{H}_{22}\text{O}_3\text{Fe}_2$ C 61.32%, H 4.72%, found C 61.37%, H 4.68%.

Pentafluorophenyl-4-biferrocenyl-4-one-butylate (6). A mixture of the carboxylic acid (**5**) (0.6 g, 1.3 mmol), pentafluorophenol (0.29 g, 1.6 mole) and DCC (0.32 g, 1.6 mmol) was dissolved in 150 ml of dry THF. The reaction was maintained in a nitrogen atmosphere and continued for 48 h at room temperature. The THF was removed in vacuo and the remainder was dissolved in CH₂Cl₂ and washed thrice with saturated NaHCO₃. The organic extract was dried over MgSO₄ and concentrated and purified by column chromatography over silica gel with CH₂Cl₂ as an eluent to give the final product as a red solid in a yield of 60% (0.5 g). m.p. 125.5-126 °C. ¹H NMR (300 MHz, CDCl₃) δ (ppm): 2.86 (s, 4H, CH₂CH₂), 3.96 (2, 5H, Cp), 4.22 (t, 2H, *J* = 1.7 Hz, Cp), 4.24 (t, 2H, *J* = 1.8 Hz, Cp), 4.35 (t, 2H, *J* = 1.7 Hz, Cp), 4.36 (t, 2H, *J* = 1.9 Hz, Cp), 4.41 (t, 2H, *J* = 1.8 Hz, Cp), (t, 2H, *J* = 1.8 Hz, Cp). ¹³C NMR (100 MHz, CDCl₃) δ (ppm): 27.12 (O(CO)CH₂), 34.25 (CH₂CO), 66.70 (Cp), 67.60 (Cp), 68.46 (Cp), 69.57 (Cp), 70.40 (Cp), 71.43 (Cp), 73.35 (Cp), 79.18 (Cp), 81.45 (Cp), 86.89 (Cp), 136.41 (CF), 137.97 (CF), 141.33 (CF), 143.17 (CF), 169.56 (CO), 200.64 (BFcCO). FAB MS Cald. For C₃₀H₂₁ O₃F₅Fe₂ *m/z* = 636.19, Found: *m/z* = 637.4 [M + H]. Elem. Analysis: C₃₀H₂₁ O₃F₅Fe₂ (636.1854) calculated: C 56.64%, H 3.33%, F 14.93%, found: C 56.54%, H 3.36%, F 13.15%.

G1-PPI-(BFc)₄ (7a). A mixture of 300 mg (0.47 mmol) of **6** and 32 mg (0.10 mmol) of G1-PPI-(NH₂)₄ dissolved in a small amount of the dry chloroform was maintained in a nitrogen atmosphere and stirred overnight at room temperature. The product was isolated by repeated precipitation from hexane. Yield: 0.202 g, 95%. MALDI TOF MS Cald. for C₁₁₂H₁₂₀Fe₈N₆O₈ *m/z* = 2125.02, Found *m/z* = 2126 [M + H]. ¹H NMR (300 MHz, CDCl₃) δ (ppm): 1.38 (br, 4H, NCH₂CH₂CH₂CH₂N), 1.70 (br, 8H, CH₂CH₂N), 2.37 (br, 8H, NHCOCH₂), 2.62 (br, 12H, CH₂NCH₂), 2.82 (br, 8H, CH₂CO), 3.24 (br, 8H, NHCH₂), 3.93 (s, 20H, Cp), 4.15 (br, 8H, Cp), 4.19 (br, 8H, Cp), 4.27 (br, 8H, Cp), 4.31 (br, 8H, Cp), 4.37 (br, 8H, Cp), 4.56 (br, 8H, Cp). ¹³C NMR (100 MHz, CDCl₃) δ (ppm): 23.49, 25.34, 30.12, 35.00, 37.54, 50.98, 53.33, 66.53, 67.62, 68.37, 69.52, 70.29, 71.39, 73.74, 79.29, 81.58, 86.79, 173.23 (NHCO), 203.46 (BFcCO).

G2-PPI-(BFc)₈ (7b). Similar procedure as described for **G1-PPI-(BFc)₄** but using 300 mg (0.47 mmol) of **6** and 39 mg (0.050 mmol) of G2-PPI-(NH₂)₈. Yield: 0.151 g, 69%. MALDI TOF MS Cald. for C₂₃₂H₂₅₆Fe₁₆N₁₄O₁₆ *m/z* = 4390.26, found *m/z* = 4393 [M + H]. ¹H NMR (300 MHz, CDCl₃) δ (ppm): 1.38 (br, 4H, NCH₂CH₂CH₂CH₂N), 1.70 (br, 28H, CH₂CH₂N), 2.37 (br, 16H, NHCOCH₂), 2.62 (br, 36H, CH₂NCH₂), 2.82 (br, 16H, CH₂CO), 3.24 (br, 16H, NHCH₂), 3.93 (s, 40H, Cp), 4.15 (br, 16H, Cp), 4.19 (br, 16H, Cp), 4.27 (br, 16H, Cp), 4.31 (br, 16H, Cp), 4.37 (br, 16H, Cp), 4.56 (br, 16H, Cp). ¹³C NMR (100 MHz, CDCl₃) δ (ppm): 22.17, 25.68, 30.01, 35.00, 37.53, 51.04, 66.55, 67.64, 68.38, 69.52, 70.31, 71.39, 73.79, 79.31, 81.60, 86.78, 173.41 (NHCO), 203.43 (BFcCO).

G3-PPI-(BFc)₁₆ (8b). Similar procedure as described for **G1-PPI-(BFc)₄** but using 300 mg (0.47 mmol) of **6** and 44 mg (0.026 mmol) of G3-PPI-(NH₂)₁₆. Yield: 0.200 g, 86%. MALDI TOF MS Cald. for C₄₇₂H₅₂₈Fe₃₂N₃₀O₃₂ *m/z* = 8920.76; found *m/z* = 8945 [M + Na]. ¹H NMR (300 MHz, CDCl₃) δ (ppm): 1.37 (br, 4H, NCH₂CH₂CH₂CH₂N), 1.67 (br, 56H, CH₂CH₂N), 2.38 (br, 32H, NHCOCH₂), 2.54 (br, 36H, CH₂NCH₂), 2.82 (br, 32H, CH₂CO), 3.23 (br, 32H, NHCH₂), 3.92 (s, 80H, Cp), 4.14 (br, 32H, Cp), 4.18 (br, 32H, Cp), 4.26 (br, 32H, Cp), 4.30 (br, 32H, Cp), 4.37 (br, 32H, Cp), 4.56 (br,

32H, Cp). ^{13}C NMR (100 MHz, CDCl_3) δ (ppm): 22.83, 26.02, 30.07, 35.05, 37.76, 51.20, 66.56, 67.65, 68.38, 69.53, 70.32, 71.40, 73.81, 79.34, 81.67, 86.71, 173.03 (NHCO), 203.34 (BFcCO).

Materials and methods. All glassware used to prepare monolayers was immersed in piranha solution (conc. H_2SO_4 and 33% H_2O_2 in a 3:1 ratio). (Warning: piranha should be handled with caution; it can detonate unexpectedly)²⁴. Next, the glassware was rinsed with large amounts of Milli-Q water. All adsorbate solutions were prepared immediately prior to use. All solvents used in monolayer preparation were of p.a. grade.

Substrate preparation. Glass-supported gold substrates for SPR and for electrochemistry (2.54 cm diameter; 47.5 nm and 200 nm metal thickness, respectively, with a 2 nm titanium adhesion layer) were obtained from SSENS bv (Hengelo, The Netherlands). Gold substrates were cleaned by brief immersion in piranha and the resulting oxide layer was removed by leaving the substrates for 10 min in absolute EtOH. The substrates were subsequently immersed in the adsorbate solution (0.1-1 mM) for ca. 16 h at 60°C. Next, the samples were removed from the solutions and rinsed thoroughly with chloroform, ethanol, and Milli-Q water. Adsorption of the dendrimers was carried out by immersing a preformed βCD SAM on Au in an aqueous solution of the corresponding dendrimer- βCD assemble solutions (0.1 mM in BFc functionality in the presence of 10 mM βCD at pH = 2) for at least 1 h. Subsequently, the samples were thoroughly rinsed with Milli-Q water (at pH = 2 to ensure full protonation of the amines) and dried in a stream of N_2 .

Isothermal titration calorimetry. Titrations were performed at 25 °C using a Microcal VP-ITC titration microcalorimeter. Sample solutions were prepared using Milli-Q water. Titrations were performed by adding native βCD aqueous solutions (10 mM or 5 mM) at pH = 12 to 4-biferrocenyl-4-one butyric acid (1 mM or 0.5 mM) at the same pH. The titrations were analyzed using a least square fitting procedure.

Electrochemistry. Electrochemical measurements were performed with an AUTOLAB PGSTAT10, in a custom built three-electrode setup equipped with a platinum counter electrode, a mercury sulfate reference electrode ($V_{\text{MSE}} = +0.61 V_{\text{NHE}}$) and a screw cap holding the gold working electrode (area exposed to the solution = 0.44 cm^2). CV of immobilized dendrimers at the βCD SAMs were recorded in an aqueous solution 0.1 M K_2SO_4 , between $-0.35 V_{\text{MSE}}$ and $0.5 V_{\text{MSE}}$ or $0.6 V_{\text{MSE}}$, at scan rates of 0.05, 0.010, 0.025, 0.05, 0.1, 0.2, 0.5, 1, 2, 5 and 10 V/s. CV spectra of the dendrimer- βCD assemblies in solution (10 mM βCD at pH = 2) at concentrations 0.5 mM, 0.2 mM and 0.2 mM in BFc functionality for **7a**, **7b** and **7c**, respectively, at bare Au electrodes and the βCD SAMs at Au were recorded at scan rates varying from 1 mV/s to 0.5 V/s. For the DPV spectra a modulation time of 0.5 s, interval time of 0.2 s, step potential of 1 mV and a modulation amplitude of 10 mV were used.

Electrochemistry and SPR combined. The electrochemistry SPR setup is very similar to that described earlier by the group of Knoll.²³ The SPR setup in the Kretschmann configuration was obtained from Resonant Probes GmbH. The beam of a NeHe laser (JDS Uniphase, 10 mW, $\lambda = 633 \text{ nm}$) passes through a chopper that is connected to a lock-in amplifier (EG&G, 7256). The modulated

beam then passes through two polarizers (Owis) by which the intensity and the plane of polarization of the laser can be adjusted. Then the beam is reflected off the base of the coupling prism (Scott, LASFN9) and is focused by a lens (50 mm, Owis) into a photodiode detector.

The glass supported Au SPR substrates at the prism were clamped against a Teflon cuvette with O-rings providing a liquid-tight seals. The CVs were performed with an AUTOLAB PGSTAT10 in a three-electrode setup with the Au SPR substrates at the prism as the working electrode, a Ag/AgCl reference electrode and a platinum wire as counter electrode. The CV induced desorption processes on gold were detected by monitoring reflectivity changes as a function of time at a fixed incident angle, θ .

5.5 References

- 1) (a) Abd-El-Aziz, A. S.; Manners, I. *J. Inorg. Organomet. Polym. Mater.* **2005**, *15*, 157. (b) Nguyen, P.; Gómez-Elipse, P.; Manners, I. *Chem. Rev.* **1999**, *99*, 1515. (c) Zou, S.; Hempenius, M. A.; Schönherr, H.; Vancso, G. J. *Macromol. Rapid Commun.* **2006**, *27*, 103.
- 2) (a) Barlow, S.; O'Hare, D.; *Chem. Rev.* **1997**, *97*, 637. (b) Nishihara, H.; Murata, M. *J. Inorg. Organomet. Polym. Mater.* **2005**, *15*, 147.
- 3) Cuadrado, I.; Casado, C. M.; Alonso, B.; Morán, M.; Losada, J.; Belsky, V. *J. Am. Chem. Soc.* **1997**, *119*, 7613.
- 4) Alvarez, J.; Ren, T.; Kaifer, A. E. *Organometallics*, **2001**, *20*, 3543-3549.
- 5) Nishihara, H.; *Bull. Chem. Soc. Jpn.* **2001**, *74*, 19.
- 6) Dong, T. -Y.; Chang, C. -K.; Cheng, C. -H.; Lee, S. -H.; Lai, L. -L.; Chiang, M. Y. -N. Lin, K. -J. *Organometallics* **1997**, *16*, 5816.
- 7) (a) Yamada, M.; Nishihara, H. *Langmuir*, **2003**, *19*, 8050. (b) Dong, T. -Y.; Chang, L. -S.; Tseng, I -M.; Huang, S. -J. *Langmuir*, **2004**, *20*, 4471. (c) Shih, H.-W.; Dong, T.-Y. *Inorg. Chem. Commun.* **2004**, *7*, 646.
- 8) Dong, T. -Y.; Chang, C. -K.; Cheng, C. -H.; Lin, K. -J. *Organometallics*, **1999**, *18*, 1911.
- 9) Fish, R. W.; Rosenblum, M. *J. Org. Chem.* **1965**, *30*, 1253.
- 10) Rausch, M. D. *J. Org. Chem.* **1961**, *26*, 1802.
- 11) Rekharsky, M. V.; Inoue, Y. *Chem. Rev.* **1998**, *98*, 1875.
- 12) De Jong, M. R.; Huskens, J.; Reinhoudt, D. N. *Chem. Eur. J.* **2001**, *7*, 4164.
- 13) Michels, J. J.; Baars, M. W. P. L.; Meijer, E. W.; Huskens, J.; Reinhoudt, D. N. *J. Chem. Soc., Perkin. Trans. 2* **2000**, 1914.
- 14) Zanello, P. *Inorganic Electrochemistry: Theory, Practice and Application* The Royal Society of Chemistry: Cambridge, **2003**
- 15) (a) Newkome, G. R.; He, E.; Moorefield, C. N. *Chem. Rev.* **1999**, *99*, 1689. (b) Cuadrado, I.; Morán, M.; Casado, C. M.; Alonso, B.; Losada, J. *Coord. Chem. Rev.* **1999**, *193-195*, 395.
- 16) (a) Nlate, S.; Ruiz, J.; Blais, J. -C.; Astruc, D. *Chem. Commun.* **2000**, 417. (b) Green, S. J.; Pietron. J. J.; Stokes, J. J.; Hostetler, M. J.; Vu, H.; Wuelfing, W. P.; Murray, R. W. *Langmuir* **1998**, *14*, 5612.
- 17) Knoll, W. *Annu. Rev. Phys. Chem.* **1998**, *49*, 569.
- 18) J. Huskens, A. Mulder, T. Auletta, C. A. Nijhuis, M. J. W. Ludden, D. N. Reinhoudt, *J. Am. Chem. Soc.* **2004**, *126*, 6784.
- 19) Mulder, A.; T. Auletta, T.; Sartori, A.; Del Ciotto, S.; Casnati, A.; Ungaro, R.; Huskens, J.; Reinhoudt D. N. *J. Am. Chem. Soc.* **2004**, *126*, 6627.
- 20) De Jong, M. R.; Huskens, J.; Reinhoudt, D. N. *Chem. Eur. J.* **2001**, *7*, 4164.
- 21) Matsue, T.; Evans, D. H.; Osa, T.; Kobayashilb, N. *J. Am. Chem. Soc.* **1985**, *107*, 3411.

- 22) Bard, A. J.; Faulkner, L. R. *Electrochemical Methods: Fundamentals and Applications* John Wiley & Sons: New York, **2001**.
- 23)(a) Xia, C.; Advincula, R. C.; Baba, A.; Knoll, W. *Langmuir* **2002**, *18*, 3555. (b) Baba, A.; Park, M.-K.; Advincula, R. C.; Knoll, W. *Langmuir* **2002**, *18*, 4648. (c) Baba, A.; Advincula, R. C.; Knoll, W. *J. Phys. Chem. B* **2002**, *106*, 1581. (d) Aust, E. F.; Ito, S.; Sawondny, M.; Knoll, W. *Trends Polym. Sci.* **1994**, *2*, 313.
- 24) Dobbs, D. A.; Bergman, R. G.; Theopold, K. H. *Chem. Eng. News* **1990**, *68*, 2.

Redox-Controlled Supramolecular Patterning of Dendrimers at Surfaces*

In chapters 3 and 5 it was demonstrated that guest dendrimers form multiple host-guest interactions with the molecular printboard resulting in stable monolayers. Therefore, these molecules are excellent candidates to employ in bottom-up nanofabrication schemes. This chapter describes supramolecular microcontact printing and dip-pen nanolithography using multivalent guest molecules as ink to print and write stable patterns at the host surfaces on Au and SiO₂. The formation of specific interactions was proven by comparing to reference hydroxyl-terminated SAMs. Electroless deposition of copper on the printboard was shown to occur selectively on the areas patterned with dendrimer-stabilized gold nanoparticles. The redox activity of patterned G3-PPI-(Fc)₁₆ dendrimers at βCD SAMs on SiO₂ was mapped by scanning electrochemical microscopy (SECM). Local oxidation of the Fc dendrimers induced by the microelectrode resulted in an effective removal of the Fc dendrimers from the host surface since the oxidation of Fc to the oxidized form (Fc⁺) leads to a loss of affinity for βCD. Additionally, SECM provided a way to induce local desorption of the redox-active dendrimers.

* Parts of this Chapter have been published in: (a) Nijhuis, C. A.; Sinha, J. K.; Wittstock, G.; Huskens, J.; Ravoo, B. J.; Reinhoudt, D. N. *Langmuir* **2006**, in press. (b) Bruinink, C. M.; Nijhuis, C. A.; Péter, M.; Dordi, B.; Crespo-Biel, O.; Auletta, T.; Mulder, A.; Schönherr, H.; Vancso, G. J.; Huskens, J.; Reinhoudt, D. N. *Chem. Eur. J.* **2005**, *11*, 3988.

6.1 Introduction

The capability to immobilize switchable molecules onto surfaces with nanometer scale precision is one of the enabling principles in the field of nanotechnology. Two strategies to transfer molecules to surfaces are commonly employed: i) the use of templates (e.g. patterns of self-assembled monolayers (SAMs) or polymers) to control the deposition of molecules from solution, or ii) active deposition onto surfaces by means of a patterning element, such as a stamp or a probe. The latter has the advantage that photolithographic techniques are not required and do not require processing conditions that are incompatible with several interesting types of functional molecules (e.g. biomolecules), or are susceptible to non-specific binding. Therefore, direct patterning strategies in the micro- and nanometer regime such as soft lithography^{1,2} and scanning probe lithography (SPL)³ are extensively used for immobilizing functional molecules on surfaces. Examples include microcontact printing (μ CP)¹ of proteins on glass,⁴ of polymers on reactive SAMs on gold,⁵ and dip-pen nanolithography (DPN)^{6,7} of DNA on gold and glass.⁸ However, positioning of molecules on surface mostly proceeds by covalent binding to the surface, or to SAMs consisting of anchoring molecules, or by non-specific physisorption.

In this chapter, supramolecular μ CP and DPN are used to immobilize dendrimers decorated with ferrocene (Fc) or adamantyl (Ad) guest end groups at the molecular printboard. These molecules form stable patterns owing to the formation of multiple supramolecular interactions of these polyfunctional guest molecules with the host surface. Supramolecular DPN was carried out to investigate the potential of this serial technique for writing local high-stability molecular patterns with sub-100 nm lateral dimensions on the printboard. Electroless deposition of copper was exploited to extend the application of molecular printboards to the fabrication of metal patterns.

However, applications in, for instance, nanofabrication require binding control not only at conducting surfaces, but also at non-conducting surfaces. Recently, our group reported the synthesis and characterization of β CD SAMs at SiO₂ surfaces.⁹ In the present chapter also the characterization of immobilized Fc dendrimers at molecular printboards on glass and the electrochemically induced desorption of the dendrimers from the host surface by scanning electrochemical microscopy (SECM) are described. This study presents a new SECM imaging technique where a monolayer of a surface-bound species is redox titrated by the SECM mediator. SECM allows electrochemical characterization or mapping of surfaces.¹⁰ Owing to the versatility and wide applicability of SECM for surface modifications and functional characterization, it has found applications such as measuring reaction rates of immobilized biomolecules¹¹ and following chemical processes in living cells,¹² fundamental studies of charge transfer processes at solid-liquid, liquid-liquid and liquid-gas interfaces,¹³ corrosion¹⁴ and electrocatalysis.¹⁵ Almost all imaging applications were performed under steady-state conditions. Only very few studies are known where interfaces were probed by a redox

compound until all the reactive material is exhausted¹⁶ although the significance of time-dependent information for kinetic studies has been emphasized recently by Unwin et al.¹⁷

6.2 Results and discussion

6.2.1 Single molecules on the molecular printboard

In chapters 3 and 5 the formation of densely packed monolayers of dendrimers at the molecular printboard was followed in time by SPR spectroscopy. To observe single or small clusters of the dendrimers immobilized at the host surface, dendrimers were adsorbed at the molecular printboard on Au using low concentrations of dendrimers and brief adsorption times. Dendrimers were adsorbed on β CD SAMs on annealed gold surfaces using aqueous solutions of G5-PPI-(Fc)₆₄-(β CD)₄₀ of 0.23 μ M or 0.05 μ M for 30 s. AFM images were recorded before and after adsorption of the dendrimers and the results are shown in Figure 6.1.

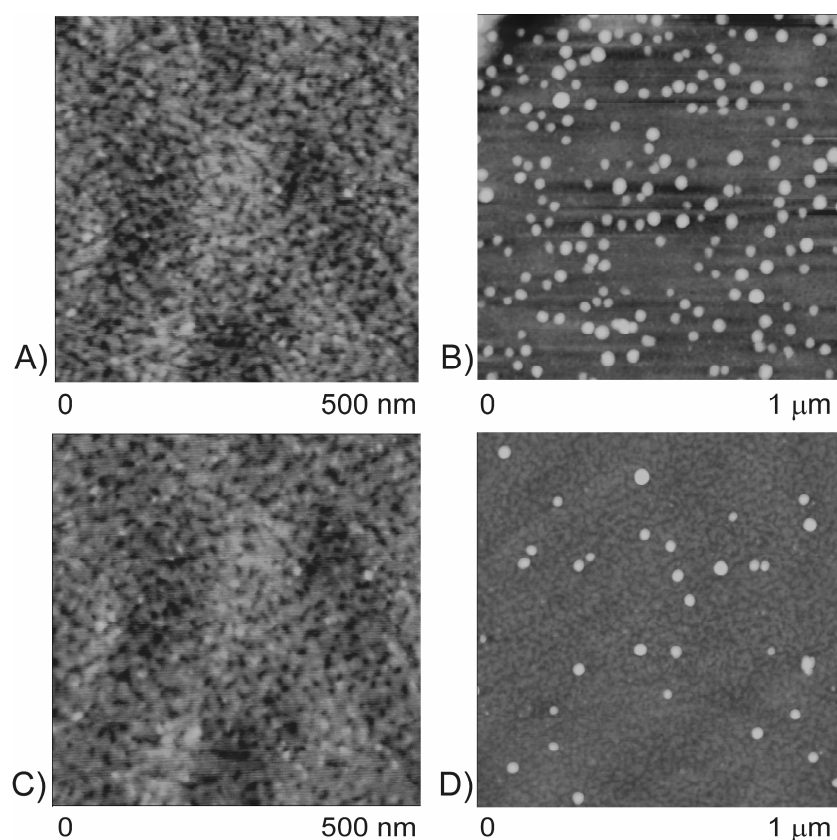


Figure 6.1: AFM images of β CD SAMs on Au before (1A and 1C) and after adsorption of a solution of 0.23 μ M (1B) or 0.05 μ M (1D) G5-PPI-(Fc)₆₄ - (β CD)₄₀ for 30 s.

The small protrusions have a height of 6.5 nm which is comparable with the estimated size as described in chapter 3 and are thus single dendrimers. The height of the larger protrusions varied and was found to be as large as 10 nm indicating that these are small aggregates of dendrimers. The density of immobilized dendrimers was higher in the case of adsorption using a solution of G5-PPI-(Fc)₆₄-(βCD)₄₀ of higher concentration (Fig. 6.1a) compared to adsorption from the 5 times more dilute solution (Fig. 6.1B) proving unambiguously that the protrusions are dendrimers. The diameter of the protrusions attributed to single dendrimers was 25 to 30 nm due to tip convolution. The fact the dendrimers can be visualized both in contact mode and in friction mode indicates that the molecules form stable multivalent assemblies at the host surface.

6.2.2 Supramolecular patterning

A fifth generation Ad dendrimer (G5-PPI-(Ad)₆₄) was dissolved in aqueous media by protonation of the core amines (pH = 2) and complexation to βCD to yield G5-PPI-(Ad)₆₄ – (βCD)₄₀.¹⁸ The number of interacting end groups of G5-PPI-(Ad)₆₄ with the host surface is expected to be similar as in the case of G5-PPI-(Fc)₆₄, since the molecular structure is the same except that the NHCOfc end groups are replaced by NHCONHAd moieties. AFM height measurements (not shown) showed that, during μCP, multilayers of guest G5-PPI-(Ad)₆₄-(βCD)₄₀ (feature height about 3 nm) were transferred onto the βCD SAM. Variations in the friction contrast within the transferred areas (Figures 6.2a and 6.2d) correlate with inhomogeneities in the layer thickness. However, rinsing with 10 mM βCD solution (Fig. 6.2c) only resulted in the removal of physisorbed G5-PPI-(Ad)₆₄-(βCD)₄₀, leaving approx. one monolayer of G5-PPI-(Ad)₆₄-(βCD)₄₀ on the βCD printboard. The feature height after rinsing is about 1 nm. Thus, the interaction of G5-PPI-(Ad)₆₄ with the βCD host surface is sufficient for the printing of stable molecular patterns of multivalent guests by supramolecular μCP.

To discriminate whether the dendrimers are bound to the host surface via physisorption or by specific interactions, printing and rinsing experiments under the same conditions were carried out on SAMs of 11-mercaptoundecanol (OH SAMs). OH SAMs were chosen since although the polarity of these SAMs is similar to that of the βCD SAMs, they are incapable of forming inclusion complexes with the guest molecules. The AFM images show that patterns of the guest at the OH SAM can be obtained after μCP (Fig. 6.2d). In sharp contrast to the results at the host surface, patterns of G5-PPI-(Ad)₆₄ can be removed using the same rinsing procedures indicating that specific multivalent interactions are required to obtain stable assemblies (Fig. 6.2e and 6.2f).

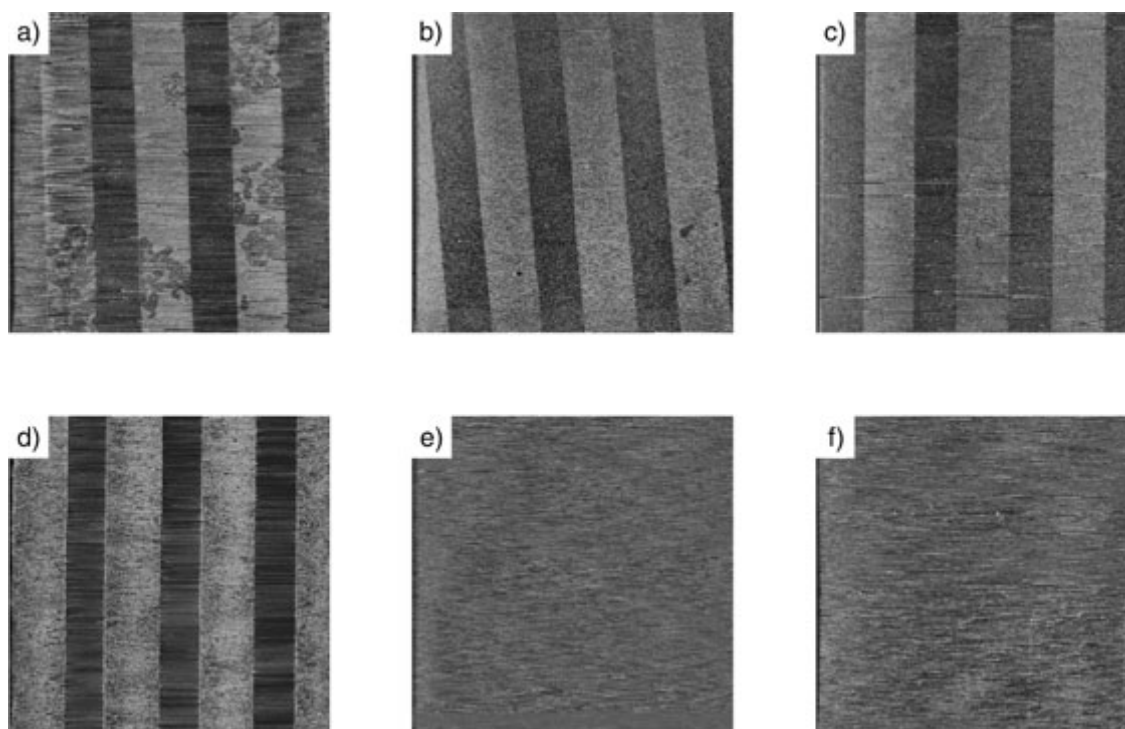


Figure 6.2: CM AFM friction images acquired in air of micrometer-size line patterns of multivalent guest G5-PPI-(Ad)₆₄-(βCD)₄₀ (brighter areas) on the βCD on Au (top) and 11-mercaptoundecanol SAMs (bottom) showing patterns present on the βCD printboard: (a,d) after μCP of the guests (brighter areas), (b,e) after rinsing with 1 mM βCD at pH 2, and (c,f) after rinsing with 10 mM βCD at pH 2 (image sizes 50x50 μm², friction forces [a.u.] increase from dark to bright contrast).

To show that the stable molecular assemblies at host surfaces can be employed in more complicated nanofabrication schemes, supramolecular μCP in combination with electroless deposition (ELD)¹⁹ of a metal was used to obtain a pattern of metal at the βCD SAM. ELD is an autocatalytic redox process of the reduction of metallic ions from solution followed by deposition at a substrate. To initiate ELD of metals on surfaces a catalyst is required which can be Au nanoparticles.²⁰ Therefore, G5-PPI-(Ad)₆₄-(βCD)₄₀-stabilized gold nanoparticles were prepared²¹ (see also chapter 7.2.1) and subsequently transferred as catalysts for ELD onto the molecular printboard by supramolecular μCP followed by ELD of Cu.²⁰ Figure 6.3a shows the AFM height image of a pattern of dendrimers loaded with Au nanoparticles after supramolecular μCP of 2 nm in height. In Figure 6.3b, an AFM height image after ELD of Cu shows the height increase of 2 nm to 64 nm.

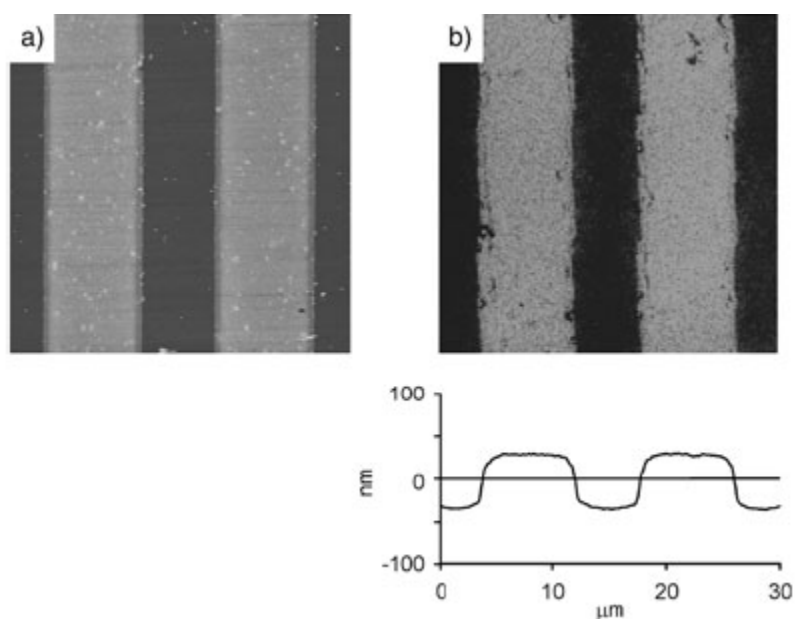


Figure 6.3: CM AFM height images acquired in air of patterns on the β CD printboard on Au (image sizes $30 \times 30 \mu\text{m}^2$): A) G5-PPI-(Ad) $_{64}$ -(β CD) $_{40}$ -stabilized gold nanoparticles by supramolecular μ CP and subsequent rinsing with 10 mM β CD solution at pH 2. (b) Copper structures fabricated by subsequent electroless deposition for 5 min.

The fact that the patterns of dendrimer-stabilized nanoparticles were stable during rinsing with 200 ml 10 mM β CD at pH 2 (Figure 6.4a) indicates that the gold particles are located in the interior of the dendrimers rather than stabilized by the exterior of several dendrimers (for additional evidence see also section 7.2.2).²¹ Nevertheless, these nanoparticles still can catalyze the ELD of copper and the deposition is highly selective. The direct placement of these catalytic centers and the protective nature of the β CD SAM for the underlying gold substrate accounts for this observation.

ELD and μ CP are readily accessible and cost-efficient to fabricate metal patterns and similar strategies have been reported before.^{20,22} However, a crucial difference between our work and previous reports is the use of multivalent supramolecular interactions between the catalyst and the surface that can subsequently serve as a strong connection between the metal patterns and the substrate.

To obtain patterns of redox-active molecules at the molecular printboard, G3-PPI-(Fc) $_{16}$ -(β CD) $_{16}$ assemblies were immobilized in hexagonal patterns of dots ($5 \mu\text{m}$ in diameter and spaced by $3 \mu\text{m}$) at the β CD host surface at SiO_2 by supramolecular μ CP. G3-PPI-(Fc) $_{16}$ -(β CD) $_{16}$ was used as the ink since according to chapters 3 and 4 the dendrimers form stable assemblies at the host surface on Au with multiple Fc- β CD interactions.

The AFM images clearly showed the transferred structures of 1 nm in height in both friction and height images (Figure 6.4A). The stability of the patterns was studied by rinsing the patterns directly after printing with Millipore water at pH = 2 (Figure 6.4B). Rinsing reduced the height of the structures to 1 nm indicating that somewhat more than a monolayer was

transferred from the stamp to the substrate. Thus rinsing removes non-specifically bound material to leave approximately a monolayer of dendrimers in the area of contact. Rinsing with water at pH = 2 for prolonged periods of time did not result in further removal of the dendrimers indicating that the molecules form stable assemblies at the β CD host surface at SiO₂.

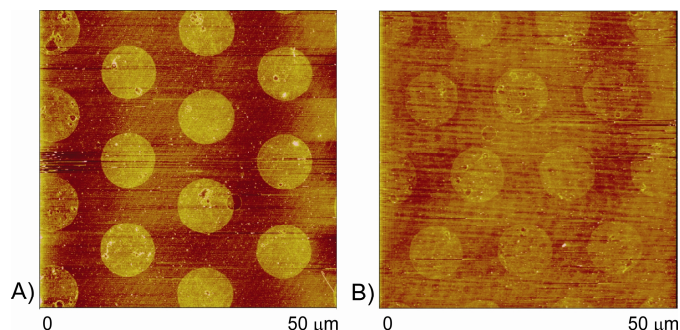


Figure 6.4: AFM height images of patterns of G3-PPI-(Fc)₁₆ on the molecular printboard on SiO₂ before (A) and after rinsing with water at pH = 2 (B).

Dip-pen nanolithography (DPN) is a lithographic technique that allows to fabricate structures in the sub-100-nm range which is difficult to achieve with μ CP.^{6,7} The sub-100-nm writing capability of supramolecular DPN is shown in Figure 6.5 by an array of lines of guest G5-PPI-(Ad)₆₄-(β CD)₄₀ on the printboard with a line width of 60 nm.²³ This specific pattern was written in three stages by adjusting the scan angle of the tip by 45° each time with respect to the previous line. In this particular experiment, gold-coated tips functionalized with a poly(ethylene glycol) SAM were used to allow a better transfer of G5-PPI-(Ad)₆₄-(β CD)₄₀ to the printboard. Scanning with a bare, uninked silicon nitride AFM tip over the β CD printboard under the same experimental conditions did not form any visible pattern, thus proving that pattern formation arises from the transfer of guest molecules and not from mechanical forces applied by the tip to the printboard.

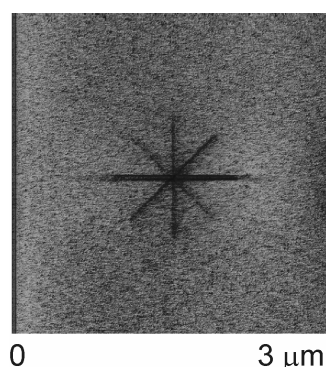
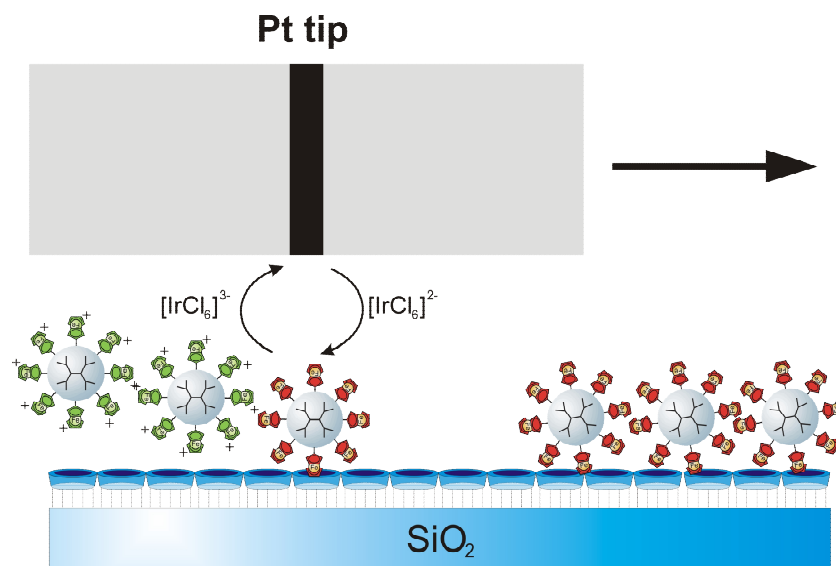


Figure 6.5: AFM friction image of an array of lines, 3 μ m long with average widths of approximately 60 ± 20 nm, of multivalent guest G5-PPI-(Ad)₆₄-(β CD)₄₀ after scanning the tip at a velocity of ~ 4 μ m/s across the β CD printboard for 10 min for each line (image size 6×6 μ m²; friction forces [a.u.] increase from dark to bright contrast). Readout of the patterns was done with the same tip by increasing the scan size and the scan velocity (approx. 15 times the writing speed).

Inversion of the relative friction contrast in the image in comparison to the friction contrasts observed in Figures 6.1 and 6.2 is probably related to the different character of the contacting surfaces (i.e. ink-covered tip vs. bare tip). This has been observed before for similar β CD systems,²⁴ as well as for poly(amidoamine) (PAMAM) dendrimers on other SAMs.²⁵

6.2.3 Imaging by scanning electrochemical microscopy (SECM)

Patterns of G3-PPI-(Fc)₁₆ obtained by supramolecular μ CP on the molecular printboard on SiO₂ as described in Section 6.2.3 were also characterized by SECM. The SECM used a disk-shaped Pt ultramicroelectrode (UME) of 25 μ m diameter. The dendrimers were printed in dots with a diameter of 50 μ m and gaps of 30 μ m which are larger than the active electrode area of the UME in order to ensure good resolution during imaging. The results were obtained by scanning the surface in aqueous solutions containing [IrCl₆]³⁻ as a mediator in the feedback mode. The UME potential E_T was kept at 0.75 V vs. Ag/AgCl such that [IrCl₆]³⁻ is oxidized at the UME under diffusion-controlled conditions. The oxidized species [IrCl₆]²⁻ diffuses to the surface and may accept an electron from Fc moieties of the dendrimers which have a lower E° . During this process Fc⁺ would be released and [IrCl₆]³⁻ regenerated. Subsequently, [IrCl₆]³⁻ may diffuse back to the UME giving rise to a positive feedback current. At locations where only a bare β CD monolayer is present the [IrCl₆]²⁻ can not be reduced, since no dendrimers are present, resulting in an UME current i_T that can be described by pure hindered diffusion of [IrCl₆]³⁻ from the solution bulk to the UME. The redox processes that occur are outlined in Scheme 6.1.



Scheme 6.1: Schematic of the mechanism of SECM-induced desorption of the dendrimers from the molecular printboard on glass. [IrCl₆]³⁻ is oxidized at the tip and diffuses to the molecular printboard where it oxidizes the patterns of Fc dendrimers. Subsequently, the oxidized Fc dendrimers desorb from the host surface and the reduced [IrCl₆]³⁻ diffuses back to the UME giving rise to positive feedback currents only at the Fc dendrimer-covered regions.

A SECM image is shown in Figure 6.6. The image clearly shows a hexagonal pattern of dots which appear with a higher feedback current compared to the background. The periodicity was determined from the profile of the image indicated by the white line and the corresponding line scan is also shown in Figure 6.6. The observed periodicity of 80 μm corresponds exactly to the printed dendrimer dots (50 μm in diameter and 30 μm gaps). Hence, SECM faithfully reveals the hexagonal pattern of a monolayer of dendrimers printed on the molecular printboard. The peak intensities of the line scan are not uniform probably due to an inhomogeneous distribution of G3-PPI-(Fc)₁₆ at the surface.

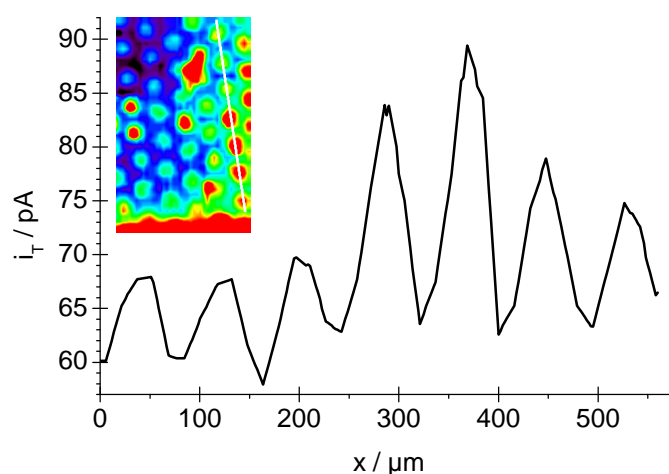


Figure 6.6: Line scan (right) obtained from the profile of the image (left) indicated by the white line in the image showing the periodicity of the printed features. $E_T = 0.75\text{ V}$, $v_T = 200\ \mu\text{m s}^{-1}$, $0.1\ \text{mM } [\text{IrCl}_6]^{3-}$.

In order to obtain the image in Figure 6.6, a very high scan rate and step size had to be used. The translation speed was $200\ \mu\text{m s}^{-1}$ and the step size in the low frequency axis (y) was $15\ \mu\text{m}$. At slower scan rates featureless images were obtained because the Fc dendrimers were completely released during the scan and mediator regeneration ceased before the current values were sampled. Even at higher scan rates the first line scans have the highest feedback current compared to the successive line scans in all obtained images. This is nicely demonstrated by the surface plot shown in Figure 6.7. Individual line scans are displayed as black lines. The first line scan is placed in the rear part of the plot. The first line scan is more intense because during the first line scan also some of the Fc-dendrimers are oxidized that are located in the area later probed by the UME. In subsequent images, sample regions outside the imaging frame can contribute to the mediator regeneration, whereas the imaged region is successively depleted.

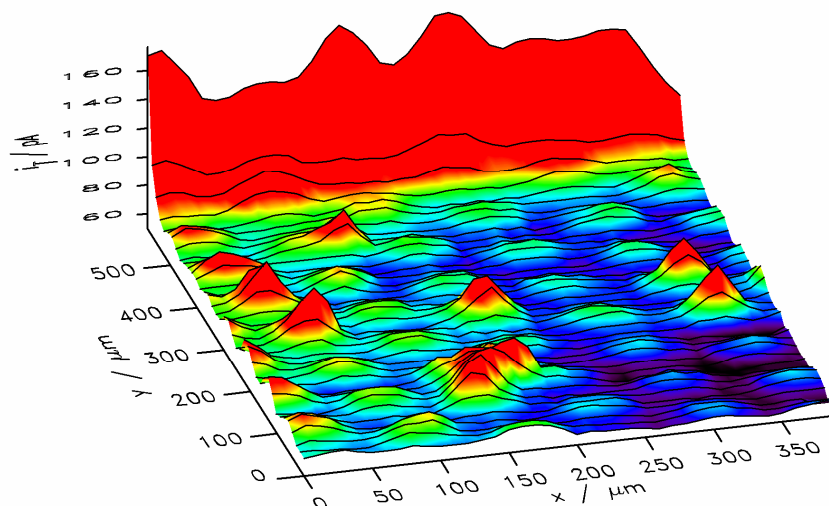
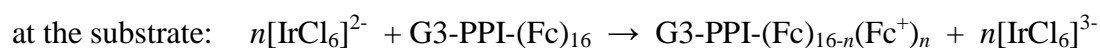


Figure 6.7: SECM image of a Fc dendrimer-modified printboard illustrating the higher intensity of the first line scan (shown in the background). Black lines correspond to individual line scans. The false color was interpolated; $E_T = 0.75$ V, $v_T = 200$ $\mu\text{m s}^{-1}$, 0.1 mM $[\text{IrCl}_6]^{3-}$.

Upon imaging by SECM the feedback currents decreased significantly due to the depletion of Fc-loaded dendrimers on the surface. Moreover, repeated imaging of the same area showed a further decrease in feedback currents. Figure 6.8 shows four images of the same sample region. Figure 6.5B and Figure 6.5D were assembled from the reverse line scans of Figure 6.5A and Figure 6.5C, respectively. The features are hardly visible in the last image.

The observations, i) the relatively high intensity of the first line scan, ii) the pattern disappearing upon scanning, and iii) the high scan rate necessary to visualize the structures, all suggest that upon scanning the dendrimers desorb from the host surface. The proposed mechanism is outlined in Scheme 6.1. At the microelectrode the mediator is oxidized and diffuses to the surface where it may oxidize Fc groups of the dendrimers.²⁶ The reduced form of the mediator may diffuse back to microelectrode. It is well known that the oxidized form of Fc is not able to form inclusion complexes with βCD at the surface resulting in an effective desorption of the dendrimers from the surface. The reactions at the UME and at the substrate are thus:



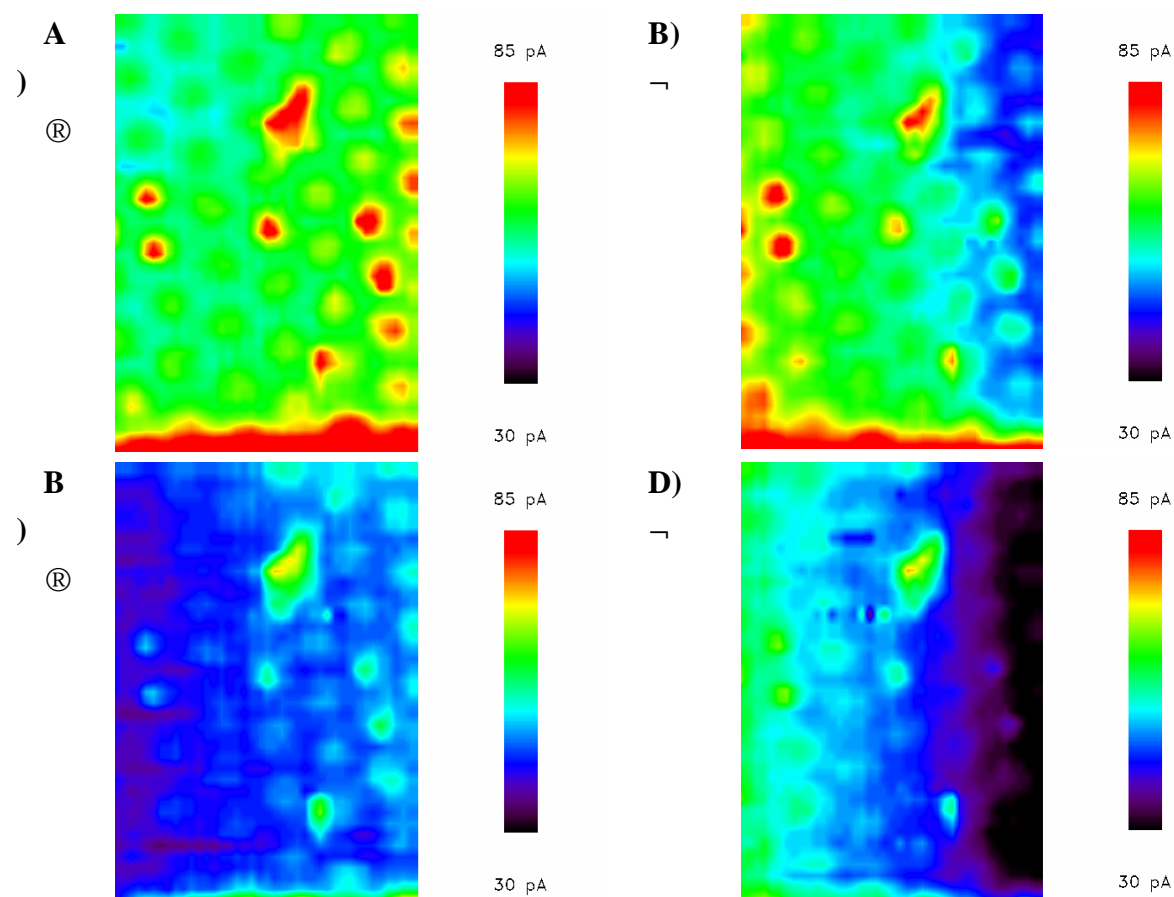


Figure 6.8: SECM images of G3-PPI-(Fc)₁₆ printed at a β CD SAM on glass: A) image composed of the forward line scans and B) backward line scans; a second SECM image of the same area composed of the forward line scans (C) and backward line scans (D); $E_T = 0.75$ V, $v_T = 200 \mu\text{m s}^{-1}$, $0.1 \text{ mM } [\text{IrCl}_6]^{3-}$.

Therefore, subsequent scans and backward scans show a significant decrease in intensity of the feedback currents. The high scan rate is required to reduce the number of redox equivalents imposed per surface area, where it oxidizes the Fc units of the dendrimers. The dendrimers desorb from the host surface and diffuse into the bulk solution. Consequently, scanning slowly may impose more redox equivalent per sample surface area than Fc units be present in the dendrimer-modified areas. For similar reasons the step size in the low frequency direction was relatively large in order to minimize oxidation during scanning the previous line scan. This also explains why the very first scan gives substantially higher positive feedback currents than the remaining line scans.

SECM-induced oxidation of the dendrimers resulted in an effective desorption of the dendrimers from the β CD SAM at SiO_2 and also provided images of the desorption process at different stages by repetitively recording images until all Fc-dendrimers were desorbed. This observation implies that the dendrimers are primarily bound via specific host-guest interactions to the host surface on SiO_2 . In principle, the monolayer is less ordered compared to monolayers on Au since the monolayer is covalently synthesized, but nevertheless, the binding behavior of the dendrimers is in full agreement to that found in studies of Fc

dendrimers binding to printboards on gold surfaces (chapter 3) and of divalent guest binding to printboards on glass.^{9,27}

6.2.4 Writing with scanning electrochemical microscopy

SECM was used to write patterns at monolayers of the Fc dendrimers of generation 2 to 5 adsorbed at the β CD SAM at SiO_2 . This was achieved by applying a voltage pulse at a distance of 15 μm from the surface using using $[\text{Ir}(\text{Cl}_6)_2]^{3-}$ as the mediator. This resulted in the local oxidation and subsequent desorption of the dendrimers from the host surface. This was repeated another three times at a distance of 100 μm with respect to the original spot resulting in a square with a hole in the corners. Figure 6.9 shows the SECM image after writing the patterns in the monolayer of the dendrimers. The spots appear with lower feedback currents since the exposed molecular printboard is not capable of reducing the mediator. This nicely demonstrates that SECM can be used to write patterns in monolayers of redox active dendrimers adsorbed at β CD SAMs. Although the resolution of SECM is inferior to DPN, SECM is complementary to supramolecular DPN and μCP , where patterns of dendrimers are written at bare β CD SAMs in an additive fashion, while SECM is subtractive.

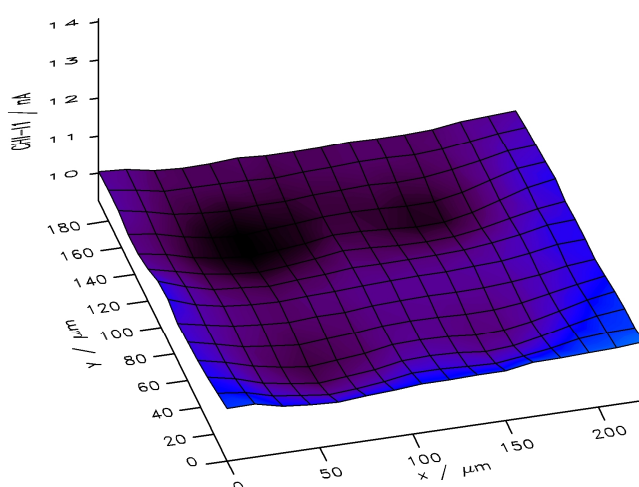


Figure 6.9: SECM image obtained after four pulses at different areas.

While writing the structures an amperogram was recorded which is shown in Figure 6.10 along with the background amperogram which was recorded at a distance of 300 μm from the surface. Integration after background subtraction gave the total charge from which the surface coverage of the Fc units, G_{Fc} , can be determined using $G_{\text{Fc}} = Q/nFA$, in which n = number of electrons per mole of reaction, F = Faraday constant, and A = surface area of the electrode, as was described in section 3.2.4 for monolayers of the dendrimers at molecular printboards on Au.²⁸ The relative coverages $G_{\beta\text{CD}}/G_{\text{Fc}}$ provide the number p_b of bound interactions per

dendrimer molecule with the host surface, using $p_b = p_{\text{tot}}G_{\beta\text{CD}}/G_{\text{Fc}}$, where p_{tot} is the total number of end groups. G_{Fc} is linearly dependent on the ratio of number of end groups of the dendrimers p_{tot} and p_b as shown in Figure 6.10 for the results obtained for monolayers of dendrimers on βCD SAMs on Au. The $G_{\beta\text{CD}}$ on SiO_2 is not known, but the βCD monolayer is expected to be less ordered and might also be less densely packed compared to βCD SAMs on Au since the monolayer is prepared in a multistep covalent synthesis. However, the number of covalent bonds of the βCD on SiO_2 is also expected to be less than the number of thioethers interacting with the Au surface (according to XPS 66% of the thioethers is interacting with the Au surface) which may lead to a higher βCD density at SiO_2 surfaces. To compare G_{Fc} of both molecular printboards, the obtained G_{Fc} values on SiO_2 by SECM were plotted using the $p_{\text{tot}}:p_b$ ratios obtained for the monolayers of dendrimers on Au as is shown in Figure 6.10.

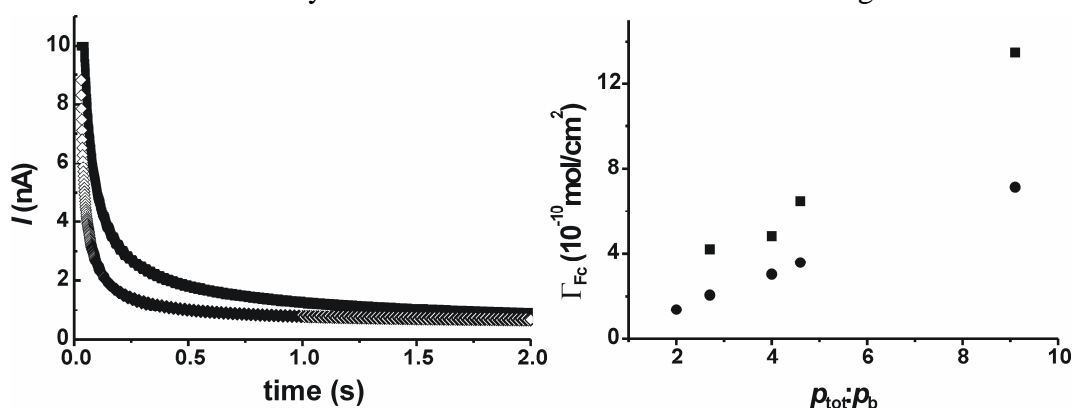


Figure 6.10: Left: background amperogram (\diamond) recorded at a distance of 300 μm from the surface and amperogram recorded while writing the structures at a distance of 15 μm (\blacksquare); Right: linear dependency of G_{Fc} measured at SiO_2 (\blacksquare) and Au (\bullet) vs. the ratio $p_{\text{tot}}:p_b$.

A striking difference between the G_{Fc} values obtained for the monolayers of dendrimer on SiO_2 and on Au is that the G_{Fc} values are approximately twice as large on SiO_2 compared to Au. This implies that the p_b values on SiO_2 are roughly half of that on Au surfaces. Apparently, the βCD monolayers on SiO_2 are less densely packed resulting in lower p_b values and, thus, in an increase of G_{Fc} . More likely is that $p_{\text{tot}}:p_b$ remains constant leading to a higher $G_{\beta\text{CD}}$ value at SiO_2 surfaces compared to the $G_{\beta\text{CD}}$ values on Au. At SiO_2 surfaces the monolayers are disordered since the βCD s are bound to the surface via covalent bonds. The monolayer formation at SiO_2 surfaces presumably proceeds via random sequential adsorption.²⁹ This results in a configuration that is generated by adding disks irreversibly to a surface while it does not overlap other disks already present at the surface. The maximum coverage of about 55% is achieved when there is no room left for other disks. However, the βCD s still can react with the surface resulting in tilted conformations and thus in higher $G_{\beta\text{CD}}$ values.⁹

6.3 Conclusions

Supramolecular μ CP and supramolecular DPN are powerful tools in bottom-up nanofabrication to yield well-defined molecular structures. The scope ranges from μm to nm sized patterns. The patterns of the dendrimers could not be removed from the host surfaces, but could be removed from a hydroxyl terminated reference surface that was not capable of forming specific interactions with the multivalent guest molecules. This proves that the pattern stability at the molecular printboard is due to the formation of multiple host-guest complexes.

SECM can electrochemically induce the desorption of Fc dendrimers from the molecular printboard at SiO_2 . The backward scans showed a decrease in positive feedback currents compared to the forward scans, and imaging the same area a second time virtually removed all redox active dendrimers from the host surface and, thus, the desorption could be imaged at different stages. The reversible adsorption results from specific host-guest chemistry since Fc in the neutral form is able to form inclusion complexes with βCD while the oxidized cationic form is not.

The combination of supramolecular and electrochemical control of dendrimer adsorption is a promising tool in the integration of “bottom-up” and “top-down” nanofabrication schemes. For instance, local desorption of guest molecules by UME electrodes or smaller conductive AFM tips may give small structures exposing the molecular printboard to which other guest molecules may bind.

6.4 Experimental

General Procedures. All moisture-sensitive reactions were carried out under argon atmosphere. Reagents were commercial and used without further purification. All dry solvents were prepared according to standard procedures. The Fc-terminated PPI dendrimers³⁰ and the per-6-amino β -cyclodextrin³¹ were synthesized according to a literature procedures.

Materials and methods. All glassware used to prepare monolayers was immersed in piranha solution (conc. H_2SO_4 and 33% H_2O_2 in a 3:1 ratio). (Warning: piranha should be handled with caution; it can detonate unexpectedly). Next, the glassware was rinsed with large amounts of Milli-Q water. All adsorbate solutions were prepared prior to use. All solvents used in monolayer preparation were of p.a. grade.

Substrate preparation. The synthesis of a βCD SAM on SiO_2 has been reported recently by our group and the same procedure was used here.⁹ Microscope glass slide were oxidized by immersion on boiling piranha (conc. H_2SO_4 and 33% H_2O_2 in a 3:1 ratio) for 15 min, rinsed with copious amounts of Millipore water and dried in a stream of N_2 . Subsequently, a monolayer was formed by reaction with 1-cyano-11-trichlorosilylundecane. Reduction gave the amino-terminated monolayer which was

converted to isothiocyanate terminated layers by reaction with 1,4-phenylene diisothiocyanate. Finally, reaction with per-6-amino β -cyclodextrin gave the host surface.

Microcontact printing. Stamps were fabricated by casting a 10:1 (v/v) mixture of PDMS and curing agent (Sylgard 184, Dow Corning) against a photolithographically patterned silicon master and curing overnight at 60 °C. Subsequently, the stamps were peeled off from the master and were mildly oxidized in a UV/ozone reactor for 60 (Ultra-Violet Products Inc., model PR-100). Directly after oxidization the stamps were immersed in aqueous solutions containing the dendrimer- β CD assemblies (1 mM in functionality and 1 mM β CD at pH = 2). The stamps were inked for at least 20-30 min and before printing the stamps were blown dry in a stream of N₂. The stamps were placed in conformal contact by hand with the host surface at SiO₂ or Au for 1 min without applying external pressure after which the stamp was carefully removed. The substrates were used as such or rinsed with water at pH = 2.

SECM. A home-built SECM was used that consisted of a stepper motor positioning system (Märzhäuser, Wetzlar, Germany) and CHI701 potentiostat used in a three-electrode configuration and operated via a home-built software. The Pt ultramicroelectrode (UME) had a radius $r_T = 13 \mu\text{m}$ and the $RG = r_{\text{glass}} / r_T = 10$ (r_{glass} is the radius of the insulating glass shielding). A Pt wire served as auxiliary electrode and was used together with a Ag/AgCl reference electrode. The aqueous solution contained 0.1 mM K₃IrCl₆ and 10 mM KClO₄. Initially the UME was positioned far from the surface and then approached to the surface with the help of the SECM instrument by monitoring the steady-state O₂ reduction current at $E_T = -0.6 \text{ V}$ until the current stayed constant when the insulating sheath of the UME mechanically touched the sample surface. The UME was retracted 10 μm from this point for horizontal scans. The sample tilt was minimized by scanning the UME horizontally over the surface for several times while monitoring the steady-state O₂ reduction current and adjusting the tilt table of the SECM. The potential was then switched to $E_T = 0.75 \text{ V}$ in order to oxidize [IrCl₆]³⁻ present in the solution. The translation speed of the UME across the surface was maintained at 200 $\mu\text{m s}^{-1}$ with a step size of 15 μm in the low frequency scan axis.

Supramolecular DPN. Si₃N₄ tips were cleaned in chloroform overnight and inked by immersion into the adsorbate solution (0.5-1.0 mM in hydrophobic constituents) with minimal delay for 15 min. After withdrawal and drying, the tip was scanned in contact mode across the surface of the β CD printboard for a certain period of time (T = 25 °C, relative humidity = 40-50%). The written patterns were recorded with the same tip by increasing the scan size and the scan velocity (ca. 15 times the writing speed).

Electroless deposition (ELD) of copper. To trigger the ELD of Cu on the printboard, G5-PPI dendrimer-stabilized gold nanoparticles were prepared according to literature procedure²¹ and transferred onto the printboard by conducting supramolecular μ CP. After rinsing with 200 ml of aqueous solutions of native β CD (10 mM at pH 2) and Milli-Q, the substrate was immersed in the copper electroless deposition bath containing 40 mM CuSO₄, 140 mM Na₂SO₄, 120 mM ethylenediaminetetraacetate sodium salt (Na₄EDTA), 300 mM NaHCOO, and 30 mM HCHO at pH 13.

After a certain immersion time, the substrate was taken out of the ELD bath, rinsed with Milli-Q and dried under a continuous stream of nitrogen for 1 min.

AFM. AFM analyses were carried out with a NanoScope III multimode AFM (Veeco/Digital Instruments, Santa Barbara, CA, USA) equipped with a J-scanner, in contact mode using Si₃N₄ cantilevers (Nanoprobes, Veeco/Digital Instruments) with a nominal spring constant of 0.1 Nm⁻¹. To ensure maximum sensitivity for lateral forces in the friction-force images, the sample was scanned in 90° with respect to the long axis of the cantilever. AFM imaging was done in ambient atmosphere (25 °C, relative humidity = 40-50%).

6.5 References

- 1) Xia, Y.; Whitesides, G. M. *Angew. Chem. Int. Ed.* **1998**, *37*, 550.
- 2) Michel, B.; Bernard, A.; Bietsch, A.; Delamarche, E.; Geissler, M.; Juncker, D.; Kind, H.; Renault, J. -P.; Rothuizen, H.; Schmid, H.; Schmid-Winkel, P.; Stutz, R.; Wolf, H. *IBM J. Res. Dev.* **2001**, *45*, 697.
- 3) Krämer, S.; Fuierer, R. R.; Gorman, C. B.; *Chem. Rev.* **2003**, *103*, 4367.
- 4) Bernard, A.; Renault, J. -P.; Michel, B.; Bosshard, H. R.; Delamarche, E. *Adv. Mater.* **2000**, *12*, 1067.
- 5) Yan, L.; Huck, W. T. S.; Zhao, X. M.; Whitesides, G. M. *Langmuir* **1999**, *15*, 1208.
- 6) Jaschke, M.; Butt, H. -J. *Langmuir* **1995**, *11*, 1061.
- 7) a) Piner, R. D.; Zhu, J.; Xu, F.; Hong, S.; Mirkin, C. A. *Science* **1999**, *283*, 661-663; b) Mirkin, C. A.; Hong, S.; Levine, R. D. *ChemPhysChem* **2001**, *2*, 37.
- 8) Demers, L. M.; Ginger, D. S.; Park, S. -J.; Li, Z.; Chung, S. -W.; Mirkin, C. A. *Science* **2002**, *296*, 1836.
- 9) Onclin, S.; Mulder, A.; Ravoo, B. J.; Huskens, J.; Reinhoudt, D. N. *Langmuir* **2004**, *20*, 5460.
- 10)(a) Mandler, D. in *Scanning Electrochemical Microscopy* (Eds. A.J. Bard, M.V. Mirkin), M. Dekker, New York **2001**, pp. 593-627. (b) Shiku, H.; Uchida, I.; Matsue, T. *Langmuir* **1997**, *13*, 7239-7244. (c) Borgwarth, K. Heinze, J. *J. Electrochem. Soc.* **1999**, *146*, 3285-3289. (d) Wilhelm, T.; Wittstock, G. *Electrochim. Acta* **2001**, *47*, 275-281. (e) Sauter, S.; Wittstock, G. *J. Solid State Electrochem.* **2001**, *5*, 205.
- 11)(a) Zhao, C.; Sinha, J. K.; Wijayawardhana, C. A.; Wittstock, G. *J. Electroanal. Chem.* **2004**, *561*, 83. (b) Zhao, C. Wittstock, G. *Anal. Chem.* **2004**, *76*, 3145-3154. (c) Wilhelm, T.; Wittstock, G. *Angew. Chem. Int. Ed.* **2003**, *42*, 2247. (d) Wittstock, G. *Fresenius J. Anal. Chem.* **2001**, *370*, 303.
- 12)(a) Bard, A. J.; Fan, F. -R. F.; Pierce, D. T.; Unwin, P.R.; Wipf, D.O.; Zhou, F. *Science* **1991**, *254*, 68. (b) Torisawa, Y. -S.; Kaa, T. Takii Y. Oyamatsu D.; Nishizawa M.; Matsue, T.; *Anal. Chem* **2003**, *75*, 2154. (c) Isik, S.; Etienne, M.; Oni, J.; Bloechl, A.; Reiter, S.; Schuhmann, W. *Anal. Chem.* **2004**, *76*, 6389. (d) Mauzeroll, J.; Bard, A. J.; Owhadian, O.; Monks, T. J. *Proc. Natl. Acad. Sci. USA* **2004**, *101*, 17587. (e) Holt, K. B.; Bard, A. J. *Biochemistry*, **2005**, *44*, 13214.
- 13) Barker, A. L.; Gonsalves, M.; Macpherson, J. V.; Slevin, C. J.; Unwin, P. R. *Anal. Chim. Acta* **1999**, *385*, 223.
- 14)(a) Basame, S. B.; White, H. S. *J. Phys. Chem B.* **1998**, *98*, 9812. (b) Zhu, Y.; Williams, D. E. *J. Electrochem Soc.* **1997**, *144*, 43. (b) Still, J. W.; Wipf, D. O. *J. Electrochem. Soc.* **1997**, *144*, 2657.
- 15)(a) Fernandez, J. L.; Walsh, D. A.; Bard, A. J. *J. Am. Chem. Soc.* **2005**, *127*, 357. (b) Shah, B. C.; Hillier, A. C. *J. Electrochem. Soc.* **2000**, *147*, 3043.
- 16) Zhang, J.; Mandler, D.; Unwin, P. R. *Chem. Commun.* **2004**, 450.
- 17)(a) Zhang, J.; Unwin, P. R. *Phys. Chem. Chem. Phys.* **2002**, *4*, 3814. (b) Barker, A. L.; Macpherson, J. V.; Slevin, C. J.; Unwin, P. R. *J. Phys. Chem B* **1998**, *102*, 1586.

- 18) Michels, J. J.; Baars, M. W. P. L.; Meijer, E. W.; Huskens, J.; Reinhoudt, D. N. *J. Chem. Soc., Perkin Trans. 2* **2000**, 1914.
- 19) G. O. Mallory, J. B. Hajdu, *Electroless Plating: Fundamentals and Applications*, American Electroplaters and Surface Finishers Society, Orlando, FL, **1990**.
- 20) A. M. Bittner, X. C. Wu, K. Kern, *Adv. Funct. Mater.* **2002**, *12*, 432.
- 21) J. J. Michels, J. Huskens, D. N. Reinhoudt, *J. Chem. Soc., Perkin Trans. 2* **2002**, 102.
- 22) X. C. Wu, A. M. Bittner, K. Kern, *Langmuir* **2002**, *18*, 4984.
- 23) Relative humidity was found to play an important role in our DPN experiments, since all successful writing experiments were carried out at humidities above 40%. These results support the currently accepted view that relative humidity is essential to the success of DPN. See: S. Rozhok, R. Piner, C. A. Mirkin, *J. Phys. Chem. B.* **2003**, *107*, 751-757.
- 24) T. Auletta, B. Dordi, A. Mulder, A. Sartori, S. Onclin, C. M. Bruinink, M. Péter, C. A. Nijhuis, H. Beijleveld, H. Schönherr, G. J. Vancso, A. Casnati, R. Ungaro, B. J. Ravoo, J. Huskens, D. N. Reinhoudt, *Angew. Chem. Int. Ed.* **2004**, *43*, 369.
- 25) G. H. Degenhart, B. Dordi, H. Schönherr, G. J. Vancso, *Langmuir* **2004**, *20*, 6216.
- 26) The use of printboards based on SiO₂ surfaces is advantageous for the SECM measurements because metal substrates (e.g. Au-thiol SAMs) may reduce the mediator by heterogeneous electron transfer which complicates the data interpretation. Wittstock, G.; Schuhmann, W. *Anal. Chem.* **1997**, *69*, 5059.
- 27) Mulder, A.; Onclin, S.; Péter, M.; Hoogenboom, J. P.; Beijleveld, H.; ter Maat, J.; García-Parajó, M.F.; Ravoo, B. J.; Huskens, J.; Van Hulst, N. F.; Reinhoudt, D. N. *Small* **2005**, *1*, 242.
- 28) Bard, A. J.; Faulkner, L. R. *Electrochemical Methods: Fundamentals and Applications* John Wiley & Sons: New York, **2001**.
- 29) Hinrichson, E. L.; Feder, J.; Jøssang, T. *Phys. Rev. A* **1990**, *41*, 4199.
- 30) Cuardo, I.; Morán, M.; Casado, C. M.; Alonso, B.; Lobete, F.; García, B.; Ibisate, M.; Losada, J. *Organometallics* **1996**, *15*, 5278.
- 31) Ashton, P. R.; Königer, R.; Stoddart, J. F.; Alker, D.; Harding, V. D. *J. Org. Chem.* **1996**, *61*, 903.

Single Electron Tunneling in Dendrimer Stabilized Gold Nanoparticles*

In chapter 6 G5-PPI-(Ad)₆₄-(βCD)₄₀ assemblies were used as nanoreactors to synthesize and stabilize Au nanoparticles with a diameter of 1.7 nm ± 0.9 nm. This chapter describes the adsorption of dendrimer-stabilized particles at βCD SAMs on Au which were characterized by scanning tunneling microscopy (STM). STM measurements showed that the particles exhibit a Coulomb staircase at room temperature under ambient conditions along with negative differential resistance (NDR) at higher voltages. Control experiments on bare βCD SAMs at which “empty” dendrimers were adsorbed did not show a Coulomb staircase. However, empty dendrimers show NDR effects at positive tip biases. Room temperature experiments under ultrahigh vacuum conditions resulted in a faint Coulomb staircase which indicates that under these conditions the dendrimers are unable to stabilize the Au nanoparticles.

* This chapter has been published in: Nijhuis, C. A.; Oncel, N.; Huskens, J.; Zandvliet, H. J. W.; Ravoo, B. J.; Poelsema, B.; Reinhoudt, D. N. *Small* **2006**, in press.

7.1 Introduction

Single-electron tunneling (SET) is a phenomenon that can be used to develop nanoelectronic devices, such as single-electron transistors, logic and memory devices, or coupled quantum dots for quantum computation.^{1,2,3,4} A variety of devices displaying SET has been prepared and characterized by STM using either small metal⁵ or semiconducting⁶ particles as central electrode, silicon-based devices⁷ or vertical quantum dots.⁸ Devices consisting of metal clusters may show Coulomb blockade due to Coulomb repulsion experienced by an incoming electron by the excess electrons at the metal cluster. Coulomb repulsion leads to equidistant steps in the (I,V) curves. Moreover, devices based on semiconductor quantum dots may show resonance tunneling and/or Coulomb blockade which give rise to non-equidistant steps in (I,V) curves. These resemble the shell structure in atoms and therefore these particles are also known as “artificial atoms”. Most devices show Coulomb staircase behavior and/or quantum confinement only at low temperatures (4 – 80 K) because then the thermal energy kT is smaller than the charging energy $e^2/2C$.⁵ Only a few examples have been reported of metallic quantum dots showing SET properties at room temperature. For instance, monolayer-capped nanoparticles directly physisorbed at self-assembled monolayers (SAMs) of alkanethiols⁹ or metal dots grown directly on a semiconducting surface¹⁰ displayed SET at room temperature. Small Pd clusters prepared by pulsed laser deposition (PLD) at decanethiol SAMs showed staircase behavior at room temperature.¹¹

SET properties are not only strongly dependent on the particle size, but also on both tunnel barriers. Self-assembled monolayers (SAMs) of organic molecules are good candidates for defining one or both of the tunnel junctions since they allow chemical control of the device characteristics and have high tunnel resistances depending on the chain length of the molecule.¹² However, it remains a challenge to obtain molecular structures containing small particles, and to immobilize the nanoparticles on SAMs at conductive substrates.¹³ Generally, the immobilization of molecules at surfaces is achieved by chemisorption, physisorption, or covalent synthesis. Disadvantages of these methods are that covalent synthesis does not allow self-correction while the thermodynamics and kinetics of chemisorption and physisorption are difficult to control. On the other hand, supramolecular interactions do allow self-correction and a wealth of information on the thermodynamics and kinetics is available, so that the intermolecular interactions can be controlled with great precision.¹⁴

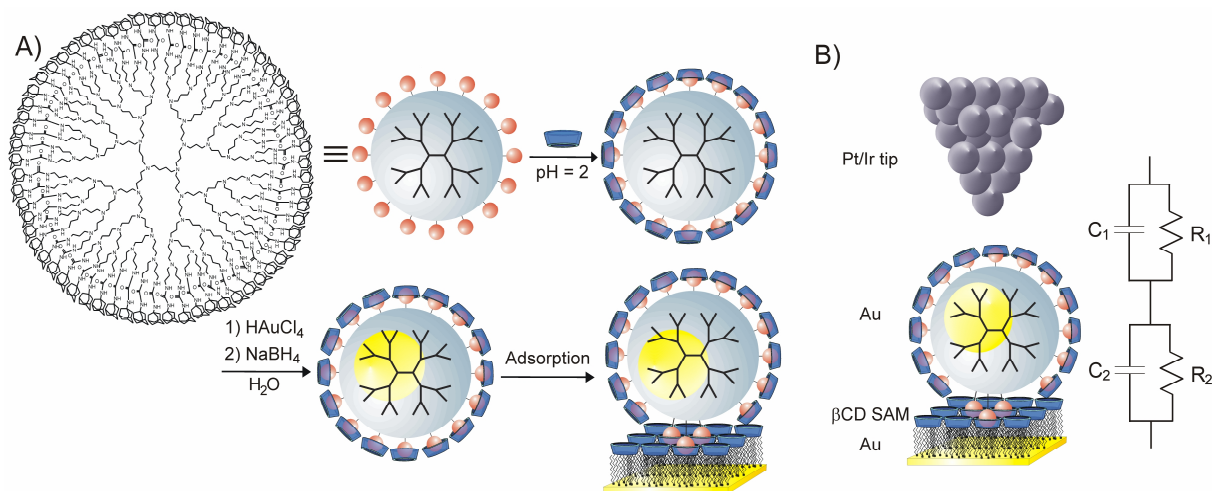
In chapter 6 the molecular printboard was successfully employed to position molecules by several techniques. As described in chapters 3, 4, and 5, the supramolecular assemblies form stable assemblies owing to the multivalent binding and retain their fully extended conformations. Furthermore, supramolecular assemblies of G5-PPI-(Ad)₆₄-(β CD)₄₀ loaded with Au nanoparticles¹⁵ were used to direct the electroless deposition of Cu (section 6.2.2). These dendrimer-encapsulated Au nanoparticles are 1.7 ± 0.9 nm in diameter and are

excellent candidates to exhibit SET by STM. These small Au nanoparticles were immobilized via multiple specific host-guest interactions at a molecular printboard. The result is a supramolecular double barrier junction composed of: Au substrate – β CD SAM tunnel barrier – dendrimer-encapsulated Au nanoparticle – air/water – PtIr STM tip.

7.2 Results and discussion

7.2.1 Immobilization of Au nanoparticles

A fifth generation Ad-functionalized poly(propylene imine) dendrimer ($G5\text{-PPI-(Ad)}_{64}$) was synthesized according to a literature procedure.¹⁶ The dendrimers were solubilized in water at low pH by complexation of the Ad end groups to β CD (Scheme 7.1). Subsequently, the dendrimers were loaded with Au nanoparticles¹⁵ as described in section 6.2.2. Finally, β CD SAMs on hydrogen flame-annealed Au substrates were immersed in solutions of dendrimer-encapsulated Au nanoparticles for 1 h resulting in a full monolayer of dendrimers at the β CD SAMs. The dendrimers bind strongly to the host surface owing to the formation of multiple host-guest interactions between the dendrimer and the host surface. In section 6.2.2 it was shown that monolayers or patterned monolayers of $G5\text{-PPI-(Ad)}_{64}$ dendrimers could not be removed from the host surface by rinsing with competitive solutions, e.g. 10 mM solution of β CD at pH = 2, indicating that the supramolecular complexation of dendrimers at the host surface is kinetically stable.



Scheme 7.1: A) Complexation of $G5\text{-PPI-(Ad)}_{64}$ to β CD resulting in water-soluble dendrimer- β CD assemblies (A, top); loading the supramolecular assemblies with Au nanoparticles by filling with AuCl_4^- ions followed by reduction and adsorption at the β CD SAM (A, bottom); B) Schematic of the supramolecular double junction tunnel barrier consisting of the PtIr STM tip – air – dendrimers loaded with Au nanoparticles – β CD SAM – Au substrate.

The Au nanoparticles are assumed to reside inside the dendrimers because: i) the periphery of the dendrimers does not contain metal particle-stabilizing groups, ii) the dendrimers are not able to expose their interior amines due to the bulkiness of the Ad moieties and the presence of β CD, and iii) the β CD complexed to the Ad moieties may act as a kinetic barrier for the metal particles preventing migration out of the assembly.¹⁵ It is important to note that, approximately, only 1 out of 5 dendrimers will contain a Au nanoparticle since initially the ratio of dendrimer to AuCl_4^- is 1:32 and a Au particle of 1.7 nm contains about 150 metal atoms. This implies that most of the dendrimers adsorbed at the surface will not contain a Au nanoparticle and that the Au nanoparticles are shielded by the dendritic shell.

7.2.2 STM

The STM measurements were performed at room temperature with two STMs: one operating in air and one in ultra highvacuum (UHV). In both cases PtIr tips were used. STM images were recorded on bare β CD SAMs (Figure 7.1d), on a monolayer of dendrimers adsorbed on a β CD SAM (Figure 7.1c), and a monolayer of dendrimers loaded with Au nanoparticles adsorbed on a β CD SAM (Figures 7.1a and 7.1b). It was not possible to record images of bare β CD SAMs or monolayers of dendrimers adsorbed at β CD SAMs under ambient conditions. In Figures 7.1a and 7.1b clear protrusions (visualized as white dots) are visible with a diameter of ~ 4 nm indicating areas of higher conductivity. The surface coverage of these protrusions is about 15%. The images recorded under UHV conditions shown in Fig. 7.1a, 7.1c and 7.1d also show pit like defects which appear as dark features, so-called vacancy islands, similar to the vacancy islands which are observed in *n*-alkylthiol SAMs.¹⁷ It is not unreasonable to expect that the β CD SAM also exhibits vacancy islands.

The white protrusions indicating higher conductivity are only visible in the case of dendrimers loaded with Au nanoparticles adsorbed at the β CD SAMs (Fig. 7.1a and 7.1b) and we assume that these are dendrimers containing a Au nanoparticle. The observed surface coverage of the dendrimers loaded with Au nanoparticles of about 15% agrees quite well with the estimated value of Au nanoparticle-loaded dendrimers in solution which amounts to $20 \pm 5\%$. Moreover, the diameter of the protrusions corresponds with the diameter of the dendrimers.

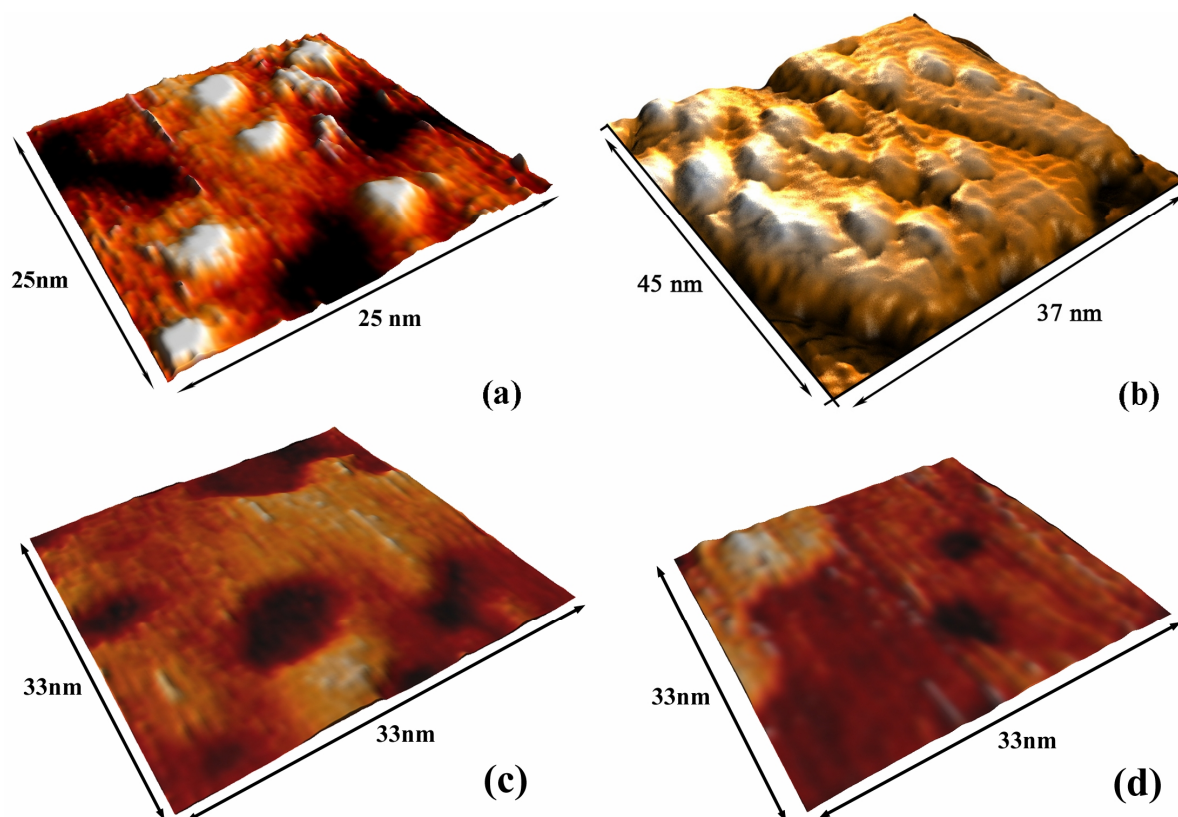


Figure 7.1: a) STM image recorded in UHV at room temperature of Au nanoparticle-loaded dendrimers immobilized at a β CD SAM. Sample bias -0.987 V, tunneling current 0.08 nA and b) recorded under ambient conditions. Tip bias 1 V, tunneling current 0.1 nA. c) STM image of a β CD SAM with a monolayer of the dendrimers recorded in UHV at room temperature, Sample bias -0.987 V, tunneling current 0.08 nA. d) STM image of a β CD SAM recorded in UHV at room temperature, Sample bias -0.987 V, tunneling current 0.08 nA.

(I, V) curves were recorded on 10 different protrusions, e.g. dendrimer-encapsulated Au nanoparticles, and were very similar. A typical (I, V) curve shown in Figure 7.2 was recorded under ambient conditions at 300 K and shows a Coulomb blockade as well as a well-resolved Coulomb staircase. Figure 7.2b shows clearly the equivalent distant steps with an average step width of 130 ± 17 meV. At higher bias voltages (≈ 1.0 V), the (I, V) curve exhibits another interesting feature, namely a strong negative differential resistance (NDR) peak. NDR is a decrease in current with increasing voltage which has been frequently observed in molecular electronics.¹⁸ The exact position of the NDR peak shifted in the range of 1.0 to 1.4 V for different particles.

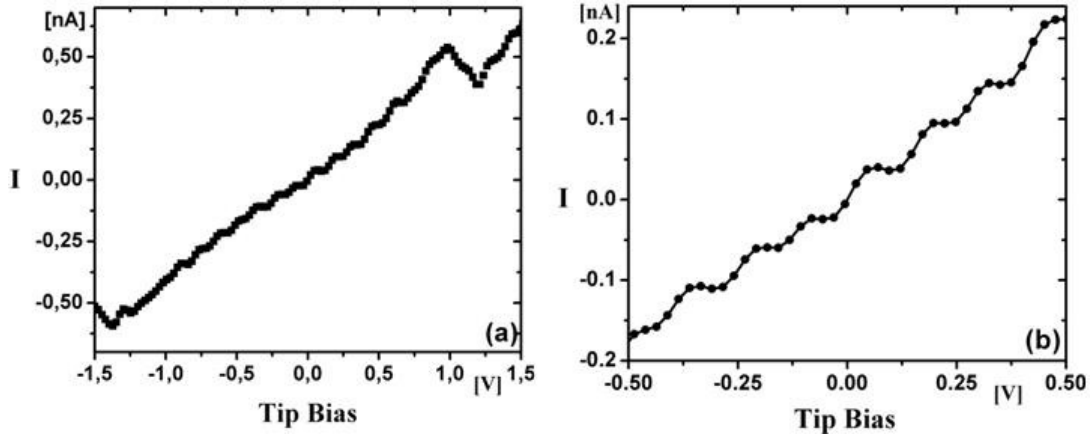


Figure 7.2: a) Typical (I,V) curve recorded at ambient conditions at one of the white protrusions shown in the STM image; b) Magnification of the (I,V) curve shown in 2a for $V = -0.5 \text{ V} - 0.5 \text{ V}$.

In order to observe a Coulomb blockade, a double junction system should fulfill two critically important conditions: i) the single electron charging energy ($e^2/(C_1 + C_2)$) must be larger than the thermal energy, kT , and ii) the resistance of the tunneling junctions must be larger than the quantum resistance (h/e^2). To observe a Coulomb staircase an additional requirement is that the double junction system should be asymmetric, i.e. $R_1C_1 \gg R_2C_2$.¹¹

Using the orthodox theory of SET, which is in principle only applicable to experiments performed at low temperatures and low biases, the resistances and the capacitances of the junctions can be estimated.^{19,20,21} The separation of consecutive steps in the (I,V) curve, e.g. the mean width of subsequent steps, is $130 \pm 17 \text{ meV}$ which is quite large compared to the thermal energy, kT , at room temperature (26 meV). According to the orthodox theory the equivalent capacitance of the system is inversely proportional to the separation of consecutive steps, thus the equivalent capacitance of the double junction system can be calculated using eq. 1:

$$\frac{e^2}{C_{eq}} = 0.13 \text{ eV} \Leftrightarrow C_{eq} = C_1 + C_2 \approx 1.2 \cdot 10^{-18} \text{ F} \quad (1)$$

The slope of the (I,V) curve at large sample bias gives the asymptotic tunneling resistance, i.e. the total resistance of the equivalent circuit, $R = R_1 + R_2$ ($\sim 2.5 \text{ G}\Omega$). A non-zero slope of the curve at zero bias is due to the negatively charged Au nanoparticles, which contain adsorbed chloride ions.²² The NDR effect can be explained by on and off resonant tunneling of electrons through molecular orbitals.

A comparison of the experimental results obtained at ambient and UHV conditions revealed a crucial difference. Despite the fact that the topographical images look rather similar (Figure 7.1), the (I,V) curves deviate significantly (Figures 7.2 and 3). (I,V) curves under UHV

conditions were recorded at bare β CD SAMs and with monolayers with empty and Au nanoparticle-loaded dendrimers adsorbed at β CD SAMs. All (I,V) curves recorded at UHV conditions do not show any signature of SET (see Figure 7.3). Nevertheless, most of the (I,V) curves show a significant NDR effect at a sample bias ~ 1 to 1.1 V, but less pronounced compared to the measurements under ambient conditions.

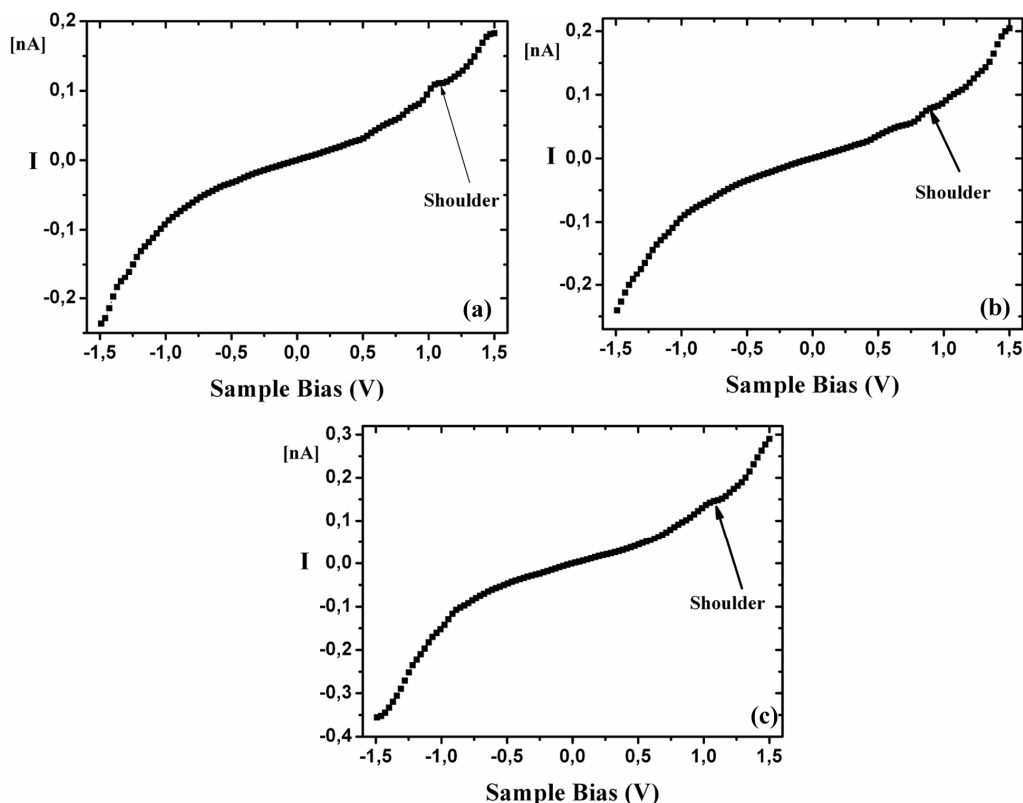


Figure 7.3: a) Typical (I,V) curve obtained under UHV at one of the white protrusions shown in the STM image; b) (I,V) curve measured on top of an empty dendrimer monolayer; c) (I,V) curve measured on a bare β CD monolayer. Tunneling current is 0.08 nA and sample bias is -0.987 V.

A possible explanation could be that under UHV conditions the structures of the supramolecular assemblies at the molecular printboard is altered significantly. The supramolecular assembly is formed by hydrophobic interactions in aqueous solution, and in aqueous conditions the 3D structures of the adsorbed assemblies are well defined. The number of β CDs complexing the dendrimers is known, the number of interactions is known, and protonation, β CD complexation and Au encapsulation cause the dendrimer to adopt an expanded and spherical conformation. For STM experiments conducted at ambient conditions a thin water film is retained and therefore the structure of the supramolecular assembly at the β CD SAM is well defined.²³ On the contrary, under UHV all water molecules are removed and possibly even the β CD that binds to the Ad end groups that are not bound to the β CD SAM, since these relatively small molecules have a certain vapor pressure. This may cause

structural changes and alter the properties of the double junction such that SET properties are not observed under these conditions. The NDR effect is still present at UHV, although it is weaker than at ambient conditions.

7.3 Conclusions

Dendrimers were successfully employed to stabilize and deliver Au nanoparticles to a β CD SAM (molecular printboard). The anchored nanoparticles show Coulomb blockade and a Coulomb staircase under ambient conditions. This indicates that the β CD SAM is an efficient tunnel barrier. The system is quite robust since the dendrimers are attached to the β CD host surface by multiple specific host-guest interactions and the metal particles are located inside the dendrimers. The fact that the Coulomb staircase behavior is observed at room temperature under ambient conditions for Au metal particles in a supramolecular system is quite unique.

The concepts of supramolecular chemistry and self-assembly were used to immobilize Au nanoparticles resulting in well-defined structures displaying SET properties. These are promising tools for large scale fabrication of devices showing SET properties which operate under ambient conditions.

7.4 Experimental

General Procedures. All moisture sensitive reactions were carried out under argon atmosphere. Reagents were commercial and used without further purification. All dry solvents were prepared according to standard procedures and stored over molecular sieves. The adamantyl-terminated PPI dendrimers¹⁶, the dendrimer encapsulated Au nanoparticle,¹⁵ and the β -cyclodextrin adsorbate²⁴ were synthesized according to literature procedures.

Materials and methods. All glassware used to prepare monolayers was immersed in piranha²⁵ solution (conc. H_2SO_4 and 33% H_2O_2 in a 3:1 ratio). (Warning: piranha should be handled with caution; it can detonate unexpectedly). Next, the glassware was rinsed with large amounts of Milli-Q water. All adsorbate solutions were prepared prior to use. All solvents used in monolayer preparation were of p.a. grade.

Substrate preparation. Glass-supported gold substrates (200 nm of gold on 5 nm of chromium on glass) were obtained from Metallhandel Schroer GmbH, Lienen, Germany. Gold substrates were rinsed with dichloromethane and subsequently flame annealed in a hydrogen flame. The substrates were cooled down and immersed in the adsorbate solution (0.1-1 mM, 1:2 ratio chloroform:ethanol) for ca. 16 h at 60°C. Next, the samples were removed from the solution and rinsed thoroughly with 3 cycles of chloroform, ethanol, and Milli-Q water. Adsorption of the dendrimers was carried out by immersing a β CD SAM on Au in an aqueous solution of the corresponding dendrimer- β CD solutions (1.0 mM in adamantyl functionality in the presence of 10 mM β CD at pH = 2) for at least 1 h and dried in a stream of N_2 .

7.5 References

- 1) Kastner, M. A. *Rev. Mod. Phys.* **1992**, *64*, 849.
- 2) Nomoto, K.; Ugajin, R.; Suzuki, T.; Hase, I. *J. Appl. Phys.* **1996**, *79*, 291.
- 3) Orlov, A. O.; Amlani, I.; Bernstein, G. H.; Lent, C. S.; Snider, G. L. *Science*, **1997**, *277*, 928.
- 4) Van der Wiel, W. G.; De Franceschi, S.; Elzerman, J. M.; Fujisawa, T.; Tarucha, S.; Kouwenhoven, L. P. *Rev. Mod. Phys.* **2003**, *75*, 1.
- 5) (a) Wang, B.; Wang, H.; Li, H.; Zeng, C.; Hou, J. G. *Phys. Rev. B* **2003**, *63*, 035403. (b) Sato, T.; Ahmed, H. *Appl. Phys. Lett.* **1997**, *70*, 2759. (c) Hou, J. G.; Wang, B.; Yang, J.; Wang, K.; Lu, W.; Li, Z.; Wang, H.; Chen, D. M.; Zhu, Q. *Phys. Rev. Lett.* **2003**, *90*, 246803.
- 6) Banin, U.; Cao, Y. W.; Katz, D.; Millo, O. *Nature*, **1999**, *400*, 542.
- 7) Tilke, A. T.; Simmel, F. C.; Blick, R. H.; Lorenz, H.; Kotthaus, J. P. *Prog. Quant. Electr.* **2001**, *25*, 97.
- 8) (a) Tokura, Y.; Kouwenhoven, L.P.; Austing, D.G.; Tarucha, S. *Physica B* **1998**, *246-247*, 83. (b) Tarucha, S.; Austing, D.G.; Tokura, Y.; Van der Wiel, W. G.; Kouwenhoven, L. P. *Phys. Rev. Lett.* **2000**, *84*, 2485.
- 9) Andres, R. P.; Bein, T.; Dorogi, M.; Feng, S.; Henderson, J. I.; Kubiak, C. P.; Mahoney, W.; Osifchin, R. G.; Reifengerger, R. *Science*, **1996**, *272*, 1323.
- 10)(a) Jiang, C. -S.; Nakayama, T.; Aono, M. *Appl. Phys. Lett.* **1999**, *74*, 1716. (b) Park, K. -H.; Ha, J. S.; Yun, W. S.; Shin, M.; Park, K. -W.; Lee, E. -H. *Appl. Phys. Lett.* **1997**, *71*, 1469.
- 11)(a) Oncel, N.; Hallbäck A.S.; Zandvliet, H. J. W.; Speets, E. A.; Ravoo B. J.; Reinhoudt, D. N.; Poelsema, B.; *J. Chem. Phys.* **2005**, *123*, 044703. (b) Speets, E. A.; Dordi, B.; Ravoo, B. J.; Oncel, N.; Hallbäck, A. S.; Zandvliet, H. J. W.; Poelsema, B.; Reinders, G.; Blank, D. H. A. Reinhoudt, D. N. *Small* **2005**, *1*, 395.
- 12)(a) Kaun, C. -C.; Guo, H. *Nano Lett.* **2003**, *3*, 1521. (b) Wang, W.; Lee, T.; Reed, M. A. *Phys. Rev. B* **2003**, *68*, 035416.
- 13)(a) Andres, R. P.; Datta, S.; Dorogi, M.; Henderson, J. I.; Janes, D. B.; Kolagunta, V. R.; Kubiak, C. P.; Mahoney, W.; Osifchin, R. F.; Reifengerger, R.; Samanta, M. P.; Tian, W. *J. Vac. Sci. Technol. A* **1996**, *14*, 1178. (b) Anselmetti, D.; Richmond, T.; Baratoff, A.; Borer, G.; Dreier, M.; Bernasconi, M.; Güntherodt, H. J.; *Europhys. Lett.* **1990**, *12*, 241. (c) Dorogi, M.; Gomez, J.; Osifchin, R.; Andres, R. P.; Reifengerger, R. *Phys. Rev. B* **1995**, *52*, 9071. (d) Ohgi, T.; Sheng, H. Y.; Nejjoh, H. *Appl. Surf. Sci.* **1998**, *130-132*, 919. (e) Ohgi, T.; Fujita, D. *Surf. Sci.* **2003**, *532-535*, 294.
- 14)Schneider, H. J.; Yatsimirsky, A. K. *Principles and Methods in Supramolecular Chemistry*, John Wiley & Sons Ltd: Chichester, **2000**.
- 15) Michels, J. J.; Huskens, J.; Reinhoudt, D. N. *J. Chem. Soc., Perkin Trans. 2* **2002**, 102.
- 16)Baars, M. W. P. L.; Karlsson, A. J.; Sorokin, V.; De Waal, B. F. W.; Meijer E. W. *Angew. Chem. Int. Ed.* **2000**, *39*, 4262.
- 17)(a) Yang, G.; Liu, G. *J. Phys. Chem. B* **2003**, *107*, 8746. (b) Poirier, G. E. *Chem. Rev.* **1997**, *97*, 1117.
- 18)(a) Pitters, J. L.; Walkow, R. A. *Nano Lett.* **2006**, *6*, 390. (b) Toisi, A.; Ratner, M. A. *Small*, **2006**, *2*, 172. (c) Joachim, C.; Ratner, M. A. *Proc. Natl. Acad. Sci. USA* **2006**, *102*, 8801.
- 19)Hanna A.E; Tinkham M. *Phys. Rev. B* **1991**, *44*, 5919.
- 20)“*Mesoscopic Electronics in Solid State Nanostructures*”, Thomas Heinzel, WILEY-VCH GmbH & Co. KGaA Winheim, Germany, **2003**.
- 21)Schonenberger C.; Van Houten H.; Donkersloot, H. C. *Europhys. Lett.* **1992**, *20*, 249.
- 22)(a) Mayer A.B.R.; Mark J.E. *J. Macromol. Sci.* **1997**, *11*, 2151. (b) M. A. Hayat, *Colloidal Gold, Principles, Methods and Applications*, Academic Press, San Diego, **1989**.
- 23)Piner, R. D.; Zhu, J.; Xu, F.; Hong, S.; Mirkin, C. A. *Science*, **1999**, *283*, 661.
- 24)Ashton, P. R.; Königer, R.; Stoddart, J. F.; Alker, D.; Harding, V. D. *J. Org. Chem.* **1996**, *61*, 903.
- 25)Dobbs, D. A.; Bergman, R. G.; Theopold, K. H. *Chem. Eng. News* **1990**, *68*, 2.

Preparation of Metal – SAM – Metal Junctions by Supramolecular Metal Transfer Printing

Metal – self-assembled monolayer (SAM) – metal junctions were prepared by a new type of metal transfer printing (mTP) that uses multiple specific β -cyclodextrin (β CD) host-guest interactions between a metal-coated stamp decorated with a monolayer of host molecules and a substrate which is also functionalized with the same host molecules. The metal transfer from the stamp to the substrate is effected by multivalent guest molecules, immobilized at either the host-functionalized stamp or the substrate, which act as a supramolecular “glue”. A β CD SAM was formed at thin Au films that were deposited onto PDMS stamps. Placing these functionalized PDMS stamps in conformal contact with monolayers of different generations of biferrocenyl- (BFc-) (chapter 5), ferrocenyl- (Fc-) (chapters 3 and 4), or adamantyl- (Ad-) terminated dendrimers at β CD SAMs resulted in the transfer of the Au from the PDMS stamp to the substrate. β CD SAMs at different substrates were used, e.g. Au and SiO₂. Also direct transfer of metal to SiO₂ surfaces is possible due to electrostatic interaction between the positively charged dendrimers and the SiO₂ substrate. Different types of patterns were used such as dots, squares or lines with sizes varying from 5 μ m to 50 μ m. Lines of 10 μ m wide and as long as 10 000 μ m could be faithfully transferred. The (I,V)-characteristics of junctions consisting of Fc- or BFc-functionalized dendrimers showed negative differential resistance (NDR). Devices with Fc dendrimers showed one NDR peak and with BFc dendrimers two NDR peaks were observed. Devices prepared using the redox-inactive Ad dendrimers showed typical tunneling behavior.

8.1 Introduction

The electronic properties of organic molecules can be designed and tuned by synthesis, and, therefore, they are attractive candidates as active components in a variety of electronic devices, such as organic light emitting diodes,¹ solar cells,² and organic field effect transistors (OFETs)³. The latter can be applied in identification tags, smart cards, and display drivers. The preparation of organic electronic devices by conventional lithography requires expensive and elaborate equipment, high temperatures, or wet chemicals. They may cause degradation of the relatively fragile organic molecules. For these reasons recently new fabrication techniques, e.g. molding, printing, and embossing, have been developed which are low cost tools with patterning capabilities over large areas and which do not suffer from the limitations of conventional techniques.⁴

In particular microcontact printing is widely used, and relies on a patterned elastomeric stamp (PDMS) from which ink molecules are transferred to a substrate resulting in a patterned self-assembled monolayer at the substrate. In close analogy, metal transfer printing⁵ or nanotransfer printing⁶ involves the transfer of a thin metal film from the stamp to the substrate. In organic electronics this method can be used for introducing top electrodes more reliably than conventional evaporation of metals on top of molecular monolayers. Metal evaporation commonly results in low yields of working devices due to short cuts. The metal transfer from the stamp to the substrate relies on the formation of covalent bonds between the metal and the substrate during conformal contact. Subsequent removal of the stamp, to which the metal film binds only weakly, transfers the metal. Au films have been successfully transferred from PDMS stamps to thiol-terminated surfaces at silicon⁷ and GaAs surfaces.⁸ During conformal contact strong thiol-Au interactions between the substrate and the Au film are formed. Other examples rely on gold welding between the Au substrate and a Au film at the PDMS stamp⁹ and a surface condensation reaction.¹⁰ Also relatively complex 3D structures have been realized by mTP.¹¹ To the best of our knowledge, there are the only two examples of mTP where noncovalent surface forces were used for directly printing a metal on a variety of polymer films at elevated temperatures.¹² However, the nature of the forces between the stamp and substrate remained elusive. Recently, Rogers et al. showed that silicon microstructures can be transferred from PDMS stamps.¹³ The silicon structures could be adhered and released to and from a PDMS stamp by changing the removal speed of the stamp. At fast removal speeds the structures were picked up from a donor substrate, while slow removal of the stamp with the structures in contact with an acceptor substrate resulted in deposition of the structures at a receiving substrate.

This chapter describes the preparation of metal – SAM – metal junctions consisting of Au – β CD SAM – monolayer of dendrimers – β CD SAM – Au or SiO₂. These multi-component junctions are prepared by mTP mediated by multivalent dendrimers to facilitate the metal transfer from β CD host-functionalized Au stamps to the host-functionalized substrates.

Different types of dendrimers were used consisting of redox-inactive Ad moieties, or redox-active BFc and Fc end groups, as described in chapters 3 to 5, and of generations ranging from 1 (4 end groups) to 5 (64 end groups). Different patterns and pattern sizes could be transferred ranging from 4 μm sized dots to lines of 10 000 μm in length. Large area crossbar junctions of 100 μm^2 without having short circuits were prepared showing tunnel characteristics at room temperature along with negative differential resistance (NDR) peaks depending on the number of different redox active groups.

8.2 Results and discussion

8.2.1 Supramolecular metal transfer printing

A uniform layer of Au of 30-40 nm was deposited by electron beam evaporation at patterned PDMS stamps (Figure 8.1). Immediately after Au deposition the stamps were immersed into an ethanolic solution of heptathioether β -cyclodextrin in order to form a β CD SAM at the thin Au film. After 16 h at 60°C the stamps were rinsed with 3 cycles of ethanol and dried in a stream of N_2 . The presence of the β CD SAM was confirmed by FT-IR, XPS and contact angle measurements on flat stamps and the results were comparable to those found for β CD SAMs on solid Au substrates.¹⁴ It is important that prior to metal deposition the stamps are ultrasonicated for at least 2 to 3 h in ethanol to remove unreacted oligomers. These are highly mobile and can easily diffuse to the surface influencing the stamp surface properties.¹⁵ It has been suggested that low molecular weight PDMS facilitates surface diffusion of the Au atoms during evaporation resulting in discontinuous metal films with large grain sizes.⁵ In our study the stamps were kept in ethanolic solutions at elevated temperatures at which low molecular weight PDMS is highly mobile and also segmental motion of the polymer chains may cause instability of the thin Au films.¹⁶ Rippling or buckling of the metal film at stamps due to temperature changes were not observed under these conditions.¹⁷ The evaporation rate is crucial in order to obtain stable Au films that could withstand all further manipulations, but not interacting too strongly with the PDMS stamp. Evaporation rates on the order of 0.6-1.0 $\text{\AA}/\text{s}$ gave optimal thin metal films for mTP. At low deposition rates the Au atoms may be engulfed by the polymer leading to metal films that strongly interact with PDMS,¹⁸ while at high deposition rates rapid nucleation and metal film growth resulted in unstable Au films.¹⁹ Moreover, high deposition rates may also cause significant heating and deformation of the stamp. It has been reported that Au films at stamps thinner than 20 nm have high sheet resistances due to the presence of low molecular weight silicone which promotes coalescence of Au.⁵ For this reason, the stamps were coated typically with 30 – 40 nm Au to ensure that the metal-SAM-metal junctions prepared by mTP consist of conductive and continuous Au top electrodes.

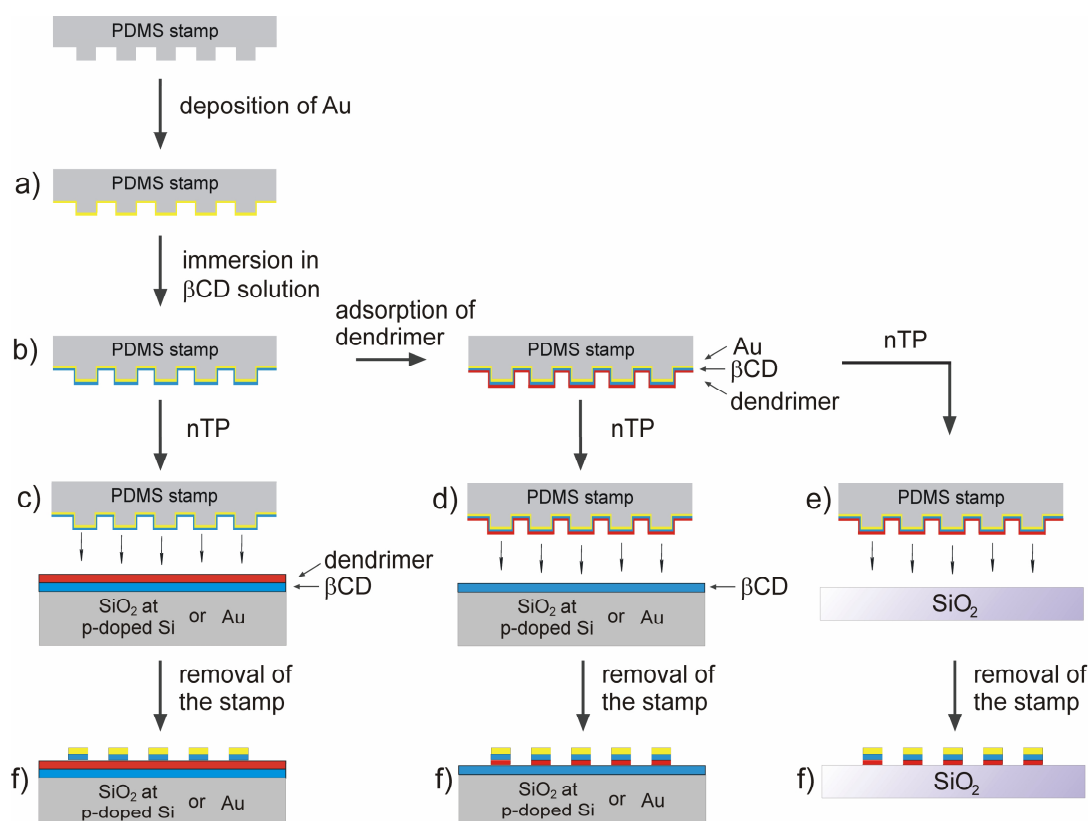
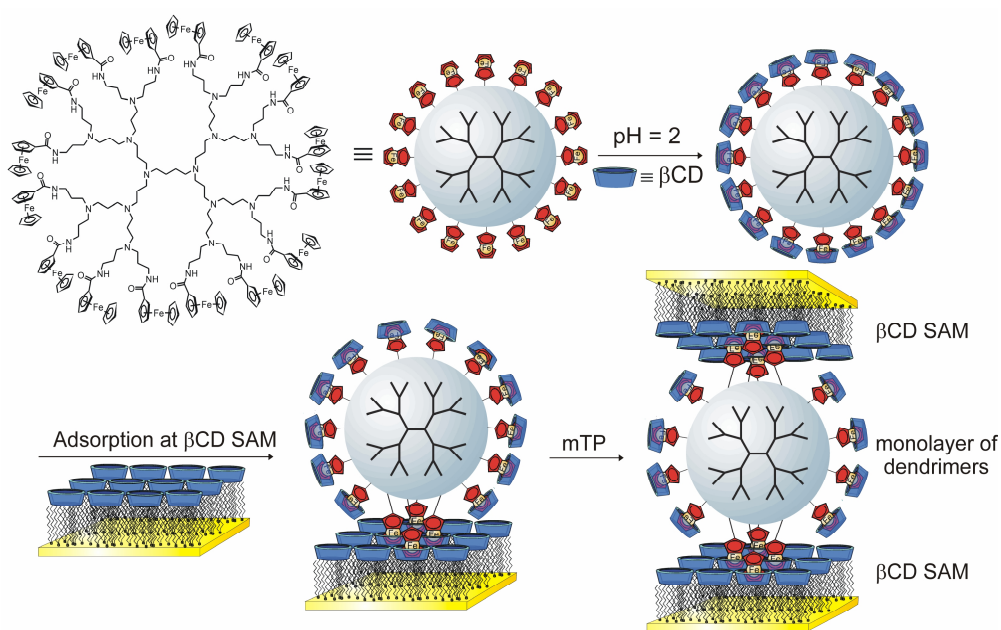


Figure 8.1: Schematic illustration of supramolecular mTP: a) coating the stamp with a layer of 30–40 nm Au; b) formation of a β CD SAM at the metal stamp by immersion in an ethanolic solution of the β CD adsorbate; c, d and e) contacting the stamp with a substrate with a β CD SAM at Au or at SiO_2 at a p-type Si-wafer, at which dendrimers are adsorbed to induce host-guest chemistry (c), or adsorption of dendrimers at the stamp by immersion in an aqueous solution of the dendrimers followed by contacting the stamp with a substrate with only a β CD SAM (d), or with a SiO_2 surface in electrostatic mTP (e); f) removal of the stamp resulting in transfer of the Au from the stamp to the substrate because the host-guest interactions or the electrostatic interactions are stronger than the inherently weak Au-PDMS interactions.

At β CD SAMs on different substrates (Au or SiO_2), redox-active dendrimers were adsorbed from aqueous solutions (Scheme 8.1): Fc PPI dendrimers of generations 1 to 5 with 4 to 64 end groups (chapters 3 and 4), generations 1 to 3 of the BFc dendrimers (chapter 5), G0-PAMAM-EG-(Fc)₄ (chapter 3), and a redox-inactive G4-PPI-(Ad)₃₂. The β CD SAM-functionalized stamps were placed in conformal contact with the substrates containing a monolayer of the dendrimers (Fig. 8.1c). At this stage, the β CD groups at the Au at the stamp may interact with free end groups of the dendrimers at the substrate (Scheme 8.1). In order to obtain good contact of the functionalized PDMS stamps with the substrate, the stamp was kept in water vapor for a few seconds before printing. The presence of water may favor the formation of host-guest complexes during printing since the host-guest chemistry is essentially a hydrophobic interaction. Additionally, the adsorbed dendrimers can change to an extended conformation upon exposure to water vapor since under relatively dry conditions the dendrimers may collapse and inhibit the formation of host-guest complexes. Thus, due to the

thin water film the dendrimers may adopt a fully extended conformation facilitating the formation of a maximal number of host-guest complexes between the functionalized stamp and substrate. Another possible explanation for the improved contact between stamp and substrate after wetting the stamp could be the action of capillary forces. Typical contact times were in the order of 2-3 h after which virtually all the excess water was evaporated and removal of the stamp left the Au behind. Transfer was efficient over large areas. This gave metal – SAM – metal junctions over larger areas consisting of a variety of molecules differing in sizes (ranging from roughly 2.5 nm up to 6 nm) and redox-activity, e.g. redox-active Fc dendrimers, electrochemically communicating BFc dendrimers, and redox-inactive Ad dendrimers. Moreover, a variety of structures could be transferred, e.g. lines, dots, and squares, of various sizes. Squares and hexagonal patterns of dots ranging from 4 μm to 50 μm in diameter could be transferred, as well as lines of 10 μm wide and 10 000 μm long. No significant differences in the effectiveness of mTP were observed using the different types of dendrimers or generations at βCD SAMs at Au or SiO_2 substrates.



Scheme 8.1: Schematic illustrating the supramolecular chemistry involved in the preparation of the metal-SAM-metal junctions shown for G3-PPI-(Fc)₁₆ on gold: complexation of the dendrimers to βCD resulting in water-soluble assemblies (top); adsorption at the molecular printboard (bottom left), and supramolecular mTP (bottom right).

Optical micrographs and AFM images of the stamps and the substrates (Figure 8.2) clearly show the selectively transferred metal structures. Optical micrographs of the stamps before and after transfer showed that metal transfer took place exclusively where the stamp made conformal contact with the substrate (4 μm dots) and not in between the dots. AFM showed that the height of the features were 40 nm which was in agreement with the metal thickness deposited at the stamp (Fig. 8.2d). AFM images revealed that the root mean square roughness

at the transferred structures was in the order of 1.3 nm. In between the structures a somewhat lower root mean square roughness of 0.8 nm was found. This indicated that the transferred structures interacted with the underlying surface and completely prevented buckling of the metal film. The somewhat higher surface roughness at the structures could be due to the fact that in between the structures a soft surface was measured, the β CD SAM with adsorbed dendrimers. XPS data revealed only trace amounts of Si at the features indicating that the Au-PDMS interaction is low and that no PDMS was transferred of the stamp during mTP and/or that unreacted PDMS oligomers were efficiently removed during ultrasonication of the stamps.

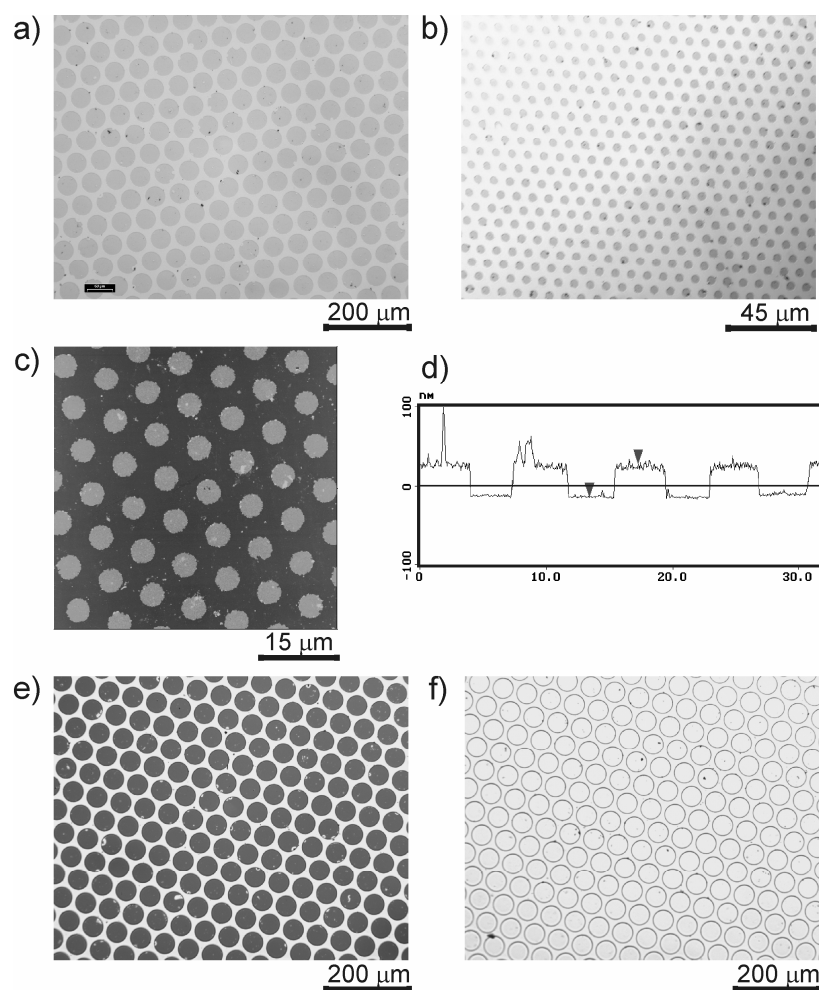


Figure 8.2: Optical micrographs of gold patterns printed by supramolecular mTP of: a) a hexagonal pattern of dots of 50 μm in diameter and a periodicity of 60 μm and b) dots of 5 μm and a periodicity of 8 μm ; c) AFM image and (d) height profile of a hexagonal pattern of dots of 5 μm and a periodicity of 8 μm ; optical micrographs of the stamp before (e) and after mTP (f).

As stated above, a thin water film was required in order to induce good conformal contact between the stamp and the surface. Therefore mTP was carried out in the absence of dendrimers in order to study the influence of the thin water film on the printing process. Some structures were transferred despite the fact that no specific host-guest complexes were formed

indicating that capillary forces are sufficient for some transfer, but the efficiency of the transfer was dramatically decreased. Subsequent brief ultrasonication (60 s) of the stamps in water resulted in an effective removal of the transferred structures while in the case of the dendrimers the structures remained intact, apart from the edges being slightly damaged. These observations suggest that multiple specific host-guest interactions are essential for having effective transfer yielding stable structures.

To fabricate structures having dendrimers in the metal-SAM-metal junctions, but not in between the structures, the dendrimers were adsorbed on the functionalized stamps instead of on the solid substrate (Fig. 8.1d). Supramolecular mTP was performed at β CD SAMs at Au or SiO₂. The metal transfer was as effective. A dendrimer with all end groups interacting with the host surface, e.g. G0-PAMAM-EG-(Fc)₄ (section 3.2.1), also showed effective mTP.²⁰ The fact that mTP is still possible indicates that end groups also interact with the host surface at the stamp. It is well known that β CD-Fc inclusion complexes are dynamic and thus formation of host-guest complexes of G0-PAMAM-EG-(Fc)₄ with the two host surfaces simultaneously is still possible. However, the number of interactions is also dependent on the effective concentration of host molecules at the surface.²¹ Thus, the β CD SAM at the stamp is sufficiently densely packed to obtain metal – SAM – metal structures even using molecules with a small number of end groups.

8.2.2 Electrostatic metal transfer printing.

Also mTP at a bare SiO₂ surface was performed with Fc PPI dendrimers of generations 4 and 5, and with G4-PPI-(Ad)₃₂, adsorbed at the functionalized Au-coated PDMS stamp (Fig. 8.1e). The stamps were placed in conformal contact with a freshly cleaned SiO₂ substrate and water vapor was used to induce good conformal contact between the stamp and the surface. Upon subsequent removal of the stamp, mTP proved highly effective as is illustrated by the optical micrograph and AFM image of the structures shown in Figure 8.3. The lines are 32 nm in height corresponding to the metal thickness deposited at the stamp (Fig. 8.3d). In this case, transfer was accomplished without specific host-guest interactions, but via electrostatic interactions since the SiO₂ surface is negatively charged and the PPI dendrimers are positively charged. A control experiment without dendrimers gave virtually no transfer indicating that indeed the electrostatic interactions of the dendrimers with the surface are essential to facilitate mTP in this case.

A relatively simple way to determine whether the transferred Au features have shortcuts with the underlying Au of the substrate is to perform electrodeposition of Cu (Fig. 8.4).²² Under the proper conditions, electrodeposition can only take place if the Au dots have shortcuts or if the monolayer in between the dots has defects. In electrodeposition of Cu, the Au layer of the substrate is used as an electrode while the counter electrode is kept in solution

together with the Cu^{2+} ions and the reference electrode. The Cu^{2+} ions are only reduced at locations where the electrode is not well protected or where the sandwiches have shortcuts.

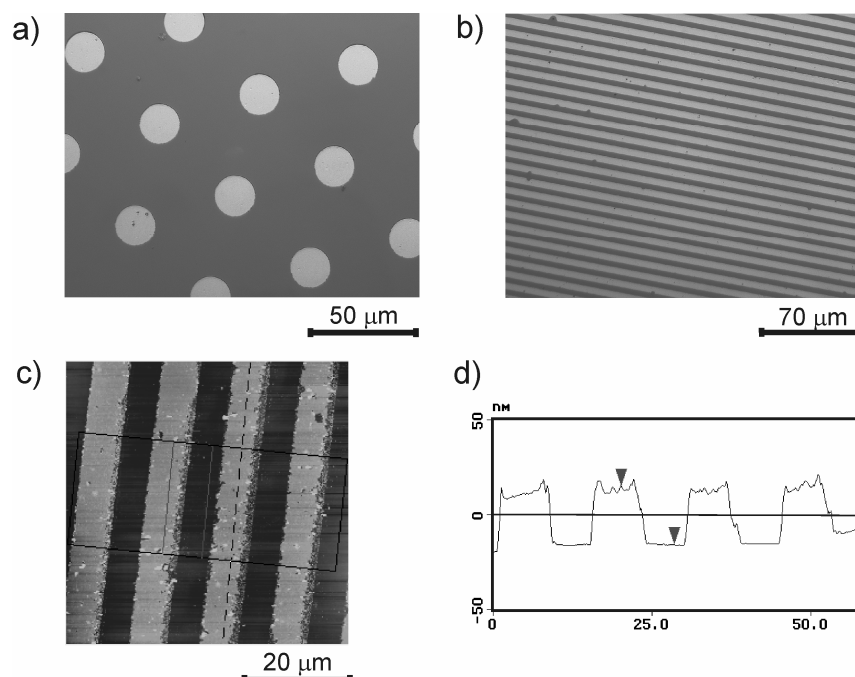


Figure 8.3: a) Optical micrographs after electrostatic mTP of hexagonal patterns of dots ($20\ \mu\text{m}$ with a periodicity of $50\ \mu\text{m}$) and b) lines of $10\ \mu\text{m}$ wide (with a periodicity of $15\ \mu\text{m}$); c) AFM image of the same line structures and a height profile (d).

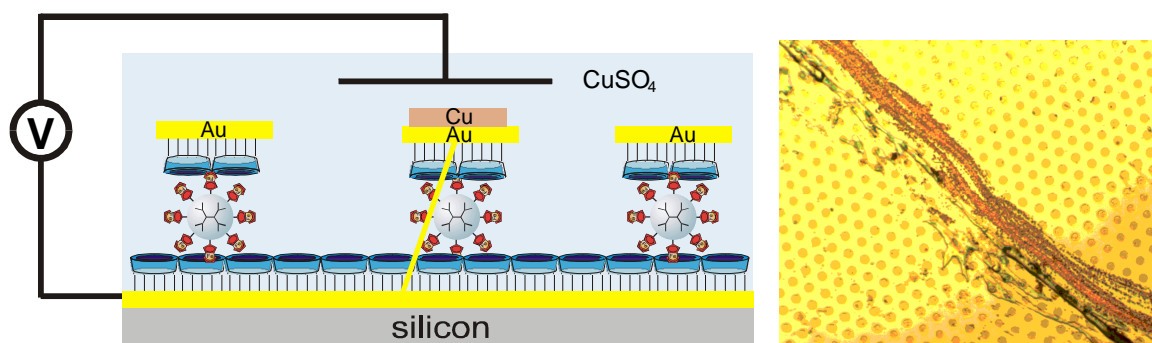


Figure 8.4: Schematic of electrodeposition of Cu: the Au at the substrate is used as a working electrode while the reference and counter electrodes are kept in the solution of $10\ \text{mM}\ \text{CuSO}_4$ at $\text{pH} = 2$; right: optical micrograph after electrodeposition: virtually no Cu was deposited at the transferred Au features or at the βCD SAM-protected Au in between, a scratch served as an internal reference at which Cu was deposited.

The aqueous solution contained $10\ \text{mM}$ of CuSO_4 at $\text{pH} = 2$ and a static potential was applied at $-0.7\ \text{V}$ for a period of $30\ \text{s}$. At this potential, Cu was deposited at an unprotected Au electrode, but not on βCD SAMs and, therefore, these conditions are suitable to determine whether the structures have shortcuts (Fig. 8.4). Prior to deposition, the structures, in this case a hexagonal pattern of dots of $4\ \mu\text{m}$ in diameter transferred using G4-PPI-(Fc)_{32} adsorbed at the substrate, were analyzed by AFM and the features were $40\ \text{nm}$ high. After applying a

potential of -0.7 V for 30 s AFM images and optical micrographs (Fig. 8.4) clearly showed that no Cu was deposited indicating that none of the devices have shortcuts with the underlying Au. As an internal reference, Cu deposition could be clearly observed by optical micrography at an intentionally made scratch.

8.2.3 Electrostatic and supramolecular mTP combined

To demonstrate the potential of supramolecular mTP in the fabrication of more complicated structures, mTP was performed at patterned Au substrates. A Au substrate at a Si wafer was patterned by printing octadecanethiol (ODT) followed by immersion in a wet etch solution to remove unprotected Au areas.²³ Next, all organic material was removed by oxygen plasma, which in addition oxidizes the Si surface in between the Au lines. Lines of Au of 10 μm wide and 10 000 μm in length were obtained on which a βCD SAM was deposited. For mTP, Au-coated stamps with a βCD SAM were used with the same line pattern onto which dendrimers, e.g. Fc PPI dendrimers of generations 1 to 5, generations 1 to 3 of the BFc dendrimers, or G4-PPI-(Ad)₃₂, were adsorbed. Cross-printing (that is 90° rotation of the stamp with respect to the substrate pattern) gave a grid-like structure since at the crossings mTP is efficient owing to the formation of multiple specific host-guest interactions while in between the crossing mTP is efficient owing to electrostatic interactions of the dendrimers with the SiO₂ surface. An AFM image and an optical micrograph shown in Figure 8.5 clearly illustrate that mTP is highly selective using two types of interactions between the stamp and substrate simultaneously to facilitate transfer of the metal film from the PDMS stamp to the substrate. Also here, no differences in mTP were observed using the different types of dendrimers.

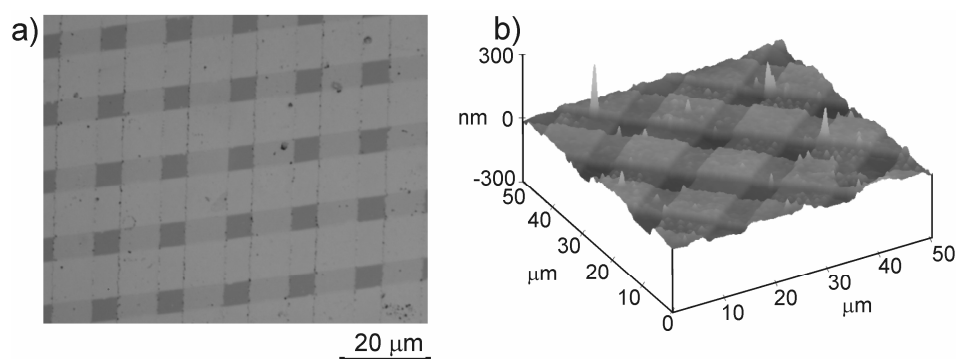


Figure 8.5: Optical micrograph (a) and an AFM image (b) of supramolecular mTP on patterned Au substrates on a Si wafer. The Au-coated wafer was patterned with lines of 10 μm wide by microcontact printing a SAM of ODT at the Au-coated wafer followed by a wet etch to remove unprotected gold areas.²³ The ODT SAM was removed in oxygen plasma and a βCD SAM was formed at the pre-patterned Au surface by immersion in ethanolic solution of the βCD adsorbate. Dendrimers were adsorbed on a PDMS stamp with the same line pattern functionalized with a βCD SAM on a thin Au film. The structures were completed by a 90° cross-print step; the metal was transferred via supramolecular interactions at the junctions and via electrostatic interactions in between.

8.2.4 Negative differential resistance in supramolecular junctions

Negative differential resistance (NDR) is a decrease in current while the voltage increases across an electronic circuit. The characteristics of NDR can be observed in resonant tunneling diodes (RTD) in conventional semiconductor-based technology and has found applications in oscillators, analog-to-digital converters, and logic.²⁴ NDR is also frequently observed in molecular electronics and received considerable attention, because molecules displaying NDR serve as nanoscale analogous of electronic switches which are presumably easier to incorporate into circuitry than three-terminal devices.

The (I,V) characteristics were measured using the cross-bar structures composed of continuous lines (Fig. 8.4) and the structures shown in Figure 8.6. The latter structures were obtained by mTP of bars of $25\ \mu\text{m} \times 10\ \mu\text{m}$ with gaps of $15\ \mu\text{m}$. The lines of rectangular shape have an overlaid structure and the top electrodes were introduced by 90° rotation of the stamp with respect to the substrate with the same pattern resulting in the structures shown in Fig. 8.6A. Rotation of less than 90° resulted in complex structures, for instance, rotation of 85° (Fig. 8.6B), 80° (Fig. 8.6C) and 75° (Fig. 8.6D) shows the change to almost continuous lines of alternating structures.

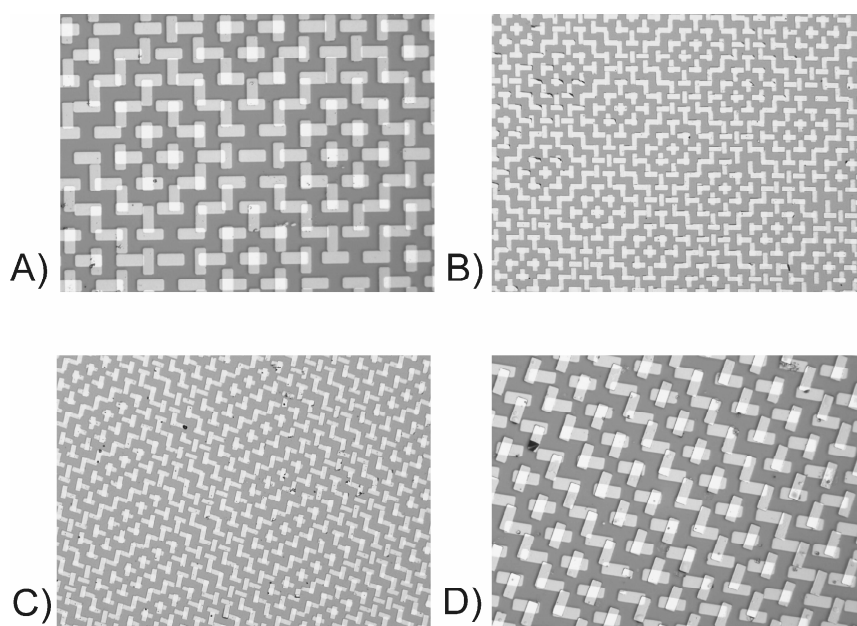


Figure 8.6: Optical micrographs of the two terminal devices prepared by mTP using bars of $25\ \mu\text{m}$ in length and $10\ \mu\text{m}$ wide. The cross-print was carried at 90° (A), 85° (B), 80° (C) and 75° (D).

A large percentage (90%) of the devices showed ohmic behavior with a resistance varying from 100 to $1000\ \Omega$ indicating short circuits, or showed no conductivity at all. The latter ones were destroyed upon applying a potential probably due to warming up of the water which is present in the junction. About 5% of the devices were found to be instable during the

measurement and gave noisy data. Water can cause random tunneling fluctuations.²⁵ Less than 5% of the devices produced (I,V)-curves that had tunnel characteristics. The low yield in working devices may be caused by the fact that the junctions have a large surface area of $100\ \mu\text{m}^2$ while the βCD SAM – dendrimer monolayer – βCD SAM is at most about 10 nm thick and, thus, prone to short circuits.

In Figure 8.7 (I,V) results are shown for junctions consisting of monolayers of G3-PPI-(BFC)₁₆ (Fig. 8.7A) and G1-PPI-(BFC)₄ (Fig. 8.7B), G4-PPI-(Fc)₃₂ (Fig. 8.7C), and G5-PPI-(Adc)₆₄ (Fig. 8.7D). The NDR peak varied from 2 V and 3 V for the Fc dendrimers and for the BFC dendrimers the first peak was found between 0.5 to 1.5 V and the second peak also between 2 V and 3 V. The peak-to-valley ratio of the NDR wave varied from 2 to 5. The currents varied three orders of magnitude between a few pA to a few nA. In the case of G3-PPI-(BFC)₁₆ around 1.5 V in the forward scan and around -1 V NDR peaks with a shoulder are visible. In the case of G1 in the forward scan the two NDR peaks are clearly visible. The backward scan is noisy at low potentials below -0.5 V. At potentials before the NDR peaks the (I,V) curves are dominated by Coulomb blockade. The Coulomb blockade ranges roughly from 3 to 4 eV where the current is effectively blocked.

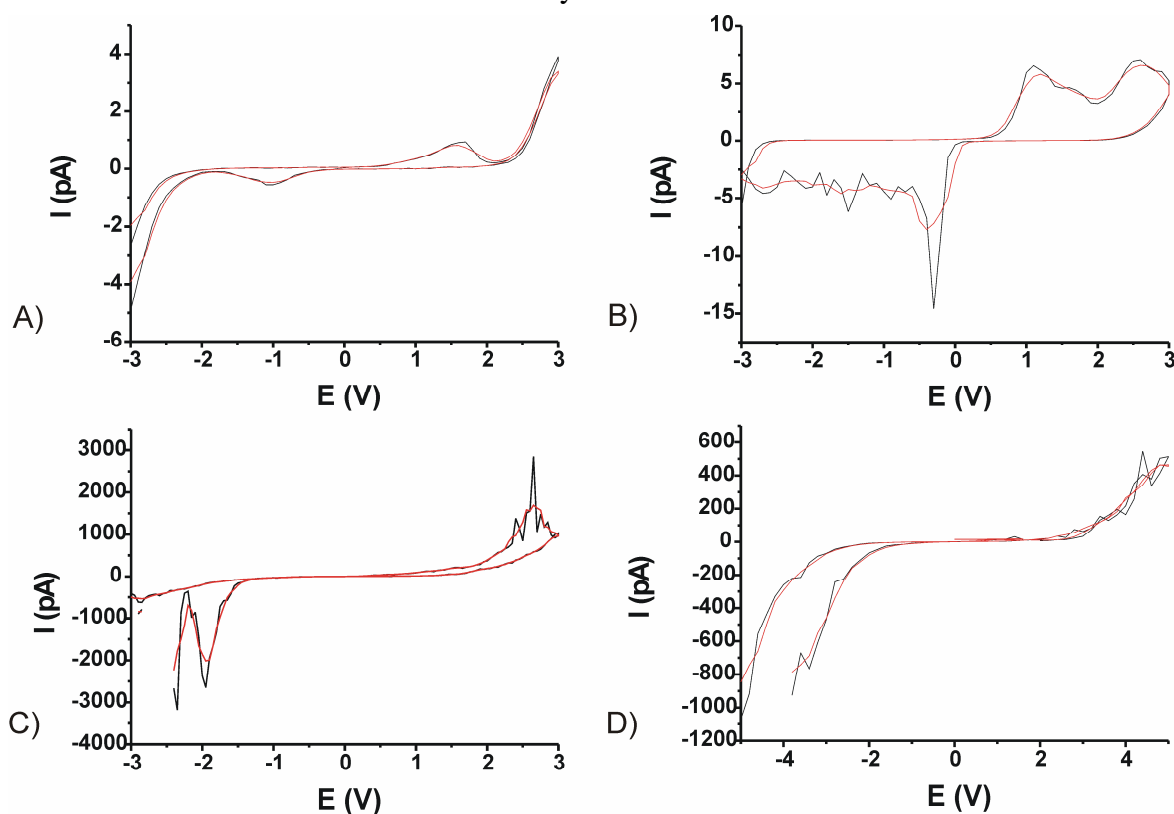


Figure 8.7: (I,V)-characteristics of G3-PPI-(BFC)₁₆ showing two NDR peaks (A), of G1-PPI-(BFC)₄ showing two NDR peaks (B), of G4-PPI-(Fc)₃₂ showing one NDR peak, and of G5-PPI-(Ad)₆₄ showing no NDR. The red lines represent smoothed data points.

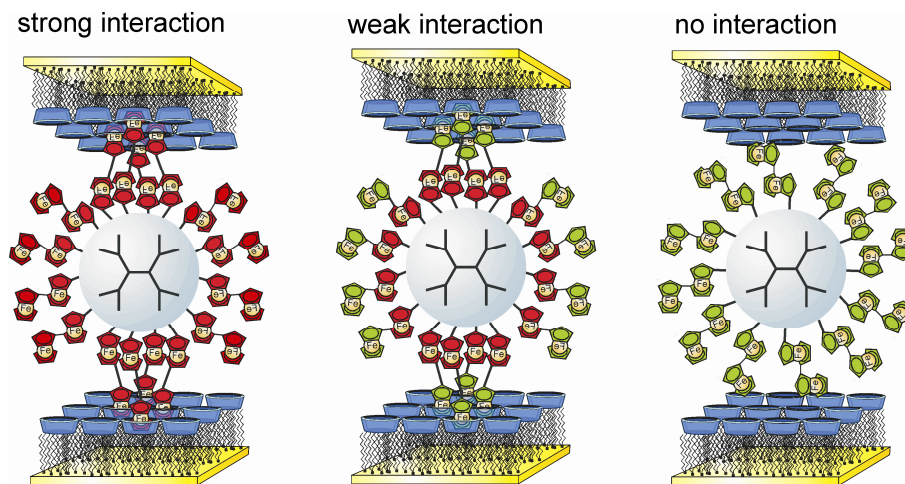
NDR has been observed in different experimental settings and molecules, but a general explanation for NDR is still under debate. Redox-active phenylacetylenes in nanopores

consisting of approx. 1000 molecules exhibit reproducible NDR.²⁶ Junctions prepared by electromigration²⁷ show NDR possibly due to redox-activity or conformational changes of the molecules.²⁸ Monolayers of arylthiols on Au measured by STM showed NDR in one or both bias directions and were attributed to narrow features on the local density of states of the tip apex atom and the adsorbed molecule.²⁹ Redox-active monolayers of ferrocene alkyl thiols on Au showed NDR which was related to a resonant tunneling mechanism involving different redox states of the Fc moiety.^{30,31} The NDR could be attenuated in a supramolecular manner by complexation of β CD to the Fc moieties.³² There is evidence that the NDR could originate from reaction under ambient conditions of the oxidized Fc with oxygen.³³ Bond fluctuation and random configuration changes of small molecules such as styrene³⁴ or vibrational changes of pyrrolidine³⁵ at Si surfaces also can account for NDR. Reductive desorption of disulfides from Hg contacts resulted in a strong and reproducible NDR.³⁶ Recently, Ratner and Nitzan reported a model to account for NDR based on polaron formation.³⁷ Other possibilities for explaining NDR are metal filament formation and dissolution due to large bias^{38,39} or the presence of impurities and defects in the monolayer.⁴⁰ NDR is frequently observed in redox-active systems and is attributed to on and off resonant tunneling.

Another explanation could be a change of carrier densities within the junction. The highest conductivity may be observed when the densities of reduced and oxidized Fc moieties are equal. Increasing either density by varying the potential may cause a decrease in conductivity resulting in a NDR wave. In the case of BFc this may happen twice resulting in a double NDR wave.

However, in this case an entirely different explanation may apply. It is well known that a strong interaction of a redox-active species with a SAM enhances the electron transfer rate. This has been thoroughly studied in wet electrochemistry involving a variety of SAMs and redox probes.⁴¹ A species that is not interacting with a SAM, for instance $\text{Fe}^{2+}(\text{CN})_6/\text{Fe}^{3+}(\text{CN})_6$, is effectively blocked, preventing electron transfer processes. In the present case, the reduced dendrimers are able to form stable inclusion complexes with the host surface. But when the potential increases the current also increases and is transported via the dendrimers most likely via an electron hopping mechanism. Electrons only hop if oxidized and reduced centres are both present, thus as the current rises so does the number of oxidized metal centres. This decreases the interaction of the BFc moieties with the β CD SAM. For this reason the current decreases when the interaction of the dendrimers with the molecular printboard is reduced. In the case of the BFc dendrimers it was found that the dendrimers in the partially mixed valence state (section 5.2.5) still have a weak interaction with the molecular printboard, but this interaction is completely lost if they are oxidized fully. Thus, as the potential increases, further oxidation of the dendrimers leads to a complete loss of specific interactions with host surface, which may result in a second decrease in current. The end result is a double NDR. Devices consisting of Fc dendrimers showed only one NDR peak, which is in agreement with the proposed mechanism shown in Scheme 8.2. The Fc moieties

undergo a single oxidation which diminishes the interaction with host surface (chapters 3 and 4). This causes a single NDR peak. In the case of the redox inactive adamantyl dendrimers the (I,V) characteristics were dominated by tunneling characteristics and no NDR peaks were observed (Fig. 8.7D).



Scheme 8.2: Schematic illustration of G3-PPI-(BFC)₁₆ in a metal – SAM – metal junction having strong, weak, or no interaction with the β CD host surface.

8.3 Conclusions

A new type of transfer printing has been introduced based on supramolecular interactions to facilitate metal transfer from a stamp to a substrate. Thin Au films at elastomeric stamps as well as the substrate were functionalized with a β CD SAM. Supramolecular transfer printing was realized by adsorption of polyfunctional guest molecules that act as supramolecular “glue” at either the stamp or at the substrate. Different metal-SAM-metal junctions were prepared, on β CD SAMs at Au or SiO₂, and five generations of redox-active Fc dendrimers, three generations of BFc dendrimers, G0-PAMAM-EG-(Fc)₄, and one redox inactive G4-PPI-(Ad)₃₂. A variety of patterns, i.e. lines (10 μ m in wide and 10 000 μ m in length), squares (50 μ m \times 50 μ m) and dots (4 μ m or 50 μ m in diameter), were used. More complicated crossbar structures could be prepared on patterned Au substrates on SiO₂ using supramolecular and electrostatic interactions simultaneously.

A variety of metal-SAM-metal structures were constructed by simple chemical modification of the molecules, e.g. Fc-, BFc-, and Ad-functionalized dendrimers, and relatively simple changes in the process steps, i.e. dendrimers adsorbed at the stamp or at the substrate. Not only specific host-guest interactions, but also electrostatic interactions are sufficient to affect metal transfer from the stamp to the substrate. Here, host-guest chemistry based on Fc, BFc, or Ad guests and β CD hosts were employed, but in principle any host-guest combination should be possible in supramolecular mTP leading to interesting devices.

The devices consisting of redox-active dendrimers showed one or two NDR peaks in the case of Fc and BFc dendrimer, respectively, while redox-inactive dendrimers, i.e. Ad-decorated dendrimers, showed no NDR. A new mechanism for NDR is proposed based on the potential dependent host-guest complex formation between the dendrimers and the host surface. The number of NDR peaks is determined by the interaction of the dendrimers with the monolayers since oxidation of the Fc and BFc dendrimers reduces the interaction with β CD SAM. Ferrocene can undergo a single oxidation which results in a lower interaction with the host surface, thus consequently lowering the current. BFc can undergo two oxidations altering the current flow twice. This is not the case for the redox passive Ad dendrimer which shows no NDR peak. This mechanism is also consistent with the mechanism for classical resonant tunneling diodes (RTDs) wherein the redox centres provide tunnel pathways depending on the redox states of the active groups. Thus, the mechanism based on supramolecular interactions is in principle a change of state of complexation of the molecules which causes a difference in interaction.

8.4 Experimental

General Procedures. All moisture sensitive reactions were carried out under argon atmosphere. Reagents were commercially available and used without further purification. All dry solvents were prepared according to standard procedures and stored over molecular sieves. ^1H NMR and ^{13}C NMR spectra were recorded on Bruker AC300 or Bruker AMX400 spectrometers. Spectra are reported in ppm downfield from TMS as internal standard. Matrix-Assisted Laser Desorption Ionization (MALDI) Time-of-Flight (TOF) mass spectra were recorded using a Perkin Elmer/PerSeptive Biosystems Voyager-DE-RP MALDI-TOF mass spectrometer. Analytical TLC was performed using Merck prepared plates (silica gel 60 F-254 on aluminum). Merck silica gel (40-63 μm) was used for flash chromatography. Column chromatography was performed using silica gel (SiO_2 , E. Merck, 0.040-0.063 mm, 230-240 mesh). The per-6-amino β -cyclodextrin,⁴² ferrocenyl⁴³ and biferrocenyl (section 5.2.1) PPI dendrimers, ferrocenyl PPI dendrimers with tetraethylene glycol tethers (section 3.2.1), and the adamantyl PPI dendrimers⁴⁴ were prepared as described previously.

Materials and methods. All glassware used to prepare monolayers was immersed in piranha solution (conc. H_2SO_4 and 33% H_2O_2 in a 3:1 ratio). (Warning: piranha should be handled with caution; it can detonate unexpectedly). Next, the glassware was rinsed with large amounts of Milli-Q water. All adsorbate solutions were prepared prior to use. All solvents used in monolayer preparation were of p.a. grade.

Substrate preparation. At gold. Gold substrates of 20 nm metal thickness with a 2 nm titanium adhesion layer were obtained from SSENS bv (Hengelo, The Netherlands). Gold substrates were cleaned by brief immersion in piranha and the resulting oxide layer was removed by leaving the substrates for 10 min in absolute EtOH. The substrates were subsequently immersed in the adsorbate

solution (0.1-1 mM) for ca. 16 h at 60°C. Next, the samples were removed from the solutions and rinsed thoroughly with chloroform, ethanol, and Milli-Q water.

At silicon. At four-inch polished, 100-cut, p-doped silicon wafers, was 50 nm of SiO₂ thermally grown and cut into 2 × 2 cm² samples which were used for monolayer preparation. The synthesis of a βCD SAM on SiO₂ has been reported recently by our group and the same procedure was used here.⁴⁵ Briefly, microscope glass slide were oxidized by immersion on boiling piranha (conc. H₂SO₄ and 33% H₂O₂ in a 3:1 ratio) for 15 min, rinsed with copious amounts of Millipore water and dried in a stream of N₂. Subsequently, a monolayer was formed by reaction with 1-cyano-11-trichlorosilylundecane. Reduction gave the amine-terminated monolayer which was converted to isothiocyanate-terminated layers by reaction with 1,4-phenylene diisothiocyanate. Finally, reaction with per-6-amino β-cyclodextrin gave the host surface.

Dendrimer adsorption. Adsorption of the dendrimers was carried out by immersing a preformed βCD SAM on Au or silicon in an aqueous solution of the corresponding dendrimer-βCD assemblies solutions (0.1 or 1.0 mM in ferrocene functionality in the presence of 11 mM βCD at pH = 2) for at least 3 h. Subsequently the samples were thoroughly rinsed with Milli-Q water (at pH = 2 to ensure full protonation of the amines) and dried in a stream of N₂.

Supramolecular metal transfer printing. Stamps were fabricated by casting a prepolymer of PDMS (DOW Sylgard 184) against a photolithographically patterned silicon master, cured for 20 h at 60°C, and released at 60°C. Subsequently the stamps were ultrasonicated in ethanol for 2 - 3 h and dried in a stream of N₂. The stamps were coated with Au by thermal deposition using a Balzers BAK-600 at deposition rates in the range of 0.6-1 Å/s at 2·10⁻⁶ bar. Directly after deposition the stamps were immersed in a suspension of βCD adsorbate in ethanol (1 mg in 20 ml). The procedure for the formation of the *b*CD SAM at a Au coated PDMS stamp is slightly different from that reported for the *b*CD SAM preparation at Au solid substrates. For solid substrates the *b*CD adsorbate is dissolved in an EtOH-CHCl₃ mixture due to the low solubility of the *b*CD adsorbate in EtOH. PDMS swells in chloroform, but only slightly in EtOH, and therefore ethanolic solutions of the adsorbate were used since at 60 °C clear solutions could be obtained (1 mg/ 20 ml). After immersion of the stamps in the *b*CD solutions at 60 °C for 16 h the stamps were removed from the warm solution and poured in pure ethanol three times for 10 min and dried in a stream of N₂. The quality of the *b*CD SAM of the modified monolayer preparation was examined at solid substrates using contact angle measurements, cyclic voltammetry, heterogeneous electron transfer and electrochemical impedance spectroscopy, and the found values were comparable to those found for the procedure for solid Au substrates.

Water vapor of 60 °C was condensed at the βCD-functionalized Au-coated stamps for 5-8 s to enhance conformal contact between the stamp and the substrate. The stamp was kept in conformal contact with the substrate for 3 h after which the stamp was removed and the metal film was left behind.

Electroless deposition of Cu. Electrochemical measurements were performed with an AUTOLAB PGSTAT10, in a custom built three-electrode setup equipped with a platinum counter electrode, a mercury sulfate reference electrode ($V_{MSE} = +0.61 V_{NHE}$) and a screw cap holding the gold working electrode (area exposed to the solution = 0.44 cm²). Electrodeposition was performed on the structures

obtained by mTP in aqueous solution containing 10 mM Cu_2SO_4 and 10 mM H_2SO_4 at a static potential of $-0.70 \text{ V}_{\text{MSE}}$.

Contact angle goniometry. Contact angles were measured with Milli-Q water on a Krüss G10 contact angle measuring instrument, equipped with a CCD camera. Advancing and receding contact angles were determined automatically during growth and shrinkage of the droplet by a drop shape analysis routine.

Optical microscopy. Optical micrographs were taken with an Olympus BH-2 microscope, equipped with CCD camera.

Atomic force microscopy. AFM analyses were carried out with a Nanoscope III multimode AFM (Digital Instruments, Santa Barbara, CA, USA) with a J-scanner in contact mode using V-shaped Si_3N_4 cantilevers (Nanoprobes, Digital Instruments) with a spring constant of 0.1 N/m. Images were acquired in ambient atmosphere (relative humidity = 30-40 % and $T = 25 \text{ }^\circ\text{C}$).

X-ray photoelectron spectroscopy. XPS spectra were obtained on a Quantera Scanning X-ray Multiprobe instrument equipped with a monochromatic Al $\text{K}\alpha$ X-ray source producing approximately 25 W of X-ray power. Spectra were referenced to the main C 1s peak at 284.0 eV. XPS data were collected from a surface area of $300 \times 300 \text{ }\mu\text{m}$.

Electrical Characterization. Electrical characterization of the devices was performed by current-voltage measurements using a Karl Süss PM8 Manual Probe station connected to a parameter analyzer (Hewlett Packard Agilent 4158B). Feather microneedles with a tip diameter of $5 \text{ }\mu\text{m}$ were used to contact the structures under a N_2 atmosphere.

8.5 References

- 1) (a) Sheatsa, J. R. *J. Mater. Res.* **2004**, *19*, 1974. (b) Braun, D. Heeger, A. J. *Appl. Phys. Lett.* **1995**, *66*, 2540.
- 2) (a) Granström, M.; Petritsch, K.; Arias, A. C.; Lux, A.; Andersson, M. R.; Friend, R. H. *Nature*, **1998**, *395*, 257. (b) Brabec, C. J.; Sariciftci, N. S.; Hummelen, J. C. *Adv. Funct. Mater.* **2001**, *11*, 15.
- 3) (a) Katz, H. E.; Bao, Z.; Gilat, S. L. *Acc. Chem. Res.* **2001**, *34*, 359. (b) Bao, Z. *Adv. Mater.* **2000**, *12*, 227.
- 4) (a) Geissler, M.; Xia, Y. *Adv. Mater.* **2004**, *16*, 1249. (b) Xia, Y.; Rogers, J. A.; Paul, K. E.; Whitesides, G. M. *Chem. Rev.* **1999**, *99*, 1823.
- 5) Schmid, H.; Wolf, H.; Allenspach, R.; Riel, H.; Karg, S.; Michel, B.; Delamarche, E. *Adv. Funct. Mater.* **2003**, *13*, 145.
- 6) Loo, Y. -L.; Willett, R. L.; Baldwin, K. W.; Rogers, J. A. *Appl. Phys. Lett.* **2002**, *81*, 562.
- 7) Loo, Y. -L.; Baldwin, K. W.; Rogers, J. A. *J. Am. Chem. Soc.* **2002**, *124*, 7654.
- 8) (a) Loo, Y. -L.; Lang, D. V.; Rogers, J. A.; Hsu, J. W. P. *Nano Lett.* **2003**, *3*, 913. (b) Loo, Y. -L.; Hsu, J. W. P.; Willett, R. L.; Baldwin, K. W.; West, K. W.; Rogers, J. A. *J. Vac. Sci. Technol.* **2002**, *B 20*, 2853.
- 9) Kim, C.; Shtein, M.; Forrest, S. R. *Appl. Phys. Lett.* **2002**, *80*, 4051.
- 10) Loo, Y. -L.; Willett, R. L.; Baldwin, K. W.; Rogers, J. A. *Appl. Phys. Lett.* **2002**, *81*, 562.

- 11)(a) Zaumseil, J.; Meitl, M. A.; Hsu, J. W. P.; Acharya, B. R.; Baldwin, K. W.; Loo, Y. -L.; Rogers, J. A. *Nano Lett.* **2003**, *3*, 1223. (b) Jeon, S.; Menard, E.; Park, J. -U.; Maria, J.; Meitl, M. A.; Rogers, J. A. *Adv. Mater.* **2004**, *16*, 1369.
- 12)(a) Hur, S. -H.; Khang, D. -Y.; Kocabas, C.; Rogers, J. A. *Appl. Phys. Lett.* **2004**, *85*, 5730. (b) Wang, Z.; Yuan, J.; Zhang, J.; Xing, R. Yan, D.; Han, Y. *Adv. Mater.* **2003**, *15*, 1009.
- 13) Meitl, M. A.; Zhu, Z. -T.; Kumar, V.; Lee, K. J.; Feng, X.; Huang, Y. Y.; Adesida, I.; Nuzzo, R. G.; Rogers, J. A. *Nature Mater.* **2006**, *5*, 33.
- 14)(a) Beulen, M. J. W.; Bügler, J.; Lammerink, B.; Geurts, F. A. J.; Biemond, E. M. E. F.; Leerdam, K. G. C.; Van Veggel, F. C. J. M.; Engbersen, J. F. J.; Reinhoudt, D. N. *Langmuir*, **1998**, *14*, 6424. (b) Beulen, M. J. W.; Bügler, J.; De Jong, M. R.; Lammerink, B.; Huskens, J.; Schönherr, H.; Vancso, G. J.; Boukamp, B. A.; Wieder, H.; Offenhäuser, A.; Knoll, W.; Van Veggel, F. C. J. M.; Reinhoudt, D.N. *Chem. Eur. J.* **2000**, *6*, 1176.
- 15) Hillborg, H.; Gedde, U. W. *IEEE Trans. Dielectr. Electr. Insul.* **1999**, *6*, 703.
- 16) Hur, S. -H.; Khang, D.-Y.; Kocabas, C.; Rogers, J.A. *Appl. Phys. Lett.* **2004**, *85*, 5730.
- 17) Bowden, N.; Brittain, S.; Evans, A.G.; Hutchinson, J. W.; Whitesides, G.M. *Nature*, **1998**, *393*, 146.
- 18) Zaporojtchenko, V.; Strunskus, T.; Behnke, K.; Bechtolsheim, C. Von; Kiene M.; Faubel F. *J. Adhesion Sci. Technol.* **2000**, *14*, 467.
- 19) Martin, G.C.; Su, T.T.; Loh, I.H.; Balizer, E.; Kowel, S.T.; Kornreich, P. *J. Appl. Phys.* **1982**, *53*, 797.
- 20) Nijhuis, C.A.; Yu, F.; Knoll, W.; Huskens, J.; Reinhoudt, D.N. *Langmuir* **2005**, *21*, 7866.
- 21) Huskens, J.; Mulder, A.; Auletta, T.; Nijhuis, C. A.; Ludden, M. J. W.; Reinhoudt, D. N. *J. Am. Chem. Soc.* **2004**, *126*, 6784.
- 22)(a) Speets, E. A.; Ravoo, B. J.; Roesthuis, F. J. G.; Vroegindewey, F.; Blank, D. H. A.; Reinhoudt, D. N. *Nano Lett.* **2004**, *4*, 841. (b) Sondag-Huethorst, J. A. M.; Fokkink, L. G. J. *Langmuir* **1995**, *11*, 4823.
- 23)(a) Xia, Y.; Whitesides, G. M. *Angew. Chem.* **1998**, *110*, 568.; *Angew. Chem. Int. Ed.* **1998**, *37*, 550. (b) Xia, Y.; Zhao, X. -M.; Kim, E.; Whitesides, G. M. *Chem. Mater.* **1995**, *7*, 2332.
- 24) Waser, R. *Nanoelectronics and Information Technology*: Wiley-VCH, Darmstadt, **2003**.
- 25) Boussaad, S.; Xu, B. Q.; Nagahara, L. A.; Amlani, I.; Schmickler, W.; Tsui, R.; Tao, N. J. *J. Chem. Phys.* **2003**, *118*, 8891.
- 26) Chen, J.; Reed, M. A.; Rawlett, A. M.; Tour, J. M. *Science*, **1999**, *286*, 1550.
- 27) Khondaker, S. I.; Zhen, Y.; Cheng, L.; Henderson, J. C.; Yao, Y.; Tour, J. M. *Appl. Phys. Lett.* **2004**, *85*, 645.
- 28) Gergel, N.; Majumdar, N.; Keyvanfar, K.; Swami, N.; Harriott, L. R.; Bean, J. C.; Pattanaik, G.; Zangari, G.; Yao, Y.; Tour, J. M. *J. Vac. Sci. Technol. A* **2005**, *23*, 880.
- 29) Xue, Y.; Datta, S.; Hong, S.; Reifenger, R.; Henderson, J. I.; Kubiak, C. P. *Phys. Rev. B.* **1999**, *59*, R7852.
- 30) Gorman, C. B.; Carroll, R. L.; Fuierer, R. R. *Langmuir* **2001**, *17*, 6923.
- 31) Tivanski, A. V.; Walker, G. C. *J. Am. Chem. Soc.* **2005**, *127*, 7647.
- 32) Wassel, R. A.; Credo, G. C.; Fuierer, R. R.; Feldheim, D. L.; Gorman, C. B. *J. Am. Chem. Soc.* **2004**, *126*, 295.
- 33) He, J.; Lindsay, S. M. *J. Am. Chem. Soc.* **2005**, *127*, 11932.
- 34) Pitters, J. L.; Wolkow, R. A.; *Nano Lett.* **2006**, *6*, 390.
- 35) Gaudioso, J.; Ho, W. *Angew. Chem. Int. Ed.* **2001**, *40*, 4080.
- 36) Salomon, A.; Arad-Yellin, R.; Shanzer, A.; Karton, A.; Cahen, D. *J. Am. Chem. Soc.* **2004**, *126*, 11648.
- 37) Galperin, M.; Ratner, M. A.; Nitzan, A. *Nano Lett.* **2005**, *5*, 125.
- 38) Troisi, A.; Ratner, M. A. *Small* **2006**, *2*, 172.
- 39) Lau, C. N.; Stewart, D. R.; Williams, R. S.; Bockrath, M.; *Nanolett.* **2004**, *4*, 569.
- 40) Larade, B.; Bratkovsky, A. M. *Phys. Rev. B* **2005**, *72*, 035440.

- 41) Bard, A. J.; Faulkner, L. R. *Electrochemical Methods: Fundamentals and Applications* John Wiley & Sons: New York, **2001**.
- 42) Ashton, P. R.; Königer, R.; Stoddart, J. F.; Alker, D.; Harding, V. D. *J. Org. Chem.* **1996**, *61*, 903.
- 43) Cuadro, I.; Morán, M.; Casado, C. M.; Alonso, B.; Lobete, F.; García, B.; Ibisate, M.; Losada, J. *Organometallics* **1996**, *15*, 5278.
- 44) Baars, M. W. P. L.; Karlsson, A. J.; Sorokin, V.; De Waal, B. F. W.; Meijer E. W. *Angew. Chem. Int. Ed.* **2000**, *39*, 4262.
- 45) Onclin, S.; Mulder, A.; Ravoo, B. J.; Huskens, J.; Reinhoudt, D. N. *Langmuir* **2004**, *20*, 5460.

Summary

This thesis describes the controlled immobilization of molecules by supramolecular chemistry and self-assembly. Unlike physisorption or covalent synthesis, the binding kinetics and thermodynamics can be controlled at will, and the immobilization is reversible. A disadvantage is that, in general, the binding strength of a single supramolecular interaction is relatively weak, but this drawback can be overcome by using multivalent interactions. To obtain functional materials it is a prerequisite that molecules form stable assemblies which can exist in at least two different states that can be controlled by external stimuli.

The first part of the thesis (Chapters 3 to 5) describes the fundamental issues of the controlled adsorption of molecules at a surface leading to well-defined and stable supramolecular surface assemblies. To achieve this, Au or SiO₂ surfaces were functionalized with self-assembled monolayers (SAMs) of β -cyclodextrin (β CD) host molecules, a so-called “molecular printboard”, to which guest molecules can bind via hydrophobic interactions in an electrochemically controlled manner. The second part of the thesis (Chapters 6 to 8) deals with the patterning of a variety of guest molecules at the molecular printboard and the preparation of supramolecular junctions for applications in molecular electronics.

Chapter 1 gives a short introduction to this thesis and in Chapter 2 a literature overview is given of supramolecular systems that respond to electrochemical conversion of one of the components. Especially, redox-active rotaxanes and catenanes are reviewed where oxidation or reduction induces, for instance, translocation of one of the interlocked molecules with respect to the other. In addition, this chapter discusses electrochemically induced host-guest complex formation and dissociation, and conformational change. Of particular interest for this thesis is the electrochemically induced dissociation of ferrocene (Fc) - β CD inclusion complexes. Fc in the neutral form forms strong inclusion complexes with β CD, but in its oxidized form, the ferrocenium cation (Fc⁺), the host-guest complexation is diminished.

Chapter 3 describes the adsorption of Fc-functionalized poly(propylene imine) (PPI) and polyamidoamine (PAMAM) dendrimers, and a PAMAM dendrimer with long tethers between the Fc end group and the dendritic core at the molecular printboard. The dendrimers are insoluble in water, but complexation of all Fc moieties to β CD led to water soluble supramolecular assemblies. The number of interacting end groups with the host surface could be determined for all dendrimers by electrochemistry. For the smaller generations, surface plasmon resonance (SPR) titrations gave also thermodynamic parameters for supramolecular

immobilization. The number of interactions increased from 2 (out of 4 end groups) for the generation 1 (G1) PPI dendrimer to 7 (or 8) out of 64 end groups for G5. The number of interactions also increased with increasing tether lengths: the number of interactions nearly doubled in the case of PAMAM dendrimers compared to the PPI analogs, and in the case of the PAMAM dendrimers consisting of long tethers all end groups were interacting with the host surface. All dendrimers, even the ones having 8 interactions, could be effectively removed from the molecular printboard upon electrochemical conversion of the Fc moieties to Fc^+ as could be followed by electrochemistry and electrochemistry combined with SPR.

While Chapter 3 describes the behavior of adsorbed guest dendrimers at the host SAM, Chapter 4 deals with the electrochemical behavior of the dendrimer- βCD assemblies in solution in equilibrium with the βCD SAM-decorated electrodes. The electrochemical system could be described in terms of an equivalent circuit which revealed detailed information about the electron transfer kinetics, adsorption and desorption processes, and diffusion processes. The dendrimers bound to the surface and adopted a fully extended conformation limited only by the number of interactions. The relative diffusion constants could be determined and showed Stokes-Einstein behavior indicating that the dendrimer- βCD assemblies behave as spheres in solution.

For various applications it is interesting to be able to switch between more than two states. The dendrimers described in Chapters 3 and 4 have only two oxidation states, i.e. Fc in the reduced or in the oxidized state. In Chapter 5, biferrocene (BFc) -functionalized PPI dendrimers are introduced that have three different oxidation states. The dendrimers can be in the fully reduced $\text{Fe}_2(\text{II,II})$ form, the mixed valence $\text{Fe}_2(\text{II,III})^+$ state, or in the fully oxidized $\text{Fe}_2(\text{III,III})^{2+}$ state. The BFc moiety formed stable inclusion complexes with βCD which had an association constant (K_{ass}) that was one order of magnitude larger compared to Fc- βCD inclusion complexes according to isothermal titration calorimetry. The complexation of BFc to βCD could be diminished by electrochemical oxidation of the BFc to the mixed valence $\text{Fe}_2(\text{II,III})^+$ state. This caused complex redox behavior of the electrochemically induced desorption of the dendrimers from the molecular printboard. At low scan rates, only surface-interacting BFc moieties were oxidized to the $\text{Fe}_2(\text{II,III})^+$ state followed by the oxidation of the remaining end groups. Finally all end groups were oxidized to the fully oxidized $\text{Fe}_2(\text{III,III})^{2+}$ form.

The second part of the thesis deals with patterning of the dendrimers at the molecular printboard and their potential use in molecular electronics. Chapter 6 describes the use of supramolecular microcontact printing (μCP) and dip-pen nanolithography (DPN) to fabricate patterns of the dendrimers at the host surface with micron and sub-micron resolution, respectively. μCP uses an elastomeric stamp which is used to transfer molecules from the stamp to a substrate during conformal contact of the stamp with substrate. The patterns were in the micrometer range and the dendrimers formed stable patterns at the host surface since the patterns were stable when exposed to rinsing procedures of competitive solutions, i.e.

aqueous β CD solutions. Supramolecular DPN uses an AFM tip as the stylus and the dendrimer- β CD assemblies as ink. Adamantyl (Ad) -terminated G5 PPI dendrimers complexed to β CD were used as ink. The large supramolecular assemblies form kinetically stable assemblies due to the formation of multiple host-guest interactions with the host surface. Structures of 60 nm wide could be written, which corresponds to 15-20 molecules. Scanning electrochemical microscopy (SECM) was used to induce the local desorption of the Fc PPI dendrimers from the molecular printboard on SiO_2 . Although the resolution of SECM is inferior to that of AFM, patterns could be written in monolayers of the dendrimers and thus SECM is complementary to DPN and μ CP, in particular because the latter techniques are additive, while SECM is subtractive. Additionally, SECM was used to determine the surface coverage of the dendrimers at the molecular printboard on SiO_2 which was found to be nearly doubled compared to the monolayers of dendrimers on β CD SAMs on Au.

The Ad-functionalized dendrimer- β CD assemblies can be used as nanoreactors to synthesize and stabilize Au nanoparticles of about 1.7 nm diameter. Chapter 7 deals with the immobilization of the dendrimer- β CD-Au nanoparticle assemblies at the molecular printboard and the characterization by scanning tunneling microscopy (STM). STM images clearly showed the dendrimers loaded with Au nanoparticles adsorbed at the β CD SAM. The (I,V) characteristics showed Coulomb staircase behavior under ambient conditions. This indicated that the β CD SAM is an efficient tunnel barrier and that the Au nanoparticles reside in the dendrimer interior resulting in a stable system.

Chapter 8 describes supramolecular metal transfer printing (mTP) which is a printing technique to introduce top contacts at monolayers via supramolecular interactions. At a PDMS stamp a thin layer of Au was deposited followed by the formation of a β CD SAM. Conformal contact of the stamp with a substrate consisting of a β CD SAM at which dendrimers were adsorbed, induced the formation of host-guest complexes in the contact areas. Removal of the stamp left the Au behind exclusively in the contact areas. A variety of structures at different length scales could be transferred and also dendrimers adsorbed at the β CD SAM at the stamp resulted in transfer of Au onto a β CD SAM at the substrate. Dendrimers adsorbed at functionalized stamps also induced the transfer directly onto SiO_2 which allowed the transfer of Au from the stamp to prepatterned Au substrates. The (I,V)-characteristics of two-terminal devices were measured consisting of the redox-active Fc and BFc dendrimers and the redox-passive Ad dendrimers. Tunnel characteristics at room temperature could be measured for devices having a surface area of $100 \mu\text{m}^2$. The devices showed one or two negative differential resistance (NDR) waves in the case of the Fc and BFc dendrimers, respectively. In the case of the Ad dendrimers, no NDR could be observed.

The results presented in this thesis showed that multivalency is an important tool in bottom-up nanofabrication to obtain stable supramolecular structures. Additionally, the electrochemically controlled adsorption of the dendrimers at the molecular printboard illustrates the advantage of using supramolecular interactions rather than physisorption or

covalent synthesis. A relatively simple printing method was introduced that yielded supramolecular junctions without destroying the supramolecular complexes on a large scale. This technique, and related ones, are promising in the field of nanoelectronics to obtain relatively complicated supramolecular junctions without destroying the relatively fragile molecules.

Samenvatting

Dit proefschrift beschrijft het gebruik van supramoleculaire interacties en zelfassemblage om moleculen gecontroleerd op oppervlakken te adsorberen. Het gebruik van specifieke interacties in plaats van fysisorptie of covalente synthese heeft het voordeel dat de bindingskinetiek en -thermodynamica gecontroleerd kunnen worden. Een nadeel is dat in het algemeen de bindingssterkte van een enkele supramoleculaire interactie relatief gering is. Multivalente binding kan de bindingssterkte echter enorm vergroten en leiden tot kinetisch stabiele systemen hetgeen een vereiste is voor veel toepassingen. Om functionele materialen te kunnen maken is het nodig dat de moleculen in verschillende toestanden kunnen bestaan en die aangesproken kunnen worden door middel van een externe stimulus.

Het eerste deel van dit proefschrift (hoofdstukken 3 t/m 5) beschrijft de fundamentele aspecten om moleculen gecontroleerd op oppervlakken te adsorberen. Om moleculen door middel van specifieke interacties op een oppervlak te kunnen adsorberen werden de oppervlakken met een monolaag van receptormoleculen gefunctionaliseerd, een zogenaamde moleculaire printplaat. De moleculaire printplaat is gebaseerd op β -cyclodextrine- (β CD-) receptoren. Op deze monolaag van gastheermoleculen kunnen vervolgens gastmoleculen binden door middel van specifieke gastheer-gast-interacties die elektrochemisch gecontroleerd kunnen worden. Het tweede deel van dit proefschrift (hoofdstukken 6 t/m 8) beschrijft het patroneren van gastmoleculen op het β CD-oppervlak en het maken van supramoleculaire schakelingen voor toepassingen in moleculaire elektronica.

Hoofdstuk 1 is een korte inleiding op dit proefschrift en in hoofdstuk 2 wordt een literatuuroverzicht gegeven van redox-actieve supramoleculaire systemen. Onder andere worden redox-actieve catenanen en rotaxanen behandeld, waarbij oxidatie of reductie beweging van het ene deel van een molecuul ten opzichte van een ander deel bewerkstelligt. Bovendien wordt aandacht besteed aan elektrochemisch geïnduceerde dissociatie en associatie van gastheer-gast-complexen, en conformatieveranderingen in een molecuul. Van primair belang van dit proefschrift is de elektrochemisch geïnduceerde dissociatie van ferrocen- (Fc-) β CD-complexen. Fc in de neutrale vorm vormt in water stabiele gastheer-gast-complexen met β CD, maar elektrochemische oxidatie leidt tot het ferroceniumkation (Fc^+) dat vrijwel niet aan β CD wordt gebonden.

In hoofdstuk 3 worden verschillende gastmoleculen, namelijk Fc-gefunctionaliseerde poly(propyleenimine)- (PPI-) dendrimeren, poly(amido-amine)- (PAMAM-) dendrimeren en

PAMAM-dendrimeren met lange verbindingsgroepen tussen de Fc-eindgroepen en de dendrimere centrum, geadsorbeerd op de moleculaire printplaat. De gastmoleculen zijn niet in water oplosbaar, maar de Fc-eindgroepen kunnen binden aan het wateroplosbare β CD, hetgeen resulteert in wateroplosbare supramoleculaire complexen. Het aantal interacties van de dendritische gastmoleculen met het receptoroppervlak is bepaald met behulp van elektrochemie. In het geval van kleine gastmoleculen was het mogelijk om met oppervlakteresonantie-spectroscopie (surface plasmon resonance, SPR) de thermodynamische bindingsparameters te bepalen. Het aantal interacties nam toe van 2 (van de 4 eindgroepen) in het geval van het generatie-1 (G1) PPI-dendrimeer tot 7 (of 8) van de 64 eindgroepen voor G5. Het aantal interacties nam ook toe met de grootte van de moleculen. Het aantal interacties verdubbelde in het geval van de PAMAM-dendrimeren (G1 t/m G3) ten opzichte van de PPI-analoga en, in het geval van de dendrimeren met de lange verbindingsgroepen (G1 en G2), konden alle Fc-eindgroepen een interactie met het receptoroppervlak aangaan. In neutrale toestand vormden de moleculen stabiele monolagen aan het β CD-oppervlak. Oxidatie van de eindgroepen gaf echter positief geladen gastmoleculen die vrijwel geen interactie met het oppervlak aangaan, hetgeen leidde tot effectieve desorptie van de dendrimeren van het β CD-oppervlak, zelfs voor moleculen met 8 interacties.

Terwijl hoofdstuk 3 uitsluitend het gedrag van de gastmoleculen geadsorbeerd aan het β CD-oppervlak behandelt, wordt in hoofdstuk 4 het gedrag van deze moleculen in waterige oplossing bestudeerd met elektrochemische methoden. Het elektrochemische systeem kon beschreven worden aan de hand van een equivalente schakeling waaruit gedetailleerde informatie verkregen kon worden over elektronoverdrachtskinetiek, adsorptie-, desorptie- en diffusieprocessen. Hieruit volgt dat de moleculen binden aan het oppervlak en daarbij een volledig uitgestrekte bolvormige conformatie hebben. De relatieve diffusieconstanten konden bepaald worden en vertoonden Stokes-Einstein-gedrag, hetgeen bewijst dat de dendrimeer- β CD-complexen zich gedragen in oplossing als bollen.

Voor veel elektronische en materiaalkundige toepassingen is het interessant om te kunnen schakelen tussen meer dan twee verschillende toestanden. In de hoofdstukken 3 en 4 wordt een systeem beschreven dat uitsluitend schakelde tussen twee toestanden, namelijk tussen geoxideerd Fc^+ en gereduceerd Fc. Hoofdstuk 5 behandelt biferroceen- (BFc-) gefunctionaliseerde dendrimeren die kunnen schakelen tussen drie verschillende toestanden. Deze moleculen kunnen zich in een neutrale $\text{Fe}_2(\text{II},\text{II})$ -toestand bevinden, in een halfgeoxideerde $\text{Fe}_2(\text{II},\text{III})^+$ -toestand en in een volledig geoxideerde $\text{Fe}_2(\text{III},\text{III})^{2+}$ -toestand. De BFc-groepen vormen complexen met β CD met een associatieconstante (K_a) die, volgens microcalorimetrie, een factor 10 groter is dan met Fc. Oxidatie tot de halfgeoxideerde $\text{Fe}_2(\text{II},\text{III})^+$ -toestand leidde tot een efficiënte dissociatie van de gastheer-gast-complexen. Dit had een grote invloed op het elektrochemische gedrag van deze complexen op het β CD-gastheeroppervlak ten opzichte van ongemodificeerde elektrodes waardoor er een extra oxidatiestap nodig was om de moleculen volledig te oxideren. Bij lage scansnelheden werden

alleen aan het oppervlak gebonden BFc-groepen geoxideerd tot $\text{Fe}_2(\text{II,III})^+$. Vervolgens werden de resterende BFc-groepen geoxideerd tot $\text{Fe}_2(\text{II,III})^+$. Uiteindelijk werden alle eindgroepen in een laatste stap geoxideerd tot de volledig geoxideerde $\text{Fe}_2(\text{III,III})^{2+}$ -toestand.

Het tweede deel van dit proefschrift beschrijft het patroneren van gastmoleculen op de moleculaire printplaten en potentiële toepassingen in de moleculaire elektronica. In hoofdstuk 6 worden zowel supramoleculaire microcontactdruk (microcontact printing, μCP) als dip-pen-nanolithografie (DPN) gebruikt om patronen van dendrimeren op de printplaten te fabriceren met respectievelijk micrometer- of submicrometerresolutie. μCP is een stempeltechniek waarbij met behulp van een rubberen stempel inktmoleculen overgedragen kunnen worden op een oppervlak. μCP leidt tot stabiele patronen op μm -schaal. De gestempelde dendrimeren op de moleculaire printplaten vormden kinetisch stabiele patronen, aangezien wasprocedures met competitieve βCD -oplossingen niet leidden tot desorptie. Supramoleculaire DPN gebruikt een AFM-naald als pen en de adamantyl- (Ad-) gefunctionaliseerde G5 PPI-dendrimeren gecomplexeerd met βCD als inkt. De grote supramoleculaire complexen vormden kinetisch stabiele monolagen vanwege de vorming van multivalente supramoleculaire interacties aan het receptoroppervlak. Hierdoor konden er patronen geschreven worden van 60 nm breed, hetgeen overeenkomt met de dikte van ongeveer 15 tot 20 moleculen. Met behulp van electrochemische rastermicroscopie (scanning electrochemical microscopy, SECM) konden plaatselijk de redox-actieve gastmoleculen geadsorbeerd worden, zodat patronen geschreven werden in de monolagen van de gastmoleculen op de monolaag van gastheermoleculen. Ofschoon de resolutie van SECM veel minder is dan die van AFM, is SECM complementair aan de twee voorafgaande technieken aangezien deze additief zijn, terwijl in de laatste materiaal verwijderd wordt. Met SECM kon ook de oppervlaktebedekking van de dendrimeren op de moleculaire printplaten of SiO_2 bepaald worden. Deze is ongeveer een factor 2 hoger vergeleken met de moleculaire printplaten op goud.

De supramoleculaire dendrimeer- βCD -complexen kunnen ook gebruikt worden om gouden nanodeeltjes van 1.7 nm te synthetiseren en te stabiliseren. In hoofdstuk 7 worden de supramoleculaire complexen met een gouddeeltje erin geadsorbeerd aan het gastheeroppervlak op goud. Met rastertunnelmicroscopie (scanning tunneling microscopy, STM) konden de aan het gastheeroppervlak geadsorbeerde dendrimeren met een gouddeeltje erin gevisualiseerd worden. De (I,V)-karakteristieken gemeten bij kamertemperatuur vertoonden de typische “getrapte” vorm van een Coulomb-blokkade. Dit impliceert dat de βCD -monolaag een efficiënte tunnelbarrière is en dat de goudnanodeeltjes in het dendrimeer zitten.

In het laatste hoofdstuk wordt supramoleculair metaalstempelen toegepast om topelektrodes op de dendrimeermonolagen te stempelen. Op een PDMS stempel wordt een dun laagje goud aangebracht waarop vervolgens een monolaag van βCD wordt gevormd. Vervolgens wordt de stempel in contact gebracht met het substraat dat bestaat uit een monolaag van dendrimeren geadsorbeerd op een gastheeroppervlak op goud. Gedurende

contact van de stempel met het substraat ontstaan er specifieke interacties tussen het substraat en de stempel. Wanneer de stempel wordt weggehaald wordt het goud overgedragen. Dendrimeren geadsorbeerd op de gefunctionaliseerde stempel induceren ook de overdracht direct op SiO₂, hetgeen ook de overdracht op gepatroneerde goudsubstraten mogelijk maakte. Aan de structuren die op deze wijze vervaardigd waren, konden tunnelstromen gemeten worden van twee-contactschakelingen met een oppervlak van 100 μm². Schakelingen verkregen met redox-actieve groepen vertoonden een zogenaamd NDR-effect, terwijl met redox-inactieve gasten geen NDR-waargenomen werd. Met de gastmoleculen met drie verschillende redox-toestanden konden twee NDR-pieken waargenomen worden, terwijl Fc-gefunctionaliseerde dendrimeren een enkele NDR-piek gaven.

Het onderzoek beschreven in dit proefschrift laat zien dat multivalentie een belangrijk stuk gereedschap is in “bottom-up”-nanotechnologie om zo stabiele supramoleculaire structuren te fabriceren. De elektrochemisch gecontroleerde adsorptie van de dendrimeren op moleculaire printplaten illustreert het voordeel van supramoleculaire interacties ten opzichte van fysisorptie en covalente synthese. Het gebruik van een relatief simpele stempelmethode resulteerde in supramoleculaire schakelingen op grote schaal zonder dat het supramoleculaire systeem beschadigd werd. Deze techniek en andere vergelijkbare technieken zijn veelbelovend in nano-elektronica om relatief complexe en fragiele moleculen in te bouwen in schakelingen op nanoschaal.

Dankwoord

Natuurlijk is al het werk beschreven in dit proefschrift niet alleen uitgevoerd, maar heb ik het geluk gehad dat veel mensen altijd bereid waren om te helpen. David Reinhoudt bedankt voor alle vrijheid die ik heb gekregen binnen mijn onderzoek. Maar ook voor veel ideeën die vaak al drie of vier stappen verderop in het onderzoek lagen dan waar ik was. Jurriaan Huskens, bedankt voor de dagelijkse supervisie in het begin van het project. Met name door jou ben ik naast de synthetische kant, ook de fysische kant binnen de chemie gaan waarderen. Bart Jan Ravoo, jij hebt de dagelijkse supervisie van Jurriaan overgenomen. Bedankt voor de prettige en vaak erg vlotte samenwerking. Bernard Boukamp van de groep Inorganic Materials Science, bedankt voor alle “lessen” elektrochemische impedantie spectroscopie en de hulp bij de interpretatie van de vele spectra. Harold “het kan altijd 1000 euro beter” Zandvliet and Nuri Oncel from the Solid State Physics group, thank you for conducting the STM experiments. Wilfred van der Wiel van de SRO NanoElectronics, de vele discussies over nanoelectronica waren altijd zeer verhelderend. Jou enthousiasme en de houding “geen idee is te gek” waren altijd zeer motiverend. Gunther Wittstock and Jatin Sinha from the Carl von Ossietzky University of Oldenburg, thanks for the pleasant collaboration and for conducting the SECM measurements. Jurriaan Schmitz, Cora Salm en Marcel Weusthof van de groep Semiconductor Components, dankzij jullie was het mogelijk om de eigenschappen van de tunnel junctions te meten. The proof of principle concerning the electrochemically controlled binding of the dendrimers was proven in the group of Wolfgang Knoll and was performed by Fang Yu from the Max Planck Institute for Polymer Research in Mainz, many thanks.

Ik heb de mazzel gehad om een aantal goede studenten te begeleiden voor een kortere of een langere periode. Een speciaal dankje gaat uit naar Jurjen ter Maat. Je afstudeeronderzoek heeft geleid tot een imposant afstudeerverslag waarvan een deel is beschreven in hoofdstuk 9. Joris Salari, ik heb je maar kort begeleid, maar toch hebben we naast het klimmen en boulderen in het gebouw ook nog wat wetenschappelijks gedaan. Karolina Dolatowska, many thanks for up-scaling the synthesis of the biferrocene dendrimers. Satria, you came all the way from Indonesia to measure “exploding” two-terminal devices, thanks.

Dankzij de “CD-groep” was er altijd ruimte voor veel discussie en het helpen bij alledaagse probleempjes. Tommaso Auletta, Olga Crespo Biel, Alart Mulder, Steffen Onclin en Manon Ludden, jullie waren altijd goed voor veel hulp en een leuke samenwerking in het alledaagse

lableven. Christiaan Bruinink wil ik bedanken voor het introduceren van microcontact printen en het maken van de masters. Many thanks go to Mária Péter for the AFM work. Emiel Speets, naast vele discussie over wetenschap en politiek, wil ik je ook bedanken voor de XPS metingen.

More or less the last six months I spent most of the time in room 1717 mainly writing. But I was not there alone: Fernando, special thanks for introducing me to the fascinating world of “crappy music” and Alessio and Kim for withstanding my frustrations about Windows.

Mark Smithers, wil ik bedanken voor de TEM-metingen van de goud nanodeeltjes. Verder heb ik vele uren door gebracht in de cleanroom om met de BAK 600 goudlagen te “bakken”. Hans Mertens, bedankt voor de vele keren dat je klaar stond.

Dan wil ik nog een paar mensen bedanken die groep draaiende houden. Marcel de Bruine, bedankt de vele koffiepauzes en ook voor het vinden van van-alles-en-nog-wat. Richard Egberink, jij was er altijd om de vele alledaagse vragen te beantwoorden en jij wist mijn computer draaiende te houden. Voor de analyses van de verbindingen moet ik Tieme Stevens en Aldrik Velders bedanken. Aldrik, ga vooral door met het “pushen” van anderen om een borrel te geven, of in ieder geval bier te halen. Ben Lammerink, wil ik bedanken voor de vele suggesties en hulp bij het uitvoeren van syntheses. Carla Weber, Izabel Can-Katalanc en Marieke Slotman bedankt voor de alledaagse administratieve handelingen.

Gerald Spijksma, Kim Wimbush, Jasper Holman and Maria Asunción Durá I would like to thank you for proof reading my thesis. Kim, good luck with continuing the project!

Matthijs “Smartie” Reinier van Calveen bedankt voor het ontwerpen van de cover die toch is anders uitgepakt dan gedacht.

En als laatste rest mij om mijn paranimfen Henk Dam en Hans Beijleveld te bedanken voor het bijstaan van de laatste momenten en de vele “memorabele” momenten daarvoor.

Curriculum Vitae

Christian Albertus Nijhuis is geboren op 17 januari 1977 te Enschede. In 1994 haalde hij het eindexamen HAVO en in 1996 het eindexamen VWO aan het Ichthus College te Enschede. Van 1996 tot 2002 studeerde hij scheikunde aan de Rijksuniversiteit Groningen en studeerde af aan de vakgroep Moleculaire Anorganische Chemie onder leiding van Prof. dr. Jan Teuben en Prof. dr. Bart Hessen. Zijn afstudeeronderzoek betrof de synthese en reactiviteit van Mn(II), Fe(II), Co(II) en Cr(II) complexen met sterisch gehinderde benzaminaat liganden. Van 2002 tot 2006 verrichtte hij zijn promotie-onderzoek in de vakgroep Supramoleculaire Chemie en Technologie onder de supervisie van Prof. dr. ir. D. N. Reinhoudt, Prof. dr. ir. J. Huskens en dr. B. J. Ravoo. De resultaten zijn beschreven in dit proefschrift. Vanaf januari 2005 zal hij werkzaam zijn als post-doc aan de Harvard University onder leiding van Prof. dr. G. M. Whitesides.